BioMed Research International

Biomechanical Properties of Biomaterials/Scaffolds for Bone Tissue Regeneration

Lead Guest Editor: Francesca Salamanna
Guest Editors: Maria Sartori and Elena Della Bella

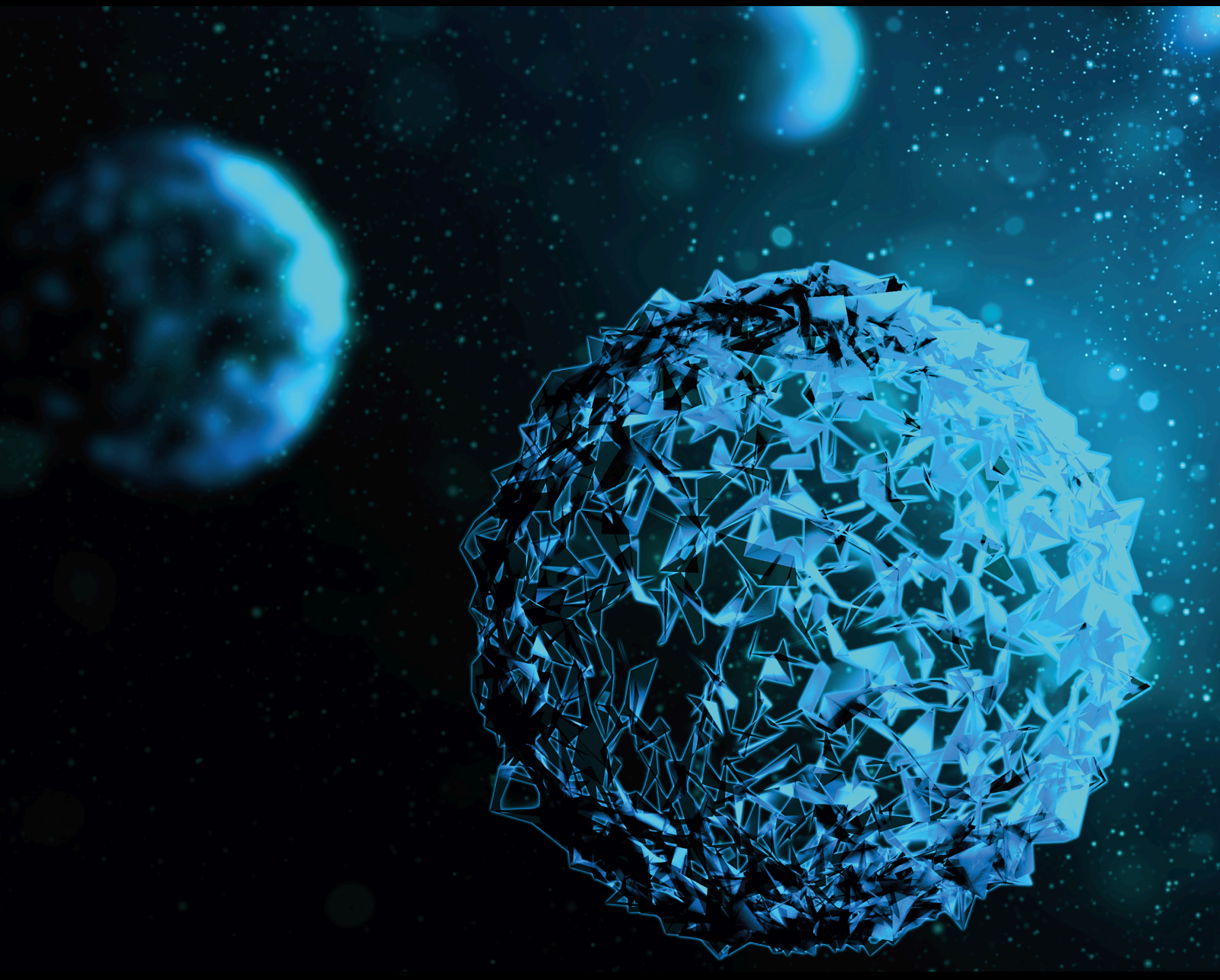

Biomechanical Properties of Biomaterials/ Scaffolds for Bone Tissue Regeneration

BioMed Research International

Biomechanical Properties of Biomaterials/Scaffolds for Bone Tissue Regeneration

Lead Guest Editor: Francesca Salamanna
Guest Editors: Maria Sartori and Elena Della Bella

Section Editors

Academic Editors

Biomaterials

Contents

Cytokine Regulation from Human Peripheral Blood Leukocytes Cultured *In Vitro* with Silver Doped Bioactive Glasses Microparticles

Jefferson Muniz de Lima, Edlainne Pinheiro Ferreira, Roberta Ferreti Bonan, David Nascimento Silva-Teixeira, Luiz Ricardo Goulart, Joelma Rodrigues de Souza, Eliton Souto de Medeiros, Paulo Rogério Ferreti Bonan, and Lúcio Roberto Cançado Castellano

Research Article (9 pages), Article ID 3210530, Volume 2019 (2019)

Evaluation and Prediction of Mass Transport Properties for Porous Implant with Different Unit Cells: A Numerical Study

Jian Li, Diansheng Chen, and Yubo Fan

Research Article (11 pages), Article ID 3610785, Volume 2019 (2019)

Hindawi
BioMed Research International
Volume 2020, Article ID 1804630, 13 pages
https://doi.org/10.1155/2020/1804630

Review Article

Histological, Histomorphometrical, and Biomechanical Studies of Bone-Implanted Medical Devices: Hard Resin Embedding

M. Maglio,[1] F. Salamanna,[1] S. Brogini,[1] V. Borsari,[1] S. Pagani,[1] N. Nicoli Aldini,[1] G. Giavaresi,[1] and M. Fini[2]

[1]*IRCCS Istituto Ortopedico Rizzoli, Laboratory of Preclinical and Surgical Studies, Bologna, Italy*
[2]*IRCCS Istituto Ortopedico Rizzoli, Laboratory of Biomechanics and Technology Innovation, Bologna, Italy*

Correspondence should be addressed to F. Salamanna; francesca.salamanna@ior.it

Received 2 July 2019; Revised 25 November 2019; Accepted 9 December 2019; Published 17 January 2020

Academic Editor: Costantino Del Gaudio

The growing incidence of degenerative musculoskeletal disorders as well as lifestyle changes has led to an increase in the surgical procedures involving implanted medical devices in orthopedics. When studying implant/tissue interface in hard materials (i.e., metals or dense plastics) and/or in large bone segments, the hard plastic embedding of the intact undecalcified tissue envelope with the implant *in situ* is needed. The aim of this work is to describe the advances and the possibilities of high-temperature methyl methacrylate (MMA) embedding for the histological, histomorphometrical, and biomechanical assessment of bone-implanted medical devices. Unlike routine techniques, undecalcified bone processing histology, using high-temperature MMA, requires a complex and precise sample processing methodology and the availability of sophisticated equipment and software for both sample preparation and analyses. MMA embedding permits the evaluation of biological responses to the presence of implanted medical devices without implant removal, allowing simultaneous qualitative and quantitative histological evaluation, both static and dynamic histomorphometry, and biomechanical analyses not possible with tissue decalcification. MMA embedding, despite being a demanding procedure, is still preferred to other kinds of resin-based embedding because of its peculiar characteristics, which allow the study of samples of big dimensions also implanted with hard materials without reducing the sample or removing the material. Dynamic measurements are allowed together with biomechanical investigations at the bone-biomaterial interface, obtaining a comprehensive and precise evaluation of the safety and effectiveness of medical devices for orthopedic regenerative, reconstructive, and reparative surgery.

1. Introduction

Orthopedic medical devices have been extremely successful in restoring mobility, reducing pain, and improving the quality of life of millions of individuals each year [1, 2]. Nowadays, different kinds of synthetic or composite materials with complex topographical features and manufacturing processing techniques are developed as bone implants and scaffolds for regenerative, reconstructive, and reparative medicine [3]. The final step of the medical device approval for the patient's use goes through an exhaustive regulatory process to prevent clinical complications or any other close or distant side effects. In this regulatory process, testing a novel material involves *in vitro* assays with cell cultures and *in vivo* tests using proper animal models. The biocompatibility, i.e., the process of evaluating materials used in the manufacture of medical devices (or a material component of such), is guided by a series of Standards International ISO 10993.

In biomedical research, when *in vitro* studies are inapplicable or not exhaustive, animal studies are mandatory to investigate the safety and to establish proof of burden on the feasibility and preclinical efficacy of medical devices as biomaterials, scaffolds, bone substitutes, and engineered constructs. In general, small laboratory animals are preferred due to the greater simplicity of management and housing and for precisely answering biological mechanisms. The use of large animals may be justified based on special

scientific considerations of the particular material under study, or if needed to accommodate implant size, with whole device testing, or to satisfy particular pathophysiological and loading conditions.

When implant/tissue interface of hard materials (i.e., metals, dense plastics) is to be studied and/or if large animals have been used with the implantation of scaled-up materials, the embedding of the intact tissue envelope with the implant *in situ* using hard plastic is needed. Plastic embedding for undecalcified bone tissues is a well-established strategy for histopathological and histomorphometric study of samples which cannot be properly evaluated with classical paraffin embedding of decalcified bone tissues. To date, high-temperature methyl methacrylate (MMA) embedding, despite being a demanding procedure, is still preferred to other kinds of resin-based embedding due to its peculiar characteristics. When compared, for example, to water-soluble MMA, such as glycol methacrylate (GMA), high-temperature MMA proves to better infiltrate samples of big dimensions and at the same time can be removed by sections in order to improve staining quality and the evaluation of tissue morphology [4]. Also, in comparison with low-temperature MMA-based resins, which allows us to obtain thinner sections and therefore a better histopathological evaluation of the section, the inclusion in high-temperature MMA could be preferred. In fact, it allows us to evaluate samples of much larger sizes in relatively shorter times and with less labor-intensive passages, since other resins allow the evaluation of samples up to 1.5 cm × 1.5 cm. However, the adoption of high-temperature MMA-based embedding solutions for histology requires that laboratories set up appropriate working spaces for all processing and embedding steps and for the subsequent phases of realization of the histological slides. The presence of adequate chemical fume hoods is mandatory for the safe manipulation and preparation, not only for formaldehyde-based fixatives but also for MMA-based infiltrating and embedding solutions, so as to avoid or minimize the exposure to vapors of monomer. In addition, the disposal of the MMA monomer and the first infiltration solution requires specific procedures. In comparison to other most common embedding techniques, such as paraffin, high-temperature MMA embedding foresees longer and alcohol consuming steps for dehydration and requires further reagents for embedding steps. Considering the high temperature of MMA polymerization, special embedding cassettes/molds resistant to temperature are needed for sample inclusion and much more attention must be paid to sample orientation because, differently from wax, MMA polymerization is an irreversible reaction. The quality of the final MMA-embedded sample depends on the correct performance of all the above-mentioned procedures; only after perfect processing, a variety of histological, histomorphometric, and biomechanical evaluations can be carried out.

Since histology, histomorphometry, and biomechanics are key methodologies for bone-implanted medical device evaluation, it is extremely important to update the concept of "hard resin embedding" as a method not allowing precise evaluations. The purpose of this work is to outline a method for the preparation of bone-implanted medical devices embedded in high-temperature MMA and to highlight the evaluations that this technique allows to carry out.

2. Materials and Methods

Once the bone-implanted medical device is collected, it is crucial to promptly carry out the processing steps in order to prevent the deterioration of the tissue triggered by proteolytic enzymes and, at a later stage, to preserve its microarchitecture, making it more resistant to subsequent processing phases.

2.1. Fixation and Dehydration. Fixation is used to prevent tissue decomposition and preservation of cell and matrix structure and to intensify subsequent staining. Bone-implanted medical devices must be fixed immediately after harvesting to avoid artifacts. Although many fixatives are available, these samples are usually fixed in 4% paraformaldehyde at room temperature. As it is essential to put samples in an excess of fixative, starting from a minimum acceptable fixative/tissue ratio of 1 : 20, also fixation times depend on sample dimensions. The minimum fixation time is considered 24 hours. After the fixation period, bone-implanted medical devices are extensively rinsed in distilled water, for at least 4–6 hours, with frequent changing of water, and then washed in running tap water for another 4 hours to eliminate all the fixative. To eliminate the entire water content of the sample, they are dehydrated in increasing concentration of alcohols in steps of at least 24 hours each, starting from 50% ethanol, 70%, twice 96%, and three times 100%, depending on sample dimension.

2.2. Embedding. After dehydration, the high-temperature MMA embedding procedure for bone-implanted medical devices is organized in the following basic steps:

(1) Infiltration of the sample with MMA monomer for 24 hours

(2) Infiltration of the sample with MMA with the addition of benzoyl peroxide and Tergitol in the solution for 24 hours

(3) Inclusion in embedding solution: MMA with the addition of benzoyl peroxide and Tergitol, to which low molecular weight polymethylmethacrylate (PMMA) is slowly added

Once the complete suspension of the PMMA is achieved, taking into account the fact that the preparation of the final embedding solution can require some hours, samples are placed in the obtained solution within specific polyethylene cassettes/molds and finally oriented according to the cutting requirements. The polymerization process is an exothermic chain reaction and is carried out in strictly controlled temperatures, as the reaction can reach very high temperatures and be very violent, causing bubble formation inside the preparation and movement of the samples, risking altering the orientation predisposed for the following cutting

phase. The polymerization time is also influenced by many factors besides temperatures, such as the sample dimension. Samples larger than 3 cm will take more time to complete embedding, also in the order of several weeks, while smaller samples can require just a few days. The whole polymerization phase, as well as MMA-based solution preparation and all infiltration steps, must be conducted under a chemical fume hood in order to avoid air dispersion of monomer when in liquid form.

2.3. Sectioning and Grinding. Once polymerized, the blocks are removed for their cassettes/molds and are sectioned by means of a surgical saw. Cutting systems are provided with diamond saw blades that can grind both fresh and embedded samples very precisely, with continuous water cooling, provided by a closed recirculation system, to avoid thermal changes that can get artifacts or friction burns. Allowing a perfect MMA "solidification" is mandatory for the successful execution of the subsequent steps; if MMA is still soft, cutting results are virtually impossible to be carried out with precision and the result in the dulling of the block surface, expected to be clear and diaphanous, can occur after contact with water. To reduce the cutting times and preserve the integrity of samples, the gripping system can oscillate and tool direction can be reverted, and a feed rate mechanism is present to adjust the cutting speed. These options are particularly useful in the presence of very hard implant like metallic materials, for which the slowing of the cutting speed and the oscillation of the sample facilitate the cutting phase, which is more difficult due to the hardness of the sample and the friction that is generated in contact with the blade. Sections obtained after cutting can usually have a thickness of $100 \pm 10\,\mu$m, which can be measured with a metric gauge for measuring thickness, subtracting the thickness of the histological slide. The obtained section must be pasted to plastic microscope slides of appropriate dimension with an adequate cyanoacrylate adhesive, with particular attention to avoid the formation of bubbles and to allow a perfect adhesion of sample to the slide in order to obtain a flat surface. This will make the subsequent steps of grinding and polishing easier and also have a clear field for the microscope observation, as well as achieving a better quality of histological preparation. Once adhesion is completed, after about 60 minutes, sections are thinned with an abrasion system using abrasive papers with different granulation, from 300 to 4000 grit (from more to less abrasive surface), in steps of about 15 minutes each, up to a thickness of $25 \pm 10\,\mu$m. This step is particularly challenging because excessive abrasion can cause the loosening of all or part of the sample, especially if the surface of the sample obtained after cutting is not completely equal or in the presence of metallic materials, which thin out more slowly than the surrounding bone. In addition, this procedure can cause the formation of lines on the surface of embedded samples, especially when the most abrasive papers are used for the thicker samples that have very hard implants. The sample surface is therefore smoothed by a polishing system using velvety cloths, sometimes in combination with diamond paste or alumina solution, indicated for surfaces difficult to polish and exposed to ceramic and ferrite materials [5–7].

2.4. Staining. In general, staining methods for plastic-embedded tissue require modifications because these procedures are usually performed without the removal of the plastic, and thus different timing regimes are utilized. However, different staining protocols can be chosen for MMA-embedded bone and the choice can be influenced by the kind of evaluations to be performed. Staining procedures that are commonly used in our laboratory reflect the attempt to primary evaluate material osseointegration or osteoinduction. Both Von Kossa and Alizarin Red staining are usually preferred for the detection of calcium deposits. Goldner's trichrome, using also hematoxylin, can better identify cellular components and distinguish newly formed bone matrix (in red) from mature ones (in green) and calcified cartilage. Van Gieson staining allows us to detect the nuclei, colored in black, and to differentiate between osteoid and collagen (red) and bone and muscle in green and can be successfully applied for the evaluation of bone-implant interface, and Stevenel's blue staining allows us to assess the presence of fibrous tissue. Perhaps one of the most utilized stains remains Safranin O/Fast green, which allows us to stain cartilage in red and bone in green. The combination of Fast Green with Toluidine Blue allows us to detect nuclei in dark blue and to distinguish old bone from newly formed bone thanks to Fast Green intensity. In fact, the staining allows appreciating a chromatic difference between the preexistent bone, whose green coloration is milder, and the newly formed bone, which is more brilliant. Such a chromatic difference is well represented in Figure 1(a), in which the bone growth around and in contact with the metallic implant is stained more intensely than the preexisting bone.

3. Results

3.1. Histological Findings of Bone-Implanted Medical Devices. The quality of the final histological slide depends on the correct performance of all the procedures described above. Histological evaluation and characterization of bone-implanted medical devices are normally done with light microscopy. However, it is also possible to use a digital pathology slide scanner, a rapid and high-resolution scanner able to convert pathology glass slides into digital slides in few minutes, obtaining in a single acquisition an image that can be observed at different real optical magnifications. Being a digital technique with very stringent acquisition parameters, only partially modifiable by the operator, the recognition and correct focusing and acquisition of the sample are functions of the quality of the histological preparation, specifically in terms of slice thickness and effective staining.

The biological response parameters that can be assessed, also following the ISO 10993-6:2016-*Biological Evaluation of Medical Devices-Part 6*: *Tests for Local Effects after Implantation*, are numerous. The most used are changes in tissue morphology, presence of fibrosis and inflammatory

Figure 1: (a) Sheep tibial diaphysis six months after a roughened titanium alloy implantation. Toluidine Blue and Fast Green stain: in black, the material; in light green, the preexisting bone; in dark green, the newly formed bone. Left: magnification 1x; right: magnification 30x. (b) Sheep tibial diaphysis three months after a sandblasted titanium implantation. Stevenel's blue and picrofuchsin stain: in black, the material; in fuchsia, the bone; in blue, the cells. Left: magnification 1x; right: magnification 30x. (c) Sheep iliac crest three months after a titanium screw implantation. Toluidine Blue and Fast Green stain: in black, the material; in light green, the preexisting bone; in dark green, the newly formed bone. Left: magnification 10x; right: magnification 30x. M: material; NB: new bone; Pr.B: preexisting bone; Ot: osteocytes; Oc: osteoclasts; OS: osteoid tissue.

cells, presence of necrosis, vascularization, fatty infiltration, foreign body reaction, mineralization, bone formation, maturation and density, materials fragmentation, bone quality, and bone ingrowth. In addition, the interface between the tissue and the materials is of critical interest. In fact, it is fundamental to evaluate the area of bone contact near the implant (osseointegration), as well as the presence of intervening noncalcified tissues. Obviously, the presence of bone resorption or new bone formation should be also recorded. Some examples of histological evaluation of bone-implanted medical devices are reported below.

Figures 1(a) and 1(b) show the histological images of a roughened titanium alloy (Figure 1(a)) and of a sandblasted titanium implant (Figure 1(b)) implanted in a sheep tibial diaphysis. Microscopic analyses, at three and six months after implantation, showed that the gap between the preexisting cortical bone and the implant is filled with newly formed lamellar bone and direct bone-to-implant contact is observed for both implants. However, in the same area of Figure 1(b), when observed at higher magnification, the newly formed bone appeared separated from the implant by a thin layer of connective tissue. Osseointegration *per se* is not linked to any particular surface characteristics, because a great number of different surfaces achieve clinical osseointegration. However, stronger or weaker bone responses may be related to the surface characteristics. Nevertheless, it is important to emphasize that higher magnification images allowed us to detect no infection signs (polymorphonuclear cells, lymphocytes, macrophages, and multinucleated cells), no implant malposition, or implant loosening (Figure 1(b)). Another example is shown in Figure 1(c) that reports a histological image of a titanium screw implanted in a sheep femoral condyle. Histological analysis three months after implantation showed complete and good osseointegration of the implant and presence of newly formed trabecular bone and active osteoid tissue

(noncalcified tissues) strictly associated with the implant surface. The new bone consisted primarily of woven bone, with the greatest density in the area closer to the native bone. The woven bone is often considered as a primitive type of bone tissue and characterized by random, felt-like orientation of its collagen fibrils, numerous, irregularly shaped osteocytes, and, at the beginning, a relatively low mineral density [8–10]. Another example is shown in Figure 2 where an entire sheep vertebra was histologically evaluated in order to assess the influence of the insertion procedure of two electrodes on bone tissue viability. At higher magnification, it is possible to see the presence of newly formed bone in the whole trabecular bone around the electrodes, thus highlighting that the insertion procedure does not influence bone tissue viability. In fact, preexisting trabeculae among the electrodes were covered by osteoblasts (OBs) with evident evenly spread osteocytes [11]. A hydroxyapatite-coated titanium implant (Figure 3) was implanted in a rabbit femoral condyle. The hydroxyapatite-coated titanium implant showed an excellent integration of the implant with newly formed trabecular bone covered by OBs and osteoid tissue (Figure 3).

Another excellent example of MMA use is reported in Figure 4, a biological failure of a human femoral neck hydroxyapatite-coated titanium screw. Histological analysis of periprosthetic tissue reactions, including necrosis, lymphocyte infiltration, histiocytosis, and intracytoplasmic metallic debris, was carried out. In addition, the evaluation of the area of bone contact near the implant and the presence of intervening noncalcified tissues and the presence of bone resorption or new bone formation were also recorded. The histological evaluations of these kinds of devices allowed us to better understand the characteristics of bone quality and its microarchitecture even after their implantation. These aspects are of significant importance in the development and improvement of future medical devices.

3.2. Histomorphometric Findings of Bone-Implanted Medical Devices. For the evaluation of bone-implanted medical devices, quantitative histomorphometry must be used in addition to the qualitative histological analysis that can suffer from operator-related bias and does not provide statistically assessable numerical data. Histomorphometry is defined as a methodology for quantitatively analyzing measurable histological parameters (as length, distance, area, number of components of interest, etc.). The first attempt to uniform the nomenclature related to bone histomorphometry dates back to the 1980s, when the first report on this topic was published, to provide standardization and to make comparable results from different studies [12]. Updated standard nomenclature, symbols, and units for bone histomorphometry can be found in the review of Dempster et al. who in 2013 published an update of the Report of the American Society for Bone and Mineral Research (ASBMR) Histomorphometry Nomenclature Committee [13]. In the histomorphometric analysis of bone-implanted medical devices, the useful parameters mostly used are reported in Table 1. The choice of the histomorphometric parameters to be measured is based on the biological and mechanical characteristics of materials implanted in bone and addresses the need to highlight if the purpose for which it has been tested, usually the evaluation of osseointegration degree and osteoconductive/inductive properties, has been reached. As for histological evaluation, the first step in approaching bone histomorphometry for bone-implanted medical devices is the definition of a region of interest (ROI), performing the measures, usually comprising implant site and/or peri-implant bone, and defining a fixed distance from the defect created for the insertion of the material. An example of the identification of the frame of measure is reported in Figure 5(a), representing a hydroxyapatite-coated titanium screw implanted in sheep vertebral pedicle [8–10]. The red frame indicates the ROI within which measures are performed and includes the implant and the peri-implant bone. Sometimes, different ROIs can be taken into account, to perform measures progressively moving away from the implant, as reported in Figure 5(b), in which concentric circles have been depicted around a circular titanium implant, defining the same number of ROI to quantify the bone growth around the material in the iliac crest of a sheep model [8–10]. Once the ROI is defined, it is fixed for all the replicates measured, discarding any samples in which the implant is not in place or that have not been cut according to the correct cutting plane, in order to minimize bias in the measurements. The quantification of area and lengths of bone and materials is at the base of many other complex evaluations to assess key properties of investigated materials. The performance of such measures requires the use of sophisticated image analysis software and specific tools, based on binary image processing, which allow automatic and semiautomatic quantifications. In the correct application of these tools, the efficacy of histological staining is to be mandatory, considering that, as shown in Figure 2(b), different features of the bone can be highlighted by brighter or milder staining, which in turn can be distinguished and quantified by the binarization process. Figure 6 shows an example of image binarization in which the implant is colored in red and the bone in green. The software is able to measure automatically the binarized surfaces, by distinguishing the different colors, quantifying both the area and perimeter. These quantifications can be made either on the entire defined ROI or in specific points of the sample, as in the case of the measure of bone ingrowth, performed on the surface between the two coils of a screw and the line that connects the top of the coils. In Figure 5(c), bone ingrowth measure and the related mirror area, in which bone growth is calculated in the space between the turns of a screw and in the exact specular area, are represented, allowing the estimate of osteoinductive/osteoconductive properties of a metallic implant. On the basis of binarization measures, the Affinity Index or Bone-to-Implant Contact (BIC) can be calculated. This is a classical parameter to assess the degree of osseointegration of an implant, measuring all the points of contact between the material and the bone, as shown in Figure 7, in which the surfaces of contact, manually marked, of a titanium implant in sheep tibial epiphyses are evidenced in orange [8–10]. The

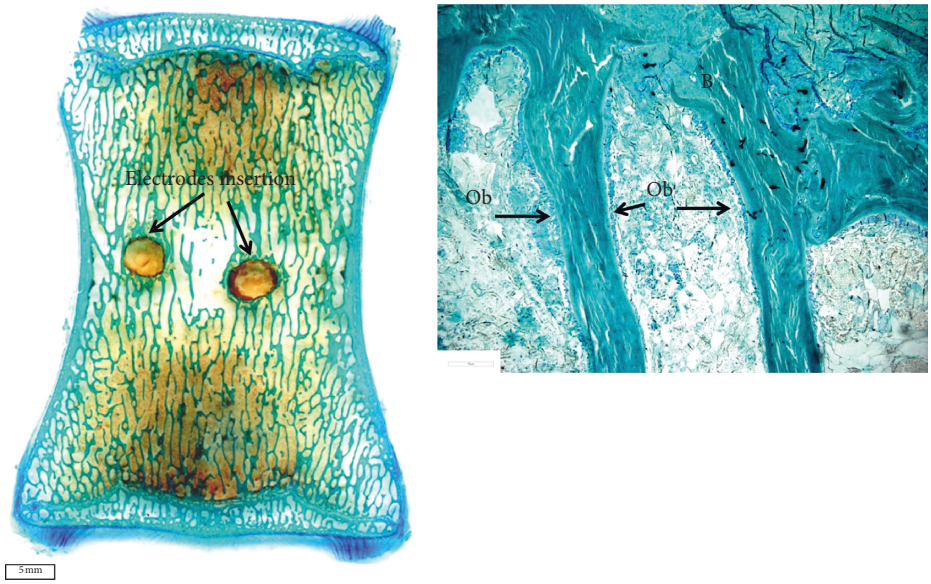

(a) (b)

Figure 2: Sheep vertebra. Toluidine Blue and Fast Green stain. Ob: osteoblasts. (a) Magnification 1x; (b) magnification 30x.

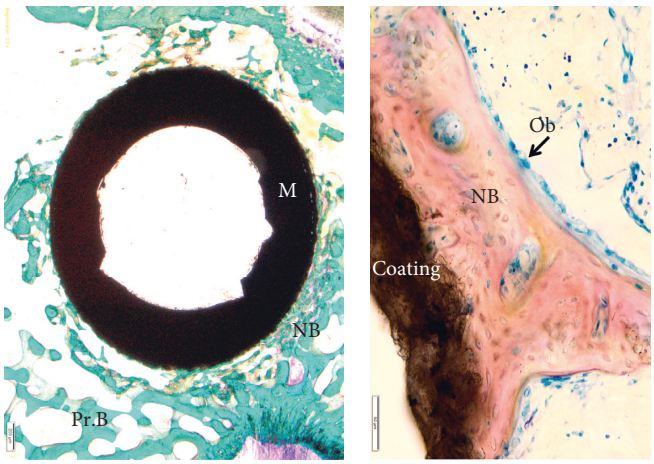

(a) (b)

Figure 3: Hydroxyapatite-coated titanium implant in a rabbit femoral condyle. (a) Toluidine Blue and Fast Green stain: in black, the material; in green, the bone. Magnification 10x. (b) Stevenel's blue and picrofuchsin stain: in black, the material; in fuchsia, the bone; in blue, the cells. Magnification 40x. M: material; NB: new bone; Pr.B: preexisting bone; Ob: osteoblasts.

analysis software is able to calculate and sum the lengths of each line. One of the major difficulties of many of these evaluations is that manually performed adjustments (for example, after binarization to avoid errors related to a specificity) or measures (as for BIC marks) are necessary, requiring well-trained operators to perform such measures which must be in any case conducted in a double-blind manner.

High-temperature MMA embedding also allows the histomorphometric evaluation of bone dynamics through the visualization of fluorescent markers. In our laboratory, we employ different fluorochromes types (tetracyclines, xylenol orange, calcein blue, alizarin red) that are administered *in vivo* at scheduled experimental times and are incorporated into the bone matrix during the new bone formation process. Figure 8 is representative of the acquisition in fluorescence of an area of rat femur after the administration of different fluorochromes over time. Bone trabeculae appear labeled progressively in different colors, marking the different steps of bone remodeling. Microscopic observation at appropriate wavelengths for fluorescence emission allows the evaluation of the mineralization status and the time intervals between remodeling processes [14]. Usually, in the presence of an implant, the evaluated ROI is at the interface between the bone and the implant to assess whether the presence of materials has stimulated bone regeneration. Tetracyclines are surely the most used fluorochrome for dynamic evaluation. Its incorporation at the

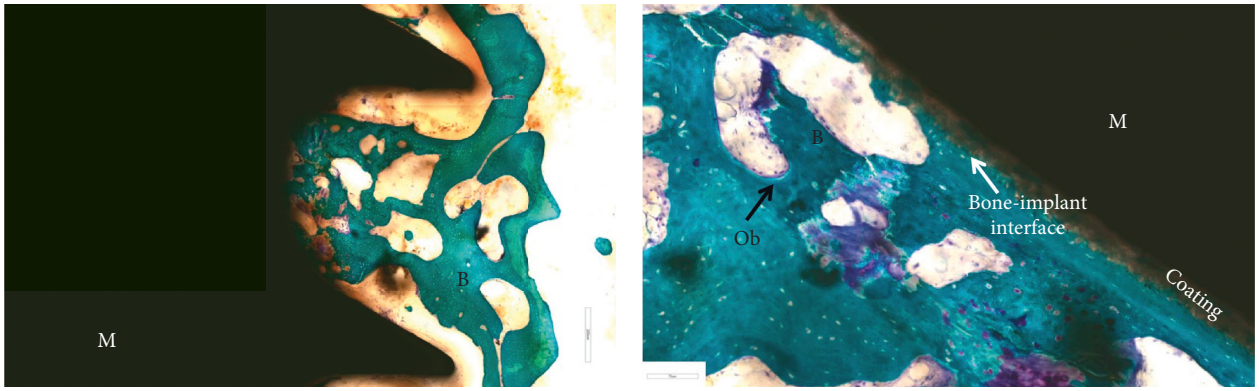

(a) (b)

Figure 4: Human femoral neck hydroxyapatite-coated titanium screw. Toluidine Blue and Fast Green stain: in green, the bone; in black, the screw; in blue, the cells. M: material; B: bone; Ob: osteoblasts. (a) Magnification 1x. (b) Magnification 10x and 30x.

Table 1: Static and dynamic histomorphometric parameters most frequently adopted for the evaluation of bone-implanted medical device.

Material total area	mm^2	Biomaterial total area
Material total perimeter	mm	Biomaterial total perimeter
Bone area (B.Ar)	mm^2	Measurement of the amount of trabecular bone
Total area (T.Ar)	mm^2	Measurement of the total amount of bone observed
Bone volume/Tissue volume (BV/TV)	%	Measure the percentage of spongy bone including the mineralized bone and the osteoid
Bone perimeter (B.Pm)	mm	Length of the observed bone surface
Bone surface/tissue volume (BS/TV)	mm^2/mm^3	Measure the percentage of spongy bone surface
Trabecular thickness (Tb.Th)	μm	Thickness of trabeculae derived from the Parfitt formula
Trabecular number (Tb.N)	mm^{-1}	Number of trabeculae per surface unit
Trabecular separation (Tb.Sp)	μm	Measure of the distance between the bone trabeculae
Affinity index or bone-to-implant contact (BIC)	%	Length of the areas of direct osseointegration without fibrous capsule interposition
Bone ingrowth	mm^2	Bone area between the screw and the line that connects the top of the coils/the total area below the top of the coils
Mirror area	mm^2	Specular image to bone ingrowth
Cortical thickness (Ct.Th)	μm	Cortical thickness
Mineral apposition rate (MAR)	μm/day	Average velocity at which individual osteoid lines are mineralized
BFR/BS	$\mu m^3/\mu m^2$/day	Amount of mineralized bone formed per unit of trabecular bone surface per day

interface of bone and osteoid is seen at a fluorescence microscope as a green line, which becomes double if more than one administration is performed. In Figure 9, alizarin red labeling of rat femoral bone is represented in red color. In the images, the double labeling of bone trabeculae is well evidenced. The length of fluorescent lines and the distance between each other are measurable parameters which can be used to evaluate bone turnover [11, 15].

MAR (Mineral Apposition Rate) is the rate at which OBs are making a matrix, which calcifies at a constant rate and incorporates the labels. Thus, it measures the average activity of the OBs in the section. BFR (Bone Formation Rate) takes into account how much of the bone surface is actively mineralizing, which depends on the number of active OBs. It multiplies the average work of each OB by the fraction of bone surface with active OBs. Both of these parameters require manually performed measures of fluorescent bands. In particular, the measure of the distance between the two bands of the same trabecula (red lines), whose average value is combined with the number of days elapsed between the two administrations, the length of the fluorescent bands (yellows lines), and the perimeter of the entire trabecula are shown in Figure 10.

3.3. Biomechanical Findings. Biomechanical tests are a fundamental tool in assessing the outcome of biomaterials/device implanted in the bone. Among the evaluation of the osteointegrative process in terms of the new bone formation and bone-to-implant contact, the evaluation of the mechanical competence provides information about the status of the newly formed bone and its ability to support the load. As the final goal is to obtain the formation of bone tissue as similar as possible to the healthy native one, it is clear that mechanical tests are an indispensable evaluation of tissue regeneration. Many of these tests are destructive and need to be performed on fresh or frozen tissue, avoiding the possibility of using the same samples for histological analysis,

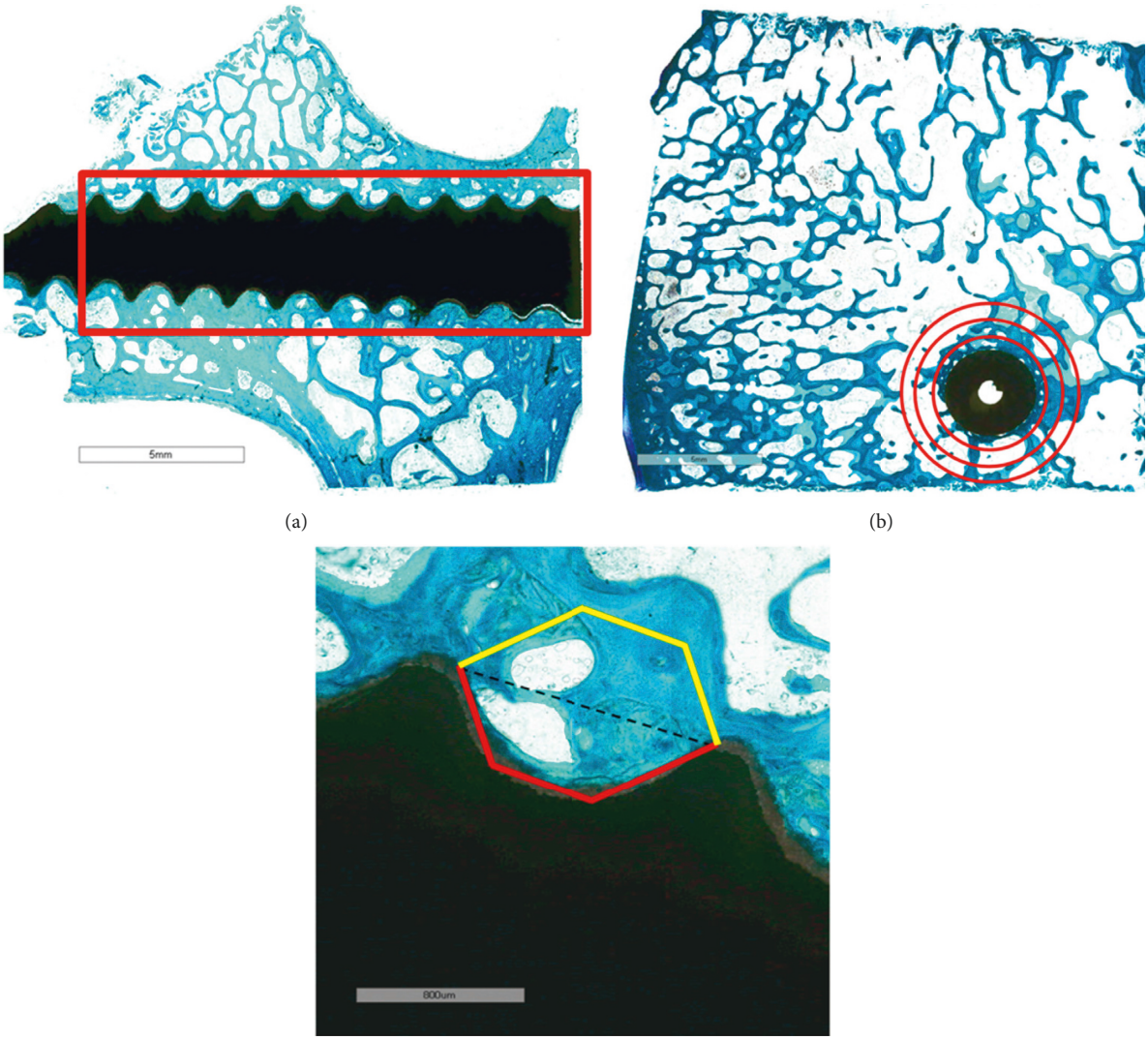

Figure 5: (a) Hydroxyapatite-coated titanium screw in sheep vertebral pedicle. The red rectangle indicates the region of interest for histomorphometric measures; Toluidine Blue/Fast Green staining; magnification 1x. (b) Cylindrical titanium implant in sagittal section in sheep iliac crest. The red circles identify regions of interest for histomorphometric measures; Toluidine Blue/Fast Green staining; magnification 1x. (c) Histomorphometrical measure of bone ingrowth and mirror area of hydroxyapatite-coated titanium screw implanted in sheep vertebral pedicle. In red, the ROI for the assessment of bone ingrowth between the two turns of the screw; in yellow, the ROI for the assessment of the mirror area; Toluidine Blue/Fast Green staining; magnification 10x.

requiring de facto the use of a huge number of animals. PMMA embedding allows us to perform on the same samples both histology and some mechanical tests, as microhardness and nanoindentation, taking into account, in the final evaluation, that the resin embedding increases microhardness by 30 to 40% [16]. For both techniques, a procedure similar to those applied in the preparation of histological slides is followed, taking care in particular of the polishing step, which needs to be particularly accurate to avoid the presence of surface scratches which can affect the test. Microhardness test is a method for measuring the hardness of a material on a microscopic scale. It is used to provide necessary data when measuring individual microstructures within a larger matrix, or testing very thin foil-like materials, or when determining the hardness gradient of a specimen along a cross section. Samples must fit in the sample stage and be perpendicular to the indenter tip. The microhardness tester needs to be isolated from vibrations. Microhardness analysis, based on the measure of the resistance of the bone to the penetration of a small diamond pyramid, yielded an accurate and reproducible measure of the mineralization degree. The degree of mineralization of bone (DMB) not only influences the mechanical resistance of bone [17] but also partly determines the bone mineral density [18]. Compared to the microhardness test, the nanoindentation test involves smaller loads and thus allows us to investigate a smaller portion of the bone tissue, down to the size of single trabeculae. Typical mechanical parameters

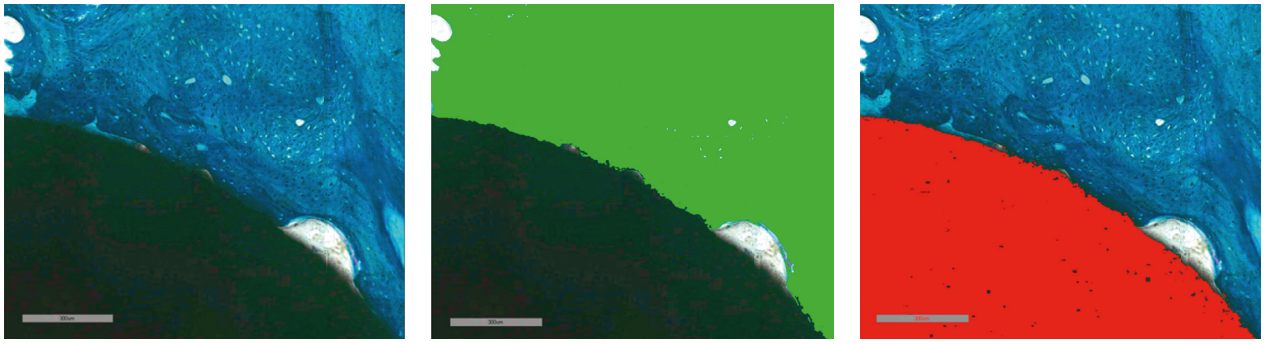

(a) (b) (c)

Figure 6: Image binarization of titanium cylindrical implant in sheep iliac crest. In sequence, (a) histological image of interface bone-implanted stained with Toluidine Blue/Fast Green; (b) binarization of bone tissue in green; (c) binarization of implant in red (magnification 20x).

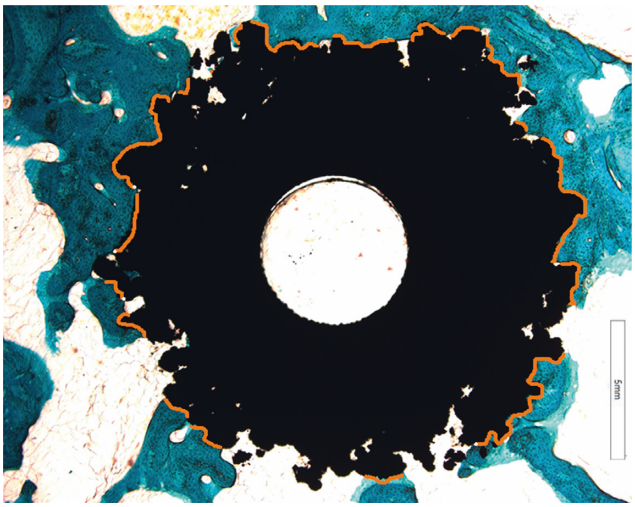

Figure 7: Evaluation of affinity index of a cylindrical titanium implant in sheep tibial epiphyses. The orange lines indicate the point of contact between the bone and the implanted material; Toluidine Blue/Fast Green staining; magnification 1x.

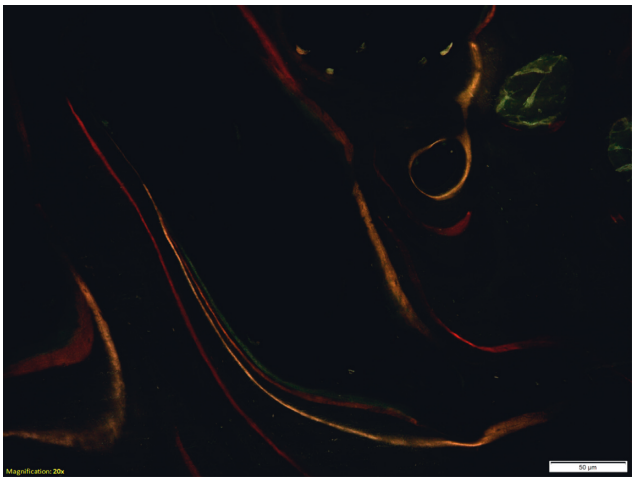

Figure 8: Fluorescence image of rat femur after overtime fluorochrome injections. Along with the profile of bone trabeculae, tetracyclines, xylenol orange, calcein blue, and alizarin red labeling are appreciable (magnification 20x).

obtained from nanoindentation tests are the reduced elastic modulus (E_R) and the indentation contact hardness (H_{IT}). Noteworthy, elastic modulus and hardness have been found to be well correlated to the degree of mineralization of the tissue [19–21].

4. Discussion

The growth of the medical device industry provides numerous novel medical devices, surfaces, biomaterials, scaffolds, and technologies to be used for orthopedic applications. The awareness of the regulatory environment and the need for testing safety, feasibility, and efficacy before clinical use is fundamental to manage the biological assessment of these materials. In this contest, the preclinical evaluation is mandatory and requires a further basic understanding of materials science and bioengineering to facilitate the interpretation of complex interface reactions between biomaterials, cellular and secretory factors, and tissue responses that modulate success or failure of medical devices. Thus, the histological assessment is the irreplaceable requisite for the evaluation of the safety and efficacy of bone-implanted medical devices.

Since the birth of histology and the setup of the techniques for the conservation, processing, and visualization of tissues, the main goal of the discipline has been to find the best way to analyze biological samples, preserving, as best possible, their structure without losing at the same time the possibility of evaluating the characteristics like protein antigenicity, mechanical properties, etc. This attempt has always been particularly complex for the bone tissue, because of its peculiar mineralized structure, which gives unique characteristics of hardness. The increasingly widespread use of biomaterials in orthopedics as the implementation of surgery for traumatic, degenerative, inflammatory, and oncologic diseases has increased the complexity of histological processing, requiring the adoption of embedding methods suitable for cutting without removing the implant, yet it is still able to allow the

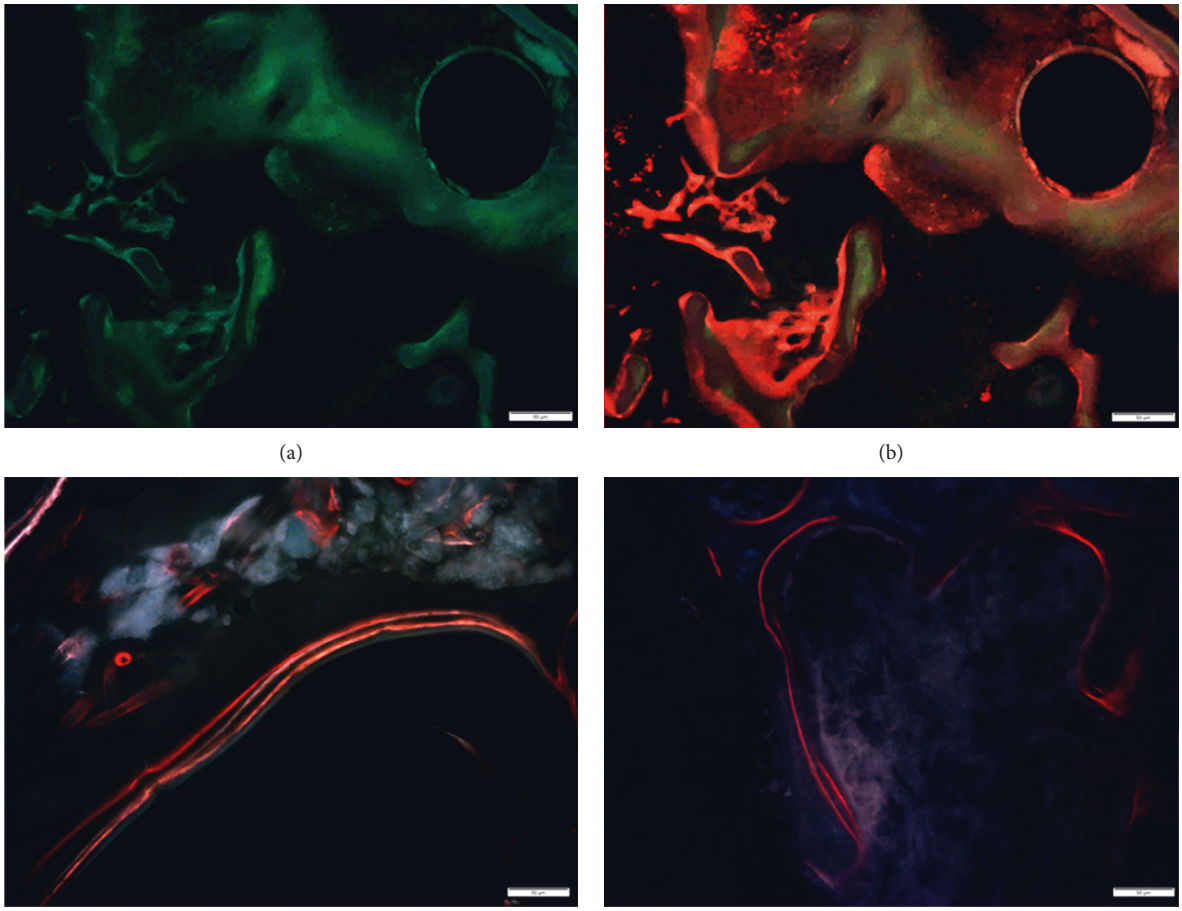

(a) (b) (c) (d)

Figure 9: Fluorescence image of alizarin red labeling of rat femur at the interface with implanted material. The double labeling of bone trabeculae is well appreciable (magnification 20x).

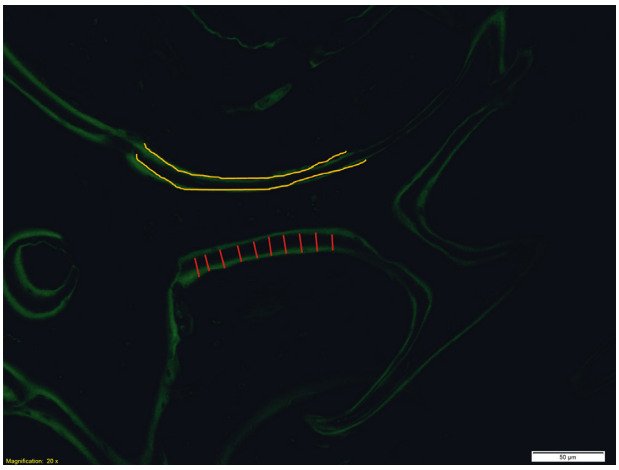

Figure 10: Fluorescence image of tetracycline labeling in sheep tibia, representative of histomorphometrical measure for MAR and BFR assessment. The red lines indicate the measure of the distance between the two bands of the same trabecula, while the yellow lines indicate the length of the fluorescent bands (magnification 20x).

biological study of the tissue. Histological processing offers a wide variety of options in terms of embedding techniques, allowing choosing the most suitable in the relationship of the tissue analyzed and the outcome to assess.

Paraffin embedding remains the most popular technique for histological evaluation, for its relative ease and speed of execution, requiring a very limited number of items of equipment. However, bone tissues need to be treated with decalcifying solutions to eliminate the mineralized component of the tissue and allow the cutting phase. This procedure is very thorny, as the exact evaluation of the degree of decalcification achieved by the sample is the discriminating factor between obtaining a sample that can be evaluated or not. An excessive decalcification would lead to the destruction of the bone architecture while a too soft decalcification would leave the sample hard, causing the formation of artifacts in the cutting phase. The small dimensions of embedding mold, which are in accordance with the dimensions of cutting microtome, limit the application of this technique to very small samples or to part of them (e.g., biopsies). The only way to evaluate the response of the

bone tissue to a material is to mechanically remove the implant and perform the histological and histomorphometrical evaluations taking into account the shadow left by the removed implant [22, 23]. However, this procedure can be feasible only with bulk materials. In fact, porous materials or materials with specific designs, aimed at allowing the bone ingrowth, cannot be removed without damaging the samples and irreparably compromising the evaluation.

Among the various embedding methods available for biological samples, the high-temperature MMA-based technique remains the only one able to address the need for embedding undecalcified samples of big dimensions without removing implanted biomaterial and allowing a satisfying biological evaluation of the tissue. Although this method requires rather long processing times and expensive and not easy to use the equipment for sample preparation, it is still preferable to other embedding solutions that are limited to very small samples and can require the removal of the implant. Among the various resins available, low-temperature MMA is probably the one with the most similar characteristics to the high-temperature MMA, with the advantage of obtaining thinner sections. However, this inclusion technique shares with high-temperature MMA the need for specific equipment and long processing times, but unlike high-temperature MMA, embedding molds allow the processing only of very small samples. Therefore, with the same equipment and procedures, the inclusion in high-temperature MMA allows working on any type of samples, in terms of both the size and type of implants. Although MMA-embedded sections can undergo a variety of histological and histomorphometric evaluations, immunohistochemical analyses still remain a challenge [24]. In fact, though, unlike other resins like GMA, MMA can be deplasticized to perform immunohistochemical analyses [25], the consensus is that the high temperatures reached during MMA polymerization, inducing the formation of reactive radicals, modify the chemical structure of tissues and simultaneously lead to irreversible loss of protein antigenicity. As a way to overcome this pitfall, low-temperature polymerization (+4° to −30°C) using blue or UV light photons as initiators can be used to preserve enzyme activity and protein antigenicity. However, this procedure is obviously highly unsuitable when samples have been *in vivo* labeled with fluorochromes for histomorphometric evaluations in fluorescence. It is well known that the observation of fluorescent histological samples must be conducted with the minimum light exposure and for a short time in order to avoid the decay of the fluorescence emission itself. It is therefore intuitive that this type of polymerization procedure can easily invalidate fluorescence assessments, when required. This aspect proves to be particularly important considering that, despite the incredible advances of non-destructive imaging methods for samples visualization and analysis, like micro positron emission tomography (PET), single-photon emission computed tomography (SPECT), and computed tomography (CT), histomorphometrical analyses remain, to date, an irreplaceable instrument for the evaluation of structural changes of bone tissue. Nevertheless, histological specimens allow the detection and evaluation of biological phenomena as inflammatory reactions, necrosis or hemorrhage, changes in cell morphology, or presence of cellular infiltrate, which cannot be highlighted by radiographic-based imaging acquisition. In addition, considering that the elevated costs of such equipment for animals imaging (i.e., micro-CT/PET) make them not suitable for any laboratories, the use of static histomorphometry stays necessary for the visualization and the measure of the bone structure and dynamic histomorphometry remains an efficient method to evaluate changes over time of the bone in the absence of radiological monitoring. Therefore, despite some limits, the possibility provided by MMA embedding to combine a comprehensive overview of the biological sample and an accurate histological and histomorphometrical analysis makes this method still the best choice for bone-implanted medical device evaluation. Not less important, the embedding in this type of resin also allows further sophisticated evaluations, such as hardness at macro- and nanolevels analyses [26–28]. These techniques are of particular interest in orthopedics as they evaluate if the presence of a material alters the mechanical properties of the surrounding bone and assesses the hardness of a newly formed bone after the implantation of osteoinductive material, allowing an even more detailed and comprehensive assessment of bone-implanted medical devices. The literature on the use of embedded sections is quite varied and not very wide, and, in some cases, the type of embedding medium is not specified [29–31]. Excluding obviously the inclusion in paraffin, which due to the nature of the inclusion medium and the need for decalcification does not lend itself to such tests, the various hard resins available for embedding might be evaluated for the purpose. However, some technical aspects must be considered; for example, GMA is softer than MMA and less suitable for the polishing steps required before microhardness tests [32]. In other cases, the use of other resins (e.g., Epofix3 cold mounting) has required additional steps before performing mechanical tests, like gold coating [33].

Thus, despite many technological advances, microscopical analyses remain an indispensable part of biomedical materials research and part of patient care. The advantages of this technique find their greatest fulfillment in the field of orthopedic translational research, such as that carried out in institutions that conjugate clinical practice and experimental research. In these contexts, in fact, the close and continuous collaboration between clinic and research implies the availability of clinical samples coming from arthroplasty surgery or prostheses substitution for usury or biological failure or from a tumor. Among the diagnostic aspects, which is not addressed in this paper, the possibility of processing and analyzing this type of samples in full allows a thorough and, wherever possible, systematic study over time to further understand the mechanisms underlying in biological reactions to implants and to evaluate mechanical limits and performance. The information related to the osseointegration degree, the presence of adverse reactions, of what kind and to what extent, greater or lesser bone growth, and the evaluations of the quality of the bone, also in terms of mechanical competence, have a great value for identifying

the weaknesses and strengths of medical devices, evaluating them in their final application. This can help the design and development of more and more effective and lasting devices, to minimize and avoid, as much as possible, the need of removal or replacement and consequently further surgery, reducing not only the cost burden for the healthcare system but above all the discomfort for the patients.

Conflicts of Interest

The authors declare that they have no conflicts of interest.

Acknowledgments

This work was supported by grants from Rizzoli Orthopedic Institute (Ricerca Corrente).

References

[1] P. H. Long, "Medical devices in orthopedic applications," *Toxicologic Pathology*, vol. 36, no. 1, pp. 85–91, 2008.

[2] F. Matassi, L. Nistri, D. Chicon Paez, and M. Innocenti, "New biomaterials for bone regeneration," *Clinical Cases in Mineral and Bone Metabolism: The Official Journal of the Italian Society of Osteoporosis, Mineral Metabolism, and Skeletal Diseases*, vol. 8, no. 8, pp. 21–24, 2011.

[3] J. J. Streit, A. Youssef, R. M. Coale, J. E. Carpenter, and R. E. Marcus, "Orthopaedic surgeons frequently underestimate the cost of orthopaedic implants," *Clinical Orthopaedics and Related Research*, vol. 471, no. 6, pp. 1744–1749, 2013.

[4] R. G. Erben, "Embedding of bone samples in methylmethacrylate: an improved method suitable for bone histomorphometry, histochemistry, and immunohistochemistry," *Journal of Histochemistry & Cytochemistry*, vol. 45, no. 2, pp. 307–313, 1997.

[5] R. A. Mukhamadiyarov, V. V. Sevostyanova, D. K. Shishkova, A. V. Nokhrin, O. D. Sidorova, and A. G. Kutikhin, "Grinding and polishing instead of sectioning for the tissue samples with a graft: implications for light and electron microscopy," *Micron*, vol. 85, pp. 1–7, 2016.

[6] J. Scheirs, *Compositional and Failure Analysis of Polymers: A Practical Approach*, Wiley, Hoboken, NJ, USA, 2000.

[7] ASM International, *Engineered Materials Handbook Desk Edition*, ASM International, Cleveland, OH, USA, 1995.

[8] G. Giavaresi, M. Fini, R. Chiesa et al., "Osseointegration of sandblasted or anodised hydrothermally-treated titanium implants: mechanical, histomorphometric and bone hardness measurements," *The International Journal of Artificial Organs*, vol. 25, no. 8, pp. 806–813, 2002.

[9] V. Borsari, M. Fini, G. Giavaresi et al., "Sandblasted titanium osteointegration in young, aged and ovariectomized sheep," *The International Journal of Artificial Organs*, vol. 30, no. 2, pp. 163–172, 2007.

[10] V. Borsari, M. Fini, G. Giavaresi et al., "Osteointegration of titanium and hydroxyapatite rough surfaces in healthy and compromised cortical and trabecular bone: in vivo comparative study on young, aged, and estrogen-deficient sheep," *Journal of Orthopaedic Research*, vol. 25, no. 9, pp. 1250–1260, 2007.

[11] M. Tschon, F. Salamanna, M. Ronchetti et al., "Feasibility of electroporation in bone and in the surrounding clinically relevant structures: a preclinical investigation," *Technology in Cancer Research & Treatment*, vol. 15, no. 6, pp. 737–748, 2016.

[12] A. M. Parfitt, M. K. Drezner, F. H. Glorieux et al., "Bone histomorphometry: standardization of nomenclature, symbols, and units. Report of the ASBMR histomorphometry nomenclature committee," *Journal of Bone and Mineral Research*, vol. 2, no. 6, pp. 595–610, 1987.

[13] D. W. Dempster, J. E. Compston, M. K. Drezner et al., "Standardized nomenclature, symbols, and units for bone histomorphometry: a 2012 update of the report of the ASBMR Histomorphometry Nomenclature Committee," *Journal of Bone and Mineral Research*, vol. 28, no. 1, pp. 2–17, 2013.

[14] M. Morra, G. Giavaresi, M. Sartori et al., "Surface chemistry and effects on bone regeneration of a novel biomimetic synthetic bone filler," *Journal of Materials Science: Materials in Medicine*, vol. 26, no. 4, p. 159, 2015.

[15] M. Fini, M. Tschon, M. Ronchetti et al., "Ablation of bone cells by electroporation," *The Journal of Bone and Joint Surgery. British Volume*, vol. 92-B, no. 11, pp. 1614–1620, 2010.

[16] Y. H. An and R. A. Draughn, *Mechanical Testing of Bone and the Bone-Implant Interface*, CRC Press, Boca Raton, FL, USA, 1999.

[17] H. Follet, G. Boivin, C. Rumelhart, and P. J. Meunier, "The degree of mineralization is a determinant of bone strength: a study on human calcanei," *Bone*, vol. 34, no. 5, pp. 783–789, 2004.

[18] G. Y. Boivin, P. M. Chavassieux, A. C. Santora, J. Yates, and P. J. Meunier, "Alendronate increases bone strength by increasing the mean degree of mineralization of bone tissue in osteoporotic women," *Bone*, vol. 27, no. 5, pp. 687–694, 2000.

[19] P. L. Leong and E. F. Morgan, "Correlations between indentation modulus and mineral density in bone-fracture calluses," *Integrative and Comparative Biology*, vol. 49, no. 1, pp. 59–68, 2009.

[20] P. Zioupos, J. D. Currey, and A. Casinos, "Exploring the effects of hypermineralisation in bone tissue by using an extreme biological example," *Connective Tissue Research*, vol. 41, no. 3, pp. 229–248, 2000.

[21] L. Mulder, J. H. Koolstra, J. M. den Toonder, and T. M. van Eijden, "Relationship between tissue stiffness and degree of mineralization of developing trabecular bone," *Journal of Biomedical Materials Research Part A*, vol. 84A, no. 2, pp. 508–515, 2008.

[22] F. Veronesi, M. Fini, M. Sartori, A. Parrilli, L. Martini, and M. Tschon, "Pulsed electromagnetic fields and platelet rich plasma alone and combined for the treatment of wear-mediated periprosthetic osteolysis: an in vivo study," *Acta Biomaterialia*, vol. 77, pp. 106–115, 2018.

[23] C. Médard, C. Ribaux, and C. Chavrier, "A histological investigation on early tissue response to titanium implants in a rat intramedullary model," *Journal of Oral Implantology*, vol. 26, no. 4, pp. 238–243, 2000.

[24] N. Keklikoglu and S. Akinci, "Comparison of three different techniques for histological tooth preparation," *Folia Histochemica et Cytobiologica*, vol. 51, no. 4, pp. 286–291, 2013.

[25] S. Rousselle and J. Wicks, "Preparation of medical devices for evaluation," *Toxicologic Pathology*, vol. 36, no. 1, pp. 81–84, 2008.

[26] F. Veronesi, G. Giavaresi, M. Maglio et al., "Chondroprotective activity of N-acetyl phenylalanine glucosamine derivative on knee joint structure and inflammation in a murine model of osteoarthritis," *Osteoarthritis and Cartilage*, vol. 25, no. 4, pp. 589–599, 2017.

[27] L. Martini, G. Staffa, G. Giavaresi et al., "Long-term results following cranial hydroxyapatite prosthesis implantation in a large skull defect model," *Plastic and Reconstructive Surgery*, vol. 129, no. 4, pp. 625e–635e, 2012.

[28] M. Bianchi, M. Boi, M. Sartori et al., "Nanomechanical mapping of bone tissue regenerated by magnetic scaffolds," *Journal of Materials Science: Materials in Medicine*, vol. 26, no. 1, p. 5363, 2015.

[29] R. B. Anchieta, M. Baldassarri, F. Guastaldi et al., "Mechanical property assessment of bone healing around a titanium-zirconium alloy dental implant," *Clinical Implant Dentistry and Related Research*, vol. 16, no. 6, pp. 913–919, 2014.

[30] H.-K. Hyun and J.-W. Kim, "Thickness and microhardness of deciduous tooth enamel with known DLX3 mutation," *Archives of Oral Biology*, vol. 54, no. 9, pp. 830–834, 2009.

[31] D. Koletsi, T. Eliades, S. Zinelis, C. Bourauel, and G. Eliades, "Disease and functional loading effect on the structural conformation and mechanical properties of the mandibular condyle in a transgenic rheumatoid arthritis murine model: an experimental study," *The European Journal of Orthodontics*, vol. 38, no. 6, pp. 615–620, 2016.

[32] S. D. Rousselle, J. R. Wicks, B. C. Tabb, A. Tellez, and M. O'Brien, "Histology strategies for medical implants and interventional device studies," *Toxicologic Pathology*, vol. 47, no. 3, pp. 235–249, 2019.

[33] R. C. Murray, N. Znaor, K. E. Tanner, R. M. DeBowes, E. M. Gaughan, and A. E. Goodship, "The effect of intra-articular methylprednisolone acetate and exercise on equine carpal subchondral and cancellous bone microhardness," *Equine Veterinary Journal*, vol. 34, no. 34, pp. 306–310, 2002.

Hindawi
BioMed Research International
Volume 2019, Article ID 2076138, 8 pages
https://doi.org/10.1155/2019/2076138

Research Article

Fabrication and *In Vitro* Evaluation of 3D Printed Porous Polyetherimide Scaffolds for Bone Tissue Engineering

Xiongfeng Tang,[1] Yanguo Qin,[1] Xinyu Xu,[1] Deming Guo,[1] Wenli Ye,[2] Wenzheng Wu,[2] and Ruiyan Li[1]

[1]*Department of Orthopedics, The Second Hospital of Jilin University, Jilin University, Changchun 130041, China*
[2]*Department of Mechanical Manufacturing and Automation, School of Mechanical Science and Engineering of Jilin University, Changchun 130025, China*

Correspondence should be addressed to Yanguo Qin; qinyg@jlu.edu.cn, Wenzheng Wu; wzwu@jlu.edu.cn, and Ruiyan Li; liyandii@msn.cn

Received 27 June 2019; Revised 15 August 2019; Accepted 24 September 2019; Published 11 November 2019

Guest Editor: Elena Della Bella

For bone tissue engineering, the porous scaffold should provide a biocompatible environment for cell adhesion, proliferation, and differentiation and match the mechanical properties of native bone tissue. In this work, we fabricated porous polyetherimide (PEI) scaffolds using a three-dimensional (3D) printing system, and the pore size was set as 800 μm. The morphology of 3D PEI scaffolds was characterized by the scanning electron microscope. To investigate the mechanical properties of the 3D PEI scaffold, the compressive mechanical test was performed via an electronic universal testing system. For the *in vitro* cell experiment, bone marrow stromal cells (BMSCs) were cultured on the surface of the 3D PEI scaffold and PEI slice, and cytotoxicity, cell adhesion, and cell proliferation were detected to verify their biocompatibility. Besides, the alkaline phosphatase staining and Alizarin Red staining were performed on the BMSCs of different samples to evaluate the osteogenic differentiation. Through these studies, we found that the 3D PEI scaffold showed an interconnected porous structure, which was consistent with the design. The elastic modulus of the 3D PEI scaffold (941.33 ± 65.26 MPa) falls in the range of modulus for the native cancellous bone. Moreover, the cell proliferation and morphology on the 3D PEI scaffold were better than those on the PEI slice, which revealed that the porous scaffold has good biocompatibility and that no toxic substances were produced during the progress of high-temperature 3D printing. The osteogenic differentiation level of the 3D PEI scaffold and PEI slice was equal and ordinary. All of these results suggest the 3D printed PEI scaffold would be a potential strategy for bone tissue engineering.

1. Introduction

Bone tissue engineering is a promising approach to heal the bone defect caused by fractures, infection, or tumor [1]. A key factor in bone tissue engineering for bone regeneration is the scaffold that plays the role of a template for cell adhesion, cell proliferation, and formation of the bone-extracellular matrix to provide structural support to the newly formed bone. The scaffolds should mimic the bone structure and function in order to optimize the integration between the scaffold and the surrounding tissue [2]. A porous structure scaffold can improve the mechanical properties to match the bone tissue [3, 4] and provide a cell-friendly structure microenvironment for the growth of osteoblasts and tissues. Furthermore, the inner surface of the porous scaffold is much larger than the solid implant, which makes it possible to carry drugs and growth factors to enhance bone healing [5]. Therefore, the porous scaffold is one of the hotspots for bone tissue engineering. Although a porous scaffold could be fabricated by traditional methods, only a randomly organized porous structure can be achievable. 3D printing, a scaffold fabrication method, can fabricate suitable customized porous scaffolds for bone tissue engineering research and orthopedics surgery [6, 7]. As the development of 3D printing technologies, such as electron beam melting (EBM), selective laser sintering (SLS), fused deposition

modeling (FDM), and stereolithography (SLA), the fabrication of scaffolds with the complex 3D structure becomes relatively easy [8, 9].

Metal and polymer are the most commonly used materials for the fabrication of 3D printed bone tissue scaffolds [10]. Among the metal materials, titanium alloy is most widely used in the research and clinical application in orthopedics [2]. However, the elastic modulus of titanium alloy is about 110 GPa, which is still much higher than that of the cortical bone (about 10–30 GPa) [11, 12]. Polymer materials, especially the degradable polymers, such as polylactide (PLA), polycaprolactone (PCL), and poly(lactic-co-glycolic acid) (PLGA), are often used as implants of non-load-bearing parts for bone defect repair because of their excellent biocompatibility and low toxicity [13, 14]. Generally, the degradable polymers are much easier to prepare compared with the metal, but their weak load-bearing capacity limits their application. Special engineering plastics combine the advantages of both metal and degradable polymers. Polyetheretherketone (PEEK) and polyetherimide (PEI), as the typical representatives, have good biocompatibility and corrosion resistance, and they have similar elastic modulus to the trabecular bone compared to titanium [15, 16]. Moreover, the melting point of them is much lower than that of titanium alloys, making them relatively easy to be 3D printed.

The mechanical properties of pure PEI are close to those of pure PEEK, and strength of both of them can be enhanced to the level of the cortical bone via doping other materials, such as carbon or glass fiber [17–19]. The usable temperature of PEI is −20° to 335°F, which is lower than that of PEEK, but it does not need to work in extreme temperatures as a bone tissue scaffold. As an advantage, the cost of PEI is lower than that of PEEK, and it has similarity to the physiological structure of the bone in charge transfer [20–22]. Meanwhile, for its biocompatibility, PEI has been proved as a potential membrane production material for biohybrid organ systems and hemodialysis [23, 24]. At present, there are a large number of researches about 3D printed PEEK scaffolds in orthopedics. However, there was no study that reported on PEI biocompatible scaffolds fabricated via 3D printing. This work is the first report to investigate the possibility of 3D printed porous PEI used as a biocompatible scaffold in bone tissue engineering.

Previous studies show that pore size had significant influence on the growth of cells in the scaffolds. The scaffolds with mean pore sizes ranging from 300 μm to 1000 μm were deemed optimal for bone tissue engineering [25, 26]. In this study, we fabricated the PEI scaffold with interconnected micropores via the FDM 3D printer, and the pore size was set as 800 μm. For analysis, its feasibility as a bone tissue scaffold and the elastic modulus, cell adhesion, cytotoxicity, cell proliferation, and osteogenic differentiation of the 3D printed scaffold were evaluated, and the results suggested that 3D printed PEI is a promising candidate as a bone tissue scaffold.

2. Materials and Methods

2.1. Fabrication of Samples. The PEI rods and grains were purchased from Sigma-Aldrich in USA. A homemade 3D printer (provided by the School of Mechanical Science and Engineering of Jilin University) was used to fabricate the 3D PEI scaffolds (3D PEI). Firstly, the PEI grains were melted and extruded into filaments ($\Phi = 1.75$ mm) (SJZS-10 twin-screw extruder, Wuhan Running Company). Secondly, the filaments were dried by keeping at a constant temperature of 60°C with desiccants for 24 hours. Then, the dried PEI filaments were added into the heated nozzle 3D printer, and the temperature was kept at 365°C. According to the options of the 3D printer and slicing data of the 3D model, the PEI filament was melted and extruded into the designed shape (length ∗ width ∗ height = 20 mm ∗ 12 mm ∗ 12mm), and the thickness of each layer was 0.8 mm, which had ordered arrays and uniform mesh.

2.2. Physical Characterizations. The compressive mechanical test was performed on the 3D PEI scaffolds (20 ∗ 12 ∗ 12 mm) and PEI rods (12.7 mm ∗ 10 mm) via the electronic universal testing system (Instron 5869, USA) with 50 kN load cells and the crosshead speed set as 1 mm/min. The compressive strength, compressive modulus, and stress-strain curve were obtained from the load recorded. The structure and the surface of the 3D PEI scaffold were observed via FE-SEM (XL-30 ESEM FEG Scanning Electron Microscope, FEI Company). The samples were sputtered with Au before SEM observation.

2.3. Cell Viability and Cytotoxicity. The rabbit bone marrow stromal cells were obtained from the 28-day fetal Japanese White rabbit (College of Veterinary Medicine, Jilin University, China). All the long limb bones were dissected from the attached soft tissues, and then BMSCs were obtained through flushing the bone marrow cavities with basic culture medium according to the previous description [27], and cells between the third and the fifth passage were used in the following *in vitro* experiments. The PEI rods were cut into PEI slices with a size of Φ 12.7 mm ∗ 1.5 mm, while the 3D PEI scaffolds were cut into 10 mm ∗ 12 mm ∗ 2 mm for cell culture. All kinds of samples were ultrasonically cleaned in deionized water and sterilized with a high-pressure steamer at 120°C for 70 min. The samples were kept sterile for subsequent experiments after drying. PEI slice, 3D PEI scaffold, and titanium alloy (Ti6Al4V) groups were, respectively, soaked in a centrifuge tube with basic culture medium (Dulbecco's modified Eagle's medium (DMEM), low glucose) for 24 hours at 37°C and then supplemented with 1% penicillin-streptomycin solution and 10% fetal bovine serum to make the leaching solution for cytotoxicity. Ten samples of each group were used to prepare the leaching solution. Ten PEI samples and ten 3D PEI samples had the same weight. Cells were cultured in a 24-well plate and a 96-well plate at a density of 1×10^4 cells/ml for 24 h, and then the medium was replaced by the leaching solution. After culturing for another 24 h, the live/dead cell staining was performed on the cells in 24-well plates using LIVE/DEAD Cell Viability Assays (Invitrogen, Life Technologies, Carlsbad, CA, USA). The dyes were component A (calcein AM, 2 mM) and component B (PI solution, 1.5 mM). The

experiment was performed as described in the manual. The samples were imaged using a scanning fluorescence microscope (Olympus BX51TF, Japan). Cells in 96-well plates were cultured for another 48 h. The plate with the normal culture group and the Ti6Al4V group was set as the control. Then, the cytotoxicity was measured using Cell Counting Kit-8 (CCK-8, Dojindo, Japan) at 450 nm using a microplate reader (Varioskan Flash, Thermo Scientific).

2.4. Cell Adhesion and Morphology. In order to investigate the adhesion of BMSCs in different groups, cells were seeded in two different samples of each group at a density of 5×10^4 cells/ml. After 12 h of incubation, the samples were transferred to a new plate and smoothly washed 3 times with PBS and then fixed with 4% paraformaldehyde for 30 min at 4°C. Fixed samples were washed again with PBS for 2 min. The cell nuclei were stained with 4′,6-diamidino-2-phenylindole (DAPI, Sigma-Aldrich, USA) for 5 min and were observed by a scanning fluorescence microscope (Olympus BX51TF, Japan). In order to directly observe the morphology of the cells on the scaffold, cells were cultured on different samples at a density of 1×10^4 cells/ml for 3 days. Then, the samples with cells were rinsed 3 times with PBS for 2 min, fixed with 2.5% v/v glutaraldehyde at 4°C for 8 h, and dehydrated through an ethanol series. The samples were sputtered with Au before SEM observation (XL-30 ESEM FEG Scanning Electron Microscope, FEI Company).

2.5. Cell Proliferation Assay. For the cell proliferation assay, which is performed twice, cells were seeded on the PEI slice and 3D PEI scaffold, at a density of 1×10^4 cells/ml in 24-well plates, and three samples in each group were treated as the parallel control. The CCK-8 reagent was used to measure the number of cells after culture for 1, 4, and 7 days. A mixed solution of CCK-8 and DMEM in a ratio of 10 : 100 was added into wells and incubated at 37°C for 2 h. The number of viable cells at each time point was measured via the absorbance of optical densities (OD) at 450 nm using a microplate reader (Varioskan Flash, Thermo Scientific).

2.6. Osteogenic Differentiation. For the evaluation of the osteogenic differentiation, the BMSCs were seeded on PEI and 3D PEI samples at a density of 1×10^4 cells/ml in 24-well culture plates with DMEM. Then, the medium was replaced by the osteogenic medium (basic culture medium containing 50 mg/L ascorbic acid, 10^{-8} M dexamethasone, and 10 mM β-glycerol phosphate; Cyagen, China).

After osteogenic induction for 7 days, the BCIP/NBT Alkaline Phosphatase Color Development Kit (Beyotime, China) was employed to quantify the alkaline phosphatase (ALP) secretion by staining the samples according to the manufacturer's instructions. Images were acquired by a zoom stereo microscope (Canon, Japan). After induction for 14 days, the samples and cells were fixed with 4% paraformaldehyde for 20 min at 4°C. Fixed samples were washed twice with PBS for 3 min, and the Alizarin Red kit was added into the well with samples. After the samples were stained with the Alizarin Red kit for 40 min in dark, the samples were washed again with PBS, and the images were observed via a zoom stereo microscope (Canon, Japan).

2.7. Statistical Analysis. Three to five samples per group per time point were used in different experiments, while 10 samples of each group were used to prepare the leaching solution. The results are presented as mean ± standard deviation (SD) for each group. Statistical differences were analyzed using an analysis of *t*-test in this study. The P value <0.05 was considered significant.

3. Results and Discussion

Figure 1 shows the design diagram (Figure 1(a)), top view (Figure 1(b)) and cross-sectional view (Figure 1(c)) photos, and SEM images (Figures 1(d) and 1(e)) for the 3D PEI scaffold. It can be seen that the sample presented a regular layer-by-layer structure with interconnected micropores, which is consistent with the design diagram. As shown in the low-magnification SEM image (Figure 1(d)), the PEI filaments were cross-stacked and formed a microporous structure. As shown in the high-magnification image (Figure 1)(e), the surface of the filament is smooth with few small pits, which may be caused by the breakdown of tiny bubbles generated during high-temperature printing. This result suggests that polyetherimide can be well fabricated into the porous scaffold via fused deposition modeling. It is well known that the microporous tissue engineering scaffold facilitates the transport of water, nutrients, and oxygen, and it also gives much more space for tissue growth into the scaffold [28–30]. In this work, the pore size was set as about 800 μm, which is in the range of the optimal pore size for porous implants [26].

Figure 2 shows the stress-strain curve for PEI and 3D PEI groups. The maximum stress of PEI was 161.0 ± 1.0 MPa, and the elastic modulus of the 3D PEI scaffold was 941.33 ± 65.26 MPa, which was lower than that of PEI (2106.67 ± 51.32 MPa). The range of elastic modulus for the cancellous bone is about 50–3000 MPa [31–33], and therefore, the mechanical behavior of the 3D PEI scaffold meets the requirement of the implant for filling cancellous bone defects.

As a bone tissue scaffold, biocompatibility is the initial requirement. Hence, the staining of nuclei, live/dead cell staining, cytotoxicity test, cell morphology, and cell proliferation were performed, and the results are shown in Figure 3. Figure 3(a) shows that lots of cells adhered on the 2D surface of the PEI group, while Figure 3(b) clearly displays the cell adhesion on the struts and corners of the porous 3D PEI. In Figure 3(c), live cells are stained green and dead cells are stained red, in which both 3D PEI scaffold and PEI slice groups show mainly living cells and rarely dead cells. Figure 3(d) shows the result of the cytotoxicity test, in which the number of cells in the 5% DMSO group is significantly lower than that in the other four groups, and there are statistical differences. There is no statistical difference between PEI, 3D PEI, and Ti6Al4V groups and plate group,

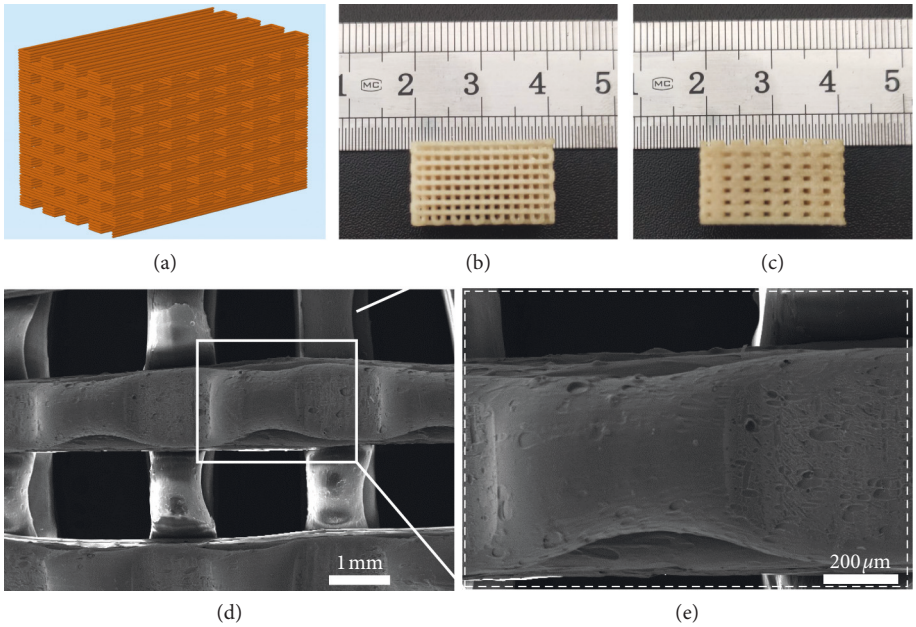

Figure 1: Visualization of the 3D PEI scaffold: design diagram (a); top view (b) and cross-sectional view (c) photos of the 3D PEI scaffold; SEM images of the structure and surface of the scaffold (d, e).

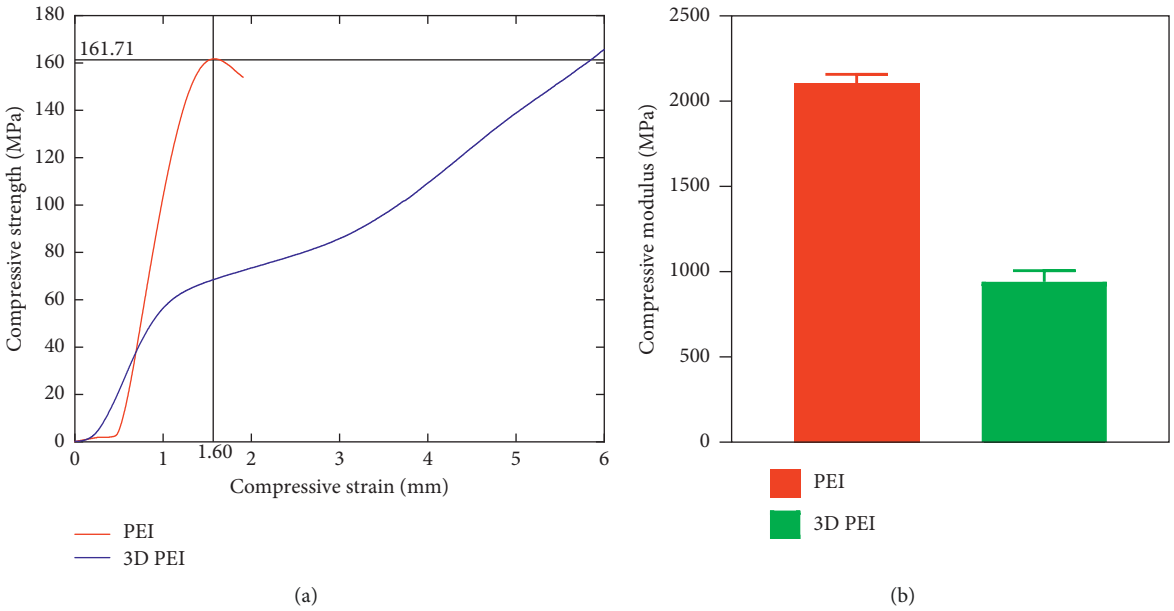

Figure 2: Stress-strain curves (a) and compressive modulus (b) of the 3D PEI scaffold and PEI slice.

whereas the performances of PEI and 3D PEI are better than that of Ti6Al4V. The result of 3D PEI is comparable to that of plate group in this cytotoxicity test, which means that they are basically nontoxic. Figure 3(e) shows the false-color SEM images of cells on the surface of PEI and 3D PEI scaffolds. Cells in the 3D PEI group show more filopodia compared with those in the PEI group. In order to analyze the effect of the 3D PEI scaffold on cell proliferation, the number of cells at 1, 4, and 7 days was detected via the CCK-8 kit. As shown in Figure 3(f), cells in both PEI group and 3D PEI group showed an increasing trend, while the number of cells in the 3D PEI group was higher than that in the PEI group at all three time points, and the difference was statistically significant after culture for 4 days. These results suggest that both PEI and 3D PEI scaffolds have good biocompatibility and that no toxic substances were produced during high-temperature 3D printing. Good cell adhesion is a prerequisite for cell proliferation and migration. The staining of nuclei and the SEM images of cell morphology demonstrate that porous 3D PEI provided a good environment conducive to cell adhesion [34]. Furthermore, the proliferation curve indicates that the 3D PEI scaffold is more

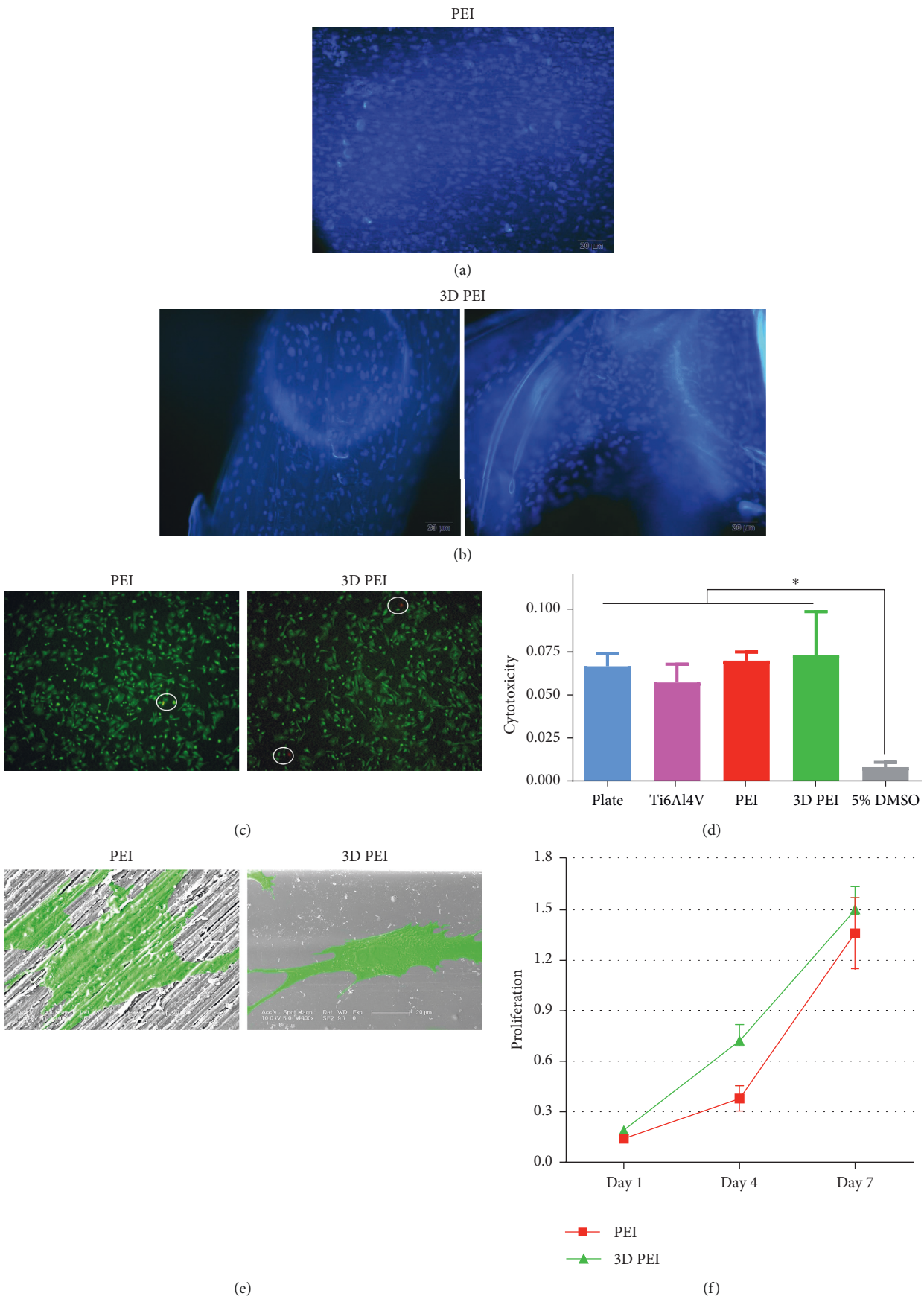

Figure 3: Results of biocompatibility analysis for the 3D PEI scaffold and PEI slice. (a, b) Fluorescence images of nuclei of different samples. Scale: 200 μm. (c) Live/dead cell staining. Scale: 100 μm. (d) Cytotoxicity test. (e) SEM images of cell morphology. Scale: 20 μm. (f) Cell proliferation. *Statistically significant at $p < 0.05$ vs. the control.

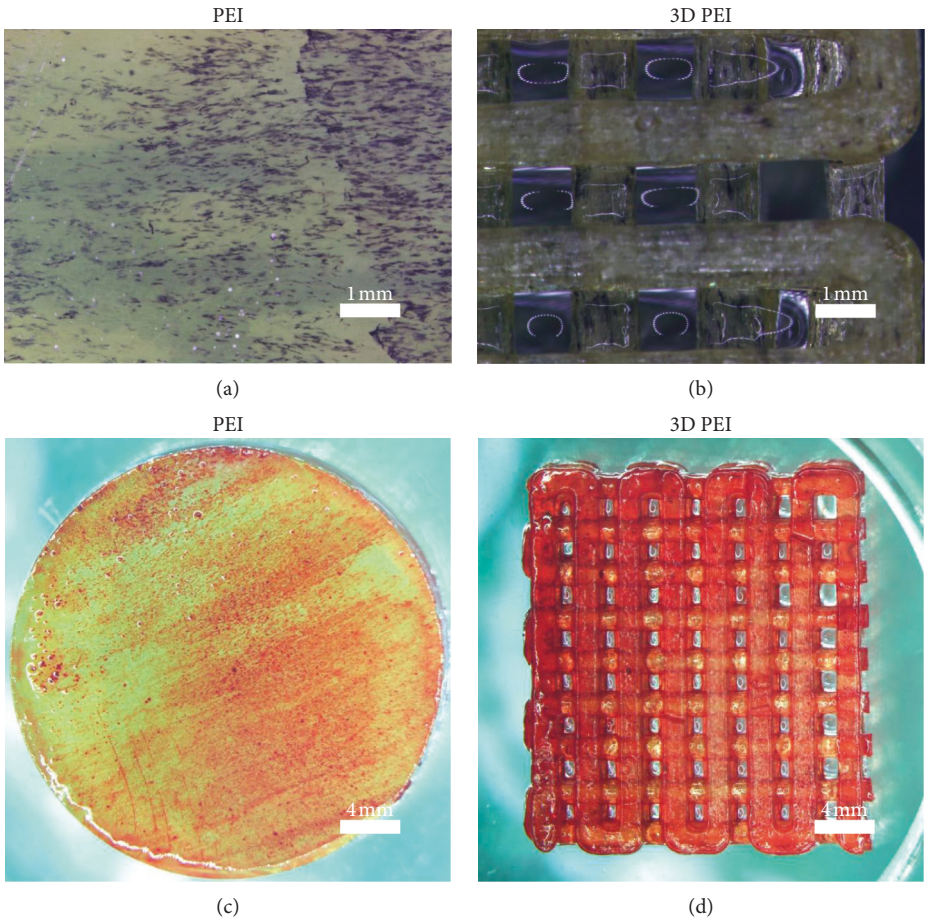

Figure 4: ALP staining (a, b) and Alizarin Red staining (c, d) images of the 3D PEI scaffold and PEI slice.

conducive to cell growth compared to the PEI slice group because of the larger inner surface of the porous structure [35]. As mentioned above, PEI has been proved as a potential membrane production material which has been applied into biohybrid organ systems and hemodialysis. Meanwhile, PEI also has been applied as bioreactors in dental and oral tissue engineering [36]. All these clinical applications indicate that both PEI and its membranes have excellent biocompatibility. Compared with the PEI membrane on other material scaffolds, 3D PEI can serve as a template for cell ingrowth and the formation of new bone tissue [37].

The secretion of ALP is an important indicator for evaluating the osteogenic differentiation of biomaterials. After osteogenic induction for 7 days, cells in 3D PEI scaffold and PEI groups were examined using ALP staining. As shown in Figures 4(a) and 4(b), both PEI and 3D PEI scaffold groups display lots of blue-purple spots (ALP-positive areas). The extracellular matrix mineralization is another important indicator for evaluating the osteogenic differentiation, and the mineralized nodules could be observed by Alizarin Red staining. Figure 4(b) shows the Alizarin Red staining of different samples after osteogenic induction for 14 days. It can be seen that the red-stained areas on the 3D PEI scaffold were slightly deeper than those on the PEI group, but the number of calcium nodules in both groups was similar. To sum up, the osteogenic differentiation level of the 3D PEI scaffold and PEI slice was equal and ordinary. In future studies, we would enhance their osteogenic differentiation through surface treatment.

4. Conclusions

In this work, we have designed and fabricated 3D scaffolds using polyetherimide as a raw material via a homemade 3D printer. The 3D PEI scaffold showed an interconnected porous structure, and its elastic modulus was 941.33 ± 65.26 MPa, which falls in the range of modulus for the native cancellous bone. The *in vitro* cell experiment demonstrates that the 3D PEI scaffold has good biocompatibility, and the porous structure provides a more suitable environment for cell proliferation compared with the PEI slice. However, the osteogenic differentiation level of the 3D PEI scaffold and PEI was ordinary. According to the biocompatibility and mechanical properties of the 3D PEI scaffold, we can consider it a potential strategy for bone tissue engineering, but the bioactivity of the surface should be improved in future studies.

Data Availability

The data used to support the findings of this study are available from the corresponding author upon request.

Conflicts of Interest

The authors declare that they have no conflicts of interest.

Acknowledgments

The authors greatly acknowledge the support from the National Natural Science Foundation of China (No. 81772456), the project supported by PhD Interdisciplinary Research Fund of Jilin University (No. 10183201845), and the Training Program of Outstanding Doctoral PhD for Norman Bethune Health Science Center of Jilin University (No. 470110000644).

References

[1] J. R. Porter, T. T. Ruckh, and K. C. Popat, "Bone tissue engineering: a review in bone biomimetics and drug delivery strategies," *Biotechnology Progress*, vol. 25, no. 6, pp. 1539–1560, 2009.

[2] X. Wang, S. Xu, S. Zhou et al., "Topological design and additive manufacturing of porous metals for bone scaffolds and orthopaedic implants: a review," *Biomaterials*, vol. 83, pp. 127–141, 2016.

[3] S. J. Hollister, "Porous scaffold design for tissue engineering," *Nature Materials*, vol. 4, no. 7, pp. 518–524, 2005.

[4] A. S. Mistry and A. G. Mikos, "Tissue engineering strategies for bone regeneration, regenerative medicine II," in *Advances in Biochemical Engineering/Biotechnology*, pp. 1–22, Springer, Berlin, Germany, 2005.

[5] J. Y. Lim, N. Kim, J.-C. Park, S. K. Yoo, D. A. Shin, and K.-W. Shim, "Exploring for the optimal structural design for the 3D-printing technology for cranial reconstruction: a biomechanical and histological study comparison of solid vs. porous structure, child's nervous system," *Child's Nervous System*, vol. 33, no. 9, pp. 1553–1562, 2017.

[6] S. C. Cox, J. A. Thornby, G. J. Gibbons, M. A. Williams, and K. K. Mallick, "3D printing of porous hydroxyapatite scaffolds intended for use in bone tissue engineering applications, materials science & engineering," *Materials Science and Engineering: C*, vol. 47, pp. 237–247, 2015.

[7] C. N. Kelly, A. T. Miller, S. J. Hollister, R. E. Guldberg, and K. Gall, "Design and structure-function characterization of 3D printed synthetic porous biomaterials for tissue engineering," *Advanced Healthcare Materials*, vol. 7, no. 7, Article ID e1701095, 2018.

[8] M. Qian-li, F. Liang, J. Nan et al., "Bone mesenchymal stem cell secretion of sRANKL/OPG/M-CSF in response to macrophage-mediated inflammatory response influences osteogenesis on nanostructured Ti surfaces," *Biomaterials*, vol. 154, pp. 234–247, 2018.

[9] L. Roseti, V. Parisi, M. Petretta et al., "Scaffolds for bone tissue engineering: state of the art and new perspectives," *Materials Science and Engineering: C*, vol. 78, pp. 1246–1262, 2017.

[10] S. Bose, M. Roy, and A. Bandyopadhyay, "Recent advances in bone tissue engineering scaffolds," *Trends in Biotechnology*, vol. 30, no. 10, pp. 546–554, 2012.

[11] C. N. Elias, J. H. C. Lima, R. Valiev, and M. A. Meyers, "Biomedical applications of titanium and its alloys," *JOM*, vol. 60, no. 3, pp. 46–49, 2008.

[12] H. Attar, S. Ehtemam-Haghighi, D. Kent et al., "Nanoindentation and wear properties of Ti and Ti-TiB composite materials produced by selective laser melting," *Materials Science and Engineering: A*, vol. 688, pp. 20–26, 2017.

[13] T. Lou, X. Wang, G. Song, Z. Gu, and Z. Yang, "Structure and properties of PLLA/β-TCP nanocomposite scaffolds for bone tissue engineering," *Journal of Materials Science: Materials in Medicine*, vol. 26, no. 1, p. 34, 2015.

[14] Q. Yao, J. G. L. Cosme, T. Xu et al., "Three dimensional electrospun PCL/PLA blend nanofibrous scaffolds with significantly improved stem cells osteogenic differentiation and cranial bone formation," *Biomaterials*, vol. 115, pp. 115–127, 2017.

[15] K. B. Sagomonyants, M. L. Jarman-Smith, N. D. John, M. S. Aronow, and G. A. Gronowicz, "The *in vitro* response of human osteoblasts to polyetheretherketone (PEEK) substrates compared to commercially pure titanium," *Biomaterials*, vol. 29, no. 11, pp. 1563–1572, 2008.

[16] Z. Yulong, Z. Zhong, Y. Mengliu et al., "Using an engineered galvanic redox system to generate positive surface potentials that promote osteogenic functions," *ACS Applied Materials & Interfaces*, vol. 10, no. 18, pp. 15449–15460, 2018.

[17] D. Garcia-Gonzalez, M. Rodriguez-Millan, A. Rusinek, and A. Arias, "Investigation of mechanical impact behavior of short carbon-fiber-reinforced PEEK composites," *Composite Structures*, vol. 133, no. 2-3, pp. 1116–1126, 2015.

[18] Y. Guo, R. Wang, P. Wang, Y. Li, and C. Wang, "Developing polyetherimide/graphitic carbon nitride floating photocatalyst with good photodegradation performance of methyl orange under light irradiation," *Chemosphere*, vol. 179, pp. 84–91, 2017.

[19] J. Li and L. Q. Zhang, "Tensile and tribological properties of a short-carbon-fiber-reinforced peek composite doped with carbon nanotubes," *Mechanics of Composite Materials*, vol. 45, no. 5, pp. 495–502, 2009.

[20] M. Razavi, *Frontiers in Biomaterials: Biomaterials for Tissue Engineering*, Bentham Science Publishers, Sharjah, UAE, 2017.

[21] A. Merolli, V. Perrone, P. T. Leali et al., "Response to polyetherimide based composite materials implanted in muscle and in bone," *Journal of Materials Science: Materials in Medicine*, vol. 10, no. 5, pp. 265–268, 1999.

[22] R. De Santis, L. Ambrosio, and L. Nicolais, "Polymer-based composite hip prostheses," *Journal of Inorganic Biochemistry*, vol. 79, no. 1–4, pp. 97–102, 2000.

[23] B. Seifert, G. Mihanetzis, T. Groth et al., "Polyetherimide: a new membrane-forming polymer for biomedical applications," *Artificial Organs*, vol. 26, no. 2, pp. 189–199, 2002.

[24] A. M. d. Santos, A. C. Habert, and H. C. Ferraz, "Development of functionalized polyetherimide/polyvinylpyrrolidone membranes for application in hemodialysis," *Journal of Materials Science: Materials in Medicine*, vol. 28, no. 9, p. 131, 2017.

[25] S. Van Bael, Y. C. Chai, S. Truscello et al., "The effect of pore geometry on the in vitro biological behavior of human periosteum-derived cells seeded on selective laser-melted Ti6Al4V bone scaffolds," *Acta Biomaterialia*, vol. 8, no. 7, pp. 2824–2834, 2012.

[26] V. Karageorgiou and D. Kaplan, "Porosity of 3D biomaterial scaffolds and osteogenesis," *Biomaterials*, vol. 26, no. 27, pp. 5474–5491, 2005.

[27] R. Li, Y. Qin, G. Liu et al., "Tantalum nitride coatings prepared by magnetron sputtering to improve the bioactivity and osteogenic activity for titanium alloy implants," *RSC Advances*, vol. 7, no. 87, pp. 55408–55417, 2017.

[28] M. H. Rich, M. K. Lee, N. Marshall et al., "Water-hydrogel binding affinity modulates freeze-drying-induced micropore architecture and skeletal myotube formation," *Biomacromolecules*, vol. 16, no. 8, pp. 2255–2264, 2015.

[29] L. Vikingsson, B. Claessens, J. A. Gómez-Tejedor, G. Gallego Ferrer, and J. L. Gómez Ribelles, "Relationship between micro-porosity, water permeability and mechanical behavior in scaffolds for cartilage engineering," *Journal of the Mechanical Behavior of Biomedical Materials*, vol. 48, pp. 60–69, 2015.

[30] Q. L. Loh and C. Choong, "Three-dimensional scaffolds for tissue engineering applications: role of porosity and pore size," *Tissue Engineering Part B: Reviews*, vol. 19, no. 6, pp. 485–502, 2013.

[31] R. Jungmann, M. E. Szabo, G. Schitter et al., "Local strain and damage mapping in single trabeculae during three-point bending tests," *Journal of the Mechanical Behavior of Biomedical Materials*, vol. 4, no. 4, pp. 523–534, 2011.

[32] R. J. Kane, H. E. Weiss-Bilka, M. J. Meagher et al., "Hydroxyapatite reinforced collagen scaffolds with improved architecture and mechanical properties," *Acta Biomaterialia*, vol. 17, no. 6, pp. 16–25, 2015.

[33] J. Wang, D. Wu, Z. Zhang et al., "Biomimetically ornamented rapid prototyping fabrication of an apatite–collagen–polycaprolactone composite construct with nano–micro–macro hierarchical structure for large bone defect treatment," *ACS Applied Materials & Interfaces*, vol. 7, no. 47, pp. 26244–26256, 2015.

[34] M. V. Cakir, U. Allenstein, M. Zink, and S. G. Mayr, "Early adhesion of cells to ferromagnetic shape memory alloys functionalized with plasma assembled biomolecules–a single cell force spectroscopy study," *Materials & Design*, vol. 158, pp. 19–27, 2018.

[35] P. E. Petrochenko, J. Torgersen, P. Gruber et al., "Laser 3D printing with sub-microscale resolution of porous elastomeric scaffolds for supporting human bone stem cells," *Advanced Healthcare Materials*, vol. 4, no. 5, pp. 739–747, 2015.

[36] L. M. Amirabad, J. Perugini, and L. Tayebi, "Application of Bioreactors in Dental and Oral Tissue Engineering," in *Applications of Biomedical Engineering in Dentistry*, pp. 89–148, Springer, Berlin, Germany, 2020.

[37] C.-T. Tao and T.-H. Young, "Polyetherimide membrane formation by the cononsolvent system and its biocompatibility of MG63 cell line," *Journal of Membrane Science*, vol. 269, no. 1-2, pp. 66–74, 2006.

Hindawi
BioMed Research International
Volume 2019, Article ID 2797210, 8 pages
https://doi.org/10.1155/2019/2797210

Clinical Study

In Situ Endoscopic Analysis of Vascular Supply and Regenerated Alveolar Bone in β-TCP Grafted and Ungrafted Postextraction Sites before Implant Placement: A Prospective Case Control Study

Víctor Beltrán,[1] Marcio Lazzarini,[2] Rodolfo Figueroa,[3] Vanessa Sousa,[4] and Wilfried Engelke[3]

[1]*Universidad de La Frontera, Dental School, Clinical Investigation and Dental Innovation Center (CIDIC) and Center for Translational Medicine (CEMT-BIOREN), Temuco, Chile*
[2]*Max Planck Institute of Experimental Medicine, Department of Molecular Biology of Neuronal Signals, Göttingen, Germany*
[3]*Universidad de La Frontera, Center of Physics and Engineering in Medicine (CFIM), Faculty of Engineering and Sciences, Temuco, Chile*
[4]*Centre for Oral Clinical Research, Institute of Dentistry, Barts & The London School of Medicine & Dentistry, QMUL, London, UK*

Correspondence should be addressed to Víctor Beltrán; victor.beltran@ufrontera.cl

Received 5 July 2019; Accepted 16 August 2019; Published 6 November 2019

Guest Editor: Maria Sartori

Background. Endoscopy has seen a significant development over recent years in various medical fields with its application expanding from the support of minimal invasive surgery to in situ imaging. In this context, the application of endoscopic techniques to assess the quality of the regenerated bone in situ in the drill hole before implant placement is an appealing approach. *Aim*. The aim of this study was to use short distance support immersion endoscopy (SD-SIE) to compare the quality of regenerated bone in healed postextraction sites, which are grafted with an in situ hardening β-TCP, against ungrafted sites, before implant placement. This assessment was based on microscopic bone analysis in combination with the blood vessel count. *Method*. 13 spontaneously healed and 13 grafted postextraction sites in 3 men and 6 women, aged 26–83 years, were evaluated using SD-SIE after 4–6 months. SD-SIE was applied in drill holes before implant placement, and videos were taken from representative central buccal areas. The video recordings were analyzed using Image J software for (1) number of blood vessels per area (NBV), (2) relative area of vessels (VA), (3) relative area of mineralized bone (MBA), (4) relative area of unmineralized bone (UMBA), and (5) relative area of bone substitute (BSA). *Results*. The grafted sites showed more (1) NBV as well as (2) VA (8.6 ± 1.1; $2.03 \pm 0.28\%$) than the ungrafted sites (2.5 ± 0.6; $1.18 \pm 0.36\%$) (independent t-test; $p < 0.05$); (3) MBA and (4) UMBA were similar to those in the grafted sites (86.3 ± 2.2 %; 13.7 ± 2.2 %) and to the ungrafted sites ($89.5 \pm 3.7\%$; $10.5 \pm 3.6\%$) (independent t-test; $p > 0.05$); and (5) BSA in the grafted sites was $18.2 \pm 5.4\%$. *Conclusion*. SD-SIE is an interesting new approach for in situ assessment of bone quality and blood supply before implant placement. The regenerated bone in β-TCP grafted extraction sockets showed an increased vascularization compared to ungrafted sites providing a vital support for subsequent implant placement.

1. Introduction

Regeneration of alveolar bone by applying the technique of guided bone regeneration has been well documented in experiments and clinical investigation [1]. Bone substitutes for the support of local regeneration must be biocompatible and osteoconductive to prevent the material becoming encapsulated by fibrous tissue, leading to device failure and the need of a second intervention. From a clinical perspective, bone graft substitutes should be moldable during application, display a self-stabilizing and hardening potential, and form a stable, but still porous, scaffold in the

defect. This approach eases the application and, at the same time, would greatly reduce the need for membranes to retain loose graft materials in the defect, resulting in a shortened and simplified surgical procedure [1]. Moldable microporous, synthetic calcium phosphate bone graft substitutes (β-TCP or β-BCP), coated with a micrometer thin layer of a degradable polymer, have been shown to be valuable materials for alveolar ridge regeneration as well as socket preservation [2, 3]. Porous calcium phosphates have been under intense investigation for more than 20 years and are widely used as bone graft substitutes. Nowadays, calcium phosphate (CaP) materials may generally vary in their rate of in vivo degradation, structure, and mechanical strength. The optimum porosity for bone should allow a vascular ingrowth and corresponding bone substitute resorption rate, since an ideal regenerative scenario would consist of a biomaterial resorption rate timed with new osseous tissue ingrowth [4].

The formation of an adequate vascular network is crucial for osteogenesis during both development and repair. Therefore, an effective bone graft for bone augmentation in the maxillofacial region shall support the formation of an adequate vascular network providing nutrition, osteoprogenitor cells, and growth factors to the site. Moreover, adequate perfusion is not only a prerequisite for bone regeneration but also for osseointegration for subsequent place dental implants [5]. Therefore, it is highly important to define the conditions for ideal bone regeneration and to investigate aspects of vascular supply of regenerated areas to improve the success of implant therapy.

Improvements of bone regeneration will rely on previous research of bone blood flow, to determine the right combination of scaffold, cell source, growth factors, and biomechanical conditions [6]. In clinical situations, as a response to bone injury, such as a fracture, robust angiogenesis occurs to relieve oxygen tension and transport osteoprogenitor cells for repair.

Vessel size and number can be robustly quantified ex vivo using histology or vascular casting. However, accurate quantification of in situ blood flow, particularly in bone, is more difficult in humans, when experimentally used techniques in animal trials such as radioactive microspheres cannot be applied.

There are two basic mechanisms of blood vessel formation: vasculogenesis (formation of a blood vessel from a progenitor cell, angioblast or hemangioblast) and angiogenesis (new vasculature development from the preexisting blood vessels). Additionally, a body of experimental work has shown that the presence or absence of the periosteum significantly affects the healing response [7].

For instance, Weigand et al. [8] hypothesized that extrinsic and intrinsic vascularization of a large-size bone tissue construct determines a successful regeneration process within a bone defect. The authors microsurgically created an arteriovenous loop and connected it with the bone substitute in either perforated titanium chambers (intrinsic/extrinsic) or tested the isolated Teflon chambers (intrinsic). In the intrinsic vascularization model, degradation of the scaffold and osteoclastic activity was significantly lower after 18 weeks, compared to the combined intrinsic-extrinsic model [8].

For observation of bone perfusion on a microscopic level, intravital microscopy has been used [9]. More recently, bone vascular parameters have been evaluated using an optical bone chamber implanted onto the calvaria of the rabbit [10]. For in vivo evaluation of soft tissues, light microscopy, in particular, epifluorescence and confocal microscopy, may be applied where the spatial resolution is typically limited to 50–100 microns of thickness of the tissue [11].

Based on earlier reports [9, 12, 13], and the refinement of the evaluation procedures, endoscopic tools have recently reached a similar magnification to the clinical observation of bone surfaces in vivo similar to the experimental setting. The short distance support immersion endoscopy (SD-SIE) allows to do an almost histological bone evaluation in vivo, not only under static, but also under dynamic conditions [12]. In this context, the field of dentistry provides a unique opportunity to get access to human bone surfaces during the preparation of implant sites prior to dental implants placement.

SD-SIE has been used as a diagnostic aid to judge the bone structure, to observe the presence of nutritional Volkmann's foramina of the alveolar bone [13]. Thus, it is possible to evaluate under high magnification, prior to implant placement, regenerated sites to detect new bone formation, to identify remnants of biomaterial, and to observe dynamic aspects of vascularization at specific sites.

The primary objective of this study was designed to evaluate the vascularization and, secondly, to microscopically evaluate the bone quality of postextractions sites grafted with a moldable microporous, synthetic beta tricalcium phosphate (β-TCP) bone graft substitute, in comparison to ungrafted sites before implant placement after 4–6 months. This assessment was performed using SD-SIE.

1.1. Patients and Methods. A pilot prospective case control study was performed in the Implant Clinic of the Dental School of Universidad de la Frontera (UFRO), Temuco, Chile, between 2017 and 2018. A total of nine patients (3 men and 6 women, aged 26 to 83 years) agreed to participate in this study, and signed informed consents were completed at the study visit at the Implant Clinic of the Dental School of UFRO. The study was conducted in line with the principles outlined in the Declaration of Helsinki (2008) on experimentation involving human participants. Ethics approval for the conduct of the study was granted by the Universidad de La Frontera Ethics Committee (Decision 118/16), DIUFRO project No. DI17-0170. These participants were selected for ridge preservation of alveolar extraction sites with a moldable self-hardening synthetic bone graft substitute (GUIDOR easy-graft CLASSIC, Sunstar Suisse SA, Etoy, Switzerland). Socket grafting was carried out following tooth extraction according to the concept of ridge preservation to maintain the lateral contour of the alveolar ridge. A total of 13 grafted and 13 ungrafted alveolar sites were analyzed with SD-SIE in the drill hole right before implant placement

(Figure 1). Details of the implant sites are given in Table 1. The sites belonged to the anterior maxillary zone including premolars, canines, and incisors. All participants' data were anonymized to ensure confidentiality and the grafted and ungrafted groups were randomized for a blind analysis.

1.2. Endoscopic Observation. For SD-SIE, a rigid STORZ endoscope with 1.9-mm diameter, 30 and 70° view angle and an integrated support-irrigation tube (Karl Storz, Tuttlingen, Germany) was used. The endoscopes were coupled to a Karl Storz Image 1 HD Camera 222200 50 (Karl Storz, Tuttlingen, Germany). Before the micromorphologic evaluation, the scope window was placed in contact with the surface of the graph paper and the scale was set to 500 micrometer (see Figures 1(a)–1(c)). The graph paper was placed inside the dental model filled with water. This model allowed us to proceed to the morphologic evaluation within a natural chamber formed by the implant cavity (see Figure 1(c)).

Videos were taken from the central buccal aspect of the drill hole. Manual jet stream irrigation was served to clean the bone surface, and the irrigation flow was stopped immediately before observation (Figure 2); thus, the bone surface could be observed without pollution through the irrigation medium (saline solution).

1.3. Image Selection. Taking the surgical reports as reference, the sites were identified and cross-checked for presence of bone substitute. The central buccal area of the augmented or native cavities was examined as a representative zone for blood vessel counts as well as microscopic bone imaging, and apical and cervical regions were not included in the evaluation. Screenshots were taken from the original digital video archives (mpg4 files) and stored in jpg format. The image analysis program (Image J, V.64, National Institutes of Health, Bethesda, MD, USA) was used to open digitized endoscopic images.

1.4. Vessels, Mineralized, and Unmineralized Bone Structure Analysis. The analysis of the bleeding bone surface was performed according to the following protocol: (1) selection of the area of interest (AoI), (2) screenshot of images after irrigation and cleaning, and (3) set of the scale bar according to the transversal diameter of the scope window (contact mode) at the center of the image and definition of the area of measurement using Image J (see Figure 1). The rectangular selection tool was used to determine the AoI with a scale of 500 micrometer and the bone structures from native ungrafted ($n = 13$) and grafted ($n = 13$) were selected from the freehand selection tool from Image J software (see Figure 3). Total number and area of vessels (red selection Figures 3(b) and 3(e)), nonmineralized bone (black selection Figures 3(c) and 3(f)), and easy-graft graft material in the bone substitute group (blue selection Figure 3(g)) were observed. Vessels were identified by observing the original video recordings that were recorded by the endoscopic procedure in vivo (Figures 3(a) and 3(d)) after cleaning the bone surface with saline solution. The percentages were calculated from area of mm^2 by (unmineralized bone or vessels) multiplied by 100 and then divided by the AoI (Figures 3(a) or 3(d)). The mineralized bone area was calculated from the difference of the AoI from the vessels area selected (Figures 3(b) and 3(e)) plus nonmineralized bone (Figures 3(c) and 3(f)). The bright white areas were selected as bone substitute (Figure 3(g)). Vessels were counted in a blinded manner by three of the authors independently, for further processing, the numbers were averaged. Sites with pulsatile extravasation from arterial vessels were excluded, if the AoI could not be cleansed sufficiently.

1.5. Statistical Analysis. Shapiro–Wilk's test ($p > 0.05$) showed that the data are normally distributed for unmineralized and mineralized bone, total area, and number of total vessels. Therefore, the independent t-test was used to see the differences of structures between ungrafted and grafted sites. The level of significance was set at $p < 0.05$. Statistical analysis was performed using SPSS, Inc., software (version 23).

2. Results

SIE applied in ungrafted and grafted sites in situ allowed for the quantitative assessment of internal bone surface. Structures such as vascular canals can be identified under variable magnification. Microscopic bone imaging analysis based on SIE allowed the identification of the quality of the localized areas of internal bone surface by the relative assessment of mineralized and unmineralized zones and vascular canals. The grafted sites showed a higher number of NBV and a larger area (VA) of blood vessels (8.6 ± 1.1; $2.03 \pm 0.28\%$) compared with the ungrafted sites (2.5 ± 0.6; $1.18 \pm 0.36\%$), as shown in Tables 2 and 3. In relation to mineralized (MBA) and unmineralized (UMBA) bone areas, the grafted sites did not show differences of percentage areas ($86.3 \pm 2.2\%$; $13.7 \pm 2.2\%$) with the ungrafted ($89.5 \pm 3.7\%$; $10.5 \pm 3.6\%$) (Table 3) (independent t-test; $p < 0.05$). The grafted sites showed a relative area of bone substitute in a mean of $18.2 \pm 5.4\%$ (Table 3).

3. Discussion

The first in vivo observation of Volkmann's channels using SIE as a microscopic tool was described by Beltrán et al. [3]. Meanwhile, the assessment of the osseous morphology to determine vascular and structural bone quality has been defined as a quantitative analysis of relative area of vessels (VA), mineralized (MBA) and unmineralized bone area (UMBA), and relative area of bone substitute (BSA) in percentages (Table 3). Grafted sites showed differences in comparison to the ungrafted sites (independent t-test; $^{*}p < 0.05$).

Engelke et al. [12] reported on microscopic bone analysis (MBA) using a SD-SIE based protocol with subsequent Image J analysis. MBA allowed a quantitative description of bone morphology such as unmineralized and mineralized areas as well as area of vascular canals under bleeding in vivo condition. The morphometric examination revealed that

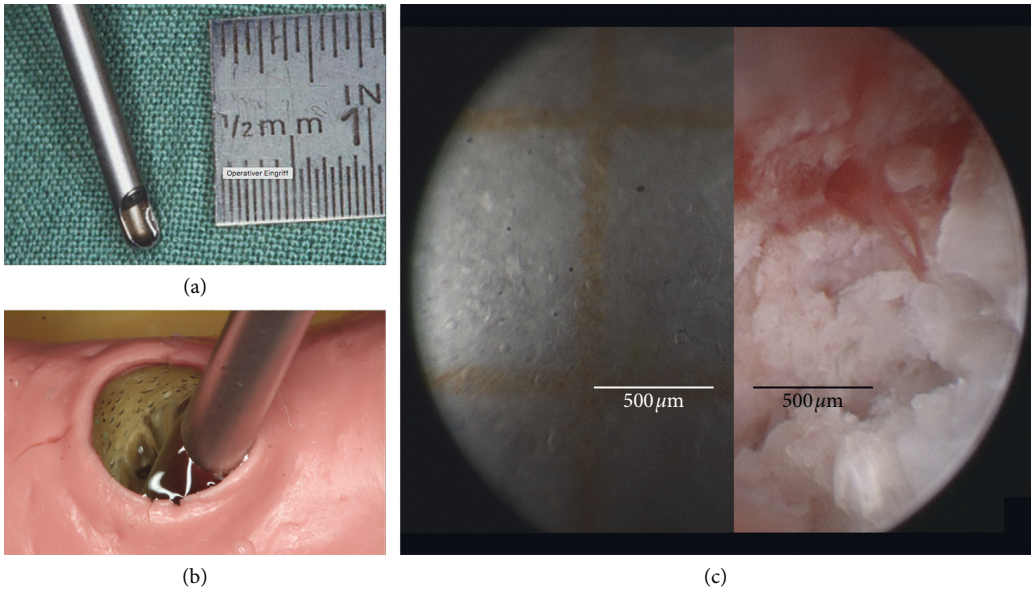

(a) (b) (c)

Figure 1: SD-SIE: (a) the endoscope is inserted into a sheath that provides both support and an irrigation system. (b) The endoscope with support immersion shaft is placed inside a dental extraction site model and implant cavity. (c) Short distance endoscopy allows observation under adequate magnification to differentiate structures for micromorphologic evaluation. When positioned at the entrance or fundus of the cavity, the endoscope can provide either a general or detailed view of the surgical field without having to make additional adjustments, thanks to its high depth of field.

Table 1: Distribution of implant sites. Second premolar (PM2), first premolar (PM1), canine (C), lateral incisive (LI), and central incisive (CI).

SITE	PM2	PM1	C	LI	CI
Ungrafted sites	3	4	2	1	4
Grafted sites	2	4	3	–	3

there was more unmineralized bone and less vascular canal area in implant sites than in the extraction sockets.

The present study was focused on the vascular supply in grafted vs. ungrafted postextraction sites, i.e., on the quantification of blood vessels per area. The study was conducted in patients who required ridge preservation with bone graft substitute following tooth extraction. Grafting of postextraction sites was performed according to the manufacturer's instruction following tooth extraction with various degrees of alveolar bone loss in the sense of ridge preservation. Since there was no primary protocol to assess the bone loss, the observation was focused on the typical area graft which is located at the buccal wall. The central buccal area was chosen in order to avoid possible influence of occlusal loading in the crestal zone or missing augmentation in the apical area. By previous observation of resting bone substitute particles, it was confirmed that the AoI corresponded to the augmented zone.

Methodically, the blood vessel count is limited by the conditions of the observation, in particular, the resolution of the optical system. The resolution of in vivo light microscopy for soft tissues using epifluorescence and confocal microscopy is typically limited to the outer 50–100 microns of the accessible tissue. With reference to Engelke et al. [12], the canal diameter of Volkmann's canals lies between 30 and 50 microns; these canals are clearly visible and confirm that the resolution of SIE is well above the average diameter of cortical canals. For the purpose of the present study, a resolution of 50 microns was assumed.

There are no in vivo data available on the number of blood vessels in alveolar bone. However, the literature offers a wide range of numbers of blood vessels per area in different bone structures, tissues, and animal models.

Sezer et al. [13] reported on bone marrow microvessel density (MVD) in immunohistochemical CD34 stained paraffin-embedded bone marrow biopsies and survival in patients with multiple myeloma. The median MVD was 48 vessels/mm^2; the range was 0–125 vessels/mm^2. The regenerated alveolar bone, however, does not represent pure bone marrow conditions as used in the clinical investigation mentioned.

There is no methodological consensus on the parameter, nomenclature and regions of interest for the quantification of bone marrow vessels. This leads to a pronounced heterogeneity of the results among the various publications.

Bone marrow vessels are heterogeneous and include small classic capillaries (10–15 μm) and a majority of sinusoid capillaries (20–30 μm), which belong to the venous capillary system [14]. These vessels probably are prone to be disregarded during a SD-SIE evaluation due to their small diameter and due to missing staining in vivo. According to our previous evaluation, these capillary structures are at the limit of the presently available resolution of SD-endoscopes of 50 μm. A comparable magnitude of vessels per tissue area were reported by Hettrich et al. [15] who evaluated the effect of rhPTH on the healing of tendon to bone in a rat model.

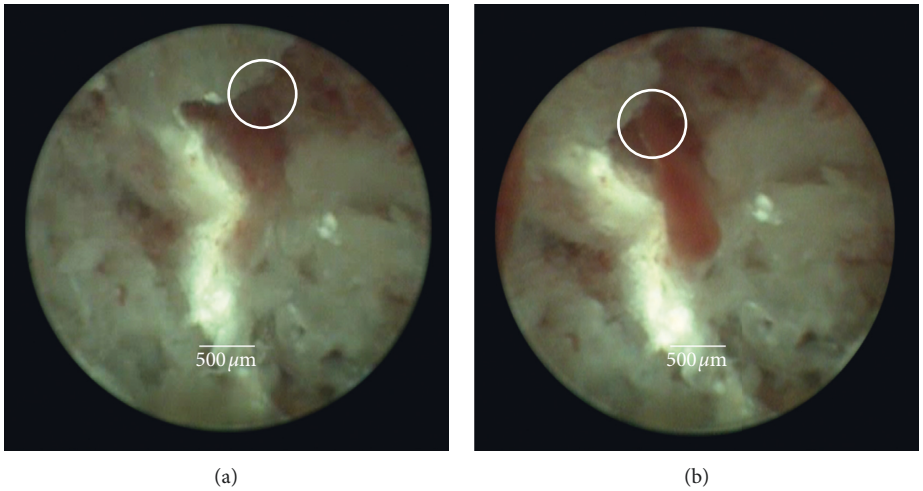

Figure 2: Observation of regenerated bone using SD-SIE: (a) region of interest showing initial bleeding of a blood vessel in regenerated bone. (b) During reduced rinsing pressure, extravasation of blood increases.

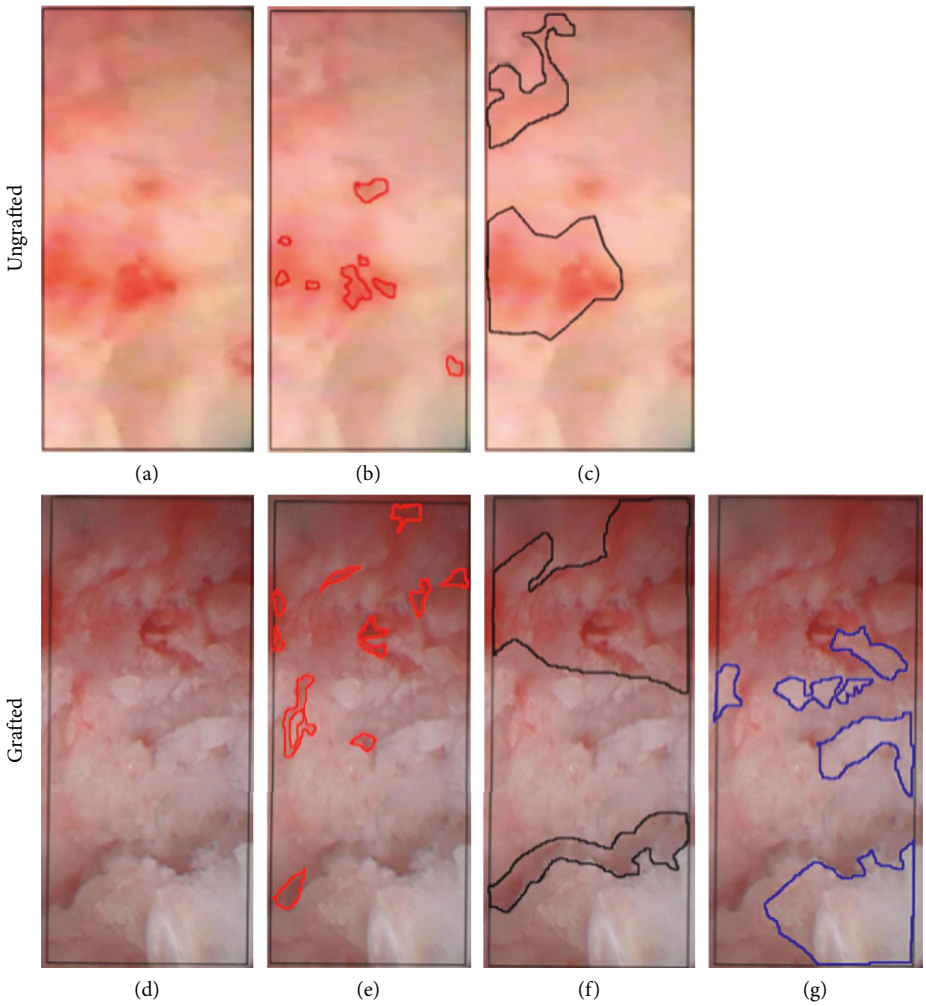

Figure 3: Micromorphology. Bone analysis of grafted and ungrafted bone: (a, d) Observation of bleeding vessels; (b, e) assessment of blood vessel area; (c, f) nonmineralized bone area; (g) grafted bone area.

Table 2: Quantitative analysis of number of blood vessels per area of interest (AoI) (NBV). Grafted sites showed more total number of vessels than ungrafted sites (independent t-test; $^{*}p < 0.05$).

	Ungrafted sites ($n = 13$)	Grafted sites ($n = 13$)
NBV		
Mean	2.538	*8.615
SD	2.259	4.011
SE	0.652	1.158
Min-max	0–6	1–14

Table 3: Quantitative analysis of relative area of vessels (VA), mineralized (MBA) and unmineralized bone area (UMBA) and relative area of bone substitute (BSA) in percentage. Grafted sites showed differences in compare the ungrafted sites (independent t-test; $^{*}p < 0.05$).

	Ungrafted sites ($n = 13$)	Grafted sites ($n = 13$)
VA		
Mean	1.82	*2.030
SD	1.274	0.967
SE	0.368	0.279
Min-max	0–4.34	0.28–3.53
MBA		
Mean	89.509	86.282
SD	12.77	7.876
SE	3.686	2.274
Min-max	60–100	62–95
UMBA		
Mean	10.491	13.718
SD	12.77	7.876
SE	3.686	2.274
Min-max	0–40	5–37
BSA		
Mean	0	18.199
SD	0	18.72
SE	0	5.404
Min-max	0	2–74

Factor VIII staining was used to evaluate angiogenesis within the supraspinatus tendon and tendon-bone interface. Microscope field images at 40x magnification were centered over the area of insertion, the vessels within these areas were counted, and the number of vessels per mm^2 was calculated. The blood count figures ranged between 0 and 3.5 vessels per mm^2, i.e., the condition of the tendon insertion appears to lie in the same range as our observations in alveolar bone.

For clinical purposes, it is highly important to define the conditions for ideal bone regeneration after tooth extraction and to investigate aspects of vascular supply of regenerated areas to improve the success of implant therapy.

Weiss et al. [16] observed the blood vessel formation in Collagen HA (CHA) scaffolds with occlusive membrane (OM) implanted in a mouse model and evaluated with μCT: CHA OM yielded the most blood vessels (8.22 ± 1.19) per unit area ($0.3588\,mm^2$), followed by Col OM (6.61 ± 0.64) and CHA acellular (6.00 ± 0.80) groups. In our in vivo observations, the grafted areas showed more vascularization (8.6 ± 1.1) per AoI than the ungrafted sites (2.5 ± 0.6) similar to previous studies in animal models. Thus, we may conclude that regenerated bone at a comparable regeneration time following extraction appears to increase the numbers of vessels.

The present in vivo observation exhibited that following the grafting of postextraction sites with a moldable in situ hardening β-TCP, a direct contact of vessels with the TCP regularly occurs. The material was in full contact with the adjacent capillaries without interposition of connective tissue or avascular zones. This may be taken as an indicator for an adequate regeneration and maturation of the sites. The findings are in accordance with reports of Valdivia-Gandur et al. [17] and Schmidlin et al. [1] who described a good biocompatibility of this bone graft substitute with an intimate distribution of newly formed bone and bone graft substitute materials.

Endomicroscopy of bone as proposed in the actual study design also allows to determine blood flow parameters and a variety of bone pathologies in vivo. For clinical purposes, it is highly important to define the conditions for ideal bone regeneration after tooth extraction and to investigate aspects of vascular supply of regenerated areas to improve the success of implant therapy.

Evaluation for bone reconstruction should focus on three levels of graft integration with surrounding tissues: osseointegration, vascular integration, and gradual substitution by bone remodeling under functional loading to achieve complete integration [18]. Osteogenic and vascular regeneration need to be complementary and should proceed at satisfactory rates for effective repair and functional restoration. The present study confirms that a similar range of vascular supply takes place within the sites grafted with in situ hardening moldable bone substitute compared to ungrafted sites. Degradation of TCP was observed close to the defect borders after 16 weeks where the formerly round granules were integrated in bone and displayed irregular shapes [1]. This could also be confirmed by nonquantified observation in vivo, where the limit of the implant cavity was located directly adjacent to the buccal border of the alveolus.

In animal trials, the number of penetrating vessels into a capsule with different bone regeneration constructs in the mouse model [19] was taken as an indicator for successful integration of constructs in vivo; however, the biomechanical conditions were significantly different from the site of implantation of the scaffold structure. Keeping this in mind, the present study provides conditions for a huge number of investigations to judge the outcome of bone regeneration constructs directly in situ before charging them with implants on a regular basis. Because there is no need for biopsies, endomicroscopy can be ethically justified due to the diagnostic value of the nondestructive evaluation of bone structure. It may deliver important parameters which could previously be acquired only by conventional evaluation of histological specimens under experimental conditions.

A precise definition of the area of observation within the clinical situs is mandatory, which can be documented directly and compared with previous 3D imaging technologies. It makes way for future outline micromorphological evaluation of regenerated sites and contributes to a newdata base for successful use of grafted alveolar sites.

However, there are some shortcomings for the method, which are mainly related to the limited image resolution. Without the use of an HD camera, the detection of capillary vessels may be impossible. Strong bleeding still impedes a clear surface observation. Furthermore, there is still a distortion of the view mainly in the vertical axis of the bone cavity and irregularities of the surface observed angle, if the endoscope cannot be placed in full contact with the surface irregularities.

4. Conclusion

SD-SIE allows for a morphometric in situ evaluation and quantification of the vascularization of human internal osseous surfaces after bone regeneration at the microscopic level. Therefore, it represents an interesting new approach for in situ assessment of bone quality and blood supply before implant placement. The regenerated bone in β-TCP grafted extraction sockets showed increased vascularization compared to ungrafted sites providing a vital support for subsequent implant placement.

Data Availability

Data that support the conclusions of this article are completely included in the manuscript.

Ethical Approval

The study was approved by the Universidad de La Frontera Ethics Committee (Decision 118/16).

Consent

All patients declared informed consent.

Conflicts of Interest

The authors declare that they have no conflicts of interest.

Authors' Contributions

WE and VB designed the study and performed the surgery. ML conducted the video-endoscopic measurements. VB, ML, RF, VS, and WE wrote the draft and WE, VB, and ML reviewed the manuscript.

Acknowledgments

Wilfried Engelke was supported in part by the MEC Project (PAI80160012) of the National Commission for Scientific and Technological Research, CONICYT, Chile, and the DI16-6009 Insertion Program. The study was supported with biomaterial from Sunstar Suisse SA, Etoy, Switzerland, to the Universidad de La Frontera, Temuco, Chile (DIUFRO project no. DI17-0170).

References

[1] P. R. Schmidlin, F. Nicholls, A. Kruse, R. A. Zwahlen, and F. E. Weber, "Evaluation of moldable, in situ hardening calcium phosphate bone graft substitutes," *Clinical Oral Implants Research*, vol. 24, no. 2, pp. 149–157, 2013.

[2] O. A. Decco, J. I. Zuchuat, A. C. Cura, J. A. Decco, and W. Engelke, "Conventional extraction vs. enucleation in anterior maxillary sites: a pilot study in humans," *International Journal of Clinical & Experimental Medicine*, vol. 10, no. 2, pp. 2147–2155, 2017.

[3] V. Beltrán, R. Fuentes, and W. Engelke, "Endoscopic visualization of anatomic structures as a support tool in oral surgery and implantology," *Journal of Oral and Maxillofacial Surgery*, vol. 70, no. 1, pp. e1–e6, 2012.

[4] S. P. Pilipchuk, A. B. Plonka, A. Monje et al., "Tissue engineering for bone regeneration and osseointegration in the oral cavity," *Dental Materials*, vol. 31, no. 4, pp. 317–338, 2015.

[5] B. H. Choi, S. M. Jeong, J. Kim, and W. Engelke, *Flapless Implantology*, Quintessence Pub. Co., London, UK, 2010.

[6] R. E. Tomlinson and M. J. Silva, "Skeletal blood flow in bone repair and maintenance," *Bone Research*, vol. 1, no. 4, pp. 311–322, 2013.

[7] C. Colnot, X. Zhang, and M. L. K. Tate, "Current insights on the regenerative potential of the periosteum: molecular, cellular, and endogenous engineering approaches," *Journal of Orthopaedic Research*, vol. 30, no. 12, pp. 1869–1878, 2012.

[8] A. Weigand, J. P. Beier, A. Hess et al., "Acceleration of vascularized bone tissue-engineered constructs in a large animal model combining intrinsic and extrinsic vascularization," *Tissue Engineering Part A*, vol. 21, no. 9-10, pp. 1680–1694, 2015.

[9] J. Nyarady, G. Farkas, G. Cseh et al., "Osteoscopy for assessment of blood supply to the femoral head: a preliminary study," *Journal of Orthopaedic Trauma*, vol. 26, no. 4, pp. 200–205, 2012.

[10] S. O. Desmons, J. Salleron, C. J. Delfosse, G. Falgayrac, G. Penel, and S. R. Mordon, "Laser preconditioning on cranial bone site: analysis of morphological vascular parameters," *Lasers in Surgery and Medicine*, vol. 42, no. 9, pp. 791–797, 2010.

[11] R. Tomer, K. Khairy, and P. J. Keller, "Light sheet microscopy in cell biology," in *Methods in Molecular Biology*, vol. 931, pp. 123–137, Humana Press, Totowa, NJ, USA, 2013.

[12] W. Engelke, M. Lazzarini, W. Stühmer, and V. Beltrán, "Support immersion endoscopy in post-extraction alveolar bone chambers: a new window for microscopic bone imaging in vivo," *PLoS One*, vol. 10, no. 12, Article ID e0145767, 2015.

[13] O. Sezer, K. Niemöller, J. Eucker et al., "Bone marrow microvessel density is a prognostic factor for survival in patients with multiple myeloma," *Annals of Hematology*, vol. 79, no. 10, pp. 574–577, 2000.

[14] M. H. Lafage-Proust, B. Roche, M. Langer et al., "Assessment of bone vascularization and its role in bone remodeling," *Bonekey Reports*, vol. 4, p. 662, 2015.

[15] C. M. Hettrich, B. S. Beamer, A. Bedi et al., "The effect of rhPTH on the healing of tendon to bone in a rat model," *Journal of Orthopaedic Research*, vol. 30, no. 5, pp. 769–774, 2012.

[16] H. E. Weiss, J. A. Gargac, M. J. Meagher, R. K. Roeder, G. L. Niebur, and D. R. Wagner, "Osteogenically treated human adult adipose-derived stem cells promote vascular invasion and de novo bone formation in hydroxyapatite-reinforced collagen scaffolds in vivo," in *Proceedings of the ORS Annual Meeting Poster No: 076*, San Antonio, TX, USA, January 2013.

[17] I. Valdivia-Gandur, W. Engelke, V. Beltrán, E. Borie, R. Fuentes, and M. C. Manzanares-Céspedes, "Novel use of

cranial epidural space in rabbits as an animal model to investigate bone volume augmentation potential of different bone graft substitutes," *Head & Face Medicine*, vol. 12, no. 1, p. 35, 2016.

[18] Áerca Mercado-Pagán, A. M. Stahl, Y. Shanjani, and Y. Yang, "Vascularization in bone tissue engineering constructs," *Annals of Biomedical Engineering*, vol. 43, no. 3, pp. 718–729, 2015.

[19] B. J. R. F. Bolland, J. M. Kanczler, D. G. Dunlop, and R. O. C. Oreffo, "Development of in vivo μCT evaluation of neovascularisation in tissue engineered bone constructs," *Bone*, vol. 43, no. 1, pp. 195–202, 2008.

Hindawi
BioMed Research International
Volume 2019, Article ID 2656503, 8 pages
https://doi.org/10.1155/2019/2656503

Clinical Study

Reconstruction of Medial Wall Blowout Fracture Defect with a Combination of Resorbable Meshed Plate and Cancellous Bone Allograft

Jongweon Shin,[1] Song I Park,[2] Yunsup Hwang,[3] Ho Kwon,[2] and Hyung-Sup Shim[4]

[1]*Department of Plastic and Reconstructive Surgery, Yeouido St. Mary's Hospital, College of Medicine, The Catholic University of Korea, Seoul, Republic of Korea*
[2]*Department of Plastic and Reconstructive Surgery, Uijeongbu St. Mary's Hospital, College of Medicine, The Catholic University of Korea, Uijeongbu-si, Gyeonggi-do, Republic of Korea*
[3]*Department of Radiology, Uijeongbu St. Mary's Hospital, College of Medicine, The Catholic University of Korea, Uijeongbu-si, Gyeonggi-do, Republic of Korea*
[4]*Department of Plastic and Reconstructive Surgery, St. Vincent's Hospital, College of Medicine, The Catholic University of Korea, Suwon-si, Gyeonggi-do, Republic of Korea*

Correspondence should be addressed to Hyung-Sup Shim; sharpshim@catholic.ac.kr

Received 4 July 2019; Revised 4 August 2019; Accepted 11 August 2019; Published 15 October 2019

Background. Various materials are available for the reconstruction of bone defects in cases of medial wall blowout fracture. This study was conducted to assess the efficacy of the combination of a resorbable meshed plate and cancellous bone allograft. *Methods.* From March 2014 to March 2017, a total of 111 patients were evaluated. Sixty-three patients received reconstruction surgery with porous polyethylene plates (control group) and the other forty-eight patients underwent operation with a resorbable meshed plate plus allogenic cancellous bone (combined group). The results were assessed by exophthalmometric measurements, width, and volume discrepancies as compared with the unaffected orbit, and operation time. *Results.* The difference in exophthalmometric measurements between the affected and unaffected orbits were 0.94 ± 0.70 mm in the control group and 1.05 ± 0.73 mm in the combined group without statistical significance ($p = 0.425$). In the analysis of computed tomography images, the width discrepancy was 1.55 ± 0.86 mm and 1.08 ± 0.69 mm, respectively ($p = 0.003$); however, the volume discrepancy demonstrated no statistically significant difference ($2.58 \pm 1.40\,cm^3$ versus $2.20 \pm 1.80\,cm^3$; $p = 0.209$). Operation time was significantly shorter in the combined group as compared with the control group (43.0 ± 7.0 versus 38.3 ± 7.0 minutes; $p = 0.001$). *Conclusion.* The combination material composed of resorbable meshed plate and cancellous bone allograft made reconstruction surgery of medial wall blowout fracture easier and quicker to perform with long-lasting results.

1. Introduction

Blowout fracture is defined as a fracture that involves the orbital walls, especially the medial wall and/or orbital floor [1]. It may be one of the most commonly encountered facial bone fractures by physicians because of the exposed position of the globe and the relatively thin properties of the orbital bone [2]. There have been numerous studies suggesting that the medial wall is the most commonly affected area among other types [3].

The management of medial wall blowout fracture remains controversial. Some surgeons suggest that small-sized defects are not a definite indication for operation. However, functional and aesthetic sequelae, such as diplopia or enophthalmos, could also occur as they do in orbital floor blowout fractures [4]. Therefore, if the patient presents with diplopia or enophthalmos and/or extensive fracture is observed in computed tomography (CT) images, then surgical reconstruction is recommended [2].

Various substances such as autogenous materials (e.g., autologous bone, cartilage, and fascia), allogenic materials, nonresorbable alloplastic materials (e.g., titanium, porous polyethylene, hydroxyapatite), and resorbable alloplastic materials (e.g., poly-L-lactic acid, polyglycolic acid, polyglactin,

composite polymers) can be used in the reconstruction of medial orbital wall fractures and defects [1, 5, 6]. Recently, resorbable alloplastic materials have become one of the most popular implant options because of their safety, simplicity, and effectiveness without donor site morbidities or permanent residues. However, debate remains about their long-term efficacy of enophthalmos prevention due to their resorbing nature.

Therefore, we attempted to evaluate a new surgical technique by using a resorbable meshed plate with allogenic cancellous bone. The flexible resorbable meshed plate was applied to enable easy insertion via a relatively small visual field of transcaruncular incision, while allogenic cancellous bone was chosen as a bone substitute because of not only its abilities for osteoconduction and osteoinduction but also for its elasticity and volume-filling effect that mimics the ethmoid sinus space.

For this study, we compared this new combination material with porous polyethylene sheeting, which is one of the most widely used permanent materials for the reconstruction of medial wall blowout fracture defects. We herein present our experience along with long-term follow-up results.

2. Patients and Methods

2.1. Ethical Statement. This study was approved by the institutional review board of the catholic university of Korea (no. UC16DISI0065). All data were analyzed anonymously and according to the principles set forth in the declaration of Helsinki (1975, revised in 2008).

2.2. Patients. From March 2014 to March 2017, a total of 273 patients with medial wall blowout fracture were enrolled. A thorough review of patients' past trauma and medical history, ophthalmic examinations including visual acuity, intraocular pressure, extraocular muscle function and other associated ocular complications was done. Fourty six patients were excluded according to the following criteria; age younger than 18 years, previous trauma history involving orbital bones, combined facial bone fractures including orbital floor, severe underlying diseases that could delay bone healing, bilateral fractures, and emergent ocular complications such as significant change in visual acuity, increased intraocular pressure, globe rupture and retrobulbar hemorrhage. As we performed the surgical intervention only when patients presented diplopia with evidence of extraocular muscle entrapment on CT scan, enophthalmos more than 2 mm, or fracture area size of more than 1 cm^2 in CT images, additional 74 patients were also excluded. Among the others, 89 patients received reconstruction surgery with porous polyethylene plates (control group) and the other 64 patients received operation with resorbable meshed plate plus allogenic cancellous bone (combined group). Because patients who underwent CT scan at least 12 months after their operation were evaluated, only 63 and 48 patients were ultimately included in this study, respectively.

2.3. Description of Reconstruction Materials. The following are two main elements of our new combination method.

First, the resorbable meshed plate implant used was Osteomesh™ (Osteopore International, Singapore), which is a bioresorbable implant often used in craniofacial surgery to fill surgical defects. It is made of polycaprolactone, which will degrade and resorb fully in vivo by hydrolysis and then is metabolized by the body over a period of 18 to 24 months. The mesh offers a rigid yet flexible scaffold with enough mechanical strength that supports bone in-growth. It degrades as bone regeneration and is replaced by autologous bone [7].

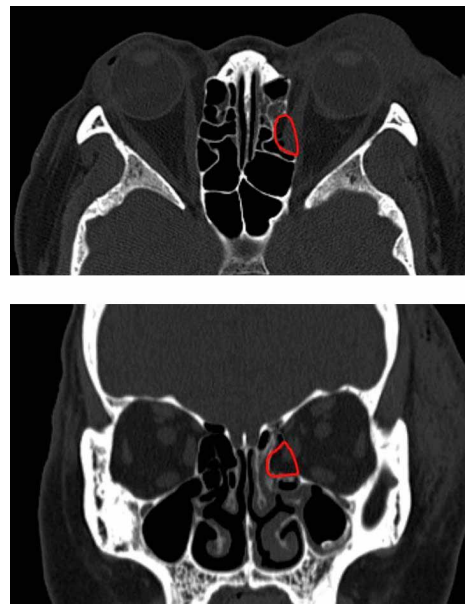

Figure 1: 3D shape of the defect was estimated based on CT images. Red line indicates the defect area to be replaced by cancellous bone allograft with inlay implantation method.

Second, the alloplastic cancellous bone used was Genesis Sponge™ (Hans Biomed Co., Seoul, Republic of Korea), a sponge-type allograft transplant material that employs the demineralized cancellous bone to induce proliferation of mesenchymal cells and osteoblast differentiation to help form normal bone. It is rapidly integrated into the recipient site and has high osteoconduction and osteoinduction properties. There are two types: block and chip. We used the former one to establish a three-dimensional (3D) structure of the defect easily [8].

In the operation room, the resorbable meshed plate was trimmed with scissors to exactly fit into the medial orbital wall defect. Then, the cancellous bone blocks were stacked upon the resorbable plate using fibrin glue after eight minutes of rehydration. The shape was sculpted according to the 3D structure of the fracture to fill the bony defect (Figure 1). The overall shape could be achieved by trimming with scissors without difficulty as the cancellous bone chips, once rehydrated, become soft as a sponge-like material. The resorbable plate and cancellous bone complex could be easily flexed and smoothly inserted through the small transcaruncular incision due to its high flexibility and elasticity (Figure 2).

2.4. Surgical Procedure. Under general endotracheal anesthesia, a transcaruncular incision was made to approach the medial wall of the orbit. Deep to the posterior lacrimal crest, a periosteal incision was performed and subperiosteal dissection was continued to expose the fracture site. After

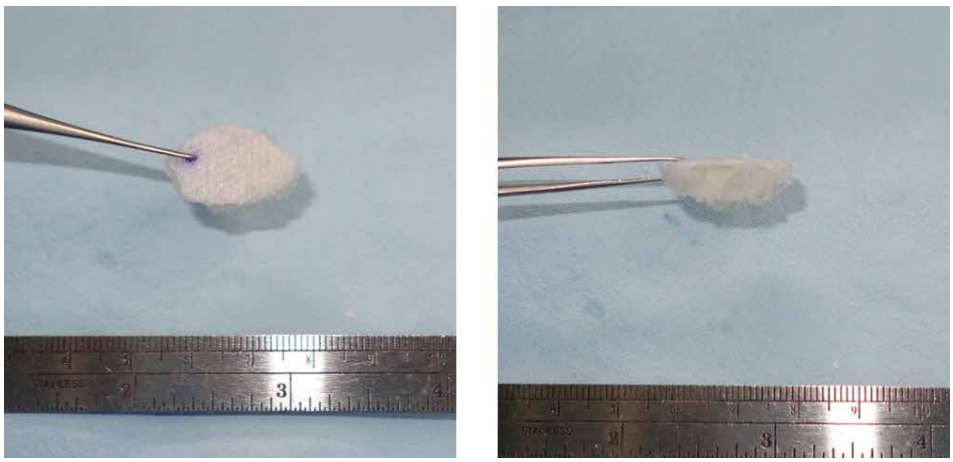

Figure 2: The reconstruction material used in the combined group was composed of resorbable meshed plate and allograft cancellous bone. Rehydrated bone sponge was sculpted according to the 3D shape of the defect based on CT images and was attached to the resorbable plate with fibrin glue.

nonvitalized bone segments were debrided, the anterior, cranial, caudal, and posterior margins of bony defect were identified.

For establishing an onlay graft using porous polyethylene sheeting, the dissection was continued slightly wider than the fracture margin, because it needs to be placed on the unfractured bone and secured. If the fracture was too large to expose all margins, at least three margins should be identified. Then, the polyethylene plate was trimmed and inserted.

In the combined group, the combination material described in the previous section was used. Because the cancellous bone was inserted into the ethmoidal sinus and the resorbable meshed plate was placed just fit to the defect, dissection over the fracture margins was not necessary. After visualization of the fracture area, the fabricated combination material was flexed using forceps and inserted into the defect. After the insertion, due to its elasticity, the combination material was automatically unfolded to fill in the orbital wall defect.

Forced duction test was performed to confirm no extraocular muscle or soft tissue entrapment after the implant insertion, and the mucosal closure was done with an absorbable suture.

2.5. Evaluation of Reconstruction Results. Pre- and postoperative clinical symptoms such as binocular visual acuity, discomfort during eyeball movement, extraocular muscle movement limitations, and diplopia were documented. Exophthalmometric measurements of both eyes were measured by hertel exophthalmometry and recorded.

All patients underwent 3D CT imaging obtained at a thickness of 1 mm for the evaluation of accurate fracture margin shape and bony defect. Postoperative CT scans were performed at 1, 3, 6, and 12 months from the surgery and images taken at least 12 months after the operation were evaluated for results. The mirror image of the patient's uninjured orbit was used as a criterion to estimate the postoperative width discrepancy. The imaginary medial wall was drawn in the coronal section of the affected orbit and the largest width difference was measured. Every coronal section of each patient was evaluated, and the highest value was selected (Figure 3). To assess the volume discrepancy, a picture-archiving communication system (PACS; Marosis m-view; Infinitt Healthcare, Seoul, Republic of Korea) with an automated region of interest was used. The calculation was done as previously described in other studies [9–12]. The area was measured by a freehand drawing cursor tracing the orbital wall in the axial section. The anterior margin of the orbit was defined as the line drawn from the anterior lacrimal crest of the maxilla to the lateral orbital rim. Volume was calculated by adding all the areas and multiplying them by the section thickness (1 mm in this study) (Figure 4). All width and volume discrepancy measurements were done twice by a single head and neck radiologist (Y. H.) and then the results were averaged to reduce measurement errors. Operation time from mucosal incision to skin closure was also recorded in all cases.

2.6. Statistical Analysis. The Statistical Package for the social sciences version 24.0 for windows software program (IBM Corp., Armonk, NY, USA) was used for statistical analysis. Mean data were analyzed with the independent samples t-test and categorical variables were evaluated by pearson's chi-square test. Statistical significance was set at $p \leq 0.05$.

3. Results

A total of 111 patients were enrolled in this study. 63 patients were assigned to the control group and the other 48 patients were placed in the combined group. The male to female ratios for each group was 2 : 1 versus 1.52 : 1 and the mean ages were 41.2 (range: 18–68) and 38.5 (range: 18–70) years, respectively. The mean follow-up periods were 19.3 months (range: 12–30) in the control group and 15.5 months (range: 12–22) in the combined group. Etiologies of the fractures included assault (43%), traffic accident (19%), fall (16%), sports injury (13%), and industrial injury (10%) in the control group, with values of 48%, 21%, 15%, 10%, and 6% for the same in the combined group, respectively. There were no statistically significant

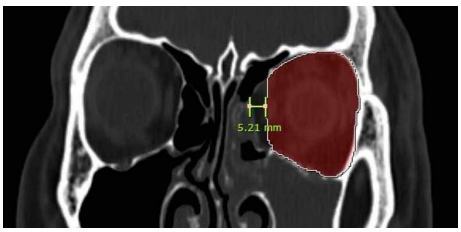

Figure 3: To evaluate width discrepancy, the mirror image of the patient's noninjured orbit was used as a criterion. The imaginary medial wall based on the mirror image of the patient's noninjured orbit was drawn and the highest width discrepancy was measured.

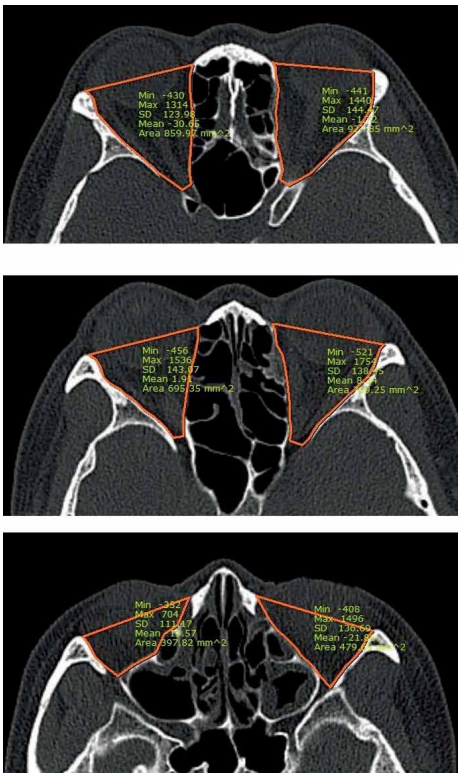

Figure 4: To calculate orbital volume discrepancy, the areas of both orbits were measured by image processing program and all areas were added and compared.

differences in male to female ratio, mean age and etiology between the two groups (Table 1).

All patients received a meticulous ophthalmic functional examination including measurement of visual acuity, intraocular pressure, extraocular muscle function and diplopia test, and exophthalmometry. Mean visual acuity in both groups were 0.87 ± 0.39 and 0.94 ± 0.45 by Landolt ring test ($p = 0.375$) and mean intraocular pressure were 14.24 ± 3.62 mmHg and 13.40 ± 3.67 mmHg, respectively ($p = 0.230$). A total of 16 patients presented extraocular movement dysfunction or diplopia in the control group (16/63, 25.40%) and 17 in the combined group (17/48, 35.42%), and this difference was not statistically significant ($p = 0.253$). Preoperative exophthalmometry discrepancy between the injured eye and the noninjured eye were 1.11 ± 0.69 mm and 1.19 ± 0.67 mm, respectively ($p = 0.505$).

Table 1: Summary of the enrolled patients' demographics ($p \leq 0.05$).

	Control group	Combined group	p value
Total number of patients	63	48	N/A
Male : Female	42 : 21 (2 : 1)	29 : 19 (1.53 : 1)	0.497
Mean age (years)	41.2 ± 14.8 (range: 18–68)	38.5 ± 16.9 (range: 18–70)	0.378
Mean follow-up (months)	19.3 (range: 12–30)	15.5 (range: 12–22)	N/A
Etiology (% (number))			0.302
Assault	43 (27)	48 (23)	
Traffic accident	19 (12)	21 (10)	
Fall	16 (10)	15 (7)	
Sports injury	13 (8)	10 (5)	
Industrial injury	10 (6)	6 (3)	

Based on preoperative CT images, the fracture area size was calculated in both groups. It was measured as $1.75 \pm 0.52\,cm^2$ in the control group and $1.85 \pm 0.66\,cm^2$ in the combined group and showed no significant difference ($p = 0.347$). These preoperative evaluations are summarized in Table 2.

Postoperative results were evaluated by exophthalmometry, CT images and the length of the operation time. Exophthalmometric measurements were obtained and compared at least 12 months after surgery. The discrepancy between the injured eye and the unaffected eye was 0.94 ± 0.70 mm in the control group and 1.05 ± 0.73 mm in the combined group. This showed no significant difference ($p = 0.425$). In the analysis of postoperative CT images, the highest width discrepancy between the reconstructed medial wall and the mirror image of the uninjured eye was evaluated. The findings were 1.55 ± 0.86 mm in the control group and 1.08 ± 0.69 mm in the combined group, and this showed a significant difference ($p = 0.003$). However, the volume discrepancy between the two groups demonstrated no statistically significant difference ($2.58 \pm 1.40\,cm^3$ versus $2.20 \pm 1.80\,cm^3$; $p = 0.209$). The length of the operation time was also recorded. As compared with the control group, operation time was significantly shorter (43.0 ± 7.0 versus 38.3 ± 7.0 minutes; $p = 0.001$) in the combined group. All postoperative results are demonstrated in Table 3.

No patients suffered from specific complications. Nine patients in the control group and seven in the combined group complained temporary diplopia after surgery but all symptoms resolved within 1 month. The other patients were discharged without complications and there were no permanent complications such as delayed diplopia, enophthalmos, and wound infection.

3.1. Case 1. A 27-year-old male patient visited the emergency department with left periorbital swelling due to a traffic accident. He complained of mild discomfort when he gazed bilaterally but no diplopia. In CT scan images, a $1.45\,cm^2$-sized fracture and bone defect were observed in the medial wall of the left orbit (Figure 5). At six days after injury, he

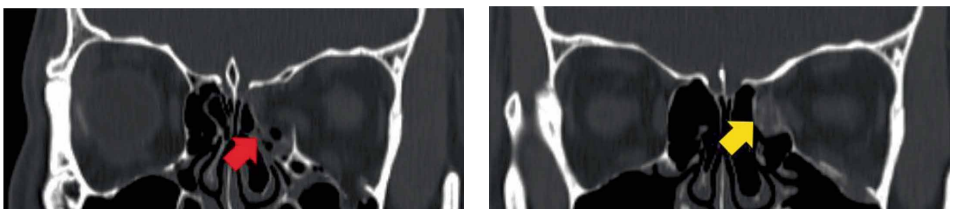

(a) (b)

Figure 5: CT images of the case 1 patient. Preoperative CT scan shows fracture and bone defect in the medial wall of the left orbit (a, red arrow). The orbital contents are well maintained inside the orbit by combination plate. Note the weak signal intensity of bone formation in the postoperative CT scan obtained at 12 months after operation (b, yellow arrow).

Table 2: Summary of the preoperative ophthalmic examinations ($p \leq 0.05$).

	Control group	Combined group	p value
Visual acuity	0.87 ± 0.39	0.94 ± 0.45	0.375
Intraocular pressure (mmHg)	14.24 ± 3.62	13.40 ± 3.67	0.230
Extraocular movement dysfunction/Diplopia (%)	25.40 (16/63)	35.42 (17/48)	0.253
Exophthalmometry discrepancy (mm)	1.11 ± 0.69	1.19 ± 0.67	0.505
Fracture area size (cm^2)	1.75 ± 0.52	1.86 ± 0.66	0.347

Table 3: Summary of the results (*$p \leq 0.05$).

	Control group	Combined group	p value
Exophthalmometry discrepancy (mm)	0.94 ± 0.70	1.05 ± 0.73	0.425
Width discrepancy (mm)	1.55 ± 0.86	1.08 ± 0.69	0.003*
Orbital volume discrepancy (cm^3)	2.58 ± 1.40	2.20 ± 1.80	0.209
Length of operation time (minutes)	43.0 ± 7.0	38.3 ± 7.0	0.001*

underwent operation with resorbable meshed plate and allogenic cancellous bone. After 12 months of follow-up, exophthalmometric measurement discrepancy between the affected and unaffected eyes was reduced from 2 to 0.5 mm. The CT images showed weak signal intensity of bone formation. The highest width discrepancy was 1.1 mm, and volume discrepancy was calculated as 1.8 cm^3. He presented no enophthalmos or other complications during the follow-up period.

3.2. Case 2. A 29-year-old male presented with diplopia upon his arrival at the emergency department. The fracture had occurred by fist injury and he was operated on two days after the assault with combined implant. Initial fracture area size was measured as 1.81 cm^2. The 15-month follow-up CT showed a well-reduced state with the highest width discrepancy being 1.06 mm and volume discrepancy being 0.8 cm^3 (Figure 6). He complained of no problems during the follow-up period except temporary diplopia, which resolved spontaneously within two weeks after surgery.

4. Discussion

Blowout fracture is one of the most frequently encountered facial bone fractures, although true incidence is unknown [2, 13]. Some studies have shown that the medial wall is the most commonly affected area in comparison with other parts of the orbit [3]. Rapid development in medical imaging technology over recent years, numbers of diagnosis and operations of medial wall blowout fractures have increased.

Various materials are available for the reconstruction of medial wall blowout fracture defects. Theoretically, using autologous bone is ideal, but it has many drawbacks such as donor site morbidity, unpredictability due to various degrees of resorption, limited availability, and patient refusal. These limitations have urged the development of alternative alloplastic materials. Nonresorbable plates such as porous polyethylene and titanium can be used as a second choice. However, they have limitations of a potential risk of infection and late presentation of extrusion. Impingement of soft tissues and the need for a relatively large incision were also disadvantages [4].

Resorbable materials are additionally available for filling the defect. They have the ability of supporting the orbital soft tissue from herniation and degradation by hydrolysis while leaving connective tissue in time. Their safety, simplicity, and effectiveness without donor site morbidity or permanent residue make them popular. However, a debate remains about their long-term efficacy because of their low strength and limited durability [1, 4].

To enhance the advantages of each material and compensate for their disadvantages, we decided to combine two materials. One is a flexible bioresorbable meshed plate and the other is alloplastic cancellous bone. We already reported our patients' data regarding orbital floor blowout fractures receiving operation with the combined materials [1]. We reconstructed a large orbital floor defect with the combination of a resorbable plate and artificial bone substitute in that study and obtained desirable results. However, when we applied this combination to medial wall blowout fracture defects, we confronted some problems. First, the resorbable plate was too rigid to pass through a transcaruncular incision. A transcaruncular incision is relatively small and there was a limit to the size of object

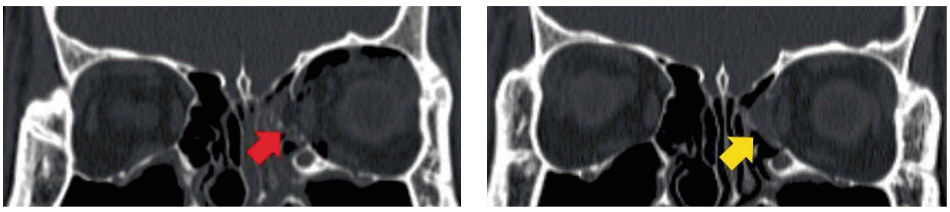

(a) (b)

Figure 6: CT images of the case 2 patient. Initial fracture and defect (a, red arrow) was well-reduced by a combination plate of resorbable meshed plate and allogenic bone substitute (b, yellow arrow).

able to be inserted. Second, for the same reason, dissection was limited for covering of the defect with this onlay-type implantation.

Therefore, we decided to change the resorbable plate from a rigid one to a flexible meshed plate. This could be flexed well with forceps grasping and, after passing the incision, it unfolded due to its elasticity. In addition, we applied alloplastic cancellous bone (Genesis Sponge™) for the inlay graft. After rehydration, it changed from a hard block into a sponge-like material. Therefore, it is simple to establish a 3D structure of the bone defect according to the preoperative CT images and easy to fold it to pass the small incision. As a result, this new combination enabled operators to insert the material easily due to folding capacity and, after insertion, it regained its original form because of elasticity. The cancellous bone unfolded according to the 3D structure of the bone defect and supported the resorbable plate to maintain its position—in other words, the plate acted as a cap. Therefore, surgeons were able to perform reduction surgery with less dissection using this inlay-type implantation method as compared with onlay grafting through a relatively limited visual field. This contributed to safer surgery without injury to the normal surrounding tissues and a reduction in operation time.

Furthermore, its long-term results were also desirable. As compared with the traditional method using polyethylene plates, there were no statistically significant differences in exophthalmometric measurement and postoperative volume discrepancy without notable complications. However, width discrepancy evaluation showed superior results versus polyethylene plate. This may be due to the elasticity of Genesis Sponge™. The nature of the resorbing process of grafted allogenic cancellous bone is not well-identified, but it maintained its initial position for at least three months in CT images according to our observations. Although not all bone substitutes formed new bone, the bony structure remained to support the resorbable plate to be successfully substituted by fibrous connective tissue in its original position, which we can identify in postoperative CT images (Figures 4 and 5). The medial wall of the orbit is a structure supported by many ethmoid air cells and multiple septa between them [14]. If the defect of the medial wall is covered by the onlay plates with septa left destroyed, the durability can be significantly decreased due to its structural instability. Hence, we used cancellous bone allograft (Genesis Sponge™) to act as the supporting material, like septa by reproducing its honeycomb structures, to push the orbital contents out from the ethmoid sinus, and maintain its structure for at least three months. This may make difference versus polyethylene plates. Nevertheless, width discrepancy did not lead to exophthalmometric measurement and postoperative volume differences in our study. While the volume values are different in various articles, an around 1.25 cm^3 increase in the orbital volume results in an increase in enophthalmos of 1 mm. This outcome may be because the amount of displacement of the orbital medial wall was too little to make a difference between the two groups in exophthalmometric measurement or orbital volume discrepancy [9, 15–18].

Various composite implants have been introduced to reconstruct orbital wall defects. The typical most commonly used material is titanium-reinforced porous polyethylene (e.g., Synpor®) [19, 20]. Titanium mesh offers high strength and stability, while polyethylene allows vascular component ingrowth into the pores with a smooth surface. However, its rigidity is a major limitation in the reconstruction of medial wall blowout fracture. Resorbable implants mixed with biological ceramics (e.g., hydroxyapatite) are also used [21, 22]. For example, Osteotrans™ is a resorbable implant composed of poly L-lactic acid and hydroxyapatite. It is provided in various shapes and it is widely used in the craniofacial reconstruction field. Although it can be a good option for the reconstruction of orbital floor defects, it is stiffer than other pure resorbable implants for the use in medial wall blowout fracture reconstruction. Newly synthesized products including bioactive glass [23], nylon foil [24], bone morphogenetic protein-loaded hydrogel [25], and bone marrow-coated polycaprolactone [26] have been introduced recently. However, most of them are still in experimental stages, need large scale studies and further rules and regulations in terms of safety. By combining the resorbable meshed plate and the alloplastic cancellous bone, our combination method has the advantages of each material with some degree of rigidity, flexibility, and elasticity. In addition to that, it can be easily trimmed into a desired shape and the safety of these materials has been already proven in various fields.

As mentioned above, the additional advantage of using our combination is shortened operation time. This may be due to no need for extensive dissection through a limited incision area. In the preliminary study, the surgery took more time with the combined plate because additional time was needed to fabricate. The fabrication process included hydration of the alloplastic cancellous bone, molding according to the 3D structure of the defect, and fixating the bone to the meshed plate. However, an assistant made the combined plates based on preoperative CT images, while the dissection was done by

the operator simultaneously and, as the assistant practiced more and more, the time for fabrication was shortened and the final operation time in the combined group was shorter than that in the control group. With a more trained assistant or 3D printing technology in the future, further shortening of the operation time will be able to be achieved.

Despite the excellent properties of resorbable plates and bone allografts, the materials are expensive. Therefore, the cost-effectiveness of our combination can be a burden to patients involved. Another major drawback of our technique is that it is limited to only medial wall blowout fracture reconstruction. Our combination materials are designed to fill into the bony defect formed by ethmoid air cells. Therefore it is not applicable in cases of blowout fractures involving the inferomedial wall or the floor. In such cases, other materials should be used instead.

In conclusion, reconstruction of orbital medial wall fracture with resorbable meshed plate and cancellous bone allograft can provide long-lasting results without significant complications. Furthermore, this technique allows not only orbital reconstruction through a relatively small incision but also effective reconstruction of large bony defects with ease and shorter operation times. We, therefore, propose this new surgical technique as an effective alternative method for orbital medial wall reconstruction.

Data Availability

The data used to support the findings of this study are included within the article.

Conflicts of Interest

None of the authors have any financial interest in this research project or any of the techniques, products, devices, or drugs mentioned in this manuscript.

References

[1] H. Kwon, H. J. Kim, B. F. Seo, Y. J. Jeong, S.-N. Jung, and H.-S. Shim, "The role of resorbable plate and artificial bone substitute in reconstruction of large orbital floor defect," *Biomed Research International*, vol. 2016, Article ID 1358312, 6 pages, 2016.

[2] L. Dubois, S. A. Steenen, P. J. Gooris, M. P. Mourits, and A. G. Becking, "Controversies in orbital reconstruction–I. Defect-driven orbital reconstruction: a systematic review," *International Journal of Oral and Maxillofacial Surgery*, vol. 44, no. 3, pp. 308–315, 2015.

[3] K.-E. Choi, J. Lee, H. Lee, M. Chang, M. Park, and S. Baek, "The paradoxical predominance of medial wall injuries in blowout fracture," *Journal of Craniofacial Surgery*, vol. 26, no. 8, pp. e752–e755, 2015.

[4] Y.-H. Kim, Y. Park, and K. J. Chung, "Considerations for the management of medial orbital wall blowout fracture," *Archives of Plastic Surgery*, vol. 43, no. 3, pp. 229–236, 2016.

[5] L. Dubois, S. A. Steenen, P. J. Gooris, R. R. Bos, and A. G. Becking, "Controversies in orbital reconstruction-III. Biomaterials for orbital reconstruction: a review with clinical recommendations," *International Journal of Oral and Maxillofacial Surgery*, vol. 45, no. 1, pp. 41–50, 2016.

[6] D. R. Gunarajah and N. Samman, "Biomaterials for repair of orbital floor blowout fractures: a systematic review," *Journal of Oral and Maxillofacial Surgery*, vol. 71, no. 3, pp. 550–570, 2013.

[7] Osteopore International, "Osteomesh™," 2018, https://www.osteopore.com/osteomesh.html.

[8] Hans Biomed, "Genesis Sponge™," 2018, https://www.hansbiomed.com/kr/product/allograft/bone_genesis_sponge.asp.

[9] H. B. Ahn, W. Y. Ryu, K. W. Yoo et al., "Prediction of enophthalmos by computer-based volume measurement of orbital fractures in a Korean population," *Ophthalmic Plastic & Reconstructive Surgery*, vol. 24, no. 1, pp. 36–39, 2008.

[10] H. H. Han, S. W. Park, and S.-H. Moon, "Comparative orbital volumes between a single incisional approach and a double incisional approach in patients with combined blowout fracture," *Biomed Research International*, vol. 2015, Article ID 982856, 6 pages, 2015.

[11] J. Kwon, J. E. Barrera, T.-Y. Jung, and S. P. Most, "Measurements of orbital volume change using computed tomography in isolated orbital blowout fractures," *Archives of Facial Plastic Surgery*, vol. 11, no. 6, pp. 395–398, 2009.

[12] J. Ye, K. H. Kook, and S. Y. Lee, "Evaluation of computer-based volume measurement and porous polyethylene channel implants in reconstruction of large orbital wall fractures," *Investigative Opthalmology & Visual Science*, vol. 47, no. 2, pp. 509–513, 2006.

[13] M. Choi and R. L. Flores, "Medial orbital wall fractures and the transcaruncular approach," *Journal of Craniofacial Surgery*, vol. 23, no. 3, pp. 696–701, 2012.

[14] W. K. Song, H. Lew, J. S. Yoon, M.-J. Oh, and S. Y. Lee, "Role of medial orbital wall morphologic properties in orbital blow-out fractures," *Investigative Opthalmology & Visual Science*, vol. 50, no. 2, pp. 495–499, 2009.

[15] X. Fan, J. Li, J. Zhu, H. Li, and D. Zhang, "Computer-assisted orbital volume measurement in the surgical correction of late enophthalmos caused by blowout fractures," *Ophthalmic Plastic & Reconstructive Surgery*, vol. 19, no. 3, pp. 207–211, 2003.

[16] O. Ploder, C. Klug, M. Voracek et al., "A computer-based method for calculation of orbital floor fractures from coronal computed tomography scans," *Journal of Oral and Maxillofacial Surgery*, vol. 59, no. 12, pp. 1437–1442, 2001.

[17] E. M. Raskin, A. L. Millman, V. Lubkin, R. C. Delia Rocca, R. D. Lisman, and E. A. Maher, "Prediction of late enophthalmos by volumetric analysis of orbital fractures," *Ophthalmic Plastic & Reconstructive Surgery*, vol. 14, no. 1, pp. 19–26, 1998.

[18] R. W. Whitehouse, M. Batterbury, A. Jackson, and J. L. Noble, "Prediction of enophthalmos by computed tomography after 'blow out' orbital fracture," *British Journal of Ophthalmology*, vol. 78, no. 8, pp. 618–620, 1994.

[19] C. Y. Kim, B. J. Jeong, S. Y. Lee, and J. S. Yoon, "Comparison of surgical outcomes of large orbital fractures reconstructed with porous polyethylene channel and porous polyethylene titan barrier implants," *Ophthalmic Plastic and Reconstructive Surgery*, vol. 28, no. 3, pp. 176–180, 2012.

[20] M. Y. Peng, S. L. Merbs, M. P. Grant, and N. R. Mahoney, "Orbital fracture repair outcomes with preformed titanium mesh implants and comparison to porous polyethylene coated

titanium sheets," *Journal of Cranio-Maxillofacial Surgery*, vol. 45, no. 2, pp. 271–274, 2017.

[21] T. Morotomi, K. Matsunaga, H. Kusuhara et al., "Long-term result of a biodegradable osteo-inductive copolymer for the treatment of orbital blowout fracture," *Journal of Cranio-Maxillofacial Surgery*, vol. 42, no. 5, pp. 443–447, 2014.

[22] C. Landes, A. Ballon, S. Ghanaati, A. Tran, and R. Sader, "Treatment of malar and midfacial fractures with osteoconductive forged unsintered hydroxyapatite and poly-L-lactide composite internal fixation," *Journal of Oral and Maxillofacial Surgery*, vol. 72, no. 7, pp. 1328–1338, 2014.

[23] M. Peltola, I. Kinnunen, and K. Aitasalo, "Reconstruction of orbital wall defects with bioactive glass plates," *Journal of Oral and Maxillofacial Surgery*, vol. 66, no. 4, pp. 639–646, 2008.

[24] D. J. J. Park, D. C. Garibaldi, N. T. Iliff, M. P. Grant, and S. L. Merbs, "Smooth nylon foil (SupraFOIL) orbital implants in orbital fractures: a case series of 181 patients," *Ophthalmic Plastic & Reconstructive Surgery*, vol. 24, no. 4, pp. 266–270, 2008.

[25] M. W. Betz, J. F. Caccamese, D. P. Coletti, J. J. Sauk, and J. P. Fisher, "Tissue response and orbital floor regeneration using cyclic acetal hydrogels," *Journal of Biomedical Materials Research Part A*, vol. 90A, no. 3, pp. 819–829, 2009.

[26] D. Rohner, D. W. Hutmacher, T. K. Cheng, M. Oberholzer, and B. Hammer, "In vivo efficacy of bone-marrow-coated polycaprolactone scaffolds for the reconstruction of orbital defects in the pig," *Journal of Biomedical Materials Research*, vol. 66B, no. 2, pp. 574–580, 2003.

Hindawi
BioMed Research International
Volume 2019, Article ID 4040236, 27 pages
https://doi.org/10.1155/2019/4040236

Review Article

Current Trends in the Evaluation of Osteochondral Lesion Treatments: Histology, Histomorphometry, and Biomechanics in Preclinical Models

M. Maglio, S. Brogini, S. Pagani, G. Giavaresi, and M. Tschon

IRCCS-Istituto Ortopedico Rizzoli, Laboratory of Preclinical and Surgical Studies, via di Barbiano 1/10, 40136 Bologna, Italy

Correspondence should be addressed to S. Brogini; silvia.brogini@ior.it

Received 4 July 2019; Revised 23 August 2019; Accepted 5 September 2019; Published 9 October 2019

Academic Editor: Jiang Du

Osteochondral lesions (OCs) are typically of traumatic origins but are also caused by degenerative conditions, in primis osteoarthritis (OA). On the other side, OC lesions themselves, getting worse over time, can lead to OA, indicating that chondral and OC defects represent a risk factor for the onset of the pathology. Many animal models have been set up for years for the study of OC regeneration, being successfully employed to test different treatment strategies, from biomaterials and cells to physical and biological adjuvant therapies. These studies rely on a plethora of post-explant investigations ranging from histological and histomorphometric analyses to biomechanical ones. The present review aims to analyze the methods employed for the evaluation of OC treatments in each animal model by screening literature data within the last 10 years. According to the selected research criteria performed in two databases, 60 works were included. Data revealed that lapine (50% of studies) and ovine (23% of studies) models are predominant, and knee joints are the most used anatomical locations for creating OC defects. Analyses are mostly conducted on paraffin-embedded samples in order to perform histological/histomorphometric analyses by applying semi-quantitative scoring systems and on fresh samples in order to perform biomechanical investigations by indentation tests on articular cartilage. Instead, a great heterogeneity is pointed out in terms of OC defect dimensions and animal's age. The choice of experimental times is generally adequate for the animal models adopted, although few studies adopt very long experimental times. Improvements in data reporting and in standardization of protocols would be desirable for a better comparison of results and for ethical reasons related to appropriate and successful animal experimentation.

1. Introduction

The treatment of osteochondral (OC) defects is still a great challenge in the orthopaedic field. Whatever the triggering cause of OC lesion formation is (osteonecrosis, osteoarthritis, sports-related injuries, and chronic overload), the progression of the lesion leads to the destruction of the normal architecture of the affected district, both in the cartilaginous component and in the subchondral bone, further aggravating the pathological picture of osteoarthritis, if already present or promoting its onset. Consequently, the functionality of the affected joint is compromised by mechanical and tribological alterations which, in the final stage, can require invasive surgical approach up to total joint replacement [1].

It is difficult to give precise numbers about the incidence of OC lesions; however, it has been observed that in about 60% of patients undergoing various types of knee surgery, it is possible to find OC lesions, frequently in the medial femoral condyle and usually involving subchondral bone [2]. Moreover, these lesions also characterize the idiopathic process of osteochondritis dissecans, which can occur from childhood through adult life in approximately 15 to 29 per 100,000 patients and for which a number of possible causes has been reported including repetitive microtrauma, vascular abnormalities, and genetic predisposition [3, 4]. The deep and well-known structural, biochemical, and biomechanical differences between cartilage and subchondral bone have prompted much of the past research in the regeneration of each compartment separately. However,

cartilage and subchondral bones are biologically and functionally linked, influencing each other physiologically and pathophysiologically to form what is considered the OC unit [5].

The observation of the OC unit detects a complex system, with great variations in terms of functions and architecture, with a progressive heterogeneity of cellular component, aggrecan presence, collagen types and contents, and cartilage fibrils thickness, starting from the articular surface up to the bone. The biomechanical skills of the districts are closely related to the mutual interaction between the various parts of the OC unit. Articular cartilage is mainly responsible for absorbing impacts, but the ability to manage weight bearing and load is strengthened by subchondral bone, also because of its key role in providing nutrition to cartilage [6].

Consequently, the complexity of the OC unit makes the approach to the setup of regenerative medicine studies quite demanding. The use of multilayered and bi/triphasic scaffolds tries to address the need to restore the functionality of this district, considering both bony and cartilaginous features and the strict dependence between chondral and subchondral status. In the last years, the combination of such scaffolds with cells from different sources seemed to be a promising approach, exploiting the ability of stem cells to differentiate towards different lineages without immunogenic effects [7].

A wide variety of animal models are employed in this research field, and the most common anatomical site in which OC lesions are created is the stifle joints (both medial and lateral condyles and trochlea). The correct dimensions of such defects, in order to obtain a lesion which cannot spontaneously heal but which, at the same time, is not so wide as to affect the effectiveness of the treatment, are still a topic of discussion. In the literature, for each animal model, lesions of very different dimensions are found, involving or not the subchondral bone. Such a variety of in vivo protocols makes it difficult to establish a standard model as well as to compare results from different studies, also because the posttreatment evaluations can vary a lot among studies [8]. The complexity of the OC district gives the possibility of using a large number of assessments, ranging from histological stains specific for bone and cartilage to specific markers for cartilage regeneration/degeneration, new bone formation, mineralization status etc. As for any regenerative medicine study, even those related to OC regeneration may be enriched by biomechanical assessments. Although these are generally destructive tests and therefore require a greater number of animals if they are to be combined with histological evaluations, their use is fundamental for an assessment of the quality of the regenerated tissue. It appears particularly important considering that OC lesions are generally located in joints subjected to mechanical loading, so that the resumption of a correct mechanical competence is essential to define the success of a treatment [9].

To have an overview about the current trend for the evaluation of treatments for OC regeneration, the recent literature about in vivo models of OC defects were reviewed, focussing on the assessments performed in terms of histological, histomorphometrical, and biomechanical evaluations.

2. Methods

2.1. Descriptive Systematic Literature Review. This systematic review was carried out according to PRISMA guidelines. Electronic database searches were performed on http://www.pubmed.com and http://www.webofknowledge.com to identify studies reporting the following key terms: (osteochondral scaffold OR osteochondral biomaterial OR osteochondral regeneration OR osteochondral tissue engineering OR osteochondral defect OR osteochondral lesion) AND (biomechanics OR biomechanical evaluation OR biomechanical test OR histomorphometric evaluation OR histomorphometric analysis OR histomorphometric test OR histomorphometry). Study eligibility was independently determined by reviewing titles and abstracts using the following inclusion criteria: preclinical studies of any level of evidence, full text, English language, and reports published from April 2009 to April 2019. Exclusion criteria were articles not in English, reviews, not in vivo studies, papers not reporting histological, histomorphometric, or biomechanical assessments, papers involving only chondral lesions, and duplicate papers. Three independent researchers performed both the screening step and subsequent data extraction (MM, SB, and MT).

2.2. Data Extraction and Management. From all studies, specific data related to the adopted experimental animal model (type and number of animals), experimental setup (site of implant, OC lesion dimension, and experimental time), type of treatment, performed histological/histomorphometric and biomechanical evaluations, and main results were extracted (Tables 1 and 2).

3. Results

3.1. Literature Results. The a priori search retrieved 149 articles from http://www.pubmed.com and 188 from http://www.webofknowledge.com. After screening, several articles (224) were excluded: 27 were clinical studies, 75 were not in vivo (in vitro and ex vivo studies, cadaveric studies), 52 were reviews, 6 did not report histological, histomorphometric, and biomechanical evaluations, and 64 were not related to the research (chondral only implants, ectopic implants, and mathematical models). Therefore, a total of 113 papers were recognized eligible for the review and after the use of a public reference manager (Mendeley 1.19.3) to eliminate duplicate articles; 60 papers remained: 33 performed in small-medium animal models (rodent and lapine) and 27 in large animal models (canine, swine, equine, and ovine) (Figure 1).

3.2. Rodent Model. Among the retrieved papers, three evaluated the osteochondral tissue regeneration of the joint by adopting a rat animal model. All papers selected the same anatomical site of implant in the trochlear groove, had

Table 1: Data extraction of papers involving small-medium animal models.

Experimental model	Anatomical site (defect dimension) and experimental time	Osteochondral treatment	Histological, histomorphometric, and biomechanical methods	Main outcomes	Author
Rodent model					
Fifty-five rats (6 weeks old)	Cartilage defect (2 mm Ø and 1 mm depth) in the patellar groove for 1 and 2 months	Bilayered collagen scaffold with or without hESC-MSC	(i) ICRS score (ii) Paraffin embedding (iii) H&E and Safranin O stainings (iv) Indentation test on fresh explants submerged in PBS: Young's equilibrium modulus	Similar trends between the histomorphometric score and biomechanical analysis	Zhang et al. [10]
Nine male athymic nude rats (11 weeks old)	Critical-size defects in the trochlear groove (1.4 mm Ø and 1 mm depth) for 2 months	Micromasses of hPDCs with or without TGF-β1	(i) Paraffin embedding (ii) Alcian Blue staining (iii) IHC: Col I, Col II, nuclei, and lubricin (iv) MicroCT: BV/TV, Tb.Th., Tb.Sp., and Tb.N.	MicroCT showed heterogeneous regeneration across the defects	Mendes et al. [11]
Fifty male Wistar rat (4 months old)	Defects in the trochlear groove (1.5 mm Ø and 1.5 mm depth) for 2 months	MeHA hydrogel seeded with MSCs or chondrogenically primed MSCs cultivated either free loading or dynamically compressed	(i) Paraffin embedding (ii) Wakitani score (iii) Safranin O staining (iv) IHC: Col II	Dynamic compression and chondrogenic priming synergistically improved regenerative properties of MSCs	Lin et al. [12]
Lapine model					
Twelve young adult NZW rabbits	Defects in the weight-bearing areas of femoral condyles (4 mm of chondral defect followed by a 2 mm hole in the centre of the 4 mm defect) for 3 months	ADM alone (rabADM) or in association with IPFP-MSCs (cells + rabADM)	(i) Paraffin embedding HC: Col I and II (ii) Quantification of the total area of cartilage repair by 2D analysis	Significant differences in type II collagen staining	Ye et al. [13]
Ten NZW male rabbits (5 months old)	Defects in the medial femoral condyles (4 mm Ø and 4 mm depth) for 40 days	Collagen scaffold alone or seeded with rabbit BMC; half of the animals stimulated by PEMFs	(i) Niederauer score (ii) Paraffin embedding (sagittal cut) (iii) Safranin-O/fast green staining (iv) Modified O'Driscoll score quantification of new cartilaginous tissue over and under the tidemark	Significant effects in Niederauer and O'Driscoll scores and in percentage of cartilage	Veronesi et al. [14]

Table 1: Continued.

Experimental model	Anatomical site (defect dimension) and experimental time	Osteochondral treatment	Histological, histomorphometric, and biomechanical methods	Main outcomes	Author
Twelve female skeletally mature NZW rabbits	Defects in the central medial femoral condyles (3.5 mm Ø and 2 mm depth) for 1.5 months	Bilayered collagen type I/III scaffold seeded with either culture-expanded allogenic chondrocytes (ACI-CHDR) or synovium-derived stem cells (ACI-SMSC)	(i) ICRS subscore and OARSI score (ii) Paraffin embedding (sagittal cut) (iii) H&E and Safranin O staining (iv) IHC: Col II, X (Remmele–Stegner score) (v) Indentation test on fresh samples: cartilage thickness, instant modulus, and shear modulus	Similar trends among instantaneous and shear modulus and OARSI score	Schmal et al. [15]
Sixteen male NZW rabbits (34 weeks old)	Defects in the patellar groove (3 mm Ø and 2–2.5 mm depth) for 3 months	3-dimensional constructs fabricated using Col II hydrogel alone (Col II) or associated with auricular chondrocytes (AU-Col II)	(i) Modified ICRS score (ii) Paraffin embedding (sagittal cut) (iii) H&E, Masson's trichrome, and Alcian Blue stainings	Significance in histological scores and defect healing	Wong et al. [16]
Ten male NZW rabbits (10 months old)	Full-thickness cartilage defects in the patellar groove (4 mm in Ø and 3 mm in depth) for 3 weeks	Autologous BMSCs seeded on type I collagen scaffold in association or not with LLLT	(i) Paraffin embedding (sagittal cut) (ii) H&E staining (iii) Quantification of new cartilage formation, new bone formation%, measure of inflammation	No significant difference in new cartilage formation and inflammation; significance in new bone formation	Fekrazad et al. [17]
48 NZW rabbits (6–8 months old)	Defects in the trochlear groove (4 mm Ø and 3 mm depth) for 3 and 9 months	Regenerated silk fibroin scaffold alone (SF) or seeded with autologous chondrocytes (SFC); fibrin glue containing autologous chondrocytes (FGC)	(i) Wakitani score (ii) Paraffin embedding (sagittal cut) (iii) Modified O'Driscoll, Keeley and Salter score (iv) H&E, Alcian Blue and Masson's trichrome stainings (v) IHC: Col II (vi) Indentation test on fresh samples: ultimate compressive strength (UCS) and compressive Young's modulus	Significant differences in histological scores but not in biomechanical data	Kazemnejad et al. [18]

Table 1: Continued.

Experimental model	Anatomical site (defect dimension) and experimental time	Osteochondral treatment	Histological, histomorphometric, and biomechanical methods	Main outcomes	Author
Twenty-eight female skeletally mature NZW rabbits	Defects in the medial femoral condyle (4 mm Ø and 5 mm depth) for 13 weeks	Autologous BMP-2-activated muscle tissue directly implanted into OC lesions	(i) Paraffin embedding (ii) Extended O'Driscoll score (iii) Safranin O/fast green stainings (iv) IHC: Col I and II (v) Quantification of bone area within the subchondral defect (v) Indentation test on fresh samples: stiffness	Similar trends between the bone area quantification and biomechanics	Betz et al. [19]
Forty-one skeletally mature NZW rabbits	Full-thickness defects in the femoral groove (5 mm Ø and 6 mm depth) for 1, 2, and 6 months	Combined material comprising a scaffold-free tissue-engineered construct (TEC) derived from synovial mesenchymal stem cells and hydroxyapatite (HA) artificial bone (TEC-HA) Control group: HA artificial bone	(i) Paraffin embedding (ii) O'Driscoll score (iii) H&E and Toluidine Blue staining (iv) Microindentation test (at 6 months): stiffness	Significance in the histological score but not in biomechanics	Shimomura et al. [20]
Nine skeletally mature male NZW rabbits	Defects in the medial femoral condyles (2.7 mm Ø and 4.0 mm depth) for 6.5 months	(i) Poly(1,8-octanediol-co-citrate) (POC) with 60 weight % hydroxyapatite nanocrystals (POC-HA) (ii) Poly-L-lactide (PLL)	(i) Paraffin embedding (longitudinal cut) (ii) Niederauer score (iii) Masson–Goldner trichrome staining (iv) Quantification of total area and range of depth of tissue ingrowth, active osteoid surface area/total trabecular bone surface area, total osteoid surface area/total trabecular bone surface area, and trabecular bone surface area/total tissue area (v) Measurement of fibrous capsule widths	No significant differences in all histomorphometric evaluations	Chung et al. [21]

Table 1: Continued.

Experimental model	Anatomical site (defect dimension) and experimental time	Osteochondral treatment	Histological, histomorphometric, and biomechanical methods	Main outcomes	Author
Seven male and female NZW rabbits (13 or 32 months old)	Defects in the trochlear groove (1.5 mm Ø and 2 mm depth drill holes) for 70 days	(i) 10 kDa chitosan/ blood implant with fluorescent chitosan tracer (ii) 40 kDa chitosan/ blood implant with fluorescent chitosan tracer	(i) Modified O'Driscoll score (ii) Paraffin embedding (sagittal cut) (iii) SafO staining (iv) IHC: Col I and II (v) Quantification of total chondral repair tissue area, (including bone overgrowth); percentage SafO, Col-1- or Col-2-positive-stained tissue (excluding bone overgrowth) (vi) MicroCT on fresh samples: Residual hole depth and residual hole area below the surface	Significant differences in bone morphometry and O'Driscoll scores	Guzmán-Morales et al. [22]
Five male and female NZW rabbits (30-months old)	Defects in the trochlea (microdrill hole defects, 1.4 mm Ø, and 2 mm depth) for 1 and 21 days	150, 40, and 10 kDa chitosan solutions, mixed with autologous rabbit whole blood and clotted with tissue factor	(i) MicroCT on fresh samples: residual hole depth and residual hole area below the surface (ii) Paraffin embedding (sagittal cut) (iii) SafO staining (iv) IHC: Col I and II (v) Quantification of GAG, col I or col II (%); distribution of repair tissues in treated defects and volume density of neutrophils and stromal cells (vi) TRAP quantification	Significant differences in microCT, GAG, col II, and col I quantifications and volume density of neutrophils	Lafantaisie-Favreau et al. [23]
Twenty NZW rabbits (18 weeks old)	Defects in the weight-bearing area of medial femoral condyles (3 mm Ø and 3 mm depth) for 2 weeks and 1, 2, and 4 months	Allogeneic scaffold-free bioengineered chondrocyte pellet (BCP)	(i) Paraffin embedding (sagittal cut) (ii) Modified O'Driscoll score (iii) H&E, Safranin O/ fast green staining (iv) IHC: Col I and II, type I and type II (v) PCNA stainings (vi) Quantification of % area filled in defect, cartilage thickness, and bone area	Significant differences in the score and cartilage thickness	Cheuk et al. [24]

Table 1: Continued.

Experimental model	Anatomical site (defect dimension) and experimental time	Osteochondral treatment	Histological, histomorphometric, and biomechanical methods	Main outcomes	Author
Forty NZW rabbits (12–15 months old)	Defects in the weight-bearing area of medial femoral condyles (2 mm Ø with 1–1,5 mm depth) for 2 and 4 months	Osteochondral defect (acute osteoarticular injury)	(i) Paraffin embedding (sagittal cut) (ii)Manking score (iii) Safranin O/fast green staining (iv) Sagittal-plane laxity measurement (at 8 and 16 weeks) (v) Contact stress test on 7 fresh cadaver knees	Significance in the histological score	Vaseenon et al. [25]
Fourty-two adult male NZW rabbits	Defects in the patellar groove (4 mm Ø and 3.5–4 mm depth) for 1.5 and 3 months	Bilayered microporous scaffold with collagen and electrospun poly-L-lactic acid nanofibers (COL-nanofiber) and bilayer COL scaffold, seeded with BMSCs	(i) ICRS score (ii) Paraffin embedding (iii) H&E and Safranin O/fast green staining (iv) Indentation test (at 12 weeks): Young's moduli on fresh samples placed in PBS at room temperature before testing. (v) microCT: subchondral bone	Similar trend between histological scoring system and biomechanical test	Zhang et al. [26]
Nine female NZW rabbits (6 months old)	Defects in the medial femoral condyle (4 mm Ø and 4 mm depth) for 3 months	(i) 70/30 poly(ethylene oxide terephthalate)/ poly(butylene terephthalate) (PEOT/ PBT) scaffold (ii) 55/45 PEOT/PBT	(i) Histological scoring system (O'Driscoll score) on 2-hydroxyethyl methacrylate (Technovit) embedded samples (thionine staining) (midsagittal cut)	Significance in the histological scoring system	Jansen et al. [27]
Forty-eight NZW rabbits (7 months old)	Defects in the patellar groove (5 mm Ø and 10 mm depth) for 2 weeks and 1, 2, and 4 months	OC defects treated with low-level He-Ne laser therapy (LLLT) 3 times a week	(i) Paraffin embedding (sagittal cut) (ii) H&E, Toluidine Blue staining (iii) Pineda score	Significant acceleration of healing at 4 and 6 weeks	Bayat et al. [28]
20 adult male NZW rabbits	Defects in the femoral epiphysis (6 mm Ø and 8 mm depth) for 2 months	Mineralized HA-alginate scaffold compared to a commercially available collagen-hydroxyapatite composite scaffold	(i) Niederauer score (ii) PMMA embedding (sagittal cut) (iii) Stevenel Blue/van Gieson pichrofucsin staining (iv) Quantification of MAR and BFR (v) MicroCT on fresh samples: defect BV/ TV; defect Tb.Th.; defect Tb.N.; defect Tb.Sp.; peri-implant BV/TV; peri-implant Tb.Th., Tb.N., and Tb.Sp.	Significance in microCT evaluations and not in dynamic morphometric analyses	Filardo et al. [29]

Table 1: Continued.

Experimental model	Anatomical site (defect dimension) and experimental time	Osteochondral treatment	Histological, histomorphometric, and biomechanical methods	Main outcomes	Author
Sixty skeletally immature male NZW rabbits (3 months old)	Full-thickness defects in the trochlear groove (4 mm Ø and 4 mm depth) for 2 and 9 months	Autogenous periosteal grafts under the influence of (i) group a— active intermittent motion (AIM), euthanized at 8 weeks; group B— continuous passive motion (CPM), euthanized at 8 weeks; group C—AIM, euthanized at 36 weeks; (ii) Group D—CPM, euthanized at 36 weeks	(i) Indentation test on fresh samples: elastic stiffness (ii) paraffin embedding (sagittal cut) (iii) O'Driscoll score (iv) H&E, Masson trichrome, and Alcian Blue staining (v) Quantification of thickness and area of the regenerated tissue; thickness of the normal cartilage surrounding the defect	Significance in thickness of regenerated tissue and in elastic stiffness	Martin-Hernandez et al. [30]
Forty-two male NZW rabbits (7 months old)	Full-thickness defects in the patellar groove (5 mm Ø and 10 mm depth) for 2 and 1, 2, and 4 months	OC defects treated with low-level He-Ne laser therapy (LLLT) 3 times a week	(i) Indentation test on previously frozen samples: instantaneous stiffness, maximum force, equilibrium load, and energy absorption	Significance only in the energy absorption	Javadieh et al. [31]
Twenty mature female NZW rabbits	Defects in the medial femoral condyle (2.5 Ø and 3 mm depth) for 1, 2, and 3 months	OC defects treated with low-dose irradiation	(i) Paraffin embedding (ii) O'Driscoll score (iii) H&E and Safranin O staining (iv) Indentation test on previously frozen samples: cartilage stiffness	No statistical significance was seen in any parameter	Öncan et al. [32]
Thirty-four male NZW rabbits	Full-thickness defects in the medial and lateral femoral condyles (3 mm Ø and 3 mm in depth) for 6 and 12 weeks	Poly(lactic-co-glycolic acid) with or without fibrin as cells carrier: (i) PLGA/Fibrin/ BMSCs (PFC group) (ii) PLGA/BMSCs (PC group)	(i) ICRS score (ii) Paraffin embedding (iii) H&E; Alcian Blue; Safranin O staining (iv) IHC: Col II (v) Cartilage-specific gene expression (vi) Quantification of sGAG (v) Compression test (at 12 weeks)	Similar significant trends in histological score, GAG content and biomechanical strength	Rahman et al. [33]

Table 1: Continued.

Experimental model	Anatomical site (defect dimension) and experimental time	Osteochondral treatment	Histological, histomorphometric, and biomechanical methods	Main outcomes	Author
Thirty-five skeletally mature NZW rabbits (24 weeks old)	Full-thickness defects in the patellar groove (5 mm Ø and 6 mm depth) for 1, 2, and 6 months	(i) Combined material: bTCP-based hybrid implant coupled with a scaffold-free tissue-engineered construct (TEC) derived from synovial mesenchymal stem cells (TEC/bTCP) (ii) Scaffold-free tissue-engineered construct (TEC) derived from synovial mesenchymal stem cells and hydroxyapatite (HA) artificial bone (TEC/HA)	(i) Histological grading system (resurfacing: 0–2) for gross examination (ii) Paraffin embedding (iii) Modified O'Driscoll score (iv) H&E and Toluidine Blue staining (v) Microindentation test: tissue stiffness	Similar trends among cellular morphology, total histological score, and biomechanics	Shimomura et al. [34]
Five NZW rabbits (5–6 months old)	Defects in the trochlear groove (3 mm Ø and 2 mm depth) for 3 and 6 months	Cell carrier prepared from articular cartilage slices, designated cartilage extracellular matrix- (ECM-) derived particles (CEDPs) seeded with rabbit ACs or ASCs	(i) ICRS score (ii) Paraffin embedding (iii) H&E, Toluidine Blue and sirius red staining (iv) OARSI score (v) IHC: Col I and II (vi) Nanoindentation tests on fresh samples (6 months): hardness, contact stiffness and reduced modulus (vii) MRI: cartilage regeneration (viii) microCT: Tb.Th. and BV/TV	Same significant trend in histological, microCT, and biomechanical evaluations	Yin et al. [35]
Eighteen NZW rabbits (15 weeks old)	Defects in the medial and lateral femoral condyles (3 mm Ø and 3 mm depth) for 2, 4, and 6 months	Expandable gelatin scaffold seeded with rabbit chondrocytes (C + S group) compared to OC defects treated with allogenic chondrocyte injection (positive control), scaffold alone (S) and empty defect	(i) O'Driscoll score (ii) Paraffin embedding (iii) H&E, Alcian Blue stainings (iv) Quantification of integration, apposition, and disintegration of regenerated tissue (v) IHC: Col I, II, and X and S-100 (vi) Compression test on fresh samples	Similar trend among the macroscopic score, histomorphometry, and compressive strength at each time point	Wang et al. [36]

Table 1: Continued.

Experimental model	Anatomical site (defect dimension) and experimental time	Osteochondral treatment	Histological, histomorphometric, and biomechanical methods	Main outcomes	Author
Twenty-seven NZW rabbits (3 months old)	Full-thickness defects in the trochlea (4 mm Ø and 4 mm depth) for 6, 12, or 24 weeks	Oriented bovine cartilage ECM-derived scaffold using thermal-induced phase separation (TIPS) technology and seeded with rabbit BMSCs: (i) cell-oriented scaffold construct; (ii) cell-random scaffold composite	(i) Paraffin embedding (ii) H&E, Toluidine Blue, and Safranin O staining (iii) Modified O'Driscoll score (iv) microCT (v) Unconfined compression test (UCC) on fresh samples: Young's modulus (v) Quantification of total DNA level, total GAG, and collagen content	Similar trends among histomorphological score, DNA, GAG, and collagen content and biomechanics	Jia et al. [37]
Fifty-two Japanese white rabbits (6 months old)	Defects in the trochlea (4.3 mm Ø and 7 mm depth) for 1, 2, 4, and 12 weeks	Hydroxyapatite- (Hap-) coated double-network (DN) hydrogel (HAp/DN gel)	(i) MMA embedding (sagittal cut) (ii) Villanueva bone staining (iii) IHC: procollagen 1A1 (iv) Pushout test (v) MicroCT: Bonding area and tissue density	Similar trend between microCT and biomechanics	Wada et al. [38]
Five female Japanese white rabbits (6 months old)	Defects in the trochlea (4.7 mm Ø and 7 mm depth) for 1 month	(i) Collagen fibril-based tough hydrogels based on the double network (DN) concept using swim bladder collagen (SBC) extracted from Bester sturgeon fish (SBC/PDMAAm) (ii) Hydroxyapatite-(Hap-) coated gel (HAp/c-SBC(ge-1)/PDMAAm)	(i) Pushout and compression test on fresh samples	Significant differences in biomechanical performance	Mredha et al. [39]
Forty-eight adult male NZW rabbits	Defects in the medial femoral condyles (4 mm Ø and 5 mm depth) for 1, 2, and 4 months	Porous tantalum (PT) loaded with BMP-7 (MPT group)	(i) SEM analysis (ii) MMA embedding (longitudinal cut) (iii) Toluidine Blue staining (iv) MicroCT (at 16 weeks): bone intertrabecular space (trabecular spacing, Tb. Sp); bone density; Tb.Th.; Tb.N.; BV/TV; (v) Launch test	Similar trend among histological grading system, micro CT, and biomechanics	Wang et al. [40]

Table 1: Continued.

Experimental model	Anatomical site (defect dimension) and experimental time	Osteochondral treatment	Histological, histomorphometric, and biomechanical methods	Main outcomes	Author
Thirty-six skeletal mature NZW rabbits (5-6 months old)	Defects in the central medial femoral condyle (4 mm Ø and 5 mm depth) for 4 months	Bilayered PLGA/ PLGA-Hap composite scaffold preseeded with BMSCs	(i) Paraffin embedding (longitudinal cut) (ii) H&E, Toluidine Blue, and Safranin O stainings (iii) IHC: Col II (iv) MicroCT on fresh samples (v) AFM test of Young's modulus and surface roughness (vi) Western blot: p-smad 1, p-smad 2, and Col I and II	Significant differences in protein expression but not in all other parameters	Xiangyu et al. [41]
Forty-two NZW rabbits (6–12 months old)	Defects in the trochlea (5 mm Ø and 5 mm depth) for 6 months	(i) Osteochondral allografts (OCA) stored in Tsmu (ii) OCA after vitrification	(i) Paraffin embedding (ii) Mankin score (iii) H&E, Safranin O/ fast green staining (iv) Quantification of chondrocyte viability (fluorescein diacetate and ethidium bromide staining), proteoglycan (PG) type II collagen (v) Compression test on fresh samples: Young's modulus	Similar trends among gross score, chondrocyte viability, PG content, type II collagen, and Young's modulus	Cao et al. [42]

Ø = diameter; IHC = immunohistochemistry; Col = collagen; hPDCs = human periosteum-derived progenitor cells; TGF-β1: transforming growth factor β1; BV/TV = bone volume/trabecular volume; Tb.Th. = trabecular thickness; Tb.Sp. = trabecular separation; Tb.N. = trabecular number; micro-CT = microcomputed tomography; hESC-MSC = human embryonic stem cell-derived mesenchymal stem cells: PBS = phosphate-buffered saline; MeHA = methacrylated hyaluronic acid; NZW = New Zealand white; ADM = acellular dermal matrix; IPFP = infrapatellar fat pad; H&E = hematoxilyn and eosin; BMC = bone marrow concentrate; HA = hydroxyapatite; PEMFs = pulsed electromagnetic field; BMP-2 = bone morphogenic protein-2; OC = osteochondral, BMSCs = bone marrow mesenchymal stem cells; LLLT = low-level laser therapy; mar = mineral apposition rate; BFR = bone formation rate; AFM = atomic force microscope; sGAG = sulphated glycosaminoglycan; bTCP = beta-tricalcium phosphate; ACs = articular chondrocytes; ASCs = adipose-derived stem cells; Tsmu = Taishan Medical University solution.

similar follow up times of 1-2 months, performed defects with similar dimensions (diameter range 1.4–2 mm and depth range 1–1.5 mm), and conducted histological/histomorphometric analyses on paraffin-embedded samples. The study by Zhang et al. was the only one that conducted both histological/histomorphometric and biomechanical analyses [10]. These analyses found similar significant results between the histomorphometric score (ICRS score) and biomechanical analysis of Young's modulus of the regenerated cartilage. Investigations on biomechanics were performed by the indentation test on freshly excised samples submerged in PBS without any inclusion, whereas the histological scoring system was made on decalcified paraffin-embedded samples.

Instead, the other two works by Mendes et al. and Lin et al. in a low weight-bearing area of the joint performed microtomographic analysis and histological score (Wakitani score), respectively, but not biomechanical evaluations of the regenerated tissue. So far, a direct comparison of results is not possible [11, 12].

3.3. Lapine Model. Thirty studies of the retried papers involved rabbits as an animal model [13–42]. The New Zealand white rabbit was adopted in 28/30 studies, whereas Japanese rabbit was used in two related studies [38, 39]. The majority of the researches claimed to use skeletally mature animals (range age: 6–32 months). However, in some studies [14, 24, 36, 37], a lower animal age until 3 months was reported. Of note, an average weight between 2.5 and 4 kg was reported in all these studies except for Cheuk et al. [24]. Finally, regarding the animal age, it is to stress that Martin-Hernandez et al. openly declared the use of 3-month-old skeletally immature rabbits [30].

Medial and/or lateral femoral condyles (14/30) and the trochlear groove (16/30) have been the selected anatomical sites where osteochondral defects were created. Between the defects created in the femoral condyles, 3 were made in the load bearing areas [13, 24, 25]. The defects dimension varied from 1.5 mm to 6 mm in diameter and from 1.5 to 10 mm in depth contributing to make the comparison difficult.

Table 2: Data extraction of papers involving large animal models.

Experimental model	Anatomical site (defect dimension and experimental time)	Osteochondral treatment	Histological, histomorphometric, and biomechanical methods	Main outcomes	Author
Canine model					
Twelve male dogs	Defects (11 mm Ø and 10 mm depth) in the load-bearing area of the femoral head for 3 and 6 months	Allogeneic BMSC-seeded DCM/DCBM scaffolds	(i) MicroCT on fresh samples: bone volume fraction (ii) Indentation test on fresh samples: stiffness	Similar trend between microCT and biomechanics (stiffness)	Qiang et al. [43]
Eight mongrel dogs	Defects (3.5 and 4.5 mm Ø and 10 mm depth) in the medial femoral condyle for 12 months	Autograft and allograft plugs	(i) Paraffin embedding (sagittal cut) (ii) Histological scoring system for proteoglycan content (iii) H&E and Safranin O stainings; (iv) MRI: MOCART score and T2 mapping (v) Indentation test on fresh samples submerged in saline solution: second shear modulus	No statistical significance was seen in any parameter	McCarty et al. [44]
Twenty-seven TOYO beagles (15 months old)	Defects in the patellar groove (5.0 mm Ø and 2.0 mm depth) for 27 weeks	Ultrapurified alginate gel with or without microfractures	(i) Paraffin embedding (longitudinal cut) (ii) Niederauer score (iii) H&E and Safranin O stainings (iv) IHC: Col I and II (v) GAGs content (vi) Changoor score for collagen orientation (vii) MicroCT on frozen samples: volume of mineralized bone (viii) Indentation test on fresh samples submerged in saline solution: stiffness	Similar trends between the histological and collagen orientation scores and biomechanical analysis of stiffness. No differences in microCT	Baba et al. [45]
Twelve male dogs (2 year-old)	High load bearing surface of femoral condyles (4.2 mm Ø and 6 mm depth) for 3 and 6 months	Decellularized OC construct with or without 1×10^6 chondrogenically induced BMSCs	(i) Paraffin embedding (ii) Solchaga score on paraffin-embedded samples (H&E and Toluidine Blue stainings); quantification of glycosaminoglycan content (iii) MicroCT on fixed samples: BVF and BRP (iv) Indentation test on samples fixed with cement and submerged in saline and EDTA solution: stiffness of cartilage and of subchondral bone (only at 6 months)	Significant on histological score and not in other parameters	Yang et al. [46]

Table 2: Continued.

Experimental model	Anatomical site (defect dimension and experimental time)	Osteochondral treatment	Histological, histomorphometric, and biomechanical methods	Main outcomes	Author
Sixteen female mongrel dogs (2–5 years old)	Defects (8 mm Ø and 8 mm depth) in the weight-bearing areas of the lateral and medial femoral condyles for 6 months	Allograft plugs stored in different storage media and temperature	(i) Paraffin embedding (ii) OARSI score (iii) H&E, Toluidine Blue, and picrosirius red stainings (iv) GAGs and collagen contents (v) Indentation test on thawed samples: instantaneous tissue and dynamic modulus	Significance in histological score and not in biomechanics	Cook et al. [47]
Sixteen female mongrel dogs (2–5 years old)	Defects (8 mm Ø and 8 mm depth) in the weight-bearing areas of the lateral and medial femoral condyles for 6 months	Allograft plugs stored in different storage media and temperatures	(i) Paraffin embedding (ii) OARSI score (at 1 week and 6 months) (iii) H&E, Toluidine Blue, and picrosirius red stainings (iv) Quantification of GAGs and collagen (v) Indentation test on thawed samples: instantaneous tissue modulus and dynamic modulus (at 6 months)	No statistical significance was seen in any parameter	Cook et al. [48]
Swine model					
Sixteen pigs (6 months old)	Defects (10 mm Ø, 4 mm depth) in the weight-bearing area of medial and lateral femoral condyles for 6 months	PGA/PLA scaffolds seeded with autologous BMSCs and cultivated in vitro for 2, 4, or 8 weeks	(i) Paraffin embedding (longitudinal cut) (ii) Wakitani and Pineda scores (iii) H&E, Safranin O, and sirius red staining (iv) IHC: Col I, Col II, and osteocalcin (v) Quantification of collagen and GAGa contents (vi) Indentation test on fresh samples: compressive load-displacement curve and Young's modulus	Similar trend between histological score and biomechanics	He et al. [49]
Yorkshire Duroc pigs (six months old)	Critical sized defects in the medial condyle and patellar groove (8 mm and 8 mm depth) for 6 months	Biphasic construct made of PCL for cartilage and PCL-TCP for bone with or without BMSCs	(i) Paraffin embedding (longitudinal cut) (ii) O'Driscoll score (iii) H&E, Toluidine blue/Safranin O, and Masson's trichrome stainings (iv) IHC: Col I and II (v) MicroCT on fresh samples: degree of mineralization (vi) Indentation test on thawed samples: Young's modulus	Inferior healing in the patellar groove than in medial condyle; similar trends and positive correlation between microCT and biomechanical tests for all groups at both locations	Ho et al. [50]

Table 2: Continued.

Experimental model	Anatomical site (defect dimension and experimental time)	Osteochondral treatment	Histological, histomorphometric, and biomechanical methods	Main outcomes	Author
Twelve male Gottingen minipigs (19.8-months old)	Critical sized defects in the medial and lateral trochlear facets (6 mm Ø and 8 mm depth) for 6 and 12 months	Autologous bone graft with or without autologous cartilage chips	(i) Resin embedding (ii) ICRS II score (iii) H&E staining (iv) Quantification of hyaline tissue, fibrocartilage, fibrous tissue, bone, bone marrow and blood vessel area (v) MicroCT on fresh samples: bone defect volume	Histomorphometric parameters showed differences between groups (articular cartilage, fibrocartilage, fibrous tissue, and ICRS II); microCT showed significant differences between experimental times but not between experimental groups	Christensen et al. [51]
Eight female Goettingen minipigs (1.5–2 years old)	Defects (5.4 mm Ø and 8 mm depth) in the trochlear groove for 2 months	Collagen type I/III membrane with or without autologous BMSCs	(i) Paraffin embedding (longitudinal cut) (ii) O'Driscoll score (iii) Safranin O and col II stainings (iv) IHC: Col II	Better significant results in the O'Driscoll score	Jung et al. [52]
Eighteen Göttingen minipig (1.5–2.5 years old)	Critical size defects (6.3 mm Ø and 10 mm depth) in the trochlear groove for 1.5, 3, and 13 months	Autologous osteoperiosteal bone plug with or without subperiosteal injection of a chondrogenic and osteogenic growth factor mixture	(i) Paraffin embedding (sagittal cut) (ii) Safranin O staining (iii) ICRS II score (iv) Indentation test on fresh samples: compressive load-displacement curve	No statistical significance was seen in any parameter	Gotterbarm et al. [53]
Eighteen minipigs (7-8 months old)	Defects (7 mm Ø, 8 mm depth) in the medial femoral condyles for 6 months	PLGA scaffold with or without autologous chondrocytes or BMSCs	(i) Paraffin embedding (longitudinal cut) (ii) ICRS score (iii) H&E and Safranin O staining (iv) MRI: MOCART score and biomechanical properties (collagen matrix and hydration) (v) Indentation test on fresh samples: compressive modulus	Similar trend among histomorphometric, MRI scores (ICRS and MOCART), and biomechanics (compressive modulus)	Zuo et al. [54]
Equine model					
Five mature ponies	Defects (13 mm Ø and 7 mm depth) in femoral condyles with an inner hole (2.5 mm Ø and 10 mm depth) for 3, 6 (MRI and CT), and 13 months (microCT and histology)	Ad-BMP2 or Ad-BMP6 or Ad-GFP	(i) qMRI (ii) CT in vivo and microCT ex vivo: lesion area and BMD for the lesion, drill, and adjacent subchondral bone (iii) Paraffin embedding (iv) O'Driscoll score (v) H&E, Toluidine Blue and Safranin O stainings	Similar trends between MRI (T1 relaxation time) and clinical CT (BMD) at 12 weeks	Menendez et al. [55]

Table 2: Continued.

Experimental model	Anatomical site (defect dimension and experimental time)	Osteochondral treatment	Histological, histomorphometric, and biomechanical methods	Main outcomes	Author
Ovine model					
16 adult female Dutch milk goats (4 years)	Defects (6 mm Ø and 6 mm depth) in each talus for 6 months	Demineralized bone matrix (DBM) with and without platelet-rich plasma (PRP)	(i) Paraffin embedding (longitudinal cut) (ii) microCT: BV/TV (iii) Goldner's trichrome and Toluidine Blue stainings (iv) Quantification of mineralized bone surface area and osteoid surface area (%), number of osteoclasts, osteoblasts, and osteocytes, MAR	No differences between groups	van Bergen et al. [56]
8 skeletally mature female Dutch milk goats	Osteochondral defects (5 mm Ø, 3.5 mm depth) were created in medial condyles and trochlear grooves for 1 and 4 months	Acellular collagen I/III scaffolds or scaffolds seeded with SVF cells or cultured ASCs	(i) Indentation test (fresh sample): 50, 100, 200, and 300 μm indentation at a constant speed of 20 μm/sec with 4 mm Ø bold tip probe (ii) Paraffin embedding (sagittal cut) (iii) H&E and Alcian Blue stainings (iv) IHC: COLLI, COLLII (v) microCT (vi) GAGs quantification	No significance in biomechanical test: better histological and immunohistochemical outcomes in acellular construct	Jurgens et al. [57]
Goat	Critical size defect 6 mm Ø × 6 mm depth in each medial femoral condyles for 6 and 12 months	(1) Maioregen scaffold (2) Articular cartilage and growth plate ECM from porcine hind limbs AC-GP-ECM-derived bilayered scaffold	(i) MicroCT (ii) Paraffin embedding (longitudinal cut) (iii) H&E, Safranin O, and picrosirius red stainings (iv) IHC: COLLII (v) ICRS score	Hyaline-like repair tissue, better collage fiber organization of repaired tissue, and parallel fiber orientation with a lower range of dispersion in the superficial cartilage region	Cunniffe et al. [58]
10 skeletally mature female Merino sheep (2–2.5 years)	Bilateral full thickness defects (4 mm Ø and 12 mm depth) created 2 mm below the calcified layer in the medial femoral condyles for 6 and 12 months	Triphasic implant engineered using β-tricalcium phosphate osseous phase and Coll I hydrogel chondral phase, with MSCs vs. autograft	(i) ICRS score (ii) O'Driscoll score (iii) Siebert semiquantitative score (iv) Toluidine Blue and Levai-Laczko stainings (v) Indentation test (maximum load 40 N) fresh sample (vi) IHC: COLLII (vii) MicroCT	No biomechanical differences between the groups	Marquass et al. [59]

Table 2: Continued.

Experimental model	Anatomical site (defect dimension and experimental time)	Osteochondral treatment	Histological, histomorphometric, and biomechanical methods	Main outcomes	Author
28 female Merino sheep (2–4 years old)	7 mm Ø and 25 mm depth osteochondral defect in the centre of the load-bearing area of the medial femoral condyle for 1.5, 3, 6.5, and 13 months	Cylindrical plugs of microporous b-TCP (Ø: 7 mm; length: 25 mm; porosity: 43.5 ± 2.4%; pore Ø: ~5 μm) seeded with autologous chondrocytes cultured for 4 weeks	(i) Paraffin embedding (sagittal cut) (ii) ICRS score (iii) ESEM (iv) TEM (v) MicroCT (vi) Masson's trichrome, Safranin O, Giemsa, and TRAP stainings (vii) O'Driscoll score (viii) IHC: COLLI, COLLII, COLLX, and ALP (ix) Quantification of mineralized bone substance and TCP proportion	Degradation of ceramic proportional to bone formation; new cartilage formation and integration, although not with the same values of native one	Bernstein et al. [60]
5 skeletally mature Arcott cross female sheep (2–4 years old)	Six 2 mm Ø, 2.5 to 8.5 mm deep Jamshidi biopsy holes were created bilaterally in the weight-bearing area of medial femoral condyle for 1 day, 3 weeks and 3 months	Presolidified chitosan-blood implant with fluorescent chitosan tracer	(i) Paraffin embedding (longitudinal cut) (ii) MicroCT (iii) Safranin O/fast green/iron hematoxylin, Gomori trichrome, and von Kossa/Toluidine Blue staining (iv) IHC: COLLI, COLLII	Bone plate-induced chondroinduction is an articular cartilage repair mechanism; Jamshidi biopsy repair takes longer than 3 months and can be influenced by subchondral chitosan-blood implant	Bell et al. [61]
24 adult goats (2–3 years old)	Osteochondral defect in the medial femoral condyles (6 mm Ø and 8 mm depth) for 3, 6, and 12 months	Multilayered scaffolds with oriented articular cartilage extracellular matrix- (ACEM-) derived cartilage layer, porous 3D printing (3DP) PLGA/TCP bone layer (BL), and an intermediate PLGA/TCP compact interfacial layer	(i) ICRS score (ii) Safranin O and Toluidine Blue staining (iii) O'Driscoll score (iv) IHC: collII (v) Compression test (initial load of 0.05 N, speed 0.01 mm/s)	MLS enhances hyaline-like tissue formation with better mechanical properties	Jia et al. S, 2018 [62]
6 crossbred adult sheep	Critical size osteochondral defect (7 mm Ø, 5 mm depth) in the medial and lateral femoral condyles for 6 months	Biphasic HA-HYA alginate- based scaffold (bony layer 1.25% alginate and 4% HA; chondral layer 1% alginate and 0.5% HYA)	(i) Fortier-modified score (ii) MicroCT: BV/TV; Tb.Sp.; Tb.Th.; and Tb.N. (iii) Paraffin embedding (sagittal cut) (iv) Safranin O/fast green staining (v) Pineda score (vi) IHC: COLLI, COLLII, VEGF	No differences were found between groups.	Filardo et al. [29]

Table 2: Continued.

Experimental model	Anatomical site (defect dimension and experimental time)	Osteochondral treatment	Histological, histomorphometric, and biomechanical methods	Main outcomes	Author
14 skeletally mature goat	Osteochondral defect (6 mm Ø, 8 mm depth) in the medial and lateral femoral condyles for 6 months	Biphasic osteochondral scaffold prepared using coralline aragonite with 1 to 2 mm depth drilled channels in the cartilage phase (+HA impregnation) or in the bone phase	(i) Fortier-modified score (ii) ICRS score (iii) paraffin embedding (longitudinal cut) (iv) Safranin-HE, Masson trichrome, Safranin O/fast green stainings (v) IHC: COLLI and COLLII (vi) O'Driscoll score	Mechanical modification with drilled channels and impregnation of HA within the coral pores enhanced the scaffold's cartilage regenerative potential	Kon et al. [63]
12 skeletally matured female adult sheep	Osteochondral lesion (7 mm Ø, 9 mm thickness) in the right medial and lateral femoral condyles for 6 months	Osteochondral biomimetic scaffold with and without PRP	(i) Paraffin embedding (sagittal cut) (ii) Safranin O/fast green staining (iii) Niederauer score (iv) IHC: COLLII	HA-coll scaffold promotes regeneration even without PRO	Kon et al. [64]
22 Sardinian sheep (5.5 years old)	Bilateral osteochondral defects in medial and lateral condyles (6 mm Ø and 2 mm depth) involving subchondral bone for 1, 2, 6, 12, and 24 months	Embryonic stem-like (ESL) cells embedded in fibrin glue	(i) Indentation test (fresh samples) (ii) H&E and Safranin O staining (iii) Score by Kaplan (iv) IHC: COLLII (v) FISH	ESL cells enhance the regeneration of hyaline cartilage	Manunta et al. [65]
24 skeletally mature female merino-mix sheep	7.3 mm Ø defect and 12 mm in height in the central weight-bearing area of the femoral condyles for 3 and 6 months	Osteochondral autograft bottomed (recipient site depth 10 mm) and unbottomed (recipient site depth 12 mm)	(i) Paraffin embedding (sagittal cut) (ii) Safranin O/von Kossa, Safranin O/fast green stainings, and TRAP staining	Full graft support improves long-term integration	Nosewicz et al. [66]
12 female Merino sheep (2 years old)	Osteochondral defects in the weight-bearing area of femoral condyles (9.4 mm Ø and 1.1 cm depth) for 6 weeks	Biphasic scaffold of hydroxyapatite/ collagen (scaffold a) and allogenous-sterilized bone/ collagen (scaffold B) with or without chondroblasts	(i) ICRS score (ii) Paraffin embedding (sagittal cut) (iii) TRAP staining (iv) H&E and Toluidine Blue stainings (v) IHC: coll II and CD68 (vi) Gene expression: Col1A1, COLIIA1, SOX9, and CEP-68	More immunocompetent cells around scaffold and a higher expression of COLLII and SOX9 for scaffold B	Schleicher et al. [67]
28 female Merino sheep (2–4 years old)	Osteochondral defect of 7 mm Ø and 25 mm in height in the center femoral condyles for 1.5, 3, 6.5, and 13 months	Microporous beta TCP scaffold (7 mm Ø and 25 mm length) preseeded with autologous chondrocytes	(i) Indentation test in a special mount (3 mm Ø indenter, 200 μm penetration, maximal load 1.5 N): achieved load, absorbed energy, and contact stiffness (ii) PMMA embedding (longitudinal cut) (iii) ICRS score	Mechanical properties of TCP scaffold were similar to native cartilage Lower score in the central area	Mayr et al. [68]

GAGs = glycosaminoglycan; OC = osteochondral; BMSCs = bone marrow-derived mesenchymal stem cells; BVF = bone volume fraction; BRP = bone regeneration percentage; PCL = polycaprolactone; PCL-TCP = olycaprolactone-tricalcium phosphate; Ad-BMP2 = adenoviral bone morphogenetic protein 2; Ad-BMP6 = adenoviral bone morphogenetic protein6; Ad-GFP = adenoviral green fluorescent protein; BMD = bone mineral density; DCM/DCBM = microfilaments of decellularized cartilage matrix/decellularized cancellous bone matrix; DMEM = Dulbecco's modified Eagle's medium; ECM = extracellular matrix; HA-HYA = hydroxyapatite-hyaluronic acid; DBM = deminerilzed bone matrix; PRP = platelet rich plasma; PMMA= poly(methyl methacrylate); TCP = tetracalciumphosphate; SVF = stromal vascular fraction; ALP = alkaline phosphatase; PLGA = poly(lactic-co-glycolic acid).

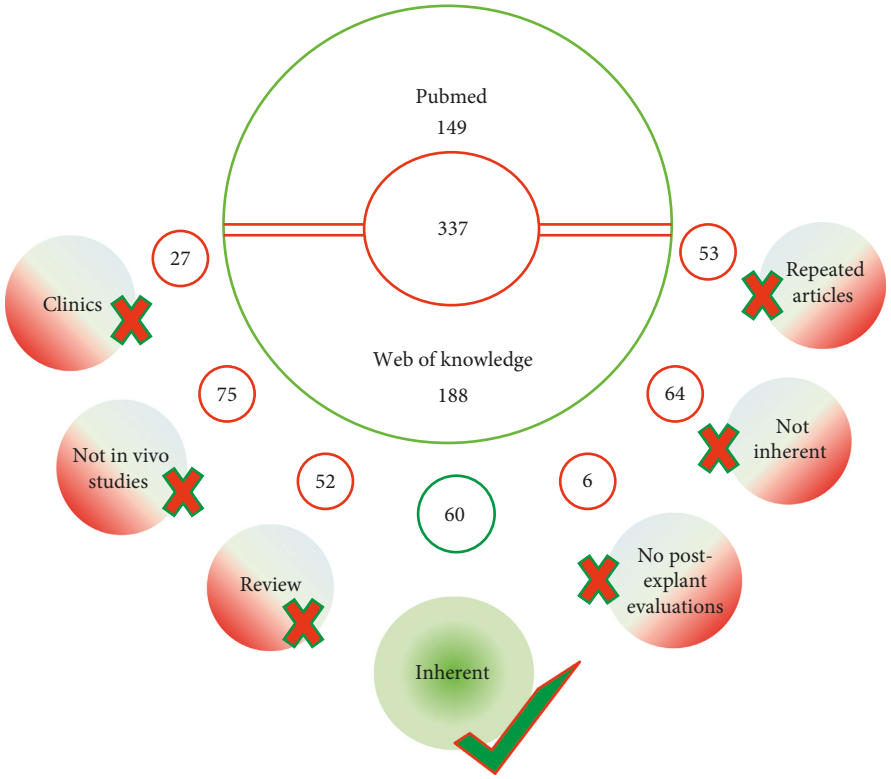

Figure 1: Flowchart of research strategy and paper selection.

Notably, the fact that, in some studies, the surgical defect performed was defined as a "full thickness" cartilage defect, but the range (diameter: 3–5 mm; depth: 2–10 mm), both in diameter and in depth of the defect, varied among studies [9, 20, 30, 31, 34, 37], indicating that an accordance is not reached yet on the issue. In terms of defect size, an extremely variation was noticed also in the experimental times, ranging from 1 day [23] to 36 weeks [18]. In 12/60 papers, the chosen experimental time was 1–1.5 months, but in the 75% of these works, also longer experimental times were taken. Overall, the most common long-term experimental times were 3 (8/30) and 6 months (7/30 papers) and only one paper arrived up to 9 months.

Except for two studies [31, 39] where only biomechanical tests were performed, all authors (28/30) conducted histological/histomorphometric analyses mainly on decalcified and paraffin-embedded (25 papers out of 30) samples. In two studies, such an analysis was performed on frozen samples [22, 23], while in three studies, 2-hydroxyethyl methacrylate (Technovit) and polymethylmetacrilate were chosen as embedded solution, respectively [27, 29, 40]. Apart from the research of Wada et al., both embedding methods were adopted [38]. Mainly, histologic analysis included the adoption of semiquantitative scoring systems both for macro- and microevaluation of samples. Where specified, both in gross evaluation and microscopic analysis, different scoring systems were adopted. Between them, the O'Driscoll score resulted as the most utilized (12 to 30), immediately followed by the ICRS (5 papers out of 30) and Niederauer (3/30) scores. As basic histological staining for the general assessment of cell and tissue morphology, the common hematoxylin-eosin (H&E) staining was used. Instead, both Safranin O (associated or not with the fast green dye for the bone compartment) and Toluidine Blue were the staining methods most frequently chosen for proteoglycans as well as glycosaminoglycans content, in addition to the Alcian Blue staining method. Only five studies utilized the two classical techniques to visualize collagen fibers in histological section, picrosrius red [35] or Goldner's trichrome [16, 18, 21, 30]. Finally, for undecalcified samples, the Stevenel Blue/Van Gieson Pichrofucsin dye [29], thionine staining [27], and Toluidine Blue were used to evaluate the osteochondral compartment. Where specified, all the abovementioned histological stainings were performed after cutting the samples according to a sagittal [14–18, 22–25, 27–30, 38] or longitudinal [13, 40, 41] plane.

Histomorphometry mainly included the quantification of osteochondral repair tissue, both of cartilage and bone compartments, microtomographic bone-related parameters, and the percentage of biochemical analytes such as collagen type I and II or proteoglycan content. Different from commonly performed analyses, one study reported osteoclasts quantification also after TRAP staining [23]; other two researches quantified cartilage specific gene expression and sulphated glycosaminoglycan (sGAG) [33, 37] or DNA content [37], as well as protein expression by mean western blot in the in vivo constructs [41]. Finally, only one study performed quantification of oxytetracycline incorporation [29]. Between imaging techniques, MRI [35] and SEM [40] was also adopted together with microCT.

Biomechanical evaluations on fresh samples or previously frozen samples [31, 32] implemented the histomorphometric results of the abovementioned studies.

Between biomechanics methods, indentation tests were used to evaluate parameters such as cartilage stiffness, instant modulus and shear modulus, compressive strength, Young's modulus, or contact stress of the cartilage compartment. Among the studies where biomechanics was performed, three studies specified which type between nanoindentation [35] or microindentation [20, 34] was used. Finally, the pushout test was conducted in two related studies [38, 39].

As far as biomechanical results were concerned, Schmal et al., Betz et al., and Zhang et al. found similar trend between histological and mechanical analysis [15, 19, 26]. In the work of Schmal et al., cartilage thickness, instant modulus, and shear modulus on fresh samples by mean indentation tests were evaluated while histomorphometry was conducted by quantification of collagen content and by adopting the semiquantitative OARSI score [15]. Mechanical stiffness and quantification of bone area within the subchondral defect and the O'Driscoll score were instead evaluated by Betz et al., finding a positive correlation between the histomorphometric parameters and higher stiffness values [19]. Significant differences between the experimental groups in comparison to other groups were found in biomechanical and microCT evaluations by Zhang et al. in [26]. Cao et al. assessed a significant higher chondrocyte viability, PG content, type II collagen, and Young's modulus on trochlea defects treated with osteochondral allografts stored in a particular medium. However, no significant results were detected in comparison to fresh osteochondral allografts [42].

On the contrary, the work by Kazemnejad et al. did not find any significant differences in quantitative histopathological and mechanical data [18].

3.4. Canine Model. Six papers analyzed the osteochondral regeneration of defects made in the knee of dogs [43–48]. Different from the studies conducted in rats, the most (5 out of 6) performed defects in the high load bearing areas in medial or lateral femoral condyles and one in the low load bearing area in the patellar groove. The dog's age was quite homogeneous (range 1.5–5 years), with the exception of two studies where dog ages were not reported [43, 44]. On the contrary, defect dimensions greatly varied from 3.5 to 11 mm in diameter and from 2 to 10 mm in depth. Also by analysing the defect dimensions in relation to the animal's breed, the three papers that used Mongrel dogs performed defects in femoral condyles with diameters ranging from 3.5 to 8 mm and height from 8 to 10 mm [43, 47, 48].

The experimental times ranged from 3 to 12 months; however, most of the papers (4 out of 6) selected the six-month period for investigations. All authors performed both histological/histomorphometric and biomechanical tests: histology was performed on decalcified and paraffin-embedded samples and biomechanics on fresh or frozen/thawed samples (4/6 papers among which 3 submerged samples in saline) or frozen/thawed samples (2/6 papers). Mainly, histology included the adoption of semiquantitative scoring systems, histomorphometry measured microtomographic bone-related parameters and quantification of biochemical analytes (collagen and/or GAGs), and biomechanics evaluated cartilage stiffness or modulus by performing the microindentation test. One work by McCarty et al. included also a MRI evaluation of MOCART score and the quantitative T2 mapping [44]. A great concern about the examined studies is that the study reporting is almost incomplete, because in some cases, there is a lack of indications about the animal's breed, age, or anatomical plane of cut.

As far as results were concerned, Quiang et al. [43] and Baba et al. [45] found similar trends between histological and biomechanical analyses; both works measured the cartilage stiffness by means of the indentation test, whereas in the work of Quiang, histomorphometry was conducted by measuring the 3D bone volume by microCT, and in the work of Baba, semiquantitative Niederauer and Changoor scores were adopted.

Yang et al. and Cook et al. found significant results only in histological/histomorphometric investigations and not in biomechanics, whereas the remaining two papers did not find any statistical significance in any of the performed analyses [46, 47].

3.5. Swine Model. Six papers [49–54] employed a swine animal model to investigate the repair and regeneration of the joint tissues: two works were made in 6-month-old pigs [49, 50] and four in miniaturized pigs with ages ranging from 7 months to 2.5 years [51–54]. The experimental times ranged from 1.5 to 13 months, but four out of six papers selected the 6-month endpoint.

In pigs, critical sized osteochondral defects, meaning that they were not able to spontaneously heal, were created. These studies found similar significant trend between histological and histomorphometric and biomechanical investigations that were conducted on paraffin-embedded samples (longitudinally cut) by adopting semiquantitative scoring systems and by the indentation test to evaluate Young's modulus. Interestingly, Ho et al. performed defects both in the high-load bearing femoral condyles and in the low-load bearing trochlear groove, finding that, for the same treatment, mechanical stimulus had beneficial effects on the tissue regeneration gaining superior healing in the condyles than in the trochlea [50]. Moreover, Ho et al. correlated the obtained results from the histomorphometric score and biomechanical test: they found positive correlation between the bone regeneration measured by microCT and Young's modulus measured by the indentation test at the two different implantation sites [50]. This study suggests a close interaction in the healing of both tissues as cartilage repair is dependent on the underlying bone for support and both histomorphometric and biomechanical tests are able to identify such improvements.

Among the four works in minipigs, three used Goettinger minipigs: all defects were created in the trochlear groove with dimension ranging from 5.4 to 7 mm in

diameter and from 8 to 10 mm in depth [51–54]. Christensen et al. and Jung et al. performed histological/histomorphometric analysis on resin-embedded [51] and paraffin-embedded samples [52], respectively, but not biomechanical ones. Gotterbarm et al. and Zuo et al. quantitatively measured the osteochondral regeneration by histological scores on paraffin-embedded samples and the compressive modulus of regenerated cartilage in fresh samples by the indentation test [53, 54]. While Gotterbarm et al. failed to observe significant differences in any of the measured parameters, Zuo et al. found corresponding trends between biomechanics and histomorphometry [53, 54].

3.6. Equine Model. One work analyzed the knee tissue regeneration in an equine animal model: osteochondral defects with a smaller and deeper core was adopted in adult ponies for the localized delivery of gene transfer vectors [55]. The work dealt with paraffin-embedded histological samples, and the follow-up experimental times were 3 and 6 months for MRI and CT investigations and 13 months for microCT and histological ones. However, the authors did not perform biomechanical analysis, and they found correspondence between MRI and clinical CT data [55]. The paucity of data regarding the use of this model, owing to huge costs and ethical reasons as companion animals, affects the relevance of their results.

3.7. Ovine Model. Among papers retrieved after research, 14 resulted to involve ovine models [29, 56–68]. Five papers out of 14 used goats, while 9 used sheep. Among works dealing with goats, 2 used Dutch milk goats while the remaining three did not report the breed. Among works dealing with sheep, 9 used Merino, 1 Sardinian, and 1 Arcott and 2 papers did not report the breed.

In contrast with an almost generalized use of macroscopic and microscopic scores (mainly ICRS score and O'Driscoll score) and histological analyses, in 7/14 papers, microtomographical assessment is reported, and in 5/14 papers, biomechanical tests are performed; among these, 4/5 were indentation tests and 1/5 compression test. When specified, the site selected for the creation of osteochondral defects was in one case the talus [56], in one paper, the trochlea and the medial condyles [57], and for the other papers, medial condyles [58–62] or both medial and lateral condyles [29, 63–75]. In some cases, the choice of central weight-bearing area was underlined [60, 61, 66, 67].

It is noticeable the wide range of defect dimensions, from 2 mm to 9.4 mm of diameter and from 11 mm to 25 mm of depth, which make it difficult to compare the studies with each other. By analysing the defect size in relation to the species, the same variability exists. In the femoral condyles of goats, the dimensions were quite homogeneous (diameter range was 5–6 mm and the height range 3.5–8 mm), while in the femoral condyles of sheep, the diameter range was 2–9.4 mm and the height range was 2–25 mm. By grouping data per breed, defects in the femoral condyles of Merino sheep (the mostly used breed in 5/9 studies of sheep) had a diameter range of 4–9.4 mm and an height range of 11–25 mm, suggesting there is no relation to the breed.

With the exception of the paper by Bell et al. in which very short experimental times were selected (one day and 3 weeks) [61], for the other studies, a minimum of 1 month to a maximum of 24 months of experimental times were chosen, but most of the studies (11/14) selected 6 months. In almost all papers (11/14), immunohistochemical evaluations were performed to investigate mainly collagen I and II reactivities, while the paper by van Bergen is the only one in which evaluation of bone mineralization was performed with MAR measure [56]. In a single case, the possibility to extract RNA from paraffin-embedded samples is exploited to perform gene expression analyses [67].

In all papers, biomechanical tests were performed before histological analyses on fresh samples, except for the paper by Mayr et al. in which PMMA embedding was performed, and achieved load, absorbed energy, and contact stiffness were evaluated [68]. Jia et al. [62] and Jurgens et al. [57] measured Young's modulus, keeping samples in PBS at room temperature during the compression and indentation tests. Marquass et al. also tried to mimic a physiological environment during the test using a polymethylmethacrilate (PMMA) tank filled with PBS (7.4 pH) [59]. Articular cartilage deformation was tested by Manunta et al. [65].

As for the region of interest evaluated, when clearly specified, Mayr et al. performed measurements both in the implant and healthy tissue at the interface with the defect [68], while Marquass et al. considered an area next to the centre of the defect [59]. As control, Marquass et al. compared the results with those obtained from tests previously performed on untreated joints, while Jurgens et al. tested the native cartilage adjacent to the osteochondral defect [57]. One paper [68] compared results with those obtained from the contralateral untreated defect.

Generally speaking, except for the cases in which the biomechanical test did not show significant differences among groups [56, 57, 59], the results from mechanical assessments are comparable with those obtained from histological evaluations.

4. Discussion

The progress of histological techniques and technological advances related to image analysis software and specific test equipment has allowed the study of the musculoskeletal tissue and the evaluation of regenerative medicine protocols more thorough and complete. The peculiarity of the OC unit, due to the presence of both cartilaginous and bone tissues, makes its evaluation quite complex and varied [69, 70]. One of the most challenging aspects can be considered the biomechanical evaluation as the different structural characteristics of bone and cartilage, even if only considering the difference in extracellular matrix composition. It requires the setup of protocols being able to perform a correct measure in relationship to the tissue and the loading expected. Consequently, it is not so rare that post-explant assessments focus mainly on one tissue rather than another, although it is now established that a full-fledged

consideration of the district is indispensable for the evaluation of a new therapy or treatment [71].

As confirmed by data extracted from this review, paraffin embedding still remains the most common embedding technique for histological evaluation. The types of treatment tested in the reviewed papers allow an easy application of this technique. In fact, the majority of the studies tested the effect of cells, mainly mesenchymal stem cells from different sources, and also chondroblasts or chondrocytes. When used in combination with scaffolds/biomaterials, the choice frequently fell on collagenic/gelatin scaffolds, biphasic constructs, and rarely ceramic or PLGA materials. Most of these materials can be easily embedded in paraffin, which has also the advantage to allow a better evaluation of cellularity and cartilage status, allowing to perform specific stainings and also immunohistochemistry evaluations. Resin embedding was applied mainly in the few cases in which hard materials, such as metals, were used. The paucity of works using resin embedding protocols might be due to the need of specific costly equipment, in particular for cutting samples, such as rotating microtomes and oscillating saws. In addition, although resin inclusion allows the study of the material-bone interface without decalcification and maintaining any type of implant in place, it is less suitable for analysing bone cellularity and cell morphology, with a different yield of histological stainings. Among these, hematoxylin/eosin and Safranin O/fast green stainings are the most adopted techniques for the OC tissue, regardless of the animal model employed. The first one is probably one of the most commonly used histological stainings. The chromatic gradation that the staining can take according to the degree of tissues mineralization makes it particularly suitable for the study of the OC district, highlighting both the presence of calcification and the predominantly collagenic areas. On the other hand, the specificity and stoichiometric affinity of Safranin O for proteoglycans make this dye ideal for the evaluation of cartilage status and for the application of most of the scores for OC regeneration [72]. There are many existing scores for the evaluation of OC regeneration, and the data extracted from the review show that these are all widely used, from the simplest and with less parameters considered (e.g., Pineda and Wakitani scores) to the more complex and complete ones (e.g., O'Driscoll, Sellers, and Forties scores). ICRS and OARSI scores are quite commonly used, sometimes in combination, although the first is usually applied for the evaluation of human joints, while the second is more specific for the evaluation of osteoarthritic cartilage staging [73]. The existing scores for OC evaluation share some fundamental parameters, for example, cell morphology, filling of the defect, and staining of matrix. Both O'Driscoll and Sellers scores specify that the extent of matrix staining is expected to be evaluated with Safranin O staining, while in the Fortier score, Toludine Blue staining is suggested for the evaluation of adjacent cartilage. This last parameter is actually evaluated only in two scores (Wakitani and Fortier), while the evaluation of subchondral bone is provided only by Sellers score. This evidence underlines a relevant gap in the perspective of a comprehensive evaluation of OC unit regeneration and suggests the need to employ at the same time different scores to evaluate all critical aspects. However, the choice to perform more than a single score seems to be not frequently adopted, while quantitative evaluations as microCT or histomorphometric measures or immunohistochemical staining are frequently used, in addition to histological scores. For an exhaustive evaluation of cartilage regeneration and acquisition of hyaline characteristics, the peculiar composition of articular cartilage requires the evaluation of both collagen I and II presence. To make the picture complete, collagen X quantification provides information about the process of cartilage calcification and bone growth, thus allowing comprehensive evaluation of both cartilagineous and bone tissues [74]. Due to the emerging role of the subchondral bone, microCT analyses have been widely performed for the evaluation of bone volume, microarchitecture, and response to treatments.

An interesting aspect emerged by the results is the widespread use of biomechanical tests in the evaluation of OC regeneration although mostly performed on the superficial articular cartilage [75]. Biomechanical tests require special equipment and are usually associated with sample destruction or alteration, unlike microtomographic assessment, which has benefits to be a nondestructive technique, so that fewer studies could have been expected involving this kind of evaluation. Considering that hard resin embedding allows to perform some mechanical evaluations, as microhardness and indentation tests, it could be reasonable to expect to find more papers using this embedding technique, as the traditional inclusion in paraffin is now accompanied by inclusion techniques in high- and low-temperature hard resins. Results instead showed that mechanical tests, mainly performed by indentation tests, are usually carried out on fresh or frozen/thawed samples, before histological processing. Specific shrewdness to avoid tissues damages and bias that could alter the subsequent analyses was applied, by keeping samples in saline solution with specific pH and temperature, or, alternatively, performing the test in the region of interest different from that employed for histology. Other technical aspects frequently reported are the stable fixation of samples, for example, with screws or cement, to guarantee the maintenance of the position of the sample perpendicular to the indenter as much as possible. In fact, one of the most critical aspects in the execution of indentation tests on fresh samples is the correct alignment with the machine, which is clearly easier when samples are already embedded in hard resin. Moreover, resin embedding allows the analysis of the biomechanical competence also of the subchondral and trabecular bone underlying articular cartilage, that in the reviewed papers always lacks. The great prevalence of indentation tests among the mechanical tests available provides a starting point for reflection on the use of this technique in the evaluation of OC regeneration. This method, in fact, has proven to be precise in evaluating tissue deformation and mechanical properties of regenerated tissues, in comparison to native ones, with possibilities to deepen the analyses at micro- and nanolevel [76]. It is reasonable to think that the improvement of these biomechanical tests as well as the progress in the level of investigation at the nanometric level will provide fundamental

indications over time not only in terms of optimization of the design and production of scaffolds and materials for OC regeneration but also in relation to the anatomical site involved.

Histomorphometry is often performed on 2D paraffin or resin-embedded specimens, different from microCT that is performed on 3D volumes. The cutting plan of the histological sections is not always clearly indicated in the papers, and it is not easy to extrapolate this information from the observation of the images, sometimes acquired at high magnification. However, the most used planes are the sagittal and frontal planes, which allow to observe the osteochondral region in its entirety, both at the level of the cartilage and of the bone. In most of the studies, it is not reported on how many slices 2D histomorphometry has been performed. If 2D morphometry is not carried out on a relevant number of sections representative of the entire defects, this might cause the lack of arising of statistically significant differences among experimental groups. Moreover, data extracted from reviewed articles show a general troubling lack of statistical analyses to evaluate the number of animals to be employed, in relationship with experimental groups, animal model, number of implants, and experimental times. An a priori power analysis to exactly define the numerical consistency of animal groups required to reach the statistical significance is imperative in primis for ethical concerns, secondly to achieve correctly the scientific objectives with related costs (Figures 2 and 3).

As far as the selected animal model is concerned, rodent result is not widely used in the literature probably because of the small dimensions, making it difficult to perform all of the above biomechanical analysis of indentation rather than histomorphometric or microtomographic ones. Despite the reduced costs of management and the availability of different strains, as well as the possibility to set up allogenic or xenogenic models, the small size of the joint and thinnest articular cartilage make their use more difficult and far from the clinical scenario. Similarly, studies involving equine models are infrequent, but in this case, the reason might be related to the demanding management of such big animals, above the ethical and affective concerns. This last aspect is particularly felt also for the canine model whose use, despite its potentiality due to the spontaneous development of joint diseases similar to humans, is not allowed in some countries. In addition, the horse is unable to maintain protected weight-bearing protocols [77]. Therefore, the location of the defect should be carefully considered to avoid early overloading. However, the thickness of equine cartilage similar to humans' and the low regeneration ability, as well as the possibility to perform specific analyses as arthroscopy, make this model quite fascinating. Porcine and ovine models share with equines some advantages, namely, the joint size, cartilage and subchondral bone thickness, accessibility for arthroscopic procedures, and limited intrinsic healing capacity. However, their management and costs can be quite challenging [77]. The most used animal model is still the rabbit, because its dimensions represent a good compromise for greater ease of management and costs and the possibility of obtaining sufficiently large anatomical segments. However, two critical aspects of this model should not be overlooked: the peculiarity of the animal's load, which makes it very different from that of humans, and its great regenerative capacity, which keeps a debate open with continuous updates on the correct size of the defects to be created to properly evaluate bone regeneration (Figure 4).

Moreover, the overview of the animal models employed shows troubling inhomogeneities in terms of defect dimensions. This observation brings to light a very common controversial aspect in regenerative medicine studies, which makes it difficult to perform an easy comparison between studies and to properly define a defect as "critical." As mentioned above, animal cartilage thickness is greatly different from that of humans (2-3 mm), with a difference of at least one millimetre in large models up to at least 2.5 millimetres in small animals. This is reflected in the dimension of the defects created, which should in any case be related to the experimental time adopted, which should not be less than 8 weeks for rabbits and 24 weeks for sheep, although longer experimental times are recommended [72]. According to these indications, the experimental times selected in the reviewed articles were coupled to the experimental models, being mostly 12 weeks for lapine and 24 weeks for canine, swine, and ovine models.

Additionally, the age of the animals must be taken into consideration since the regenerative abilities, as well as the effects of the load, are different depending on the age. A great variety has been observed in almost all animal models reviewed; perhaps, a greater homogeneity has been found only in the ovine model, in which age ranged between 2 and 4 years. Unfortunately, in many studies, age is not reported and "skeletally mature" is the only indication provided.

Apart from the Ho et al.'s study, there are no studies that compare the histological/histomorphometric and biomechanical characteristics of OC regeneration between areas subjected to high or low mechanical loads (such as femoral condyles as a high mechanical load area or as the trochlea as an area subjected to low mechanical load) in the same animal model [50]. This is important because it is known that the mechanical load has a positive effect on the repair/regeneration of both the chondral and bone tissues. Mechanical regulation of cartilage with the beneficial effects during cartilage regeneration have long been known [78]. The biomechanical environment of articular cartilage and subchondral bone, consisting of compressive and shear stresses and hydrostatic and osmotic pressures, governs with appropriate magnitudes the development and homeostasis of the tissue, as well as its regeneration. Chondrocytes are able to differently respond to biomechanical stimulations [79]: hydrostatic pressure increases the expression of metabolism related factors and activates the expression of genes associated with various cellular processes, such as extracellular matrix synthesis (cartilage oligomeric matrix protein COMP, type II and IX collagen, and GAGs) [80, 81] and proinflammatory gene suppression [82].

Another valuable aspect is what kind of data mechanical results is compared with. In some papers, results obtained from treated lesions were compared with the contralateral untreated limb or with data from healthy tissue. Another

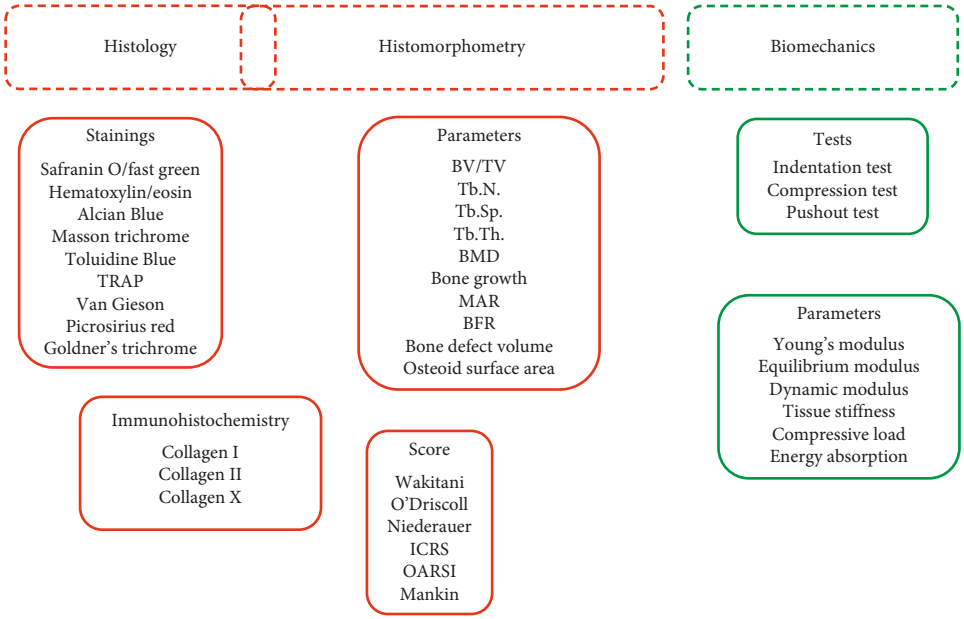

Figure 2: Overview of methods employed for histological, histomorphometrical, and biomechanical evaluations.

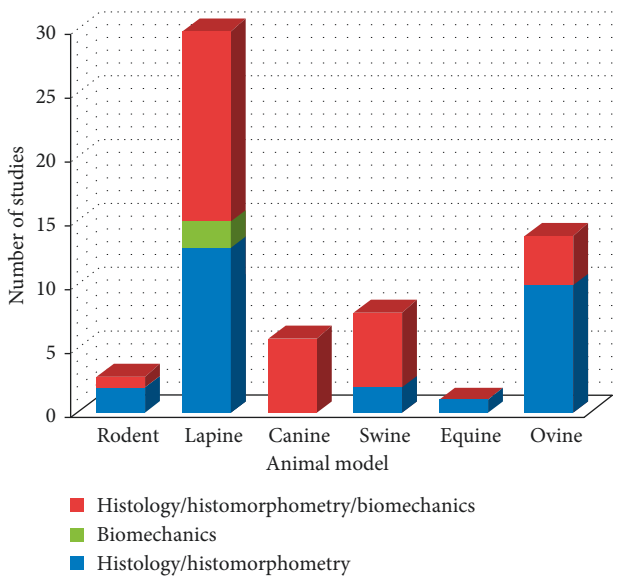

Figure 3: Number of studies in relationship with the animal model employed in which histology and/or histomorphometry and/or biomechanics are performed.

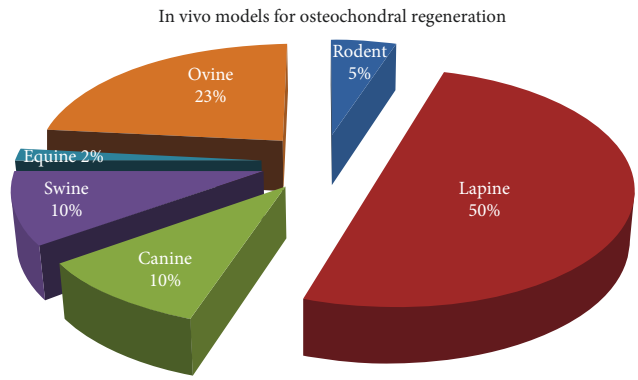

Figure 4: Distribution (%) of in vivo models employed in the reviewed studies for osteochondral regeneration.

trend found is performing the evaluation on the adjacent native tissue, especially for cartilage. However, it must be considered that, though close but not within the treated region, they still suffer from the effects related to surgical and treatment procedures and the consequent alterations of the load by the animal. In fact, some works have observed in the areas adjacent to those treated mechanical characteristics halfway between those of the regenerated tissue and the healthy one [9].

Many reviews in the literature have addressed the topic of the most used animal models or current trends in treatments for OC defects, but to our knowledge, there are none that focuses on the type of evaluation performed.

In recent years, very different studies have been carried out; all in all, some points can be focussed and reference points were considered for the development of new studies. Among histological techniques, paraffin embedding combines the possibility to perform the evaluation of the cellularity and structure of cartilage and subchondral bone, thanks also to the better yield of stainings such as Safranin O, which are able to highlight fundamental histological aspects for assessing osteochondral regeneration. Although the existing scores have many criteria in common, it is advisable to combine more than one to cover all the aspects necessary for the evaluation of both the cartilaginous and the bony district. Among all scores, the most complete still scores are O'Driscoll score and Sellers score. The immunohistochemical quantification of the collagen component remains indispensable, and it would be important to place it with assessments of subchondral bone in terms of bone metabolism/regeneration, among the evaluation of architecture with imaging methods. Finally, more effort should be put for biomechanical tests to assess the quality of regenerated

cartilage, in terms of load absorption capacity, stiffness, etc., as well as the evaluation of microhardness techniques for the evaluation of the mechanical competence of the subchondral bone, a field still little explored.

The use of comparable methods and the standardization of protocols for biomechanical tests will be essential to make the results obtained by such studies comparable and more reliable.

Conflicts of Interest

The authors declare that they have no conflicts of interest.

Acknowledgments

The work was partly supported by the Project "5×1000" 2016: "Sviluppo di modelli di valutazione preclinica per un sicuro ed efficace trasferimento in clinica delle ricerche in ambito muscoloscheletrico" and partly by Ricerca Corrente funding to the Rizzoli Orthopaedic Institute. The authors thank Dr. Lucy Scioscia for the linguistic revision of the manuscript.

References

[1] P. Bowland, E. Ingham, L. Jennings, and J. Fisher, "Review of the biomechanics and biotribology of osteochondral grafts used for surgical interventions in the knee," *Proceedings of the Institution of Mechanical Engineers, Part H: Journal of Engineering in Medicine*, vol. 229, no. 12, pp. 879–888, 2015.

[2] W. Widuchowski, J. Widuchowski, and T. Trzaska, "Articular cartilage defects: study of 25,124 knee arthroscopies," *The Knee*, vol. 14, no. 3, pp. 177–182, 2007.

[3] L. Andriolo, D. C. Crawford, D. Reale et al., "Osteochondritis dissecans of the knee: etiology and pathogenetic mechanisms. A systematic review," *Cartilage*, 2018.

[4] P. Niemeyer, M. J. Feucht, J. Fritz, D. Albrecht, G. Spahn, and P. Angele, "Cartilage repair surgery for full-thickness defects of the knee in Germany: indications and epidemiological data from the German Cartilage Registry (KnorpelRegister DGOU)," *Archives of Orthopaedic and Trauma Surgery*, vol. 136, no. 7, pp. 891–897, 2016.

[5] M. Sartori, S. Pagani, A. Ferrari et al., "A new bi-layered scaffold for osteochondral tissue regeneration: in vitro and in vivo preclinical investigations," *Materials Science and Engineering: C*, vol. 70, no. 1, pp. 101–111, 2017.

[6] M. Tamaddon, L. Wang, Z. Liu, and C. Liu, "Osteochondral tissue repair in osteoarthritic joints: clinical challenges and opportunities in tissue engineering," *Bio-Design and Manufacturing*, vol. 1, no. 2, pp. 101–114, 2018.

[7] C. Deng, J. Chang, and C. Wu, "Bioactive scaffolds for osteochondral regeneration," *Journal of Orthopaedic Translation*, vol. 17, pp. 15–25, 2019.

[8] I. R. Dias, C. A. Viegas, and P. P. Carvalho, "Large animal models for osteochondral regeneration," in *Osteochondral Tissue Engineering. Advances in Experimental Medicine and Biology*, J. Oliveira, S. Pina, R. Reis, and J. San Roman, Eds., Vol. 1059, Springer, Cham, Switzerland, 2018.

[9] E. J. Strauss, L. R. Goodrich, C.-T. Chen, C. Hidaka, and A. J. Nixon, "Biochemical and biomechanical properties of lesion and adjacent articular cartilage after chondral defect repair in an equine model," *The American Journal of Sports Medicine*, vol. 33, no. 11, pp. 1647–1653, 2005.

[10] S. Zhang, Y. Z. Jiang, W. Zhang et al., "Neonatal desensitization supports long-term survival and functional integration of human embryonic stem cell-derived mesenchymal stem cells in rat joint cartilage without immunosuppression," *Stem Cells and Development*, vol. 22, no. 1, pp. 90–101, 2013.

[11] L. F. Mendes, H. Katagiri, W. L. Tam et al., "Advancing osteochondral tissue engineering: bone morphogenetic protein, transforming growth factor, and fibroblast growth factor signaling drive ordered differentiation of periosteal cells resulting in stable cartilage and bone formation in vivo," *Stem Cell Research and Therapy*, vol. 9, no. 1, p. 42, 2018.

[12] S. Lin, W. Y. W. Lee, Q. Feng et al., "Synergistic effects on mesenchymal stem cell-based cartilage regeneration by chondrogenic preconditioning and mechanical stimulation," *Stem Cell Research and Therapy*, vol. 8, no. 1, p. 221, 2017.

[13] K. Ye, K. Traianedes, S. A. Robins, P. F. M. Choong, and D. E. Myers, "Osteochondral repair using an acellular dermal matrix-pilot in vivo study in a rabbit osteochondral defect model," *Journal of Orthopaedic Research*, vol. 36, no. 7, pp. 1919–1928, 2018.

[14] F. Veronesi, M. Cadossi, G Giavaresi et al., "Pulsed electromagnetic fields combined with a collagenous scaffold and bone marrow concentrate enhance osteochondral regeneration: an in vivo study Orthopedics and biomechanics," *BMC Musculoskeletal Disorders*, vol. 16, no. 1, p. 233, 2015.

[15] H. Schmal, J. Kowal, M. Kassem et al., "Comparison of regenerative tissue quality following matrix-associated cell implantation using amplified chondrocytes compared to synovium-derived stem cells in a rabbit model for cartilage lesions," *Stem Cells Int*, vol. 2018, p. 4142031, 2018.

[16] C.-C. Wong, C.-H. Chen, L.-H. Chiu et al., "Facilitating in vivo articular cartilage repair by tissue-engineered cartilage grafts produced from auricular chondrocytes," *The American Journal of Sports Medicine*, vol. 46, no. 3, pp. 713–727, 2018.

[17] R. Fekrazad, M. B. Eslaminejad, A. M. Shayan et al., "Effects of photobiomodulation and mesenchymal stem cells on articular cartilage defects in a rabbit model," *Photomedicine and Laser Surgery*, vol. 34, no. 11, pp. 543–549, 2016.

[18] S. Kazemnejad, M. Khanmohammadi, S. Mobini et al., "Comparative repair capacity of knee osteochondral defects using regenerated silk fiber scaffolds and fibrin glue with/without autologous chondrocytes during 36 weeks in rabbit model," *Cell and Tissue Research*, vol. 364, no. 3, pp. 559–572, 2016.

[19] V. M. Betz, A. Keller, P. Foehr et al., "BMP-2 gene activated muscle tissue fragments for osteochondral defect regeneration in the rabbit knee," *The Journal of Gene Medicine*, vol. 19, no. 9-10, p. e2972, 2017.

[20] K. Shimomura, Y. Moriguchi, W. Ando et al., "Osteochondral repair using a scaffold-free tissue-engineered construct derived from synovial mesenchymal stem cells and a hydroxyapatite-based artificial bone," *Tissue Engineering Part A*, vol. 20, no. 17-18, pp. 2291–2304, 2014.

[21] E. J. Chung, P. Kodali, W. Laskin, J. L. Koh, and G. A. Ameer, "Long-term in vivo response to citric acid-based nanocomposites for orthopaedic tissue engineering," *Journal of Materials Science: Materials in Medicine*, vol. 22, no. 9, pp. 2131–2138, 2011.

[22] J. Guzmán-Morales, C.-H. Lafantaisie-Favreau, G. Chen, and C. D. Hoemann, "Subchondral chitosan/blood implant-guided bone plate resorption and woven bone repair is coupled to hyaline cartilage regeneration from microdrill

holes in aged rabbit knees," *Osteoarthritis and Cartilage*, vol. 22, no. 2, pp. 323–333, 2014.

[23] C. H. Lafantaisie-Favreau, J. Guzmán-Morales, J. Sun et al., "Subchondral pre-solidified chitosan/blood implants elicit reproducible early osteochondral wound-repair responses including neutrophil and stromal cell chemotaxis, bone resorption and repair, enhanced repair tissue integration and delayed matrix deposition," *BMC Musculoskeletal Disorders*, vol. 14, no. 1, p. 27, 2013.

[24] Y.-C. Cheuk, M. W.-N. Wong, K.-M. Lee, and S.-C. Fu, "Use of allogeneic scaffold-free chondrocyte pellet in repair of osteochondral defect in a rabbit model," *Journal of Orthopaedic Research*, vol. 29, no. 9, pp. 1343–1350, 2011.

[25] T. Vaseenon, Y. Tochigi, A. D. Heiner et al., "Organ-level histological and biomechanical responses from localized osteoarticular injury in the rabbit knee," *Journal of Orthopaedic Research*, vol. 29, no. 3, pp. 340–346, 2011.

[26] S. Zhang, L. Chen, Y. Jiang et al., "Bi-layer collagen/microporous electrospun nanofiber scaffold improves the osteochondral regeneration," *Acta Biomaterialia*, vol. 9, no. 7, pp. 7236–7247, 2013.

[27] E. J. P. Jansen, J. Pieper, M. J. J. Gijbels et al., "PEOT/PBT based scaffolds with low mechanical properties improve cartilage repair tissue formation in osteochondral defects," *Journal of Biomedical Materials Research Part A*, vol. 89A, no. 2, pp. 444–452, 2009.

[28] M. Bayat, F. Javadieh, and M. Dadpay, "Effect of He-Ne laser radiation on healing of osteochondral defect in rabbit: a histological study," *The Journal of Rehabilitation Research and Development*, vol. 46, no. 9, pp. 1135–1142, 2009.

[29] G. Filardo, F. Perdisa, M. Gelinsky et al., "Novel alginate biphasic scaffold for osteochondral regeneration: an in vivo evaluation in rabbit and sheep models," *Journal of Materials Science: Materials in Medicine*, vol. 29, no. 6, p. 74, 2018.

[30] C. Martin-Hernandez, J. Cebamanos-Celma, A. Molina-Ros, J. J. Ballester-Jimenez, and J. Ballester-Soleda, "Regenerated cartilage produced by autogenous periosteal grafts: a histologic and mechanical study in rabbits under the influence of continuous passive motion," *Arthroscopy: The Journal of Arthroscopic and Related Surgery*, vol. 26, no. 1, pp. 76–83, 2010.

[31] F. Javadieh, M. Bayat, and G. Torkaman, "Evaluation of low-level laser therapy with a He-Ne laser on the healing of an osteochondral defect using a biomechanical test," *Photomedicine and Laser Surgery*, vol. 28, no. 3, pp. 423–428, 2010.

[32] T. Oncan, B. Demirağ, C. Ermutlu, U. Yalçinkaya, and L. Özkan, "Effect of low-dose irradiation on structural and mechanical properties of hyaline cartilage-like fibrocartilage," *Acta Orthopaedica et Traumatologica Turcica*, vol. 47, no. 2, pp. 127–133, 2013.

[33] R. Rahman, N. Mohamad Sukri, N. Md Nazir et al., "Evaluation of three dimensional construct engineered from poly(Lactic-co-glycolic acid)/fibrin hybrid scaffold using rabbit bone marrow mesenchymal stem cells for osteochondral defect repair," *Jurnal Teknologi*, vol. 77, no. 25, pp. 77–82, 2015.

[34] K. Shimomura, Y. Moriguchi, R. Nansai et al., "Comparison of 2 different formulations of artificial bone for a hybrid implant with a tissue-engineered construct derived from synovial mesenchymal stem cells: a study using a rabbit osteochondral defect model," *The American Journal of Sports Medicine*, vol. 45, no. 3, pp. 666–675, 2017.

[35] H. Yin, Y. Wang, X. Sun et al., "Functional tissue-engineered microtissue derived from cartilage extracellular matrix for articular cartilage regeneration," *Acta Biomaterialia*, vol. 77, pp. 127–141, 2018.

[36] C. C. Wang, K. C. Yang, K. H. Lin et al., "Expandable scaffold improves integration of tissue-engineered cartilage: an in vivo study in a rabbit model," *Tissue Engineering Part A*, vol. 22, no. 11-12, pp. 873–884, 2016.

[37] S. Jia, T. Zhang, Z. Xiong, W. Pan, J. Liu, and W. Sun, "In vivo evaluation of a novel oriented scaffold-BMSC construct for enhancing full-thickness articular cartilage repair in a rabbit model," *PLoS One*, vol. 10, no. 12, Article ID e0145667, 2015.

[38] S. Wada, N. Kitamura, T. Nonoyama et al., "Hydroxyapatite-coated double network hydrogel directly bondable to the bone: biological and biomechanical evaluations of the bonding property in an osteochondral defect," *Acta Biomaterialia*, vol. 44, pp. 125–134, 2016.

[39] M. T. I. Mredha, N. Kitamura, T. Nonoyama et al., "Anisotropic tough double network hydrogel from fish collagen and its spontaneous in vivo bonding to bone," *Biomaterials*, vol. 132, pp. 85–95, 2017.

[40] Q. Wang, H. Zhang, H. Gan, H. Wang, Q. Li, and Z. Wang, "Application of combined porous tantalum scaffolds loaded with bone morphogenetic protein 7 to repair of osteochondral defect in rabbits *," *International Orthopaedics*, vol. 42, no. 7, pp. 1437–1448, 2018.

[41] L. Xiangyu, D. Pingguo, G. Jingming et al., "Bilayered PLGA/PLGA-HAp composite scaffold for osteochondral tissue engineering and tissue regeneration," *ACS Biomaterials Science and Engineering*, vol. 4, pp. 3506–3521, 2018.

[42] F. Cao, J. Qi, H. Song et al., "Tsmu solution improves rabbit osteochondral allograft preservation and transplantation outcome," *Cell and Tissue Banking*, vol. 19, no. 4, pp. 549–558, 2018.

[43] Y. Qiang, Z. Yanhong, P. Jiang et al., "Xenoimplantation of an extracellular-matrix-derived, biphasic, cell-scaffold construct for repairing a large femoral-head high-load-bearing osteochondral defect in a canine model," *The ScientificWorld Journal*, vol. 2014, p. 127084, 2014.

[44] E. C. McCarty, R. R. Fader, J. J. Mitchell, R. E. Glenn Jr., H. G. Potter, and K. P. Spindler, "Fresh osteochondral allograft versus autograft," *The American Journal of Sports Medicine*, vol. 44, no. 9, pp. 2354–2365, 2016.

[45] R. Baba, T. Onodera, M. Matsuoka et al., "Bone marrow stimulation technique augmented by an ultrapurified alginate gel enhances cartilage repair in a canine model," *The American Journal of Sports Medicine*, vol. 46, no. 8, pp. 1970–1979, 2018.

[46] Q. Yang, J. Peng, S. B. Lu et al., "Evaluation of an extracellular matrix-derived acellular biphasic scaffold/cell construct in the repair of a large articular high-load-bearing osteochondral defect in a canine model," *Chinese Medical Journal*, vol. 124, no. 23, pp. 3930–3938, 2011.

[47] J. L. Cook, J. P. Stannard, A. M. Stoker et al., "Importance of donor chondrocyte viability for osteochondral allografts," *The American Journal of Sports Medicine*, vol. 44, no. 5, pp. 1260–1268, 2016.

[48] J. L. Cook, A. M. Stoker, J. P. Stannard et al., "A novel system improves preservation of osteochondral allografts," *Clinical Orthopaedics and Related Research*, vol. 472, no. 11, pp. 3404–3414, 2014.

[49] A. He, L. Liu, X. Luo et al., "Repair of osteochondral defects with in vitro engineered cartilage based on autologous bone marrow stromal cells in a swine model," *Scientific Reports*, vol. 7, p. 40489, 2017.

[50] S. T. B. Ho, D. W. Hutmacher, A. K. Ekaputra, D. Hitendra, and J. H. Hui, "The evaluation of a biphasic osteochondral implant coupled with an electrospun membrane in a large animal model," *Tissue Engineering Part A*, vol. 16, no. 4, pp. 1123–1141, 2010.

[51] B. B. Christensen, C. B. Foldager, M. L. Olesen, K. C. Hede, and M. Lind, "Implantation of autologous cartilage chips improves cartilage repair tissue quality in osteochondral defects," *The American Journal of Sports Medicine*, vol. 44, no. 6, pp. 1597–1604, 2016.

[52] M. Jung, B. Kaszap, A. Redöhl et al., "Enhanced early tissue regeneration after matrix-assisted autologous mesenchymal stem cell transplantation in full thickness chondral defects in a minipig model," *Cell Transplantation*, vol. 18, no. 8, pp. 923–932, 2009.

[53] T. Gotterbarm, S. J. Breusch, S. B. Vilei, P. Mainil-Varlet, W. Richter, and M. Jung, "No effect of subperiosteal growth factor application on periosteal neo-chondrogenesis in osteoperiosteal bone grafts for osteochondral defect repair," *International Orthopaedics*, vol. 37, no. 6, pp. 1171–1178, 2013.

[54] Q. Zuo, W. Cui, F. Liu, Q. Wang, Z. Chen, and W. Fan, "Utilizing tissue-engineered cartilage or BMNC-PLGA composites to fill empty spaces during autologous osteochondral mosaicplasty in porcine knees," *Journal of Tissue Engineering and Regenerative Medicine*, vol. 10, no. 11, pp. 916–926, 2016.

[55] M. I. Menendez, D. J. Clark, M. Carlton et al., "Direct delayed human adenoviral BMP-2 or BMP-6 gene therapy for bone and cartilage regeneration in a pony osteochondral model," *Osteoarthritis and Cartilage*, vol. 19, no. 8, pp. 1066–1075, 2011.

[56] C. J. A. van Bergen, G. M. M. J. Kerkhoffs, M. Özdemir et al., "Demineralized bone matrix and platelet-rich plasma do not improve healing of osteochondral defects of the talus: an experimental goat study," *Osteoarthritis and Cartilage*, vol. 21, no. 11, pp. 1746–1754, 2013.

[57] W. J. F. M. Jurgens, R. J. Kroeze, B. Zandieh-Doulabi et al., "One-step surgical procedure for the treatment of osteochondral defects with adipose-derived stem cells in a caprine knee defect: a pilot study," *BioResearch Open Access*, vol. 2, no. 4, pp. 315–325, 2013.

[58] G. M. Cunniffe, P. J. Díaz-Payno, E. J. Sheehy et al., "Tissue-specific extracellular matrix scaffolds for the regeneration of spatially complex musculoskeletal tissues," *Biomaterials*, vol. 188, pp. 63–73, 2019.

[59] B. Marquass, J. S. Somerson, P. Hepp et al., "A novel MSC-seeded triphasic construct for the repair of osteochondral defects," *Journal of Orthopaedic Research*, vol. 28, no. 12, pp. 1586–1599, 2010.

[60] A. Bernstein, P. Niemeyer, G. Salzmann et al., "Microporous calcium phosphate ceramics as tissue engineering scaffolds for the repair of osteochondral defects: histological results," *Acta Biomaterialia*, vol. 9, no. 7, pp. 7490–7505, 2013.

[61] A. D. Bell, V. Lascau-Coman, J. Sun et al., "Bone-induced chondroinduction in sheep Jamshidi biopsy defects with and without treatment by subchondral chitosan-blood implant," *Cartilage*, vol. 4, no. 2, pp. 131–143, 2013.

[62] S. Jia, J. Wang, T. Zhang et al., "Multilayered scaffold with a compact interfacial layer enhances osteochondral defect repair," *ACS Applied Materials and Interfaces*, vol. 10, no. 24, pp. 20296–20305, 2018.

[63] E. Kon, G. Filardo, D. Robinson et al., "Osteochondral regeneration using a novel aragonite-hyaluronate bi-phasic scaffold in a goat model," *Knee Surgery, Sports Traumatology, Arthroscopy*, vol. 22, no. 6, pp. 1452–1464, 2014.

[64] E. Kon, G. Filardo, M. Delcogliano et al., "Platelet autologous growth factors decrease the osteochondral regeneration capability of a collagen-hydroxyapatite scaffold in a sheep model," *BMC Musculoskeletal Disorders*, vol. 11, no. 1, p. 220, 2010.

[65] A. F. Manunta, P. Zedde, S. Pilicchi et al., "The use of embryonic cells in the treatment of osteochondral defects of the knee: an ovine in vivo study," *Joints*, vol. 4, no. 2, pp. 70–79, 2016.

[66] T. L. Nosewicz, M. L. Reilingh, M. Wolny, C. N. van Dijk, G. N. Duda, and H. Schell, "Influence of basal support and early loading on bone cartilage healing in press-fitted osteochondral autografts," *Knee Surgery, Sports Traumatology, Arthroscopy*, vol. 22, no. 6, pp. 1445–1451, 2014.

[67] I. Schleicher, K. S. Lips, U. Sommer et al., "Biphasic scaffolds for repair of deep osteochondral defects in a sheep model," *Journal of Surgical Research*, vol. 183, no. 1, pp. 184–192, 2013.

[68] H. O. Mayr, J. Klehm, S. Schwan et al., "Microporous calcium phosphate ceramics as tissue engineering scaffolds for the repair of osteochondral defects: biomechanical results," *Acta Biomaterialia*, vol. 9, no. 1, pp. 4845–4855, 2013.

[69] F. R. Maia, M. R. Carvalho, J. M. Oliveira, and R. L. Reis, "Tissue engineering strategies for osteochondral repair," *Osteochondral Tissue Engineering*, vol. 1059, pp. 353–371, 2018.

[70] F. M. M. da Cunha Cavalcanti, D. Doca, M. Cohen, and M. Ferretti, "Updating on diagnosis and treatment of chondral lesion of the knee," *Revista Brasileira de Ortopedia (English Edition)*, vol. 47, no. 1, pp. 12–20, 2012.

[71] D. J. Kelly and P. J. Prendergast, "Prediction of the optimal mechanical properties for a scaffold used in osteochondral defect repair," *Tissue Engineering*, vol. 12, no. 9, pp. 2509–2519, 2006.

[72] C. Hoemann, R. Kandel, S. Roberts et al., "International cartilage repair society (ICRS) recommended guidelines for histological endpoints for cartilage repair studies in animal models and clinical trials," *Cartilage*, vol. 2, no. 2, pp. 153–172, 2011.

[73] M. Rutgers, M. J. P. van Pelt, W. J. A. Dhert, L. B. Creemers, and D. B. F. Saris, "Evaluation of histological scoring systems for tissue-engineered, repaired and osteoarthritic cartilage," *Osteoarthritis and Cartilage*, vol. 18, no. 1, pp. 12–23, 2010.

[74] P. Orth, D. Zurakowski, D. Wincheringer, and H. Madry, "Reliability, reproducibility, and validation of five major histological scoring systems for experimental articular cartilage repair in the rabbit model," *Tissue Engineering Part C: Methods*, vol. 18, no. 5, pp. 329–339, 2012.

[75] C. Erisken, D. M. Kalyon, and H. Wang, "Viscoelastic and biomechanical properties of osteochondral tissue constructs generated from graded polycaprolactone and beta-tricalcium phosphate composites," *Journal of Biomechanical Engineering*, vol. 132, no. 9, p. 91013, 2010.

[76] M. Boi, G. Marchiori, M. Berni et al., "Nanoindentation: an advanced procedure to investigate osteochondral engineered tissues," *Journal of the Mechanical Behavior of Biomedical Materials*, vol. 96, pp. 79–87, 2019.

[77] C. R. Chu, M. Szczodry, and S. Bruno, "Animal models for cartilage regeneration and repair," *Tissue Engineering Part B: Reviews*, vol. 16, no. 1, pp. 105–115, 2010.

[78] V. Glatt, C. H. Evans, and M. J. Stoddart, "Regenerative rehabilitation: the role of mechanotransduction in orthopaedic

regenerative medicine," *Journal of Orthopaedic Research*, vol. 37, no. 6, pp. 1263–1269, 2019.

[79] N. Fahy, M. Alini, and M. J. Stoddart, "Mechanical stimulation of mesenchymal stem cells: implications for cartilage tissue engineering," *Journal of Orthopaedic Research*, vol. 36, no. 1, pp. 52–63, 2018.

[80] R. L. Mauck, M. A. Soltz, and C. C. Wang, "Functional tissue engineering of articular cartilage through dynamic loading of chondrocyte-seeded agarose gels," *Journal of Biomechanical Engineering*, vol. 122, no. 3, pp. 252–260, 2000.

[81] K. W. Ng, R. L. Mauck, and C. C. Wang, "Duty cycle of deformational loading influences the growth of engineered articular cartilage," *Cellular and Molecular Bioengineering*, vol. 2, no. 3, pp. 386–394, 2009.

[82] A. Dossumbekova, M. Anghelina, and S. Madhavan, "Biomechanical signals inhibit IKK activity to attenuate NF-κB transcription activity in inflamed chondrocytes," *Arthritis and Rheumatology*, vol. 56, no. 10, pp. 3284–3296, 2007.

Hindawi
BioMed Research International
Volume 2019, Article ID 8483658, 6 pages
https://doi.org/10.1155/2019/8483658

Clinical Study

Observational Study on the Preparation of the Implant Site with Piezosurgery vs. Drill: Comparison between the Two Methods in terms of Postoperative Pain, Surgical Times, and Operational Advantages

Michele Maglione,[1] Lorenzo Bevilacqua,[1] Federica Dotto,[1] Fulvia Costantinides,[1] Felice Lorusso,[2] and Antonio Scarano[2,3]

[1]*Department of Medical Sciences, University of Trieste, 34127 Trieste, Italy*
[2]*Department of Medical, Oral and Biotechnological Sciences and CeSi-MeT, University of Chieti-Pescara, Via Dei Vestini 31, 66100 Chieti, Italy*
[3]*Department of Oral Implantology, Dental Research Division, College Ingà, UNINGÁ, Cachoeiro de Itapemirim 29312, Brazil*

Correspondence should be addressed to Antonio Scarano; ascarano@unich.it

Received 26 May 2019; Revised 9 August 2019; Accepted 12 September 2019; Published 29 September 2019

Guest Editor: Elena Della Bella

Purpose. Recent advances show that ultrasonic implant site osteotomy is related to a decreased trauma and a better postoperative healing of the surgical site when compared to traditional drilling techniques. The micrometric bone cutting control and the operative advantages related to the piezoelectric approach are also characterized by a learning curve for the clinician in surgical practice and an increased operative duration of the procedure. The aim of this investigation is to compare the operative time, the postoperative pain, and the amount of painkillers taken by the patient during the healing period. *Methods*. A total of 65 patients were treated at the Unit of Oral Surgery (Department of Medical Sciences, Surgery and Health, University of Trieste, Italy) using a split mouth model: 75 drill-inserted implants (G1) and 75 piezoelectric device-inserted implants (G2) were placed. The Visual Analogue Scale (VAS) was performed to evaluate the postoperative pain at 15 days from surgery. The operative time and frequency of intake of painkillers were measured. *Results*. The G1 and G2 groups showed a significant difference with a higher use of painkillers observed for G1. The G2 patients showed a lower level of pain (VAS) at all experimental times between 8 hours to 7 days ($p < 0.01$) postsurgery. At 15 days, the pain levels were similar for both groups. No differences were found in site preparation duration between the study groups. *Conclusions*. The evidence supports the application of the piezoelectric approach compared to the drill's osteotomy as a useful technique for implant site preparation. This trial is registered with NCT03978923.

1. Introduction

Piezosurgery has long been applied in implantology for the preparation of implant sites because of its selective cut, cavitational effect, and preservation of soft tissues [1–3]. It achieves the most correct positioning of implants and allows for a more predictable osteointegration while providing an increased respect of bone vitality.

Recent studies have suggested that there are no statistically significant differences in terms of primary stability between implant sites prepared with piezosurgery and those using the traditional technique with dedicated drills [4]. Numerous histological studies conducted both in vitro and in vivo have shown that ultrasonic microvibrations minimize trauma during the cutting action [5]. As a result, bone healing is much faster from both histological and histochemical points of view [6–8].

Furthermore, clinical benefits were highlighted both intraoperatively and postoperatively. The day after surgery, the postoperative edema resulted smaller than those in the sites

treated with traditional methods and numerous advantages were found regarding patients' symptoms, both in terms of greater intraoperative comfort and a better postoperative course [9]. Multiple implant rehabilitative protocols involve the use of the piezoelectric technique not only in complex clinical conditions that require, for example, ridge expansion (split crest) or maxillary sinus lift but also in simpler cases, limited only to the preparation of the implant site.

In fact, even in nonadvanced implantology, there are some clinical conditions of objective difficulty regarding the initial stages of surgery. The initial preparation of the implant site using only the pilot drills on the handpiece present in the implant kit, in some circumstances, can be complex; this is due to the fact that the rotation of the cutter, and therefore the macromovements, makes the implant difficult to precisely stabilize at the point established by the operator. In these cases, ultrasound systems are important aids for the surgeon, as a safe, reliable, and advantageous method from an intraoperative (technical-related) point of view.

The main technical and executive advantages of piezoelectric surgery for the operator can be summarized as follows:

(i) More stable positioning of the guide inserts on the crestal profile for the creation of the first implant site

(ii) Definition of a more correct implant axis that helps in the success of the implant-prosthetic rehabilitation

(iii) Possibility of intraoperative corrections of the implant axis

(iv) Execution of the cortical crestal osteotomy in a more secure way, thanks to the fact that the piezoelectric handpiece is ergonomically pivoted and free from the initial "waving" phenomena typical of rotating systems

(v) Realization of the initial osteotomy in a less traumatic way and with a greater visibility of the operative field, thanks to the cavitational process with constant irrigation

(vi) Reduction of the emotional impact on the patient, who does not perceive the annoying vibrations caused by the use of drills on the handpiece

The biological advantages, that are however technically related, can be listed as follows:

(i) Reduction of thermal stress on bone tissue

(ii) Maintenance of a better bone vitality

(iii) Greater respect for osteoblastic turnover and better postresective bone response

(iv) Preservation of the soft tissues and of any noble anatomical structures (inferior alveolar nerve, Schneiderian membrane, etc.) contiguous to the osteotomy [10–12]

Undoubtedly today, ultrasonic surgery techniques are superior to traditional, rotating, or manual instruments, thanks to greater cutting precision and to the possibility of creating more conservative surgical access, as there is no risk of damaging the soft tissues, less operator fatigue, and minimal risk of developing bone thermonecrosis although they present a reduced speed of execution [13–15]. In a previous study, we compared two different implant site preparation techniques using piezoelectric surgery vs. conventional drills with evaluation of pain in patients who were prescribed painkillers, and this research showed less pain in the site prepared with an ultrasonic device [16]. In light of these premises, the main objective of this study was to verify if there were differences between the traditional method with micromotor and dedicated drills and the piezoelectric technique with dedicated tips. The preparation time of the implant site was compared for the two methods, both in absolute terms and according to the type of bone. Then, the operator's learning curve implant survival and the presence of postoperative complications were also evaluated with the piezoelectric method. Finally, attention was paid to the intra- and postoperative pain and to the need for pain medication in the postoperative phases through the use of painkillers.

2. Materials and Methods

The study was conducted with the approval of the local ethical committee (n. 88-10.05.2018) of University of Trieste.

The following study included adult patients undergoing implant therapy with insertion of two contralateral conical implants with a diameter between 3.8 and 4.5 mm with a maximum torque of 35 Ncm. In a single sitting, one site was prepared with Ultrasonic device (Esacrom, Imola, Italy), while the contralateral site was prepared with micromotor and dedicated drills. All patients were treated at the Unit of Oral Surgery (Department of Medical Sciences, Surgery and Health, University of Trieste, Italy). Seventy-five patients were enrolled in the study, 44 women and 31 men, aged between 45 and 70, who underwent implant therapy in the period between January 2013 and December 2017. The inclusion criteria were edentulous or partly edentulous with a bilateral loss of teeth in the maxillary or mandible and bone type D2 or D3, according to Misch classification [17]. In general, it is easy to differentiate these bone qualities D2 and D3 than bone types D1 or D4.

The exclusion criteria included general contraindications to implant surgery, severe coagulation disorders, leukocyte or metabolic diseases, immunosuppressed or immunocompromised patients, patients receiving chemotherapy for less than 1 year, patients on therapy or having taken aminobisphosphonates intravenously, patients irradiated at the head or neck, patients with uncontrolled diabetes, pregnant, and lactating patients, patients with poor oral hygiene and motivation, patients needing maxillary sinus lift concomitant with implant insertion, and postextraction sites with acute or purulent infections.

The final sample of the implants inserted was 150 (75 per technique) divided into two groups: the drill-inserted implants (G1) and the ultrasonic device-inserted implants (G2). Each patient subscribed an informed written consent and underwent a preoperative oral hygiene session. Two

grams of amoxicillin was administered to each patient in the preoperative phase.

Before surgery, each patient used a 0.2% chlorhexidine mouthwash for one minute.

The surgery was always performed by the same operator (M. M.) to reduce the bias of the study. Locoregional anesthesia was performed with mepivacaine hydrochloride with 1 : 100000 adrenaline.

For the preparation of implant sites using traditional methods, the drills used, following the manufacturer's protocol, were specific for the implant system in use (WINSIX®- BioSAF IN srl, Trezzano Rosa, Trezzano Rosa, Milano, Italy).

For the preparation of the other sites, an ultrasonic device was used (Surgysonic II, Esacrom S.R.L., Imola, Italy). For the final preparation and insertion of implants, 5-6 ultrasound inserts were used in sequence as follows: tip-shape 1st insert (ES012X) and 2nd insert (ES052XG), crown-shape 3rd insert (ES040), 4th insert (ES041), 5th insert (ES043), and 6th insert (ES044).

The implant insertions were performed with a maximum torque of 35 Ncm with manual calibrated torque gauge ratchet. Finally, the cap screws were positioned, and the flaps were sutured with Vycril® 3.0.

Each patient was prescribed a 0.2% chlorhexidine mouthwash to be used twice a day for two weeks and paracetamol 1000 mg (maximum 3 tablets a day) as a pain-relieving therapy.

Each patient included in the study was in possession of two questionnaires, one per technique, for the evaluation of the treatment. In the questionnaires, the patient was asked to trace an "X" representing the level of pain experienced. The questionnaire recorded the individual symptoms experienced during the surgery, after 8 hours, from the 1st to the 7th postoperative day and finally any persistence of the symptoms on the 15th day after surgery. In the same questionnaire, it was also asked to indicate the possible intake of painkillers and the related dose after surgery and in the following six days; moreover, after the fifteenth day, the patient was asked if he would have repeated the experience of the implant surgery. Then, for each patient, a postoperative check was scheduled: after one week, all the patients were recalled for a postoperative control and the removal of the sutures.

For the subjective analysis of the effects of the two methods, it was decided to use the Visual Analogue Scale (VAS). This linear scale is the visual representation of the amplitude of pain that the patient perceives. It is a horizontal line of 100 mm long, in which one end indicates the absence of pain, while the other represents the worst pain imaginable.

During the surgical procedure, the preparation times of the implant site were measured from the preparation of the flap up to the insertion of the implant.

Immediately after the end of the surgical procedure, a questionnaire on the operative difficulty was compiled by the operator. In particular, the two techniques were compared considering two factors: the easiness in obtaining a correct axis of implant insertion and the quality of visibility.

Furthermore, a cumulative judgement was done for the whole procedure, as "simple," "medium difficulty," or "difficult."

3. Statistical Analysis

SPSS software (SPSS Inc. Chicago, IL) was used for statistical analysis. A value of $p < 0.05$ was used in rejecting the null hypothesis.

In addition, continuous data were analyzed using nonparametric tests given the asymmetric distribution of some data sets.

The Friedman test was used to evaluate the significance of VAS differences between the groups over time. The Wilcoxon test was used to intercept differences between the groups at each time point. The Wilcoxon rank signed test was used as the post hoc test for pairwise comparison to evaluate the significance of VAS differences between the groups.

A Cochran test was used to assess the significance of differences in the frequency of intake of painkillers between the groups over time. Subsequently, a McNemar test was used for post hoc analysis and to assess the significance of differences in the frequency of intake of painkillers between groups each time point.

After having calculated the mean operative times for G1 and G2, the Mann–Whitney test was used to compare the differences in surgical times between D2 and D3 bone types within each group, while the Wilcoxon test was used to intercept the differences between the groups in bone types D2 and D3, respectively.

The Cochran test was used to test the differences in the operator questionnaire answers between the groups.

4. Results

From the analysis carried out on the comparison of the VAS scale of the statistical units treated with drill and piezoelectric methodology, a statistically significant difference was found in regard to the intraoperative symptomatology between each group over time (Friedman test: G1, $p < 0.001$; G2, $p < 0.001$). Differences of VAS values within the groups and between the groups at each time point are reported in Table 1.

The differences in the frequency of intake of painkillers between the groups over time showed statistical significance (Cochran test; G1, $p < 0.001$; G2, $p < 0.001$) (Figure 1).

From the analysis carried out on the comparison between the average surgical times of preparation of the implant sites in the experimental groups, it was found that the average time in the G1 was 9.7 minutes (±4.7), whereas in G2, it was 13.1 minutes (±6.2) (Figure 2).

Considering the different bone types, no differences were found in preparation times within the study groups (Mann–Whitney test, p = NS), whereas a significant difference was found between the groups, both for D2 and D3 densities (Wilcoxon test: D2, $p < 0.05$; D3, $p < 0.001$) (Table 2).

Table 1: Pain rate of patients in intraoperative and postoperative times recorded by VAS Score.

Group	VAS										
	Intraop.	8 hours	1 day	2 days	3 days	4 days	5 days	6 days	7 days	15 days	Diff.*
G1	4.05	3.58[a]	2.72[b]	2.28[c]	1.67[d]	0.86[e]	0.77	0.49[f]	0.33[g]	0.05[h]	$p = 0.000$
G2	2.51	2.09	1.47[b]	1.02[j]	0.70[k]	0.42[l]	0.26	0.12	0.09	0.02	$p = 0.000$
Diff.**	$p = 0.000$	$p = 0.000$	$p = 0.000$	$p = 0.000$	$p = 0.000$	$p = 0.002$	$p = 0.001$	$p = 0.007$	$p = 0.014$	$p = 0.317$	

*Friedman test; **Wilcoxon test. [a]Significant difference with "intraop." VAS; Wilcoxon test, $p < 0.05$. [b]Significant difference with "8 hours" VAS; Wilcoxon test, $p < 0.001$. [c]Significant difference with "1 day" VAS; Wilcoxon test, $p < 0.05$. [d]Significant difference with "2 days" VAS; Wilcoxon test, $p < 0.001$. [e]Significant difference with "3 days" VAS; Wilcoxon test, $p < 0.001$. [f]Significant difference with "5 days" VAS; Wilcoxon test, $p < 0.05$. [g]Significant difference with "6 days" VAS; Wilcoxon test, $p < 0.05$. [h]Significant difference with "7 days" VAS; Wilcoxon test, $p < 0.05$. [j]Significant difference with "1 day" VAS; Wilcoxon test, $p < 0.001$. [k]Significant difference with "2 days" VAS; Wilcoxon test, $p < 0.05$. [l]Significant difference with "3 days" VAS; Wilcoxon test, $p < 0.05$.

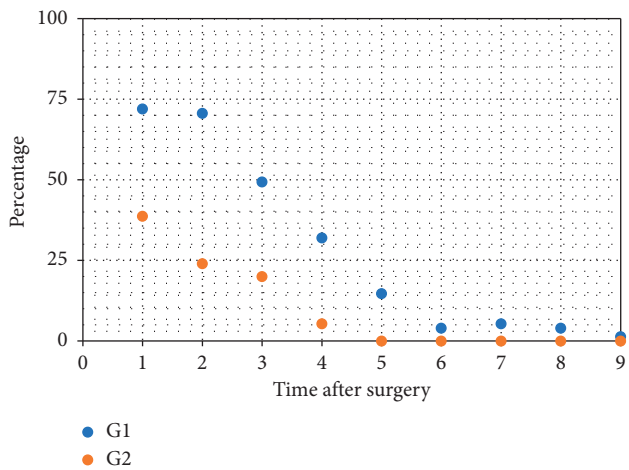

Figure 1: Frequency of intake of painkillers in percentage.

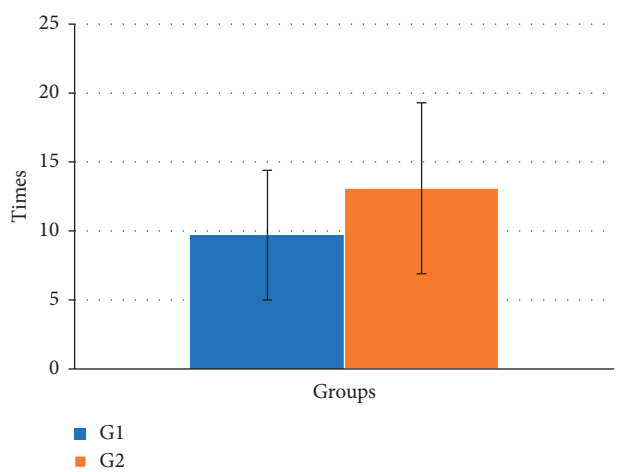

Figure 2: Operative surgery duration evaluated for the two study groups (min.). Significant difference with G1; Mann–Whitney test, $p < 0.005$.

Answers given by the oral surgeon to the questionnaires showed a significant difference between G1 and G2 only for the quality of visibility (McNemar test, $p < 0.05$). Easiness in reaching the correct axis of insertion and the global judgement on the difficulty of the surgery did not show significant differences (Cochran test, $p <$ NS).

Table 2: Operative surgery duration evaluated considering the different bone types.

Groups	D2 mean times (min)	D3 mean times (min)	Diff.*
G1	10.74 ± 5	8.6 ± 4.6	$p = 0.133$
G2	13.04 ± 6.9	13.15 ± 5.5	$p = 0.516$
Diff.**	$p = 0.000$	$p = 0.000$	

*Mann–Whitney test. **Wilcoxon test.

5. Discussion

The objective of the present investigation was firstly to monitor postoperative pain of implants placed in sites prepared with drills and ultrasonic inserts.

The results of this clinical study showed significant effectiveness of the ultrasonic technique for performing implant preparation with reduction of pain.

The results also suggest that these benefits may be at the cost of increased operating time with the piezoelectric device. The findings therefore raise the possibility of improved clinical healing after osteotomy with the piezoelectric device compared with conventional rotary burs, and this is consistent with clinical and histological studies in rats [1, 18].

Also, the painkiller assumption showed a significant difference between G1 and G2. Until the fifth day after surgery, a higher use of painkillers was observed for G1. The reduced intake of painkillers in G2 allowed the patient to experience the implant insertion as a less invasive intervention.

However, the results of our study showed that the osteotomy performed with ultrasound extends the surgical times in respect to the drill preparation.

In the literature, it has been shown that piezoelectric osteotomy requires a longer intervention time than osteotomy with conventional drills [13, 15, 19–21]. As reported in some studies, piezoelectric bone surgery causes an acceleration of the healing processes at the level of the bone matrix, stimulating cell proliferation and its synthesis [22]. These advantages are the consequence of a more secure crestal osteotomy, as the ergonomic piezoelectric pivoting handpiece, without the initial "waving" phenomena typical of each rotating system, allows a more stable positioning of the guide insert on the crest profile, for the creation of the first implant hole, making the initial osteotomy less traumatic by exploiting the cavitational process with constant irrigation. All this, in biological terms, translates into a

reduction of thermal stress on the bone tissue, maintenance of a better bone vitality, better compliance with osteoblastic turnover, and a possible respect of soft tissues and any noble anatomical structures (inferior alveolar nerve, Schneiderian membrane, etc.) contiguous to the osteotomy [13–15].

The prospect of using piezosurgery promises to revolutionize implantology, but the professional skill and training for its use should be taken into consideration because the technique requires a longer surgical time compared with the use of conventional rotary and oscillating saws. This occurs when deep cuts into the bone are necessary, and the system is less efficient. Although the cutting speed decreased, temperatures rose, so pauses were necessary to let the system cool down. In these cases, the combination of piezosurgery for the initial incision and a chisel for the final osteotomy of the bone was useful [23]. But the majority of studies agree that the piezoelectric device is extremely efficient and precise and recommend its use [24]. These observations were also supported by the present study; in fact, a lower pain was present for osteotomies performed by an ultrasonic device. The piezoelectric technique, in addition to being more tolerable, in terms of intraoperative comfort, and in the phases following surgery for the patient, has shown surgical advantages for the operator [25–27]. Although the operative times are higher for G2, they had no substantial influence on the global evaluation of the surgery. In fact, when the operator had to evaluate the difficulty of the implant insertion, no differences were found in comparison with G1 except for the visibility of the operative field that was better in G2. This is allowed by the cavitational effect of the piezoelectric device which allows for a clean and sterile operating field, ensuring the operator greater visibility, with the advantage of safer surgery.

Furthermore, comparative histological studies between piezoelectric devices, saws, and burs highlighted the superiority of the piezoelectric device in terms of protection of anatomic structures and, consequently, a better healing process. A remarkable feature of the piezoelectric device is its good manageability, which makes it easy for the surgeon to create a straight osteotomy line, without any learning period [28]. In this sense, a promising technical evolution is the combination of the intraoral navigation system with ultrasonic drilling to achieve a more safe and precise implant site preparation with a reduced invasiveness [29].

Within the limits of the present study, such as the choice of a single operator for the evaluation of the easiness of surgery or the choice of few parameters (VAS and painkillers assumption) for the evaluation of the patient's comfort, the results showed that piezosurgery was more comfortable in the implant phases and less painful in the postoperative one, bringing advantages in terms of acceptance of implant-supported prosthetic rehabilitation.

6. Conclusions

In recent years, the excellent results in the use of dental implants have greatly expanded the treatment options related to the replacement of missing teeth. Implantology has now reached levels of reliability and predictability of success over time that, associated with a high rate of safety, makes it a daily surgical practice.

The evolution of materials and techniques, with an increasing knowledge of the mechanism of healing processes, has also contributed to a reduction of numerous rehabilitative limitations. However, the success of a therapy is often determined only by the clinical result based on objective parameters, without taking into account the subjectivity of the patient and the operator.

The present study took these aspects into consideration, finding a positive response in implant surgery with the piezoelectric method compared to the traditional technique.

In light of the above, traditional surgery undoubtedly maintains the record for the speed of execution of the techniques. However, ultrasounds applied to the implant site preparation are a method of bone surgery that presents fewer risks related to operative maneuvers and greater comfort for the patient.

Data Availability

All data used (pain rate of patients in intraoperative and postoperative times recorded by VAS Score) to support the findings of this study are available from the corresponding author upon request. We have annotated the entire data building process and empirical techniques presented in the paper.

Conflicts of Interest

The authors declare that they have no conflicts of interest.

References

[1] J. E. Horton, T. M. Tarpley, and L. D. Wood, "The healing of surgical defects in alveolar bone produced with ultrasonic instrumentation, chisel, and rotary bur," *Oral Surgery, Oral Medicine, Oral Pathology*, vol. 39, no. 4, pp. 536–546, 1975.

[2] A. Patel, "The role of piezosurgery in implant dentistry," *Implant dentistry*, vol. 5, pp. 1–15, 2014.

[3] S. Siervo, S. Ruggli-Milic, M. Radici, P. Siervo, and K. Jäger, "Piezoelectric surgery: an alternative method of minimally invasive surgery," *Schweizer Monatsschrift für Zahnmedizin*, vol. 114, no. 4, pp. 365–377, 2004.

[4] J. A. Baker, S. Vora, L. Bairam, H. Kim, E. L. Davis, and S. Andreana, "Piezoelectric vs. conventional implant site preparation: ex vivo implant primary stability," *Clinical Oral Implants Research*, vol. 23, no. 4, pp. 433–437, 2012.

[5] A. Scarano, G. Iezzi, V. Perrotti et al., "Ultrasonic versus drills implant site preparation: a histologic analysis in bovine ribs," *Journal of Craniofacial Surgery*, vol. 25, no. 3, pp. 814–817, 2014.

[6] P. Maurer, M. S. Kriwalsky, R. Block Veras, J. Vogel, F. Syrowatka, and C. Heiss, "Micromorphometrical analysis of conventional osteotomy techniques and ultrasonic osteotomy at the rabbit skull," *Clinical Oral Implants Research*, vol. 19, no. 6, pp. 570–575, 2008.

[7] A. Scarano, A. Piattelli, B. Assenza et al., "Infrared thermographic evaluation of temperature modifications induced during implant site preparation with cylindrical versus conical drills," *Clinical Implant Dentistry and Related Research*, vol. 13, no. 4, pp. 319–323, 2011.

[8] A. Scarano, S. Noumbissi, S. Gupta, F. Inchingolo, P. Stilla, and F. Lorusso, "Scanning electron microscopy analysis and energy dispersion X-ray microanalysis to evaluate the effects of decontamination chemicals and heat sterilization on implant surgical drills: zirconia vs. steel," *Applied Sciences*, vol. 9, no. 14, p. 2837, 2019.

[9] A. Itro, G. Lupo, A. Marra et al., "The piezoelectric osteotomy technique compared to the one with rotary instruments in the surgery of included third molars: a clinical study," *Minerva Stomatologica*, vol. 61, no. 6, pp. 247–253, 2012.

[10] M. Pasi, R. Vinci, D. Di Stefano, and E. F. Gherlone, "La chirurgia orale piezoelettrica," *Italian Oral Surgery*, vol. 7, no. 5, pp. 7–18, 2008.

[11] S. Pappalardo, V. Carlino, S. Distefano, and D. T. Cantalupo Milazzo, "Tecnologia piezoelettrica e sequele postoperatorie," *Dental Clinics*, vol. 4, pp. 19–25, 2008.

[12] M. Labanca, L. F. Rodella, and P. B. Binello, "Una nuova tecnica per la preparazione del sito implantare con l'impiego della chirurgia piezoelettrica (PES)," *Implants*, vol. 1, 2015.

[13] F. Stelzle, C. Frenkel, M. Riemann, C. Knipfer, P. Stockmann, and E. Nkenke, "The effect of load on heat production, thermal effects and expenditure of time during implant site preparation— an experimental ex vivo comparison between piezosurgery and conventional drilling," *Clinical Oral Implants Research*, vol. 25, no. 2, pp. e140–148, 2014.

[14] A. Rashad, A. Kaiser, N. Prochnow, I. Schmitz, E. Hoffmann, and P. Maurer, "Heat production during different ultrasonic and conventional osteotomy preparations for dental implants," *Clinical Oral Implants Research*, vol. 22, no. 12, pp. 1361–1365, 2011.

[15] F. Stelzle, F. W. Neukam, and E. Nkenke, "Load-dependent heat development, thermal effects, duration, and soft tissue preservation in piezosurgical implant site preparation: an experimental ex vivo study," *The International Journal of Oral & Maxillofacial Implants*, vol. 27, no. 3, pp. 513–522, 2012.

[16] A. Scarano, F. Carinci, F. Lorusso et al., "Ultrasonic vs. drill implant site preparation: post-operative pain measurement through VAS, swelling and crestal bone remodeling: a randomized clinical study," *Materials*, vol. 11, no. 12, p. 2516, 2018.

[17] C. E. Misch, "Root form surgery in the edentulous anterior and posterior mandible: implant insertion," in *Contemporary Implant Dentistry*, pp. 221–226, Mosby Elsevier, St Louis, MO, USA, 2008.

[18] M. Sirolli, C. E. S. Mafra, R. A. B. D. Santos, L. S. M. Holzhausen, J. B. César Neto, and J. B. César, "Influence of piezosurgery on bone healing around titanium implants: a histological study in rats," *Brazilian Dental Journal*, vol. 27, no. 3, pp. 278–283, 2016.

[19] J.-L. Beziat, J.-C. Bera, B. Lavandier, and A. Gleizal, "Ultrasonic osteotomy as a new technique in craniomaxillofacial surgery," *International Journal of Oral and Maxillofacial Surgery*, vol. 36, no. 6, pp. 493–500, 2007.

[20] A. Gleizal, J.-C. Bera, B. Lavandier, and J.-L. Beziat, "Piezoelectric osteotomy: a new technique for bone surgery-advantages in craniofacial surgery," *Child's Nervous System*, vol. 23, no. 5, pp. 509–513, 2007.

[21] M. Rana, N.-C. Gellrich, M. Rana, J. Piffkó, and W. Kater, "Evaluation of surgically assisted rapid maxillary expansion with piezosurgery versus oscillating saw and chisel osteotomy—a randomized prospective trial," *Trials*, vol. 14, no. 1, p. 49, 2013.

[22] G. Preti, G. Martinasso, B. Peirone et al., "Cytokines and growth factors involved in the osseointegration of oral titanium implants positioned using piezoelectric bone surgery versus a drill technique: a pilot study in minipigs," *Journal of Periodontology*, vol. 78, no. 4, pp. 716–722, 2007.

[23] G. Eggers, J. Klein, J. Blank, and S. Hassfeld, "Piezosurgery®: an ultrasound device for cutting bone and its use and limitations in maxillofacial surgery," *British Journal of Oral and Maxillofacial Surgery*, vol. 42, no. 5, pp. 451–453, 2004.

[24] C. C. S. Pereira, W. C. Gealh, L. Meorin-Nogueira, I. R. Garcia-Júnior, and R. Okamoto, "Piezosurgery applied to implant dentistry: clinical and biological aspects," *Journal of Oral Implantology*, vol. 40, no. 1, pp. 401–408, 2014.

[25] L. Piersanti, M. Dilorenzo, G. Monaco, and C. Marchetti, "Piezosurgery or conventional rotatory instruments for inferior third molar extractions?," *Journal of Oral and Maxillofacial Surgery*, vol. 72, no. 9, pp. 1647–1652, 2014.

[26] G. Pavlíková, R. Foltán, M. Burian et al., "Piezosurgery prevents brain tissue damage: an experimental study on a new rat model," *International Journal of Oral and Maxillofacial Surgery*, vol. 40, no. 8, pp. 840–844, 2011.

[27] L. Boioli, T. Vercellotti, and J. Teucianu, "Piezoelectric surgery: an alternative to conventional bone-surgery techniques," *L' Information Dentaire*, vol. 86, no. 41, pp. 2887–2893, 2004.

[28] C. A. Landes, S. Stübinger, J. Rieger, B. Williger, T. K. L. Ha, and R. Sader, "Critical evaluation of piezoelectric osteotomy in orthognathic surgery: operative technique, blood loss, time requirement, nerve and vessel integrity," *Journal of Oral and Maxillofacial Surgery*, vol. 66, no. 4, pp. 657–674, 2008.

[29] G. Pellegrino, V. Taraschi, T. Vercellotti, B. Ben-Nissan, and C. Marchetti, "Three-dimensional implant positioning with a piezosurgery implant site preparation technique and an intraoral surgical navigation system: case report," *The International Journal of Oral & Maxillofacial Implants*, vol. 32, no. 3, pp. e163–e165, 2017.

Hindawi
BioMed Research International
Volume 2019, Article ID 2587245, 14 pages
https://doi.org/10.1155/2019/2587245

Review Article

The Additional Effect of Autologous Platelet Concentrates to Coronally Advanced Flap in the Treatment of Gingival Recessions: A Systematic Review and Meta-Analysis

Rong Li,[1] Yanqing Liu,[1] Tong Xu,[1] Haijiao Zhao,[1] Jingya Hou,[1] Yun Wu,[1] and Dongmei Zhang[1,2]

[1]*Department of Periodontology, School of Stomatology, China Medical University, Shenyang, Liaoning 110002, China*
[2]*Department of Oral Biology, School of Stomatology, China Medical University, Shenyang, Liaoning 110002, China*

Correspondence should be addressed to Dongmei Zhang; juliyia@163.com

Received 31 May 2019; Accepted 9 July 2019; Published 25 July 2019

Guest Editor: Francesca Salamanna

Background. To improve the efficacy of regenerative treatment for gingival recessions, the autologous platelet concentrates (APCs) combined with coronally advanced flap (CAF) have been investigated. However, few studies systematically assess the complementary effect of APCs in periodontal regeneration. The present study aims to evaluate the additional effect of different types of APCs to CAF in the treatment of gingival recessions. *Methods.* Electronic databases (EMBASE, MEDLINE, and Cochrane Central Register of Controlled Trails) and relevant journals were searched until May 15, 2019. Only randomized controlled trials (RCTs) in English were included. Outcome variables include root coverage (RC), recession depth (RD), clinical attachment level (CAL), keratinized tissue width (KTW), and gingival thickness (GT). Data were analyzed with Revman5.3. The estimate of effect sizes was expressed as the mean differences and the 95% confidence interval. *Results.* 8 RCTs involving 170 patients (328 sites) were included. Our meta-analysis indicated RC, RD, CAL, KTW, and GT were better improved in the CAF plus APCs groups than the CAF alone. The subgroup analyses revealed that platelet-rich fibrin (PRF) brought significant improvement in RC, RD, CAL, and GT. Concentrated growth factors (CGF) lead clinic beneficial in CAL, KTW, and GT. No significant effect of platelet-rich plasma (PRP) could be found in any clinical parameters when combined with CAF. *Conclusions.* PRF could exert additional effect to CAF; the preferred treatment for gingival recessions was considered. Based on the limited studies, it seemed that PRP failed to show any additional effect and it was not suggested for gingival recessions. Given the limited research and high risk of bias, it is still needed to confirm the additional effect of CGF by more high-quality studies.

1. Introduction

Gingival recession is a common, undesirable problem attribute to the apical migration of the margin tissue beyond the cemento-enamel junction (CEJ). There is a higher probability of root caries, loss of attachment, and hypersensitivity in teeth with gingival recession [1]. Various mucogingival procedures have been evolved to obtain root coverage such as free gingival grafts, laterally positioned flaps, or guided tissue regeneration, as well as connective tissue grafting (CTG) and coronally advanced flaps (CAF) [2–4]. CAF is a surgical procedure to shift the gingival tissue coronally on the exposed root surface. It has proven to be an effective and predictable technique because of the optimum root coverage results, the good color blending of the treated area, and the recuperation of the original morphology of the soft tissue margin [5]. What is more, it is convenient and the invasiveness is reduced since graft harvesting is not required in CAF. However, it was reported that root coverage treated with CAF alone is unstable in a long time. The root coverage was 89.0% at 1 month postoperatively and decreased to 58.8% at 6 months [6]. Therefore, CAF is frequently combined with various regenerative materials or biological factors.

In the past several years, autologous platelet concentrates (APCs) had emerged as a potential regenerative material; it can be used alone or with other techniques [7]. APC has

been proven to play a pivotal role in soft tissue healing. Their effectiveness lies on the continuous release of multiple cytokines, such as transforming growth factor-β1 (TGF-β1), vascular endothelial growth factor (VEGF), insulin growth factor (IGF), platelet-derived growth factor-AB (PDGF-AB), and interleukin-1β (IL-1β) [8]. Until now, three generations of APCs have been developed, including platelet-rich plasma (PRP), platelet-rich fibrin (PRF), and concentrated growth factors (CGF). PRP is the first generation of APCs; it contains a high concentration of platelets obtained by special centrifugation from fresh whole blood. It is required to induce fibrin polymerization by chemical additives including anticoagulant, thrombin, or calcium chloride before applying to the surgical site [9]. PRF is the second generation of APCs originally proposed by Choukroun et al. [10] based on the PRP. It is platelet-rich fibrin with a simple preparation process without adding any chemical additives. CGF is the latest generation of APCs introduced by Sacco in 2006 [11]; it is concentrated by varying the centrifuge speed [12]. In addition, CGF is produced without the addition of any exogenous products and is therefore free from cross-contamination [13].

Recently, APC has gradually attracted the attention of scholars in the treatment of gingival recessions. However, the additional effect of APCs remains controversial. Luo et al. [14] in 2015 assessed the supplementary role of APCs with CAF in the treatment of gingival recessions. Their meta-analysis results showed significant improvement in RD and KTW. The combined application of APCs also had a positive effect on soft tissue healing postoperative. They deemed that APCs could exert a positive impact on CAF. On the contrary, a review by Del Fabbro et al. [15] in 2011 evaluated the adjuvant role of APCs in the prevention of gingival recessions. The outcomes showed no significant improvement in RC and KTW with APCs. Another meta-analysis by Vittorio Moraschini et al. [16] in 2016 evaluated the effects of PRF membranes on the outcomes of clinical treatments in patients with Classes I and II gingival recessions. Their results indicated there was no difference in improving RC, KTW, and CAL with or without APCs.

In summary, the current clinical evidence is still unclear for practitioners. Considering these controversial options, it is our aim to supplement and update the understanding of the role of APCs. The present meta-analysis aims to systematically evaluate whether the three generations of APCs could provide additional effect to CAF for gingival recessions, thus to provide guidance to practitioners in their clinical work.

2. Materials and Methods

2.1. Focused PICOS Question. This meta-analysis was conducted and reported according to the PRISMA (Preferred Reporting Project Guidelines for Systematic Review and Meta-analysis) protocols [17]. The following statements were used to conduct a systematic search.

The participants (P) included system healthy adults with Class I or II gingival recessions; the intervention (I) was the APCs combined with CAF for gingival recessions; the comparison (C) was conducted with CAF alone; the outcomes (O) comprised clinical parameters including RC, RD, CAL, KTW, and GT; the study (S) was designed for humans and only randomized control trials (RCTs) were enrolled.

2.2. Search Strategies. Three electronic databases including Medline, EMBASE, and Cochrane Central Register of Controlled Trials were searched. The search strategy was performed by using the following terms: ("platelet concentrates" OR "platelet-rich plasma" OR "platelet-rich fibrin" OR "concentrated growth factors") AND ("coronally advanced flap") AND ("Class I" OR "Class II") AND ("gingival recessions" OR "root coverage") AND ("randomized controlled trial"). Only English articles were included. An additional hand search of the following Periodontology journals was performed on the official websites: *Journal of Periodontology*, *Journal of Clinical Periodontology*, *Journal of Dental Research*, *Journal of Dentistry* and *Journal of Periodontal Research*. In addition, the bibliographies of all selected articles and relevant reviews were also searched for missing articles. In addition, grey literature was obtained from Google Scholars (https://xue.glgoo.org/). Unpublished and ongoing trials were obtained from the trial registries (EU Clinical Trials Register: https://www.clinicaltrialsregister.eu). The final search was conducted on May 15, 2019.

2.3. Inclusion and Exclusion Criteria

Inclusion Criteria. (1) Randomized clinical trials on healthy patients aged 18~60 years old.

(2) Maxillary or mandibular anterior and premolar teeth with Miller's Class I or II gingival recessions confirmed by radiographic and clinical evidence.

(3) Ability to maintain good oral hygiene (O'Leary plaque score [18] ≤20%).

(4) Recession depth ≥2.0 mm, gingival thickness ≥0.5 mm, the width of keratinized gingival ≥2.0 mm after scaling, and root planning.

(5) The only difference between the control and experimental group being that the latter was supplemented with APC.

(6) The language of publication being English.

Exclusion Criteria. (1) Pregnancy or lactation for women.

(2) Individuals allergic to medications.

(3) Smoking or use of alcohol or narcotic drugs.

(4) Using drugs that effect periodontal healing such as corticosteroids or calcium channel blockers.

2.4. Study Selection and Data Extraction Process. Two reviewers (Rong Li, Yanqing Liu) independently screened the titles and abstracts of the articles retrieved. The same authors also performed the full-text reading of possible relevant articles. If there was any objection, the senior reviewer (Dongmei Zhang) was consulted. Publications that did not meet the inclusion criteria were excluded, and the reasons for exclusion were recorded.

The mean values and standard deviation were collected in an excel sheet by two independent reviewers (Jingya

Hou, Yun Wu). The following characteristics of the studies were also extracted, including author, publication year, study design, duration, number of patients and sites, sex, mean age of the patients, smoking, tooth type, site of recessions, and intervention.

2.5. Data Items. The primary outcome measures were as follows.

(1) Gingival recessions that attained RC (the percentage of RC was calculated by the following formula [19]:

Percentage of root coverage = ([Preoperative RD - Postoperative RD]/ Preoperative RD)×100%).

(2) Change in RD was expressed as a reduction in recession at the final evaluation (RD was measured at the mid-buccal from CEJ to the gingival margin).

The secondary outcome measures were as follows.

(1) Change in CAL expressed as CAL gain at the final evaluation (CAL referred to the distance from the CEJ to the most apical part of the sulcus).

(2) Change in KTW expressed as KTW gain at the final evaluation (KTW referred to the distance from the mucogingival junction to the free gingival margin).

(3) Change in GT expressed as GT gain at the final evaluation (GT was measured 3 mm below the gingival margin at the attached gingival).

2.6. Methodological Quality Assessment. Two individuals (Tong Xu, Haijiao Zhao) independently assessed the methodological quality of each selected study according to the standard for evaluating the risk of bias in the Cochrane Handbook for Systematic Reviews of Interventions (Version 5.1.0) [20]. Seven main quality criteria were examined: (1) random sequence generation method; (2) allocation concealment; (3) blinding of participants and personnel; (4) blinding of outcome assessors; (5) incomplete outcome data; (6) selective outcome reporting; and (7) other bias. All the parameters were assessed as adequate (yes), unclear, or inadequate (no) [21]. When a discrepancy occurred, the discussion was made to reach an agreement. After the quality assessment, the studies were classified into the following categories: (1) low risk: all criteria were met or one criterion was unclear/not met; (2) moderate risk: two criteria were unclear/not met; (3) high risk: more than two criteria were not met. Quality assessment across studies was presented in the form of a graph. According to the Cochrane handbook, Chi-square and Higgins index (I^2) were used to judge whether there was heterogeneity.

2.7. Data Analysis. The software Revman5.3 (Review Manager version 5.3; The Cochrane Collaboration, Copenhagen, Denmark) was used for meta-analysis. The continuous data (including RC, RD, CAL, KTW, and GT) were expressed as mean difference (MD) and 95% confidence interval (CI), with $P<0.05$ being statistically significant. When the homogeneity between the studies was good ($P\geq0.10$, $I^2 \leq 50\%$), the fixed-effect model was used for meta-analysis. When significantly heterogeneity existed between the studies ($P<0.10$, $I^2 > 50\%$), the random-effects models were used. The heterogeneity across studies in RC, RD, CAL, KTW, and GT was compared through subgroup analysis. The results of our meta-analysis and responding publication bias were summarized in the forest and funnel plots, respectively.

3. Results

3.1. Description of Enrolled Studies. The initial electronic search provided 224 papers. Only one study was identified by the hand searching. After duplicates removal, 121 records were screened. After reviewing the titles and abstracts, 14 articles were about APCs for Classes I and II gingival recessions, and the rest 110 papers were excluded. After reviewing the full-text, 3 papers were excluded from the full-text evaluation. The reasons for exclusion were as follows: case series [22, 23] and no control group [24]. The selection process was summarized in Figure 1.

Finally, 8 RCTs [25–32] were selected in our meta-analysis. A total of 170 patients with 328 gingival recessions sites (166 test and 162 control sites) under treatment were enrolled. Three articles adopted a parallel design and five articles adopted a split-mouth design. The characteristics of the included papers were summarized in Table 1. The data of the included studies were extracted in Table 2.

3.2. Quality of Studies. The quality assessment of the selected studies was presented in Figure 2. Sequence generation was reported by six articles: four articles used a coin tossing [26, 29, 31, 32] and two [25, 27] used envelopes; the remaining two articles [28, 30] did not explain the methods of random generation. All enrolled articles did not report allocation concealment which was considered an uncertain risk of bias. Concerning the surgery process, it was impossible to be blind to the personnel. Four articles [25, 27, 31, 32] were blind to the assessors: one article [29] blind both to the patients and the assessor while the remaining three articles were unclear. Follow-up reports were completed for all papers, except one article [25] reporting that one subject in the experiment group dropped out of the study after a 1-month follow-up. No selective reporting and other biases were found. After the evaluation, four articles [27, 29, 31, 32] were classified as moderate risk (two criteria were not met or unclear) and four [25, 26, 28, 30] as high risk (three or four criteria were not met or unclear).

3.3. Additional Effect of APCs. RC gain: altogether, seven articles [25–31] were analyzed. Dixit et al.'s article was excluded from the analysis because it did not report specific data. The random-effects model was conducted due to its high heterogeneity (I^2=73%). The results of the analysis showed that APCs exerted a greater RC gain when added to CAF compared with CAF alone (Figure 3(a)). In the subgroup analysis of PRF, there was significant difference between the test and the control groups in RC, with an MD of 16.04 mm (95% CI: 4.44~27.63 mm; P=0.007), while PRP subgroup and CGF subgroup showed no significant differences between the two groups.

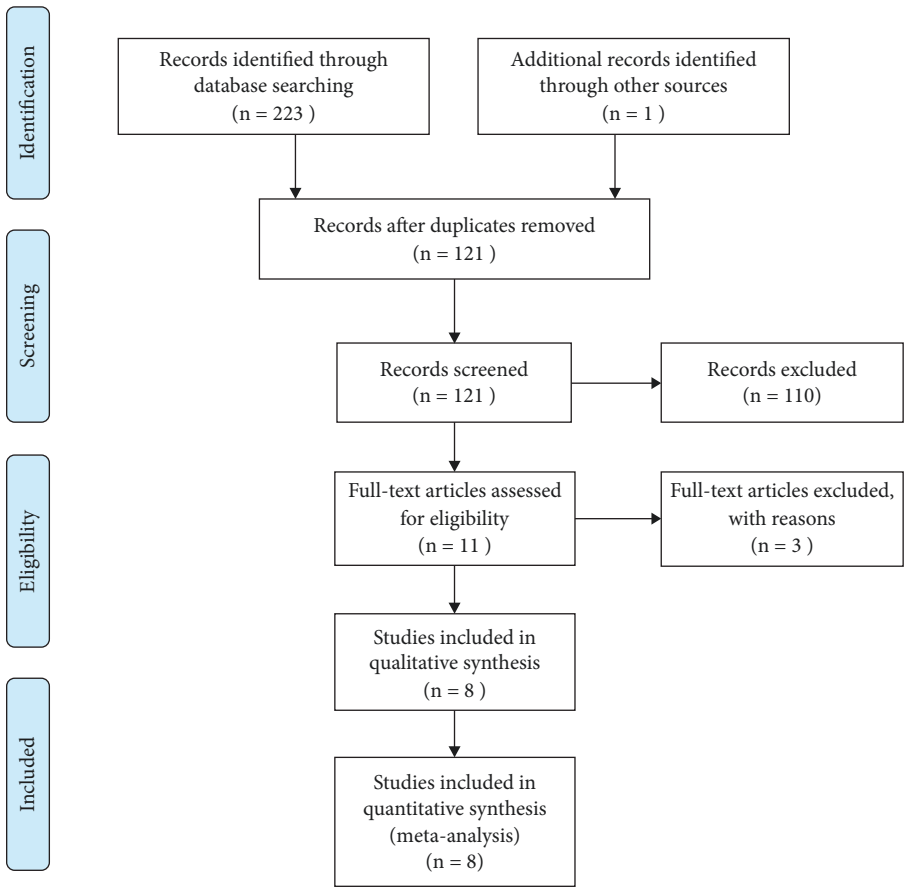

Figure 1: PRISMA flow diagram illustrating the selection process.

RD reduction: meta-analysis was conducted among all the eight records. A fixed-effects model was applied (I^2=45%). In terms of the results, the APCs group showed more RD reduction compared with CAF alone (Figure 3(b)). A beneficial effect with an MD of 0.33 mm (95%CI: 0.18~0.49 mm; P<0.001) was found in the subgroups of PRF. In contrast, no significant RD reduction was shown in subgroups of PRP and CGF.

CAL reduction: meta-analysis was performed in 8 studies. A fixed-effects model was used (I^2=31%). The results showed that the use of APCs determined a significant gain of CAL when added to CAF in the treatment of gingival recessions (Figure 3(c)). Statistical differences between the test and the control in the subgroup of PRF and CGF were found, with an MD of 0.44 mm (95%CI: 0.24~0.65 mm; P<0.001) and an MD of 0.25 mm (95%CI: 0.03~0.47 mm; P=0.03), respectively. No difference was found in the subgroup of PRP.

KTW gain: The meta-analysis of keratinized tissue increasing was performed on seven studies. Dixit et al.'s article was excluded from the analysis because it did not provide specific data. A fixed-effects model was used (I^2=40%). The results of the included studies showed that the use of APCs determines a greater KTW gain than CAF alone (Figure 3(d)). From the results of the subgroup analysis, only CGF membrane could significantly improve the KTW, with an MD of 0.21 mm (95%CI: 0.08~0.34 mm; P<0.001). The PRP and PRF failed to show any improvement.

GT gain: two records [26, 30] were excluded from our meta-analysis for its incomplete data. The heterogeneity was high (I^2=96%), so a random-effects model was used. The results of our meta-analysis showed that APCs groups obtained a greater GT gain than CAF alone groups (Figure 3(e)). Subgroup analysis revealed significant differences for PRF and CGF, with an MD of 0.31 mm (95%CI: 0.02~0.59 mm; P=0.03) and an MD of 0.26 mm (95%CI: 0.23~0.29 mm; P<0.001), respectively. Nevertheless, no significant difference was found in the subgroup of PRP.

3.4. Sensitivity Analyses. Sensitivity analyses were investigated by discarding one research every time to assess the impact of single research on the general outcomes. Except excluding the research of Bozkurt et al. [28], the overall stability of our results was shown in Figures 4(d) and 4(e).

3.5. Publication Bias. It was considered that there was no publication bias by the Begg's and Egger's test (P>0.05), which further supported the reliability of the enrolled studies (Figures 5, 6, 7, 8, and 9).

Table 1: General information of enrolled articles.

References (year)	Study Design (Duration)	Sample size (No. of patients)	Population Sex	Age (Range)	Smoking (Yes, No?)	Miller Class	Site of Recessions	Intervention (No. of sites)	
								Test	Control
Huang et al. (2005)	RCT/parallel (6 months)	23 sites (23)	17F/6M	43.8±11.9	No	I	Maxillary or mandibular anterior and premolar teeth,	CAF + PRP (11)	CAF (12)
Padma et al. (2013)	RCT/split-mouth (6 months)	30 sites (15)	NR	18~35	No	I and II	NR	CAF+PRF (15)	CAF (15)
Thamaraiselvan et al. (2015)	RCT//parallel (6 months)	20 sites (20)	2F/18M	21~47	No	I and II	Maxillary or mandibular anterior and premolar teeth,	CAF+PRF (10)	CAF (10)
Bozkurt et al. (2015)	RCT/split-mouth (6 months)	119 sites (20)	13F/7M	37.10±1.03	No	I and II	NR	CAF+CGF (60)	CAF (59)
Gupta et al. (2015)	RCT/split-mouth (6 months)	30 sites (26)	NR	20~50	No	I and II	Maxillary anterior and premolar teeth,	CAF+PRF (15)	CAF (15)
Biradar et al. (2015)	RCT/ parallel (4 months)	30 sites (30)	NR	18~45	No	I and II	Maxillary or mandibular anterior, premolar and molar teeth,	CAF+PRP (15)	CAF (15)
Kuka et al. (2017)	RCT/split-mouth (12 months)	52 sites (24)	13F/11M	32.35±6.41	No	I	Maxillary or mandibular anterior and premolar teeth,	CAF+PRF (28)	CAF (24)
Dixit et al. (2018)	RCT/split-mouth (6 months)	24 sites (12)	5F/7M	18~50	No	I and II	NR	CAF+PRF (12)	CAF (12)

NR: Not Reported CAF: Coronally Advanced Flap PRP: Platelet-Rich Plasma PRF: Platelet-Rich Fibrin CGF: Concentrated Growth Factor.

Table 2: The data of the included articles.

References(Year)	*MD* in *PD* Between Baseline and Final Follow-Up (mm)	*MD* in *CAL* Between Baseline and Final Follow-Up (mm)	*MD* in *RC* Between Baseline and Final Follow-Up (%)	*MD* in *KMW* Between Baseline and Final Follow-Up (mm)	*MD* in *GT* Between Baseline and Final Follow-Up (mm)	*MD* in *RD* Between Baseline and Final Follow-Up (mm)	Other Outcomes
Huang et al. (2005)	NR	2.5 ± 1.4(T)	81.0 ± 28.7 (T)	0.3 ± 0.9 (T)	0.6± 0.4 (T)	2.3 ± 0.9 (T)	RW PI GI
	NR	3.0 ± 1.4 (C)	83.5 ± 21.8 (C)	0.6 ± 0.7 (C)	0.3± 0.4 (C)	2.5± 0.8 (C)	
Padma et al. (2013)	NR	3.75 ± 1.90 (T)	100 ± 19.12 (T)	2.44 ± 0.90 (T)	NR	3.44 ± 1.009 (T)	RD
	NR	2.69 ± 0.36 (C)	68.40 ± 17.42 (C)	2.19 ± 0.81 (C)	NR	2.31 ± 0.49 (C)	
Thamaraiselvan et al. (2015)	0.40 ± 0.51 (T)	2.50 ± 1.17 (T)	74.16 ± 28.98 (T)	0.40 ± 0.69 (T)	0.30 ± 0.10 (T)	1.60 ± 0.51 (T)	RW CRC PI GI
	0.30± 0.48 (C)	1.80 ± 0.91 (C)	65.00 ± 44.47 (C)	0.40 ± 0.69 (C)	0.03 ± 0.04 (C)	1.30 ± 0.91 (C)	
Bozkurt et al. (2015)	0.37 ± 0.49 (T)	2.83 ± 0.62 (T)	86.67 ±1 5.59 (T)	0.58 ± 0.53 (T)	0.32 ± 0.10 (T)	2.47 ± 0.54 (T)	RW CRC
	0.29 ± 0.46 (C)	2.58 ± 0.62 (C)	82.06 ± 17.49 (C)	0.14 ± 0.63 (C)	0.06 ± 0.09 (C)	2.29 ± 0.56 (C)	
Gupta et al. (2015)	0.73 ± 0.46 (T)	3.27 ± 0.80 (T)	91.00 ± 19.98 (T)	1.60 ± 0.63 (T)	0.07 ± 0.03 (T)	2.53 ± 0.64 (T)	
	0.41 ± 0.51 (C)	2.47 ± 0.74 (C)	86.60 ± 23.83 (C)	1.40 ± 0.51 (C)	0.04 ± 0.05 (C)	2.07 ± 0.59 (C)	
Biradar et al. (2015)	0.90 ± 1.68 (T)	3.18 ± 0.78 (T)	75.00 ± 8.30 (T)	0.51 ± 0.89 (T)	NR	2.15 ± 0.66 (T)	RW
	0.87 ± 0.32 (C)	3.17 ± 0.90 (C)	73.10 ± 7.30 (C)	0.57 ± 0.55 (C)	NR	2.08 ± 0.68 (C)	
Kuka et al. (2017)	0.65 ± 0.24 (T)	2.10 ± 0.61 (T)	88.36 ± 15.45 (T)	0.70 ± 0.42 (T)	0.53 ± 0.05 (T)	2.75 ± 0.35 (T)	RW PI GI BOP CRC
	0.78 ± 0.34 (C)	1.74 ± 0.24 (C)	74.63 ± 8.05 (C)	0.65 ± 0.47 (C)	0.07 ± 0.05 (C)	2.51 ± 0.33 (C)	
Dixit et al. (2018)	NR	2.42 ± 0.88 (T)	NR	NR	0.63 ± 0.38 (T)	2.42 ± 0.78 (T)	SBI RW
	NR	2.50 ± 1.14 (C)	NR	NR	0.08 ± 0.50 (C)	2.25 ± 1.07 (C)	

T: Test Group C: Control Group *MD*: Medium Difference PD: Probe Depth CAL: Clinical Attachment Level RC: Root Coverage KTW: Keratinized Tissue Width GT: Gingival Thickness.
RD: Recession Depth NR: Not Reported RW: Recession Width PI: Periodontal Index GI: Gingival Index CRC: Completely Root Coverage BOP: Bleeding on Probing SBI: Sulcus Bleeding Index.

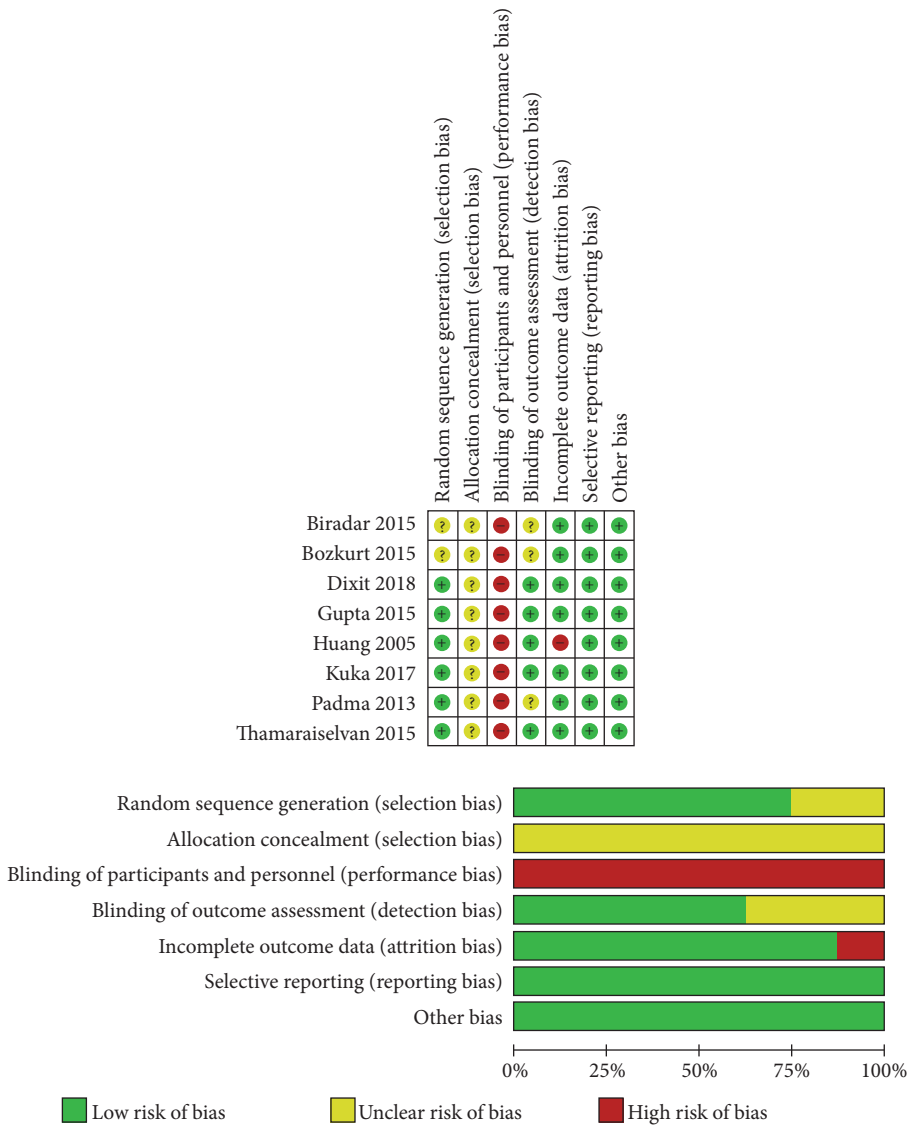

Figure 2: Risk of bias summary of the included studies.

4. Discussion

To achieve safe and effective outcomes for gingival recessions, researchers have done numerous works to improve CAF surgical procedures, including the usage of regeneration materials. As APCs can be easily obtained and it can promote wound healing and minimize the occurrence of infection, the additional effect of APCs to CAF for gingival recessions has been investigated. However, there was a lack of clinical evidence to confirm this effect. The present meta-analysis was intended to assess the adjunctive efficacy of three types of APCs when combined with CAF for the treatment of Classes I and II gingival recessions.

On the whole, the results of the present meta-analysis showed the three types of APCs had beneficial effects in all effect sizes compared with CAF alone. Regarding the primary outcomes RC and RD, only PRF and CGF showed significant differences compared with the CAF alone. It seemed that PRP would not bring a significant difference in primary outcomes. The heterogeneity of RC seems to be related to the studies of Padma and Kuka. A modified CAF (full and split flap design were combined) was used in Padma's study other than the traditional CAF. And the duration of Kuka's study was 12 months, while the duration was 6 months in other studies. We believed that the different surgical method and duration might lead to the heterogeneity. Actually, after excluding these two studies, our subgroup analysis found that the heterogeneity was low (I^2 = 0%). As to the secondary outcomes of CAL, KTW, and GT, PRF and CGF showed significant results in CAL and GT. Only CGF showed a significant result in KTW. PRP showed no significant results in any secondary outcomes. The heterogeneity of GT seems to be related to the study of Bozkurt because of the different prepare process of CGF. In fact, the results of our subgroup analysis found that I^2 was 0% after excluding this one.

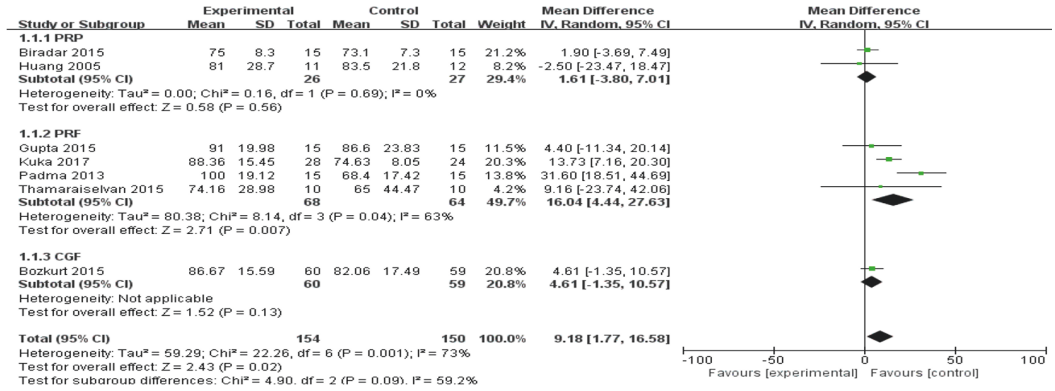

(a)

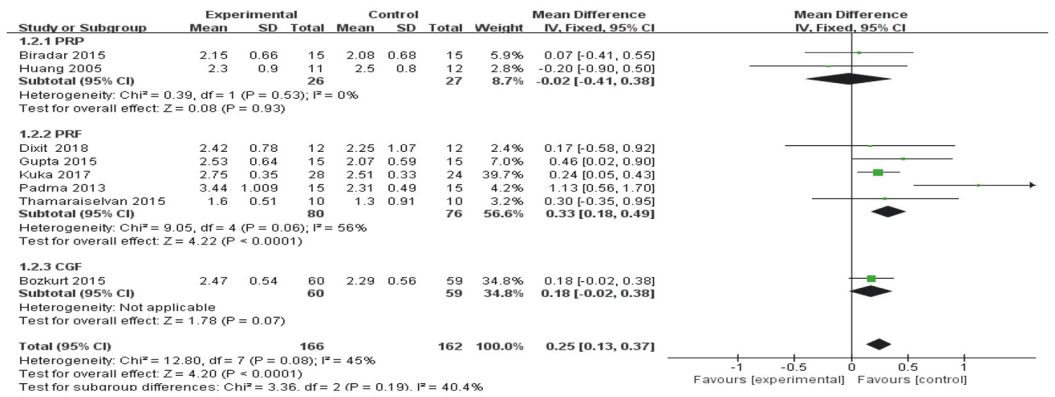

(b)

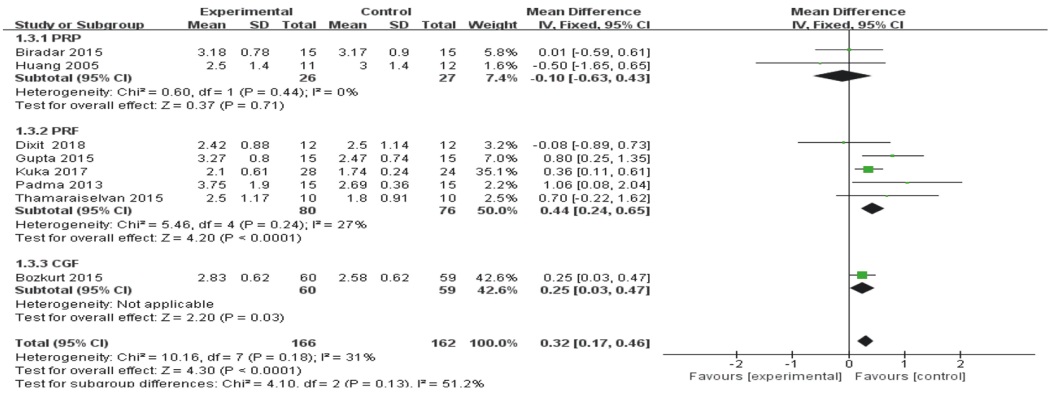

(c)

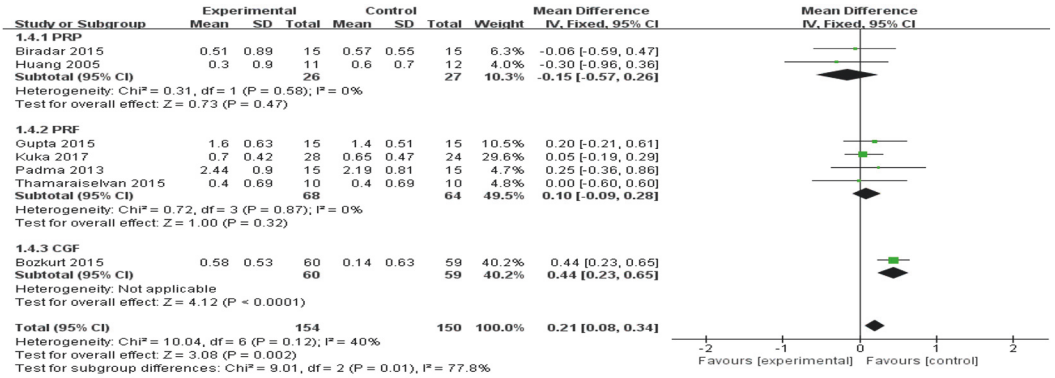

(d)

Figure 3: Continued.

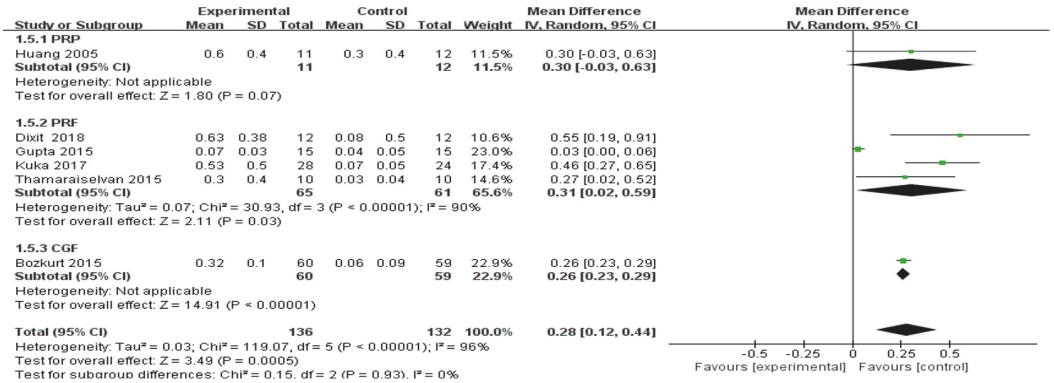

(e)

Figure 3: Forest plots for RC change (a), RD reduction (b), CAL gain (c), KTW gain (d), and GT gain (e).

According to the subgroup analysis results, the three types of APCs did not have the same therapeutic effects on gingival recessions in the CAF procedure. The results of PRP subgroup analysis, especially, showed no significant difference in all the outcome variables. This result was in accordance with Keceli et al. [19]. They compared the CTG+PRP and the CTG alone in the treatment of Miller's I/ II recessions. Their results showed PRP provides no additional benefits to CTG in terms of RC, RD, CAL, and KTW at the 6- and 12-month follow-up. The reasons could be ascribed as follows: First, as the first generation of platelet products, there were certain limitations and deficiencies in the production process of PRP. The preparation of PRP required the artificial addition of thrombin and other preparations. The resulting fibrin had a dense four-molecule structure with small interfibrous pores, which was not conducive to the attachment of cytokines and proliferation of cells [33]. Secondly, PRP released a series of growth factors for 7 days, which peaked on the first day of application [34]. The growth factors in PRP cannot be supplied stably and continuously. But controversially, many previous studies reported that PRP had the ability to promote bone regeneration and soft tissue repair [35–37]. As we know, CAF is one of the safe and effective surgical methods to treat gingival recessions, the clinical effects of it alone in the gingival recessions have been reported in a previous review [38]. We considered the function of PRP might be counteracted by the CAF. On the other hand, based on the limited two studies, our results of PRP need to be further confirmed by more researches.

The results of PRF showed that it had a wide range of effects, including significant improvement on RC, RD, CAL, and GT. The concentration of growth factors and matrix proteins in PRF is higher than PRP [33]. In addition, the fibrin of PRF has a three-dimensional structure. Such a fibrin network will lead to more efficient cell migration and proliferation and can protect the growth factors from proteolysis, thus lengthening the release of growth factors, prolonging the duration of action and promoting tissue healing [7, 39]. Scholar's molecular research has shown PRF can continuously release growth factors within 21 days and peak in 7 days [40]. Dohan Ehrenfest [41] and Zumstein [42] compared the PRP and PRF membranes in vitro. They found the two gels presented 2 very different profiles: the PRP released its most growth factors in the first hours and completely dissolved after 3 days. In contrast, the PRF membrane remained solid and intact after 7 days and continuously released numerous growth factors and matrix molecules. Another superiority of PRF over PRP lies on that PRF fibers aggregate a large number of white blood cells, which have anti-inflammatory and antibacterial effects [43, 44]. Among the four included PRF records, both the test and the control groups had a mild gain of KTW between baseline and 6 months. Nevertheless, the difference of intergroup was statistically nonsignificant (MD: 0.10 mm; 95%CI: -0.09~0.28 mm; P=0.32), which is in line with the results of Del Fabbro et al. [15]. Their meta-analysis of platelet concentrates for keratinized tissue enhancement showed no significant effect (MD: 0.18 mm; 95% CI: -0.19 ~ 0.54 mm; P = 0.34).

Only one record [28] on CGF was selected in this analysis. The subgroup analysis of CGF showed no significant difference in RC and RD, while there were some positive effects in CAL, KTW, and GT. Keratinized gingival is attached to the root surface or underlying bone; the presence of keratinized gingival is an important aspect for the maintenance of gingival health and the prevention of periodontal disease progression [45]. The reduction of gingival thickness can lead to periodontal attachment loss and marginal tissue recession, which is a major concern for periodontal disease progression [46]. Teeth with sufficient KTW and GT are more resistant to inflammation or trauma [47]. In other words, the augmentation of KTW and GT may enhance the long-term predictability of CAF surgery through reducing postoperative recurrence and provide long-term stability [48]. On the other hand, since only one study was qualified to be enrolled, the results of CGF analysis were limited and could not be used universally. The benefits of CGF as an adjunction to gingival recessions remain questionable. We expect more researches to be conducted in this area.

At present, several meta-analyses on APCs for intrabony defects, maxillary sinus elevation, and furcation defects

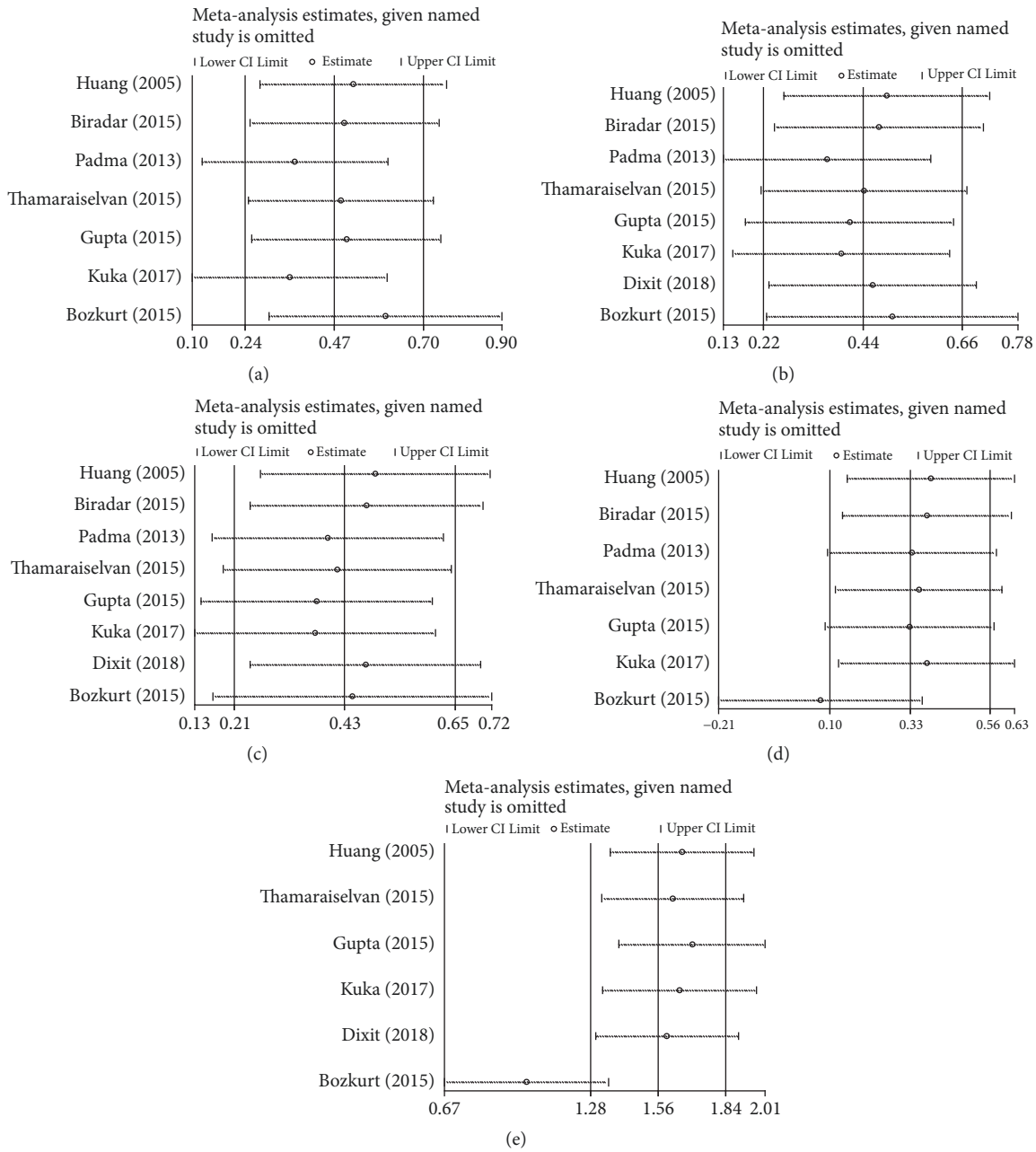

Figure 4: Sensitivity analysis was applied by comparing CAF+PRP/PRF/CGF with CAF alone. (a) RC change; (b) RD reduction; (c) CAL gain; (d) KTW gain; (e) GT gain.

had been published. However, unlike intrabony defects or furcation defects, there is a significant soft tissue defect when the gingival recession occurs, and the available tissue engineering treatment is limited. Different from the existing articles on the application of APCs for gingival recessions, we choose the simplest surgical method (CAF) without other confounding factors like reconstructive techniques, to minimize the clinical heterogeneity caused by the surgical method. Furthermore, unlike other articles, we set the RC as the primary outcome. This outcome variable is more suitable for evaluating gingival recessions because the ultimate goal of gingival recessions treatment is to gain the coverage of root surface and to obtain an optimal aesthetic outcome. To the best of our knowledge, this is the first meta-analysis that included the third generation of APCs (named CGF), which helps us to have a more comprehensive understanding of APCs in the treatment of gingival recessions.

However, there were also some limitations to this meta-analysis. Firstly, there was an inherent heterogeneity between the included articles. Two articles [25, 31] were Class I gingival recessions and the remaining six were Classes I and II recessions. One article [30] included molar teeth and four articles [25, 27, 29, 31] included anterior and premolar teeth. Due to the limited studies that could be searched, the

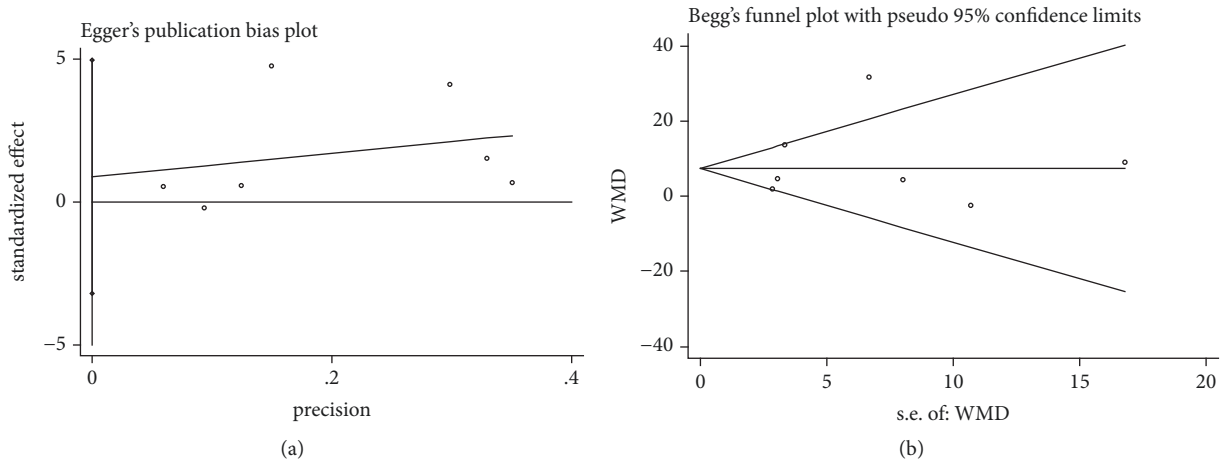

Figure 5: Publication bias of RC change was applied by comparing CAF+PRP/PRF/CGF with CAF alone. (a) Egger's linear regression; (b) Begg's funnel plot.

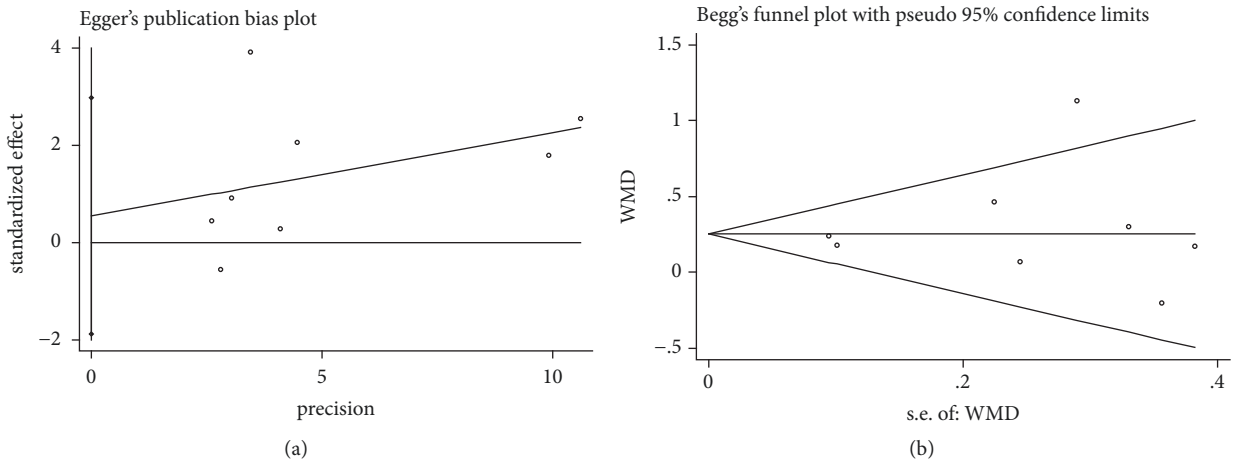

Figure 6: Publication bias of RD reduction was applied by comparing CAF+PRP/PRF/CGF with CAF alone. (a) Egger's linear regression; (b) Begg's funnel plot.

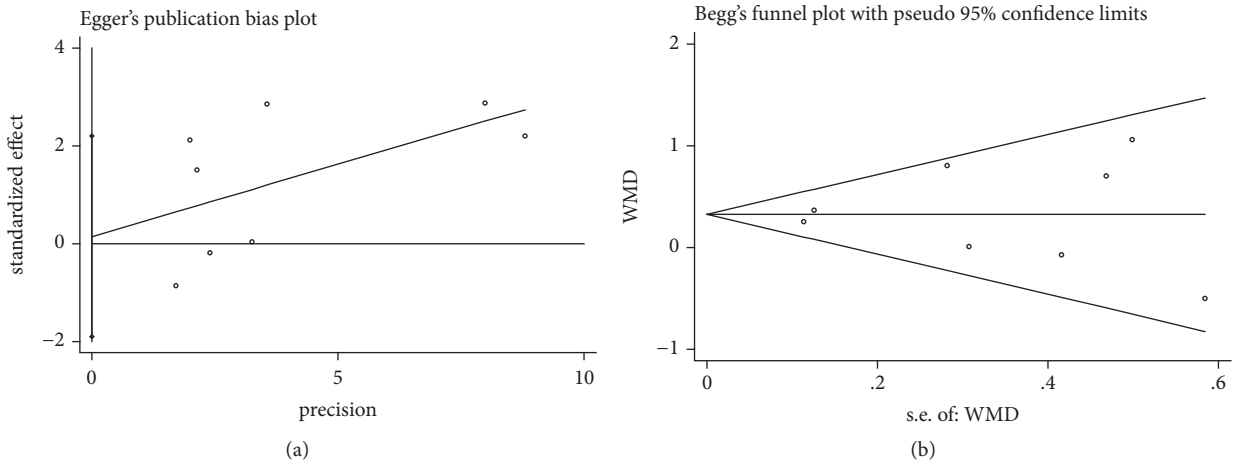

Figure 7: Publication bias of CAL gain was applied by comparing CAF+PRP/PRF/CGF with CAF alone. (a) Egger's linear regression; (b) Begg's funnel plot.

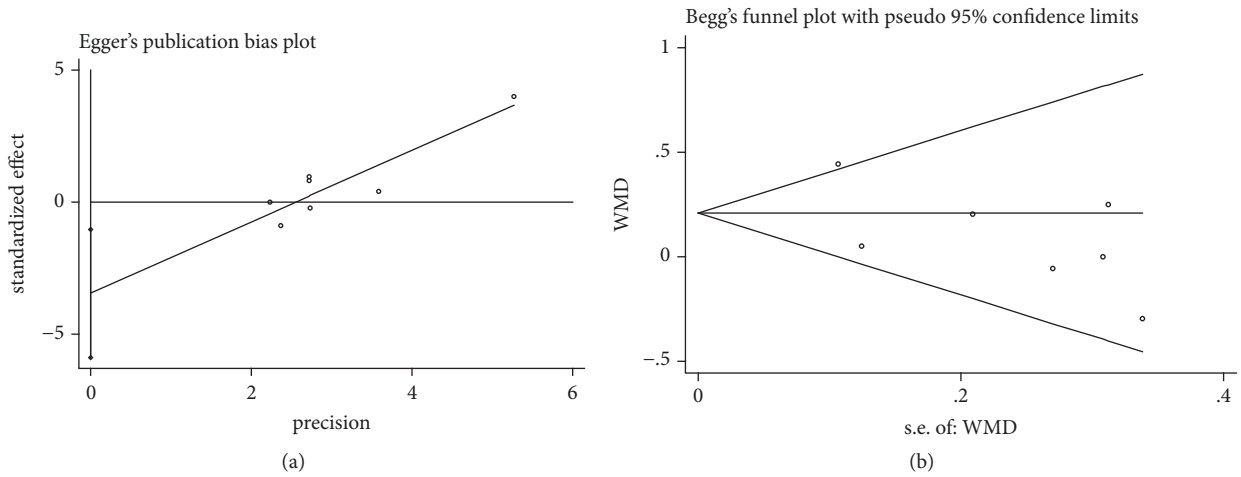

Figure 8: Publication bias of KTW gain was applied by comparing CAF+PRP/PRF/CGF with CAF alone. (a) Egger's linear regression; (b) Begg's funnel plot.

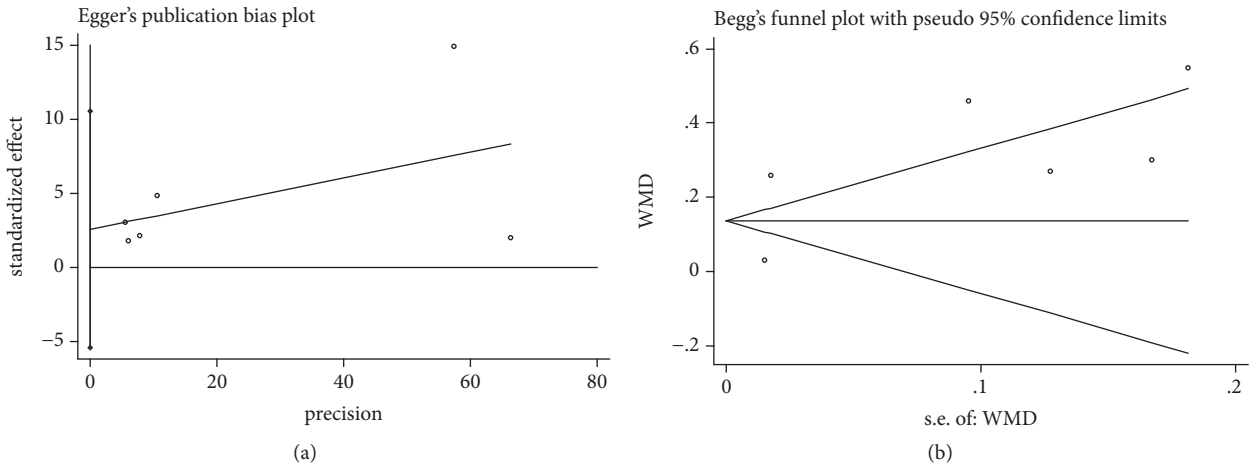

Figure 9: Publication bias of GT gain was applied by comparing CAF+PRP/PRF/CGF with CAF alone. (a) Egger's linear regression; (b) Begg's funnel plot.

entire Class I and Class II gingival recessions, anterior teeth, premolar teeth, and molar teeth were considered together, whereas the depth of the recession defects and the types of teeth can also affect the prognosis of regenerative surgeries. All these taken together may be drawbacks in this analysis. Other heterogeneities should also be considered in future clinical studies, including patient populations, methods of preparation of APCs, and duration of follow-up. Another limitation of this paper was the high risk of bias in the selected studies. Because of the different production processes of APCs, it was impossible to conduct the allocation concealment strictly or to be blind to the personnel. Our risk of bias assessment results showed that among 8 included studies, 4 studies were classified as moderate risk, and 4 as high risk. Taken together, the conclusions of our analysis are limited, and more studies with low risk of bias in this field are needed in the future to provide definitive clinical guidance for periodontal treatment.

5. Conclusions

After the system review and meta-analysis, we can initially get the following conclusions:.

(1) According to the results of our meta-analysis which enrolled five studies, PRF could exert additional effect to CAF. We considered that PRF should be preferred for the treatment of Classes I and II gingival recessions.

(2) Based on the limited studies, it seemed that PRP failed to show any additional effect when combined with CAF. It was not suggested for the therapy of Classes I and II gingival recessions, so as to alleviate the preoperative pain of patients.

(3) Given the limited research and high risk of bias, it is still needed to confirm the additional effect of CGF by more high-quality studies.

(4) Overall, the risk of bias of the articles included in APCs was high, and more low-risk and high-quality researches were needed.

Conflicts of Interest

The authors declare that there are no conflicts of interest.

Acknowledgments

The present article was supported by the Provincial Natural Science Foundation of Liaoning (201800506)

References

[1] S. G. George, A. K. Kanakamedala, J. Mahendra, N. Kareem, L. Mahendra, and J. J. Jerry, "Treatment of gingival recession using a coronally-advanced flap procedure with or without placental membrane," *Journal of Investigative and Clinical Dentistry*, vol. 9, no. 3, p. 2340, 2018.

[2] G. Zucchelli, M. Stefanini, S Ganz et al., "Coronally advanced flap with different designs in the treatment of gingival recessions: A Comparative controlled randomized clinical trial," *International Journal of Periodontics & Restorative Dentistry*, vol. 36, no. 3, pp. 319–327, 2016.

[3] M. P. Santamaria, L. A. Queiroz, I. F. Mathias et al., "Resin composite plus connective tissue graft to treat single maxillary gingival recession associated with non-carious cervical lesion: Randomized clinical trial," *Journal of Clinical Periodontology*, vol. 43, no. 5, pp. 461–468, 2016.

[4] P. S. G. Henriques, M. P. Nunes, and A. A. Pelegrine, "Treatment of gingival recession in two surgical stages: Free gingival graft and connective tissue grafting," *General dentistry*, vol. 59, no. 6, pp. e238–e241, 2011.

[5] M. Rehan, M. Khatri, M. Bansal, K. Puri, and A. Kumar, "Comparative evaluation of coronally advanced flap using amniotic membrane and platelet-rich fibrin membrane in gingival recession: An 18-month clinical study," *Contemporary Clinical Dentistry*, vol. 9, no. 2, pp. 188–194, 2018.

[6] M. K. McGuire and D. L. Cochran, "Evaluation of human recession defects treated with coronally advanced flaps and either enamel matrix derivative or connective tissue. Part 2: histological evaluation," *Journal of Periodontology*, vol. 74, no. 8, pp. 1126–1135, 2003.

[7] A. B. Castro, N. Meschi, A. Temmerman et al., "Regenerative potential of leucocyte- and platelet-rich fibrin. Part A: intra-bony defects, furcation defects and periodontal plastic surgery. A systematic review and meta-analysis," *Journal of Clinical Periodontology*, vol. 44, no. 1, pp. 67–82, 2017.

[8] M. O. Schär, J. Diaz-Romero, S. Kohl, M. A. Zumstein, and D. Nesic, "Platelet-rich concentrates differentially release growth factors and induce cell migration in vitro," *Clinical Orthopaedics and Related Research*, vol. 473, no. 5, pp. 1635–1643, 2015.

[9] R. Al-Azem, N. Ali, and D. Mostafa, "The effectiveness of platelet concentrations in periodontal surgeries," *International Journal of Dental Research*, vol. 6, no. 2, pp. 61–65, 2018.

[10] J. Choukroun, F. Adda, C. Schoeffler et al., "The opportunity in period-implantology: The PRF," *Implantodontie*, vol. 42, pp. 55–62, 2001.

[11] H. Park, S. Kim, J. Oh et al., "Early Bone Formation at a Femur Defect Using CGF and PRF Grafts in Adult Dogs," *Implant Dentistry*, vol. 25, no. 3, pp. 387–393, 2016.

[12] S. Bernardi, S. Mummolo, S. Tecco, M. A. Continenza, and G. Marzo, "Histological characterization of Sacco's concentrated growth factors membrane," *International Journal of Morphology*, vol. 35, no. 1, pp. 114–119, 2017.

[13] L. F. Rodella, G. Favero, R. Boninsegna et al., "Growth factors, CD34 positive cells, and fibrin network analysis in concentrated growth factors fraction," *Microscopy Research and Technique*, vol. 74, no. 8, pp. 772–777, 2011.

[14] H. Luo, R. Li, C. Wang, L. Peng, and L. Ye, "The adjunctive use of platelet concentrates in the therapy of gingival recessions: a systematic review and meta-analysis," *Journal of Oral Rehabilitation*, vol. 42, no. 7, pp. 552–561, 2015.

[15] M. del Fabbro, M. Bortolin, S. Taschieri, and R. Weinstein, "Is platelet concentrate advantageous for the surgical treatment of periodontal diseases? A systematic review and meta-analysis," *Journal of Periodontology*, vol. 82, no. 8, pp. 1100–1111, 2011.

[16] V. Moraschini and E. Dos Santos Porto Barboza, "Use of platelet-rich fibrin membrane in the treatment of gingival recession: A systematic review and meta-analysis," *Journal of Periodontology*, vol. 87, no. 3, pp. 281–290, 2016.

[17] L. Shamseer, D. Moher, M. Clarke et al., "Preferred reporting items for systematic review and meta-analysis protocols (prisma-p) 2015: Elaboration and explanation," *British Medical Journal*, vol. 349, Article ID g7647, 2015.

[18] T. J. O'Leary, R. B. Drake, and J. E. Naylor, "The plaque control record," *Journal of Periodontology*, vol. 43, no. 1, pp. 38-39, 1972.

[19] H. G. Keceli, D. Sengun, A. Berberoğlu, and E. Karabulut, "Use of platelet gel with connective tissue grafts for root coverage: a randomized-controlled trial," *Journal of Clinical Periodontology*, vol. 35, no. 3, pp. 255–262, 2008.

[20] J. Higgins and S. Green, *Cochrane Handbook for Systematic Reviews of Interventions: Cochrane Book Series*, 2008.

[21] I. Tsesis, E. Rosen, S. Taschieri, Y. Telishevsky Strauss, V. Ceresoli, and M. Del Fabbro, "Outcomes of surgical endodontic treatment performed by a modern technique: an updated meta-analysis of the literature," *Journal of Endodontics*, vol. 39, no. 3, pp. 332–339, 2013.

[22] P. S. Petrungaro, "Using platelet-rich plasma to accelerate soft tissue maturation in esthetic periodontal surgery," *Compendium of Continuing Education in Dentistry*, vol. 22, no. 9, pp. 729–732, 2001.

[23] A. P. Saadoun, "Current trends in gingival recession coverage–Part II: Enamel matrix derivative and platelet-rich plasma.," *Practical procedures & aesthetic dentistry : PPAD*, vol. 18, no. 8, pp. 521–528, 2006.

[24] A. R. Naik, A. V. Ramesh, C. D. Dwarkanath, M. S. Naik, and A. B. Chinnappa, "Use of autologous platelet rich plasma to treat gingival recession in esthetic periodontal surgery," *Journal of Indian Society of Periodontology*, vol. 17, no. 3, pp. 345–353, 2013.

[25] L. Huang, R. E. Neiva, S. E. Soehren, W. V. Giannobile, and H. Wang, "The effect of platelet-rich plasma on the coronally advanced flap root coverage procedure: a pilot human trial," *Journal of Periodontology*, vol. 76, no. 10, pp. 1768–1777, 2005.

[26] R. Padma, A. Shilpa, P. A. Kumar, M. Nagasri, C. Kumar, and A. Sreedhar, "A split mouth randomized controlled study to evaluate the adjunctive effect of platelet-rich fibrin to coronally advanced flap in Miller's class-I and II recession defects," *Journal of Indian Society of Periodontology*, vol. 17, no. 5, pp. 631–636, 2013.

[27] M. Thamaraiselvan, S. Elavarasu, S. Thangakumaran, J. Gadagi, and T. Arthie, "Comparative clinical evaluation of coronally advanced flap with or without platelet rich fibrin membrane in the treatment of isolated gingival recession," *Journal of Indian Society of Periodontology*, vol. 19, no. 1, pp. 66–71, 2015.

[28] Ş. Bozkurt Doğan, F. Öngöz Dede, U. Ballı, E. N. Atalay, and M. C. Durmuşlar, "Concentrated growth factor in the treatment

of adjacent multiple gingival recessions: a split-mouth randomized clinical trial," *Journal of Clinical Periodontology*, vol. 42, no. 9, pp. 868–875, 2015.

[29] S. Gupta, R. Banthia, P. Singh, P. Banthia, S. Raje, and N. Aggarwal, "Clinical evaluation and comparison of the efficacy of coronally advanced flap alone and in combination with platelet rich fibrin membrane in the treatment of Miller Class I and II gingival recessions," *Contemporary Clinical Dentistry*, vol. 6, no. 2, pp. 153–160, 2015.

[30] S. M. Biradar, A. Satyanarayan, A. J. Kulkarni, B. Patti, S. K. Mysore, and A. Patil, "Clinical evaluation of the effect of platelet rich plasma on the coronally advanced flap root coverage procedure," *Dental Research Journal*, vol. 12, no. 5, pp. 469–475, 2015.

[31] S. Kuka, S. D. Ipci, G. Cakar, and S. Yılmaz, "Clinical evaluation of coronally advanced flap with or without platelet-rich fibrin for the treatment of multiple gingival recessions," *Clinical Oral Investigations*, vol. 22, no. 3, pp. 1551–1558, 2018.

[32] N. Dixit, A. Lamba, F. Faraz, S. Tandon, K. Aggarwal, and A. Ahad, "Root coverage by modified coronally advanced flap with and without platelet-rich fibrin: A clinical study," *Indian Journal of Dental Research*, vol. 29, no. 5, p. 600, 2018.

[33] T.-H. Kim, S.-H. Kim, G. K. Sádor, and Y.-D. Kim, "Comparison of platelet-rich plasma (PRP), platelet-rich fibrin (PRF), and concentrated growth factor (CGF) in rabbit-skull defect healing," *Archives of Oral Biolog*, vol. 59, no. 5, pp. 550–558, 2014.

[34] D. M. Dohan Ehrenfest, L. Rasmusson, and T. Albrektsson, "Classification of platelet concentrates: from pure platelet-rich plasma (P-PRP) to leucocyte- and platelet-rich fibrin (L-PRF)," *Trends in Biotechnology*, vol. 27, no. 3, pp. 158–167, 2009.

[35] A. Albanese, M. E. Licata, B. Polizzi, and G. Campisi, "Platelet-rich plasma (PRP) in dental and oral surgery: from the wound healing to bone regeneration," *Immunity & Ageing*, vol. 10, no. 1, p. 23, 2013.

[36] M. Jalaluddin, J. Mahesh, R. Mahesh et al., "Effectiveness of platelet rich plasma and bone graft in the treatment of intrabony defects: A clinico-radiographic study," *The Open Dentistry Journal* , vol. 12, pp. 133–154, 2018.

[37] D. J. B. Menezes, J. A. Shibli, S. A. Gehrke, A. M. Beder, and W. R. Sendyk, "Effect of platelet-rich plasma in alveolar distraction osteogenesis: a controlled clinical trial," *British Journal of Oral and Maxillofacial Surgery*, vol. 54, no. 1, pp. 83–87, 2016.

[38] F. Cairo, M. Nieri, and U. Pagliaro, "Efficacy of periodontal plastic surgery procedures in the treatment of localized facial gingival recessions. A systematic review," *Journal of Clinical Periodontology*, vol. 41, pp. S44–S62, 2014.

[39] S. Zhou, C. Sun, S. Huang et al., "Efficacy of adjunctive bioactive materials in the treatment of periodontal intrabony defects: a systematic review and meta-analysis," *BioMed Research International*, vol. 2018, Article ID 8670832, 15 pages, 2018.

[40] R. J. Carroll, S. P. Amoczky, S. Graham et al., *Characterization of Autologous Growth Factors in Cascade Platelet-Rich Fibrin Matrix (PRFM)*, N. J. Edison, Ed., Musculoskeletal Transplant Foundation, 2005.

[41] D. M. D. Ehrenfest, T. Bielecki, R. Jimbo et al., "Do the fibrin architecture and leukocyte content influence the growth factor release of platelet concentrates? An evidence-based answer comparing a pure Platelet-Rich Plasma (P-PRP) gel and a leukocyte- and Platelet-Rich Fibrin (L-PRF)," *Current Pharmaceutical Biotechnology*, vol. 13, no. 7, pp. 1145–1152, 2012.

[42] M. A. Zumstein, T. Bielecki, and D. M. Dohan Ehrenfest, "The future of platelet concentrates in sports medicine: platelet-rich plasma, platelet-rich fibrin, and the impact of scaffolds and cells on the long-term delivery of growth factors," *Operative Techniques in Sports Medicine*, vol. 19, no. 3, pp. 190–197, 2011.

[43] D. M. Dohan, J. Choukroun, A. Diss et al., "Platelet-rich fibrin (PRF): a second-generation platelet concentrate. Part I. Technological concepts and evolution," *Oral Surgery, Oral Medicine, Oral Pathology, Oral Radiology, and Endodontolog*y, vol. 101, no. 3, pp. E37–E44, 2006.

[44] D. M. D. Ehrenfest, M. Del Corso, A. Diss, J. Mouhyi, and J.-B. Charrier, "Three-dimensional architecture and cell composition of a Choukroun's platelet-rich fibrin clot and membrane," *Journal of Periodontology*, vol. 81, no. 4, pp. 546–555, 2010.

[45] J. Carnio, P. M. Camargo, P. R. Klokkevold, Y.-L. Lin, and F. Q. Pirih, "Use of the modified apically repositioned flap technique to create attached gingiva in areas of no keratinized tissue: A clinical and histologic evaluation," *International Journal of Periodontics and Restorative Dentistry*, vol. 37, no. 3, pp. 362–369, 2017.

[46] R. G. S. Manjunath, A. Rana, and A. Sarkar, "Gingival biotype assessment in a healthy periodontium: transgingival probing method," *Journal of Clinical and Diagnostic Research*, vol. 9, no. 5, pp. 66–69, 2015.

[47] F. Liu, G. Pelekos, and L. J. Jin, "The gingival biotype in a cohort of Chinese subjects with and without history of periodontal disease," *Journal of Periodontal Research*, vol. 52, no. 6, pp. 1004–1010, 2017.

[48] Z. Aleksić, S. Janković, B. Dimitrijević, T. Divnić-Resnik, I. Milinković, and V. Leković, "The use of platelet-rich fibrin membrane in gingival recession treatment," *Srpski Arhiv za Celokupno Lekarstvo*, vol. 138, no. 1-2, pp. 11–18, 2010.

Hindawi
BioMed Research International
Volume 2019, Article ID 1680158, 8 pages
https://doi.org/10.1155/2019/1680158

Research Article

Evaluation of Implant Success in Patients with Dental Aplasia

Sameh Attia,[1] Ella Schaper,[1] Heidrun Schaaf,[1] Jörn Pons-Kühnemann,[2] Maximiliane Amelie Schlenz,[3] Philipp Streckbein,[1] Sebastian Böttger,[1] Hans-Peter Howaldt,[1] and Jan-Falco Wilbrand[1]

[1] *Department of Cranio-Maxillofacial Surgery, Faculty of Medicine, Justus-Liebig University Giessen, Klinik Str. 33, 35392 Giessen, Germany*
[2] *Institute for Medical Informatics and Medical Statistics, Faculty of Medicine, Justus-Liebig University Giessen, Rudolf-Buchheim Str. 6, 35392 Giessen, Germany*
[3] *Justus-Liebig-University Giessen, Department of Prosthodontics, Schlangenzahl 14, 35392 Giessen, Germany*

Correspondence should be addressed to Sameh Attia; sameh.attia@dentist.med.uni-giessen.de

Received 26 February 2019; Revised 30 April 2019; Accepted 30 May 2019; Published 19 June 2019

Guest Editor: Maria Sartori

Introduction. Dental aplasia is an anomaly in which the number of teeth is reduced. It is the most commonly occurring dental anomaly during tooth development. Treatment management of patients with dental aplasia is challenging. *Objectives.* The aim of this retrospective clinical study was to analyze the survival and success rates of dental implants placed in hypodontic patients, rated with different criteria. *Methods.* Forty-three patients were diagnosed with dental aplasia and treated with dental implants between November 2000 and February 2016. The variables assessed included the plaque level, bleeding on probing, probing depth, implant mobility, implant stability, and implant loss. To analyze the peri-implant bone level, a panoramic X-ray of each patient was taken. The results were compared with X-rays taken immediately after implantation. *Results*. Thirty-seven patients (16 males; 21 females) participated in this study. In total, 155 implants (86 maxillary; 69 mandibular) were inserted. Two of the 155 implants failed; the *in situ* survival rate was 98.7%. The success rate according to the criteria of Buser et al. was 96.8%, and that according to the criteria of Albrektsson et al. was 88.4%. *Conclusion.* The survival and success rates of dental implants in patients with congenitally absent teeth were very high and did not differ significantly from results achieved in an unaffected population. Dental implants are a reliable therapy for patients with dental aplasia.

1. Introduction

Types of dental aplasia include hypodontia, oligodontia, and anodontia. Hypodontia is the absence of one to five teeth, and oligodontia is the absence of more than five teeth, excluding the wisdom teeth [1]. Anodontia is characterized by the partial or complete absence of deciduous and permanent dentition [2]. The prevalence of dental aplasia in the deciduous dentition varies among countries, with a reported range of 0.2% to 0.9% [3, 4]. Agenesis of the primary dentition is associated with an increased risk of tooth absence in the secondary dentition [5]. The prevalence of hypodontia in the permanent dentition is 2–10% [6, 7]. Several studies have documented an uneven sex distribution for dental aplasia, with a greater prevalence among females than among males [8–10]. The most frequently absent teeth in the permanent dentition are the mandibular second premolars (1–5%), maxillary lateral incisors (0.5–3%), maxillary second premolars (1–2.5%), and mandibular lateral incisors (0.5%). The prevalence of wisdom tooth absence is 10–35% [6]. Dental aplasia is associated with several syndromes, such as ectodermal dysplasia, cleft lip, cleft palate, Rieger syndrome, and Down's syndrome [11]. The etiology of hypodontia may involve genetic (nonsyndromal) factors [12]. Seven genes are known to be associated with the development of dental aplasia: *MSX1*, *PAX9*, *AXIN2*, *EDA*, *EDARADD*, *NEMO*, and *KRT17141* [13]. However, the exact etiopathogenesis of dental aplasia is not completely clear [14]. Although there is no clear relationship between dental aplasia and bone metabolic disease recorded, many clinical signs are generally observed.

Table 1: Summarize the clinical and radiological parameters with the selected scoring system.

Clinical/Radiological Parameters	Scoring system
Plaque index	the modified Mombelli plaque index [31]: (i) Grade 0: no plaque detected by inspection and probing. (ii) Grade 1: accumulation of plaque that is visible only by probing the sulcus with a probe but not with the eye. (iii) Grade 2: visible plaque deposition. Grade 3: massive plaque deposition.
Probing depth	measured using the Click-Probe (Kerr Corporation, Orange, CA, USA) The measurement takes place in four sites around the implant - mesial, vestibular, distal and oral. The maximum measurements in mm were recorded.
Bleeding on probing	The bleeding index is determined parallel to the probing depths. If bleeding occurs during probing, this is indicated in the patient's sheet with a plus sign [+]
Mobility grade/Osseointegration	Periotest® device (Gulden, Modautal, Germany) The manufacturer specifies a scale from -08 to +50. The smaller the measured value is, the better the osseointegration is assessed: (i) Values from -08 to 00: good osseointegration of the implant (ii) Values +01 to +09: A clinical review is needed to investigate osseointegration (iii) Values from +10 to +50: Insufficient osseointegration of the implant
Vertical bone loss	the difference in alveolar bone height between panoramic X-rays taken immediately after implantation and at the follow-up examination in millimeters

These clinical features include tooth morphology (microdontia) and tooth malposition in different manner such as infraocclusion of primary molars, ectopia, and transposition of permanent teeth [15, 16]. Dental aplasia can seriously affect young patients physically and psychologically, particularly during puberty. Interdisciplinary cooperation among dental practitioners is important to achieve optimal treatment outcomes for these patients [2]. Therapeutic options for dental aplasia depend on the number and location of absent teeth, dental implants, resin-bonded or conventionally fixed dental prostheses, autotransplantation sites, and sites of orthodontic tooth gap closure [14, 17–19]. Dental implant placement is a reliable and effective method for the rehabilitation of even augmented jaws [20]. A deciduous tooth can serve as a space maintainer until cranial bone growth is complete and a dental implant can be inserted [21].

Many studies have evaluated dental implants in patients with dental aplasia, with a focus on the implant survival rate [22–27]. Soft-tissue parameters were not evaluated in most of these studies, and implant success was evaluated with self-defined parameters. Standard success criteria were not used in any of these studies. The aim of the present retrospective study was to determine the success and survival rates of dental implants in patients with dental aplasia. Implant success was evaluated using the Buser and Albrektsson criteria [28, 29]. An individual questionnaire was used to collect general patient data and record patient satisfaction.

2. Materials and Methods

Forty-three patients with dental aplasia were treated with endosseous implants at the Department of Oral and Maxillofacial Surgery, University Hospital Giessen, Germany, during 2000–2016. Data collected from patient records included age, sex, number and location of absent teeth, and implant- and prosthetic-based rehabilitation. All selected patients who fulfilled the inclusion criteria were invited to undergo clinical and radiological examinations and an interview that included the administration of a customized questionnaire. The main purpose of the assessment was to evaluate implant success according to the criteria of Albrektsson and Buser [29, 30]. Implant success was defined as the fulfillment of all criteria, and implant failure was defined as the failure to satisfy at least one criterion. Explanted implants, regardless of the reason for removal, were also considered to have failed.

The following clinical parameters were recorded in the assessment of dental implant success: the modified Mombelli plaque index [31], probing depth measured using the Click-Probe (Kerr Corporation, Orange, CA, USA) [32], bleeding on probing (*the mobility grade inferred the osteointegration and stability and was calculated for each dental implant* using the Periotest® device (Gulden, Modautal, Germany)), and the absence or presence of keratinized gingiva (Table 1).

The presence of peri-implant infection was assessed clinically and radiologically at the same time and defined as the presence of a pocket depth ≥ 4 mm, bleeding on probing, and/or exudate and vertical bone loss > 1.5 mm + [0.2 mm × (years − 1)].

Vertical bone loss was determined by calculating the difference in alveolar bone height between panoramic X-rays taken immediately after implantation and at the follow-up examination. The presence of radiolucency around dental implants was assessed on the panoramic X-rays. To exclude measurement error, all panoramic X-rays were obtained with the same device (Sirona®, Bensheim, Germany) and evaluated by the same examiner. The data were collected from the patients' digital files (KAOS software, University Hospital Giessen clinical administration system) and categorized using Microsoft Excel® software (version 2017; Microsoft Corporation, Redmond, WA, USA).

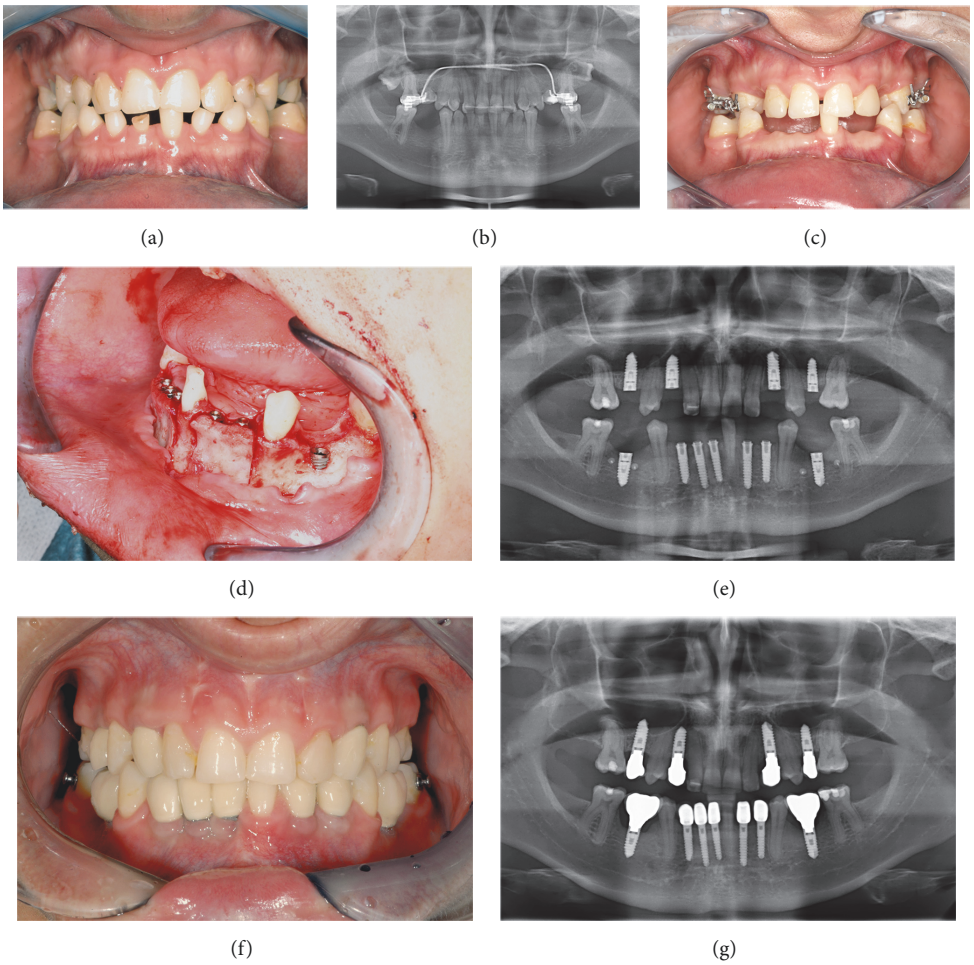

Figure 1: Treatment procedures of patient with oligodontia until oral rehabilitation. (a) Initial condition, patient with oligodontia (13 teeth absent). (b) Panoramic X-ray of the initial case. (c) After deciduous tooth extraction. (d) Intraoperative surgical view, insertion of implant and bone splitting. (e) Postoperative panoramic X-ray showing implant position. (f) Prosthetic rehabilitation with single tooth crowns. (g) Panoramic X-ray, 3 years after implantation.

The research ethics committee of the Faculty of Medicine, Justus Liebig University Giessen, approved this study (no. 209/15).

2.1. Statistical Analysis. Implant survival probability was calculated in a Kaplan–Meier analysis performed in collaboration with the Institute of Medical Informatics of Justus Liebig University Giessen using SPSS software (version 24.0; IBM Corporation, Armonk, NY, USA). *The Chi-square test (χ^2)- or Fischer's more accurate test for categorical variables was applied to investigate the correlation between implant systems used, the type of graft, and age or sex of patients.*

3. Results

Forty-three patients with hypodontia or oligodontia (25 females; 18 males) received dental implants for functional and aesthetic rehabilitation during November 2000–September 2016. All patients were treated surgically at the Department of Oral and Maxillofacial Surgery and prosthodontically at the Department of Prosthodontics of the University Hospital Giessen, Germany. Data on the patients' general condition and personal habits were collected at the time of the follow-up examination. Treatment outcomes were evaluated in 37 patients using a customized questionnaire during the clinical examination. Six patients refused to participate in the study and were counted as dropouts. Patient age at the time of implantation ranged from 17 to 44 years (mean, 21.4 years). The majority (n = 33) of patients treated with dental implants were young. Bone augmentation from the mandibular angle was performed in five (13.5%) patients with eight (5.2%) implants. Iliac crest bone grafts were used in 13 (35.1%) patients with 89 (57.4%) implants. Figure 1 shows a patient with oligodontia and treatment procedures until oral rehabilitation.

3.1. Dental Implants and Survival. In total, 155 implants (86 maxillary; 69 mandibular) were inserted (94 in males; 61 in females; Figure 2).

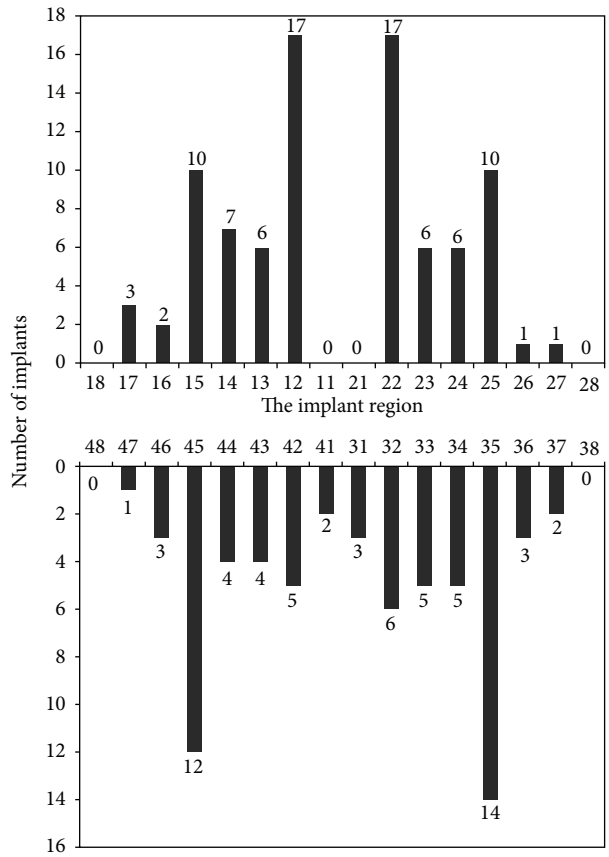

Figure 2: Implant distribution according to dental region.

Three different implant systems were used over the time of observation. In the beginning (Year 2000) mainly Straumann Standard® Implants with a parallel macrogeometry (Straumann, Basel, Switzerland; $n = 10$) were inserted. Within the following years (until 2016) mainly two different implant systems (Xive Plus® with a parallel and self-cutting shape, Friadent, Mannheim, Germany, $n = 105$, and Bego Semados® RI with a conical and condensing shape $n = 28$, and Bego Mini $n = 12$, Bego Implant Systems, Bremen, Germany; total $n = 40$) were inserted. Two implants were explanted at 6 (BEGO-Mini) and 34 months (Xive) after implantation, respectively. The overall implant survival rate over 189 months as determined by Kaplan–Meier Analysis was 98.7% (Figure 3).

3.2. Clinical and Radiological Characteristics of Dental Implants. Clinical and radiological evaluation was performed for 155 implants. Two implants were lost due to explanation. The following parameters were examined: plaque index, probing depth, bleeding on probing, implant mobility, and keratinized gingiva.

Inspection and probing revealed no plaque on 67 (43.8%) implants, grade 1 plaque according to the Mombelli index [31] on 48 (31.4%) implants, grade 2 plaque on 32 (20.9%) implants, and grade 3 plaque on 6 (3.9%) implants.

In total, 128 implants had maximum probing depths of 1.0–4.0 mm, which are considered to be physiologically normal. Probing depths were ≥ 4 mm for 24 implants. At the follow-up examinations, most ($n = 93$) implants did not bleed on probing. None of the 153 dental implants examined showed mobility, as measured manually. Periotest® values for 122 implants ranged from −7 to 0, indicating good osseointegration. Twenty-five implants had scores of 1–9, indicating the requirement for clinical reevaluation. One implant had a score of 13, which represents insufficient osseointegration. Keratinized gingiva was observed around the crowns of most ($n = 137$) implants.

Bone loss was determined radiologically for each implant by comparing bone levels on postoperative and follow-up panoramic X-rays. Bone loss of 0–0.5 mm was recorded for 33 implants, and loss of 0.5–3.5 mm was recorded for 103 implants. Bone loss > 3.5 mm was observed around 17 implants. *No correlation was found between implant systems used, the type of graft, and age or sex of patients in Fischer's exact test, and bilateral correlation testing of all parameters resulted in a p-value <= 0.05.*

3.3. Implant Success according to the Buser Criteria. According to Buser's success criteria, five implants in our sample failed due to explantation ($n = 2$), radiolucency ($n = 2$), and dysesthesia ($n = 1$). Thus, the implant success rate according to these criteria was 96.8%.

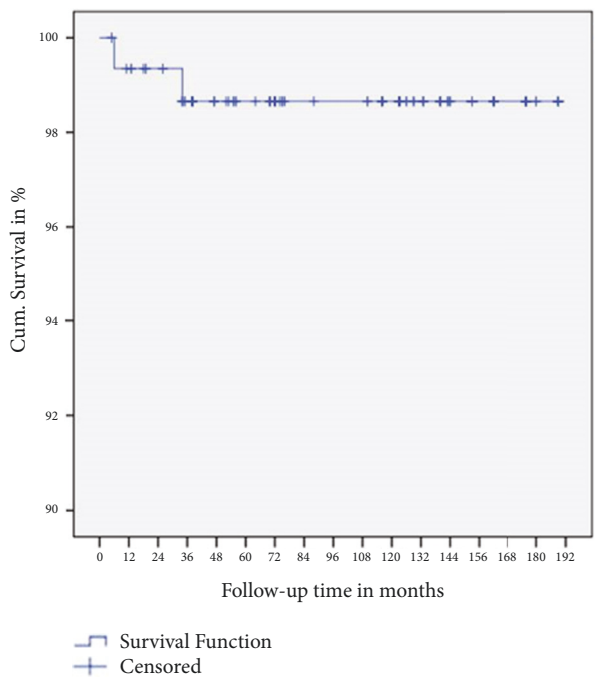

Figure 3: Cumulative Kaplan–Meier survival curve for dental implants.

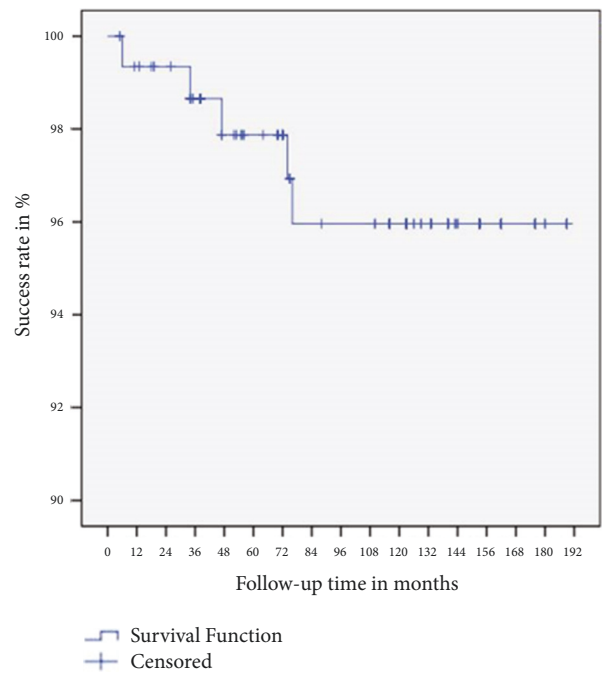

Figure 4: Cumulative success rate according to the Buser criteria.

The Kaplan–Meier curve for these data (Figure 4) shows that five of 155 implants failed during the 189-month (15.75-year) observation period, resulting in a cumulative success rate of 96%.

3.4. Implant Success according to the Albrektsson Criteria. One or more parameters (explantation, radiolucency, dysesthesia, vertical bone loss, and infection) led to the failure of 18 implants. Thus, the implant success rate according to the Albrektsson criteria was 88.4%.

The Kaplan–Meier curve for these data (Figure 5) shows that 18 of 155 implants failed during the 189-month (15.75-year) observation period, resulting in a cumulative success rate of 61%.

4. Discussion

This study considered patients who had received dental implants due to dental aplasia, regardless of whether the condition was hypodontia, oligodontia, ectodermal dysplasia, or cleft lip or palate. Limitations of this study were related to the numbers of patients (n = 37) and dental implants (n = 155) included. This relatively small sample is not representative of a larger population. Due to the rareness of dental aplasia, smaller numbers of patients and implants were included in previous studies [27, 33, 34]. The sex distribution in this study was 43.2% male and 56.8% female patients (ratio, 1:1.3). Similar distributions have been reported in the literature [8, 9]. Patient age at the time of implantation in this study ranged from 17 to 44 years (mean, 20 years), and 89.2% (n = 33) of patients were aged 17–23 years. Other studies have included similarly young patient groups [35, 36]. A possible explanation for the predominance of young patients is that early implant treatment planning commences at the age of 17–21 years, when cranial growth is complete. The most frequently absent teeth replaced with dental implants in this study were the maxillary lateral incisors and maxillary and mandibular second premolars. This prevalence distribution is comparable to results from the literature [7, 9]. The implant loss rate in this study was 1.3% (n = 2), and the *in situ* implant survival rate was 98.7% (n = 153/155). One implant was lost after 34 months due to osseointegration failure, and another was lost after 6 months due to peri-implantitis. Notably, the latter was a mini-implant with a diameter of 2.9 mm and length of 11.5 mm. Becelli et al reported a survival rate of 96.6% for 60 implants in 8 oligodontic patients [34]. In a review and meta-analysis of 19 articles on this topic, survival rates ranged from 76.6% to 100%, and the overall survival rate was 95.3% [37]. Comparable results were recorded in the present study.

4.1. Implant Success Criteria. The survival of dental implants is not necessarily equivalent to their success. The assessment of implant success in addition to survival is very important in the evaluation of treatment outcomes. Many similar studies of dental implants in patients with dental aplasia did not involve the use of implant success criteria [37]. In studies assessing implant success, self-defined criteria or the sole criterion of the marginal bone level had been applied [38–40]. Therefore, comparison of implant success rates between this study and previous studies is not meaningful. In this study, implant success was evaluated using the criteria of Buser et al. [30] and Albrektsson et al. [29]. Two sets of

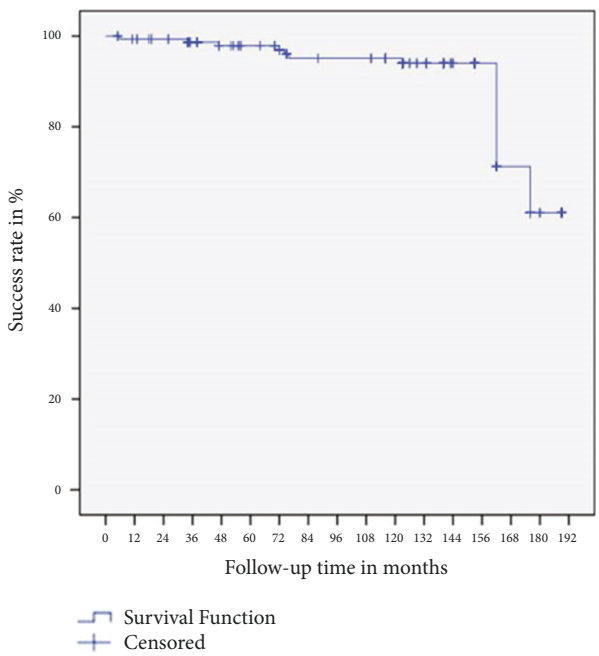

Figure 5: Cumulative success rate according to the Albrektsson criteria.

criteria were used to enable the consideration of differences in implant success in an identical patient sample resulting from the use of different measures. Depending on the criteria used, the implant success rate in the same patient sample may vary. According to the Buser criteria, five implants in this study were considered to have failed (two due to radiolucency and one due to paresthesia). According to the Albrektsson criteria, an additional 13 implants from the same sample failed (total, n= 18). Unlike the Buser criteria, the Albrektsson criteria include vertical bone loss and the presence of infection (peri-implantitis). As a result, the peri-implant hard and soft tissues were evaluated more stringently, which explains the lower success rate. However, neither of these criteria includes subjective assessment of dental implants. Only the success criteria of Jahn and d'Hoedt [41] consider patient satisfaction. Buch et al. criticized the use of only hard- and soft-tissue evaluations for the assessment of implant success and recommended additional subjective assessment of patient satisfaction [42]. About 30 years ago, researchers used primarily measurable clinical parameters to detect disease-related impairments and evaluate therapeutic success; today, patients' perceived satisfaction has become focal [43]. For this reason, patient satisfaction should be taken into consideration in the future establishment of success criteria. The Buser and Albrektsson criteria also neglect the assessment of prosthetic outcome, which should be considered in future development of success criteria. A new implant success assessment tool could also employ score calculation in which criteria (clinical and radiological parameters, prosthetic outcome, and patient satisfaction) are differentially weighted statistically. The classification of implant success should be graded (e.g., very good, good, medium, and bad), so that a less successful implant does not necessarily mean complete failure.

5. Conclusion

In this retrospective study, 155 implants were inserted in patients with dental aplasia (risk group) and examined during a median observation period of 10.25 years. The survival rate (98.7%) was comparable to those of other studies conducted with normal cohorts. Patient satisfaction parameters are planned to be acquired, addressed, and discussed in a future manuscript. In this study, two sets of criteria were used to measure implant success. The implant success rate was higher according to the Buser criteria (96.8%) than according to the Albrektsson criteria (88.4%). The main reason for the lower Albrektsson implant success rate is the assessment of marginal bone loss. Further development of a complex implant success scoring system might be useful for standardized follow-up evaluation of dental implants.

Data Availability

The data used to support the findings of this study are available from the corresponding author upon request.

Conflicts of Interest

The authors declare no conflicts of interest.

Acknowledgments

The authors extend their thanks to PD. Dr. Thaqif El Khassawna of the Experimental Trauma Surgery, Justus-Liebig University Giessen, Germany, for his support in finalizing the manuscript.

References

[1] S. L. Singer, P. J. Henry, and I. D. Lander, "A treatment planning classification for oligodontia," *International Journal of Prosthodontics*, vol. 23, no. 2, pp. 99–106, 2010.

[2] J. H. Nunn, N. E. Carter, T. J. Gillgrass et al., "The interdisciplinary management of hypodontia: background and role of paediatric dentistry," *British Dental Journal*, vol. 194, no. 5, pp. 245–251, 2003.

[3] S. Järvinen and L. Lehtinen, "Supernumerary and congenitally missing primary teeth in finnish children: An epidemiologic study," *Acta Odontologica Scandinavica*, vol. 39, no. 2, pp. 83–86, 1981.

[4] A. Kapdan, A. Kustarci, B. Buldur, D. Arslan, and A. Kapdan, "Dental anomalies in the primary dentition of Turkish children," *European Journal of Dentistry*, vol. 6, no. 2, pp. 178–183, 2012.

[5] J. Daugaard-Jensen, M. Nodal, L. T. Skovgaard, and I. Kjær, "Comparison of the pattern of agenesis in the primary and permanent dentitions in a population characterized by agenesis in the primary dentition," *International Journal of Paediatric Dentistry*, vol. 7, no. 3, pp. 143–148, 1997.

[6] K. Pieper, "Zahnanomalien und ihre Versorgung," in *Kinderzahnheilkunde*, J. Einwag, Ed., vol. 16, Elsevier, Urban & Fischer, München, Jena, Germany, 3rd edition, 2008.

[7] A. L. Gracco, S. Zanatta, F. F. Valvecchi, D. Bignotti, A. Perri, and F. Baciliero, "Prevalence of dental agenesis in a sample of Italian orthodontic patients: an epidemiological study," *Progress in Orthodontics*, vol. 18, no. 1, p. 33, 2017.

[8] N. N. Nik-Hussein, "Hypodontia in the permanent dentition: a study of its prevalence in Malaysian children," *Australasian Orthodontic Journal*, vol. 11, no. 2, pp. 93–95, 1989.

[9] B. J. Polder, M. A. Van't Hof, F. P. G. M. Van Der Linden, and A. M. Kuijpers-Jagtman, "A meta-analysis of the prevalence of dental agenesis of permanent teeth," *Community Dentistry and Oral Epidemiology*, vol. 32, no. 3, pp. 217–226, 2004.

[10] R. S. Meza, "Radiographic assessment of congenitally missing teeth in orthodontic patients," *International Journal of Paediatric Dentistry*, vol. 13, no. 2, pp. 112–116, 2003.

[11] C. J. Larmour, P. A. Mossey, B. S. Thind, A. H. Forgie, and D. R. Stirrups, "Hypodontia—a retrospective review of prevalence and etiology. Part I," *Quintessence International*, vol. 36, no. 4, pp. 263–270, 2005.

[12] F. J. Kolenc-Fuse, "Tooth agenesis: in search of mutations behind failed dental development," *Medicina Oral Patologia Oral y Cirugia Bucal*, vol. 9, no. 5, pp. 385–390, 2004.

[13] S. Ruf, D. Klimas, M. Hönemann, and S. Jabir, "Genetic background of nonsyndromic oligodontia: a systematic review and meta-analysis," *Journal of Orofacial Orthopedics*, vol. 74, no. 4, pp. 295–308, 2013.

[14] J. Hourfar, C. Lux, and B. Ludwig, "Kieferorthopädische Therapieoptionen von Nichtanlagen permanenter Zähne," *Zahnmedizin up2date*, vol. 8, no. 2, pp. 167–188, 2014.

[15] Al-Ani and A. Husam, *Genetic and Environmental Factors Associated with Hypodontia*, University of Otago, 2016.

[16] A. H. Al-Ani, J. S. Antoun, W. M. Thomson, T. R. Merriman, and M. Farella, "Hypodontia: an update on its etiology, classification, and clinical management," *BioMed Research International*, vol. 2017, Article ID 9378325, 9 pages, 2017.

[17] M. G. Botelho, A. W. Chan, N. C. Leung, and W. Y. Lam, "Long-term evaluation of cantilevered versus fixed–fixed resin-bonded fixed partial dentures for missing maxillary incisors," *Journal of Dentistry*, vol. 45, pp. 59–66, 2016.

[18] B. Bergendal, "When should we extract deciduous teeth and place implants in young individuals with tooth agenesis?" *Journal of Oral Rehabilitation*, vol. 35, no. s1, pp. 55–63, 2008.

[19] Y. Akhlef, O. Schwartz, J. O. Andreasen, and S. S. Jensen, "Autotransplantation of teeth to the anterior maxilla: A systematic review of survival and success, aesthetic presentation and patient-reported outcome," *Dental Traumatology*, vol. 34, no. 1, pp. 20–27, 2018.

[20] S. Attia, J. Wiltfang, J. Pons-Kühnemann et al., "Survival of dental implants placed in vascularised fibula free flaps after jaw reconstruction," *Journal of Cranio-Maxillo-Facial Surgery*, vol. 46, no. 8, pp. 1205–1210, 2018.

[21] V. G. Kokich and V. O. Kokich, "Congenitally missing mandibular second premolars: clinical options," *American Journal of Orthodontics and Dentofacial Orthopedics*, vol. 130, no. 4, pp. 437–444, 2006.

[22] K. J. Finnema, G. M. Raghoebar, H. J. A. Meijer, and A. Vissink, "Oral rehabilitation with dental implants in oligodontia patients," *International Journal of Prosthodontics*, vol. 18, no. 3, pp. 203–209, 2005.

[23] M. Créton, M. Cune, W. Verhoeven, M. Muradin, D. Wismeijer, and G. Meijer, "Implant treatment in patients with severe hypodontia: a retrospective evaluation," *Journal of Oral and Maxillofacial Surgery*, vol. 68, no. 3, pp. 530–538, 2010.

[24] C. Mangano, L. Levrini, A. Mangano, F. Mangano, A. MacChi, and A. Caprioglio, "Esthetic evaluation of implants placed after orthodontic treatment in patients with congenitally missing lateral incisors," *Journal of Esthetic and Restorative Dentistry*, vol. 26, no. 1, pp. 61–71, 2014.

[25] P. F. Allen, S. Lee, and P. Brady, "Clinical and subjective evaluation of implants in patients with hypodontia: a two-year observation study," *Clinical Oral Implants Research*, vol. 28, no. 10, pp. 1258–1262, 2017.

[26] C. L. Hvaring, B. Øgaard, and K. Birkeland, "Tooth replacements in young adults with severe hypodontia: Orthodontic space closure, dental implants, and tooth-supported fixed dental prostheses. A follow-up study," *American Journal of Orthodontics and Dentofacial Orthopedics*, vol. 150, no. 4, pp. 620–626, 2016.

[27] B. Burns, V. Grieg, V. Bissell, and L. Savarrio, "A review of implant provision for hypodontia patients within a Scottish referral centre," *British Dental Journal*, vol. 223, no. 2, pp. 96–99, 2017.

[28] D. Buser, W. Martin, and U. C. Belser, "Optimizing esthetics for implant restorations in the anterior maxilla: anatomic and surgical considerations," *The International Journal of Oral & Maxillofacial Implants*, vol. 19, no. 7, pp. 43–61, 2004.

[29] T. Albrektsson, G. Zarb, P. Worthington, and A. R. Eriksson, "The long-term efficacy of currently used dental implants: a review and proposed criteria of success," *The International Journal of Oral & Maxillofacial Implants*, vol. 1, no. 1, pp. 11–25, 1986.

[30] D. Buser, H. P. Weber, and N. P. Lang, "Tissue integration of non-submerged implants. 1-year results of a prospective study with 100 ITI hollow-cylinder and hollow-screw implants," *Clinical Oral Implants Research*, vol. 1, no. 1, pp. 33–40, 1990.

[31] A. Mombelli and N. P. Lang, "Clinical parameters for the evaluation of dental implants," *Periodontology 2000*, vol. 4, no. 1, pp. 81–86, 1994.

[32] K. Al Shayeb, W. Turner, and D. Gillam, "In-vitro accuracy and reproducibility evaluation of probing depth measurements of selected periodontal probes," *The Saudi Dental Journal*, vol. 26, no. 1, pp. 19–24, 2014.

[33] S. Heuberer, G. Dvorak, K. Zauza, and G. Watzek, "The use of onplants and implants in children with severe oligodontia: a retrospective evaluation," *Clinical Oral Implants Research*, vol. 23, no. 7, pp. 827–831, 2012.

[34] R. Becelli, R. Morello, G. Renzi, and C. Dominici, "Treatment of oligodontia with endo-osseous fixtures: experience in eight consecutive patients at the end of dental growth," *The Journal of Craniofacial Surgery*, vol. 18, no. 6, pp. 1327–1330, 2007.

[35] D. Zou, Y. Wu, X. D. Wang, W. Huang, Z. Zhang, and Z. Zhang, "A retrospective 3- to 5-year study of the reconstruction of oral function using implant-supported prostheses in patients with hypohidrotic ectodermal dysplasia," *Journal of Oral Implantology*, vol. 40, no. 5, pp. 571–580, 2014.

[36] M. Hosseini, N. Worsaae, M. Schiødt, and K. Gotfredsen, "A 3-year prospective study of implant-supported, single-tooth restorations of all-ceramic and metal-ceramic materials in patients with tooth agenesis," *Clinical Oral Implants Research*, vol. 24, no. 10, pp. 1078–1087, 2013.

[37] H. Terheyden and F. Wüsthoff, "Occlusal rehabilitation in patients with congenitally missing teeth—dental implants, conventional prosthetics, tooth autotransplants, and preservation of deciduous teeth—a systematic review," *International Journal of Implant Dentistry*, vol. 1, no. 1, p. 30, 2015.

[38] I. P. Sweeney, J. W. Ferguson, A. A. Heggie, and J. O. Lucas, "Treatment outcomes for adolescent ectodermal dysplasia patients treated with dental implants," *International Journal of Paediatric Dentistry*, vol. 15, no. 4, pp. 241–248, 2005.

[39] F. Zarone, R. Sorrentino, F. Vaccaro, and S. Russo, "Prosthetic treatment of maxillary lateral incisor agenesis with osseointegrated implants: a 24-39-month prospective clinical study," *Clinical Oral Implants Research*, vol. 17, no. 1, pp. 94–101, 2006.

[40] F. Grecchi, L. Pagliani, G. E. Mancini, I. Zollino, and F. Carinci, "Implant treatment in grafted and native bone in patients affected by ectodermal dysplasia," *The Journal of Craniofacial Surgery*, vol. 21, no. 6, pp. 1776–1780, 2010.

[41] M. Jahn and B. d'Hoedt, "Zur definition des erfolges bei dentalen implantaten," *Zeitschrift für zahnärztliche Implantologie*, vol. 8, pp. 221–226, 1992.

[42] R. Buch, G. Weibrich, and W. Wagner, "Erfolgskriterien in der ImplantologieCriteria of success in implantology," *Mund-, Kiefer- und Gesichtschirurgie*, vol. 7, no. 1, pp. 42–46, 2003.

[43] O. Schierz, H. Christian, T. Mike John, and R. D. Reißmann, "Mundgesundheitsbezogene Lebensqualität–Maßstab Mensch in der Zahnmedizin," *Seniorenzahnmedizin*, vol. 3, pp. 17–22, 2015.

Hindawi
BioMed Research International
Volume 2019, Article ID 3210530, 9 pages
https://doi.org/10.1155/2019/3210530

Research Article

Cytokine Regulation from Human Peripheral Blood Leukocytes Cultured *In Vitro* with Silver Doped Bioactive Glasses Microparticles

Jefferson Muniz de Lima,[1] Edlainne Pinheiro Ferreira,[1] Roberta Ferreti Bonan,[1] David Nascimento Silva-Teixeira,[2] Luiz Ricardo Goulart,[3,4] Joelma Rodrigues de Souza,[1,5] Eliton Souto de Medeiros,[6] Paulo Rogério Ferreti Bonan,[1] and Lúcio Roberto Cançado Castellano[1]

[1] *Human Immunology Research and Education Group-GEPIH, Escola Técnica de Saúde da UFPB, Universidade Federal da Paraíba, João Pessoa, Brazil*
[2] *Institute of Health Sciences, Department of Clinical Medicine, Universidade Federal do Triângulo Mineiro Federal, Uberaba, Brazil*
[3] *Laboratory of Nanobiotechnology, Institute of Genetics and Biochemistry, Universidade Federal de Uberlandia, Uberlandia, Brazil*
[4] *Department of Medical Microbiology and Immunology, University of California Davis, Davis, CA, USA*
[5] *Department of Physiology and Pathology, Universidade Federal da Paraíba, João Pessoa, Brazil*
[6] *Materials and Biosystems Laboratory, Universidade Federal da Paraíba, João Pessoa, Brazil*

Correspondence should be addressed to Lúcio Roberto Cançado Castellano; luciocastellano@gmail.com

Received 18 March 2019; Revised 12 April 2019; Accepted 21 April 2019; Published 11 June 2019

Guest Editor: Francesca Salamanna

Bioactive glasses (BG) applications include tissue engineering for bone regeneration, coating for implants, and scaffolds for wound healing. BG can be conjugated to ions like silver, which might add some antimicrobial properties to this biomaterial. The immunomodulatory activity of ion-doped bioactive glasses particles was not investigated before. The aim of this work was to evaluate the cytotoxic and immunomodulatory effect of BG and silver-doped bioactive glass (BGAg) in human peripheral blood cells. BG and BGAg samples belonging to the system $58SiO_2 \bullet (36\text{-}x)CaO \cdot 6P_2O_5 \cdot xAg_2O$, where x = 0 and 1 mol%, respectively, were synthesized via sol–gel method and characterized. Cytotoxicity, modulation of cytokine production (TNF-α, IL-1β, IL-6, IL-4, and IL-10), and oxidative stress response were investigated in human polymorphonuclear cells (PMNs) and peripheral blood mononuclear cells (PBMCs) cultures. Cell viability in the presence of BG or BGAg was concentration-dependent. In addition, BGAg presented higher PBMCs toxicity (LC50 = 0.005%) when compared to BG (LC50 = 0.106%). Interestingly, interleukin4 was produced by PBMCs in response to BG and BGAg in absence of phytohemagglutinin (PHA) and did not modulate PHA-induced cytokine levels. Subtoxic concentrations (0.031% for BG and 0.0008% for BGAg) did not change other cytokines in PBMCs nor reactive oxygen species (ROS) production by PMN. However, BG and BGAg particles decreased zymosan-induced ROS levels in PMN. Although ion incorporation increased BG cytotoxicity, the bioactive glass particles demonstrated a *in vitro* anti-inflammatory potencial. Future studies are needed to clarify the scavenger potential of the BG/BGAg particles/scaffolds as well as elucidate the effect of the anti-inflammatory potential in modulating tissue growth *in vivo*.

1. Introduction

Bioactive glass (BG) consists of a SiO_2 network, having P_2O_5 as an adjuvant and CaO and Na2O as modifiers [1, 2]. The bioactivity of this material allows its application in the field of regeneration and tissue engineering [3]. It can be used in a wide range of applications, such as bioactive fillers in bone regeneration [4], coating for implants, dental grafting [5, 6], and scaffold for tissue repair, with porous arrangements similar to trabecular bone [3, 7]. BG is most used as hard tissue replacement material, although some studies show remarkable properties in soft tissues repair, as observed in

decreased blood coagulation time, angiogenesis, and reduced wound healing time [8].

Recently, BGs have been associated with inorganic materials such as ions for nonbone therapeutic applications [9]. Silver-doped glasses showed antibacterial and antifungal effect against *Escherichia coli, Staphylococcus aureus* [10–12], *Pseudomonas aeruginosa,* and *Candida albicans* [13] in comparison to neat BG. Such proprieties may minimize complications on bone surgery like bacterial infection by topical drug delivering in a controlled and continuous manner [14]. However, silver loading may increase hypersensitivity, chronic inflammation, and immune stimulation due to materials exposure [15].

The potential immunomodulatory activity of bioactive glasses has been tested before [7, 16]. Results indicated that differences in immune response modulation are dependent on material composition or on a particular system from which the bioactive glasses are selected. Some samples indicated an ability to inhibit the secretion of inflammatory cytokines in the presence of an inflammatory stimulus [16]. However, the immunomodulatory activity of bioactive glasses doped with silver ions has not been investigated before. Little is known about the effects of Ag^{2+} on healthy primary cells of the human immune system. The complete understanding of the specific interactions and response dynamics of the immune system to different materials is still inconclusive, especially for health applications or safety recommendations [17]. Therefore, the aim of this work was to evaluate the cytotoxic and immunomodulatory effect of BG and silver-doped bioactive silica over human leukocytes.

2. Materials and Methods

2.1. BG Synthesis. Samples belonging to the system $58SiO_2$•(36-x)CaO·$6P_2O_5$·x Ag_2O with x = 0 or 1 mol% (Neat BG and BGAg) were previously synthesized and fully characterized by physical-chemical analysis and gently provided by Pires et al. [18]. Briefly, hydrolysis and condensation of tetraethyl orthosilicate (TEOS), calcium nitrate tetrahydrate ($Ca(NO_3)_2$•$4H_2O$), triethyl phosphate (TEP; Sigma Aldrich), and silver nitrate ($AgNO_3$; PlatLab) were used to obtain the gels. The molar ratio of EtOH: TEOS was of 1:1. The other precursors were dissolved in distilled water. The pH of solutions was adjusted to 2 by addition of HNO_3. The obtained gels were dried for 3 days at room temperature and 2 days in a drying oven, at 120°C. The dried BG gels were heated up to 700°C for 1/2h, at a constant rate of 3°C min^{-1}. Herein, the glasses were passed through a 200-mesh British Standard Sieve (final particles diameter smaller than 74μm). The samples synthesis was performed under aseptic conditions and the surface disinfection was made by exposure to germicidal UV light for 30 minutes [19].

Information regarding BG and BGAg characterization and composition are available at https://doi.org/10.1111/ijag.12285. Briefly, the samples were characterized by scanning electron (SEM), atomic force (AFM) microscopy, X-ray diffraction (XRD), Fourier-transform Infrared (FTIR), and surface-enhanced Raman (Raman-SERS) spectroscopy. SEM and AFM images showed particles with irregular morphology and rough surface. XRD and FTIR analyses confirmed amorphous structure corresponding to BG formation, incipient crystallization, and the presence of Si-O-Si groups typical from glass structure even with silver inclusion within BG.

2.2. Samples. Materials and Methods section was structured following the minimal information about T cell assay [20] and this study was approved by local ethics committee. Initial blood samples were kindly provided by three male healthy volunteers following the inclusion criteria: seronegative for HIV and HCV, vaccinated against HBV and with no signs or symptoms of acute infections at the time of blood sampling and leukocytes isolation. To ensure the safety of blood donors and maintenance of cell integrity, the specimen collection followed the guidelines established by the Clinical and Laboratory Standards Institute [21]. The healthy volunteers signed a written consent to participate according to the Helsinki Declaration of ethical guidelines.

2.3. Peripheral Blood Mononuclear Cells (PBMC) and Polymorphonuclear Neutrophil (PMN) Isolation and Stimulation. For PBMC and PMN isolation, 18 ml of heparinized whole blood was collected by venipuncture and aliquots of 12 ml and 9 ml were processed by density gradient centrifugation. Two different ficoll densities were applied: Histopaque® 1077, for PBMC separation, and Histopaque® 1119 for PMN isolation (Sigma-Aldrich, St. Louis, USA) [22]. The buffy coats of PBMCs and PMNs were collected and washed three times with phosphate buffer and counted in Countess® FL Automated Cell Counter (Thermo Fisher Scientific, Waltham, USA) using Trypan blue (Sigma-Aldrich, St. Louis, USA) exclusion method. Cell suspensions (PBMC and PMNs) presented at least 95% cell viability and purity as determined by morphological examination of Giemsa-stained cytocentrifuged slides (Shandon, Pittsburgh, PA, USA). Cells were suspended in equal aliquots of $2x10^6$ PBMC/ml and 10^6 PMN/ml in RPMI 1640 medium (Gibco, Life Technologies, UK) supplemented with 10% heat-inactivated fetal bovine serum, 1% PenStrep, and 20mM HEPES. All procedures were conducted at room temperature.

2.4. PBMCs Viability Assay. 100 μl of PBMC's suspension was cultured in 96 black polystyrene wells flat bottom microplates (Greiner Bio- One, USA) and stimulated with 5 μg/ml of phytohemagglutinin (PHA-P; Sigma-Aldrich, St. Louis, USA) and incubated 1:1 with BG (range 1-0.0075% wt/vl) or BGAg (range 1-0.0002% wt/vl) in culture medium for 24 hours at 37°C in a humidified atmosphere at 5% CO_2.

Cell viability was measured using alamarBlue® according to kit protocol (Bio-Rad, Hercules, EUA). Fluorescence was measured at GloMax®-Multi Microplate Reader (Promega, Madison, USA) and percentage of viability was calculated as follows:

$$\text{Cytotoxicity (\%)} = \left[\left(\frac{\text{FI 590 of treated samples}}{\text{FI 590 of untreated cells}}\right)(100)\right] \quad (1)$$

where FI 590 = fluorescent intensity at 590 nm emission (560 nm excitation).

The lethal concentration 50 (LC50) was determined by semilog graph plotted as percent of untreated control for each BG and BGAg suspensions.

2.5. PMNs Viability Assay. Cell death was assayed by the LIVE/DEAD™ viability/cytotoxicity kit (Thermo Fisher, Rockford, IL, USA) according to kit instructions. Briefly, 10^5 PMNs were incubated with BG and BGAg samples for 4 hours at 37°C in a humidified atmosphere at 5% CO_2. Cells were incubated with 80% methanol for death control. Twenty minutes after staining with 1 μM calcein and ethidium homodimer, fluorescence visualization was performed using epifluorescence microscope EVOS FL cell imaging system (Life Technologies, Eugene, OR, USA) equipped with a 40x objective, GFP and RFP filter cubes. Quantification of live and dead cells was analyzed in 3 aleatory fields using ImageJ (National Institutes of Health, Bethesda, MD) software according to recommendations [23].

2.6. Luminol-Enhanced Chemiluminescence Assay. Production of intra- and extracellular ROS was analyzed by luminol-enhanced chemiluminescence. Briefly, the PMN suspension ($2x10^5$ cells/ml) was incubated for 45 min at 37°C and 5% CO_2 with the BG and BGAg samples in white polystyrene 96-wells flat bottom (Greiner Bio-One, USA). Serum-opsonized zymosan (final concentration of 1,62 mg/ml; Sigma-Aldrich, St. Louis, USA) or medium alone were the positive and negative control, respectively. After incubation, 10^{-4} M luminol (Sigma-Aldrich, St. Louis, USA) was added and chemiluminescence was measured at 2-minute intervals with a luminometer GloMax®-Multi Microplate Reader (Promega, Madison, USA) for a period of 1h at 37°C. Chemiluminescence was expressed as relative light units (RLU) and the area under the curve (AUC) was determined for each stimulus.

2.7. Quantification of Cytokine Release. PBMCs (10^6 cells/ml) were cultured for 24 hours at 48-well plates with the larger subtoxic concentration (0.031% for BG and 0.0008% for BGAg) at 37°C in 5% CO_2. In order to induce the maximum PBMC activation and release of largest mediators amounts, PHA was used as *in vitro* model of immune cells stimulation [24]. Then, the supernatants of PBMCs cultures (with or without 5 μg/ml PHA stimulation) were analyzed for IL-1β, TNF-α, IL-4, IL-6, and IL-10 concentrations by sandwich ELISA assay using OptEIA Kit (Becton Dickinson, Franklin Lakes, New Jersey, USA) according to kit protocol.

2.8. Statistical Analysis. Significant differences on cell viability, cytokine production, and ROS release between the groups were determined by Kruskal Wallis test with Dunn's post hoc (α=0.05) using the software GraphPad Prism 7 (GraphPad Software Inc., San Diego, USA).

3. Results and Discussion

3.1. Cell Viability in the Presence of BG and BGAg. With the objective of observing acute cytotoxicity, cell viability of PBMC was accessed after 24h incubation with BG and BGAg by determining the metabolic capacity of cells to reduce the indicator dye resazurin to fluorescent resorufin. A dose-dependent reduction in cell viability was observed in both samples of BG (Figure 1). The cell viability decreased to values less than 50% of control cells at the highest treatment concentration of 0.125 and 0.0075% for BG and BGAg, respectively. Calculated LC50 values were 0.106% for BG and 0.005% for BGAg.

Over the range of BG concentrations, BG 0.031% was the highest value that did not compromise PBMC viability in comparison to growth control (P>0.05). This result is above the subtoxic concentration of 0.01% observed in a previous work [16]. The range of BGAg concentrations 1–0,0016% had a drastic effect on PBMC viability. Notably, the BGAg nontoxic concentration was 0.0008% (P>0.05) when compared with the control cells.

Therefore, these remarkable differences in cytotoxicity of the BG and BGAg against PBMCs might be associated with free Ag^{2+} in culture medium. An earlier study demonstrated that Ag^{2+} cytotoxicity against PBMCs was dose- and time-dependent [15]. BG and BGAg subtoxic doses in PBMCs did not influence the PMN viability according to LIVE/DEAD. Fluorescence images of PMN cultures stained with ethidium homodimer (damaged cell marker) did not show quantitative differences between sample wells and growth control wells (Figure 2). For avoiding PMN death due the natural short-lived cell cycle, the cell viability was quantified after incubation of 4 hours.

The discrepant results in PBMC viability may be explained by silver addiction at BG synthesis and its release in culture medium. The ion in question can induce inflammation, cell activation and oxidative stress, ROS production, protein inactivation, inhibition of respiratory chain dehydrogenase, alteration of ionic channels, misbalance of cations/anions metabolism, organelle, and DNA damage [17, 25, 26]. The soluble Ag2+ can form complexes with biomolecules causing protein dysfunction and loss of enzyme activity (inactivation, loss of tertiary structure, replacement of cofactors, exchange of structural metals, breakage of disulfide bonds, among others), impaired membrane function caused by the loss of membrane potential, mechanical damage, and interference with nutrient uptake [25]. Taken together, these events lead to cell wall breakdown and cytolysis [26]. Further probes aiming to evaluate cellular growth inhibition and quantifies cell populations as healthy, dead, apoptotic, or necrotic when exposed to BG and BGAg under different conditions of time and concentrations are necessary to complete enlighten the cytotoxic mechanism of modified bioactive glasses.

Despite undesirable effects to human cells, silver-doped glasses produced under sol–gel method were bactericidal to *Staphylococcus aureus* and *E. coli* but not toxic to human osteoblasts, under controlled concentrations [14]. Other studies [27] demonstrated growth inhibition of *S. aureus*, *E. coli*, and *P. aeruginosa* cultures under Ag^{2+} released in medium by silver-doped bioactive glasses. The antibacterial mechanism of the silver-doped bioactive glass was investigated before

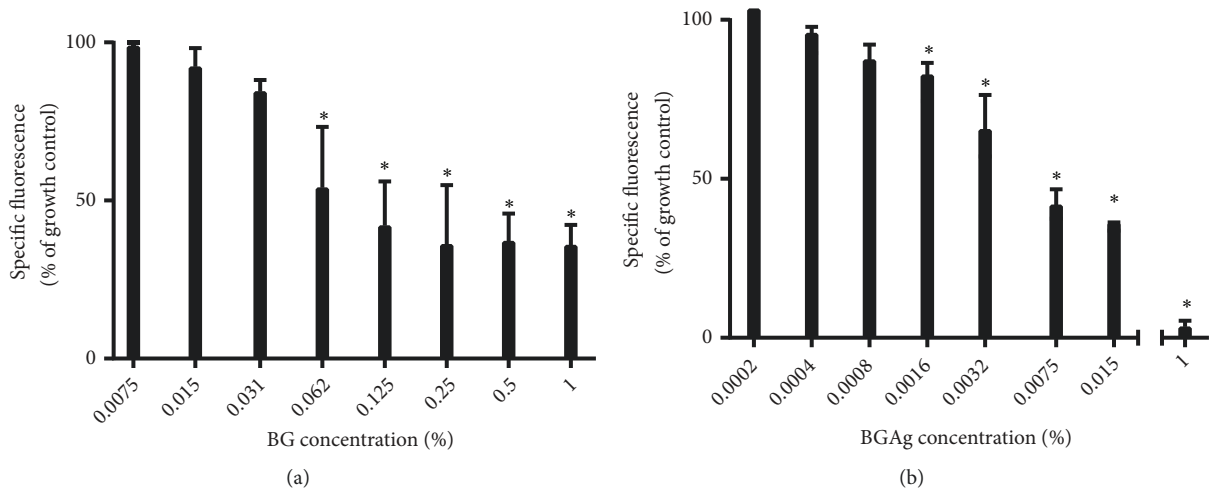

Figure 1: *BG (a) and BGAg (b) effects on PBMC viability*. Cell viability after treatment with increasing concentrations of BG and BGAg expressed as percentage of baseline viability. Results are shown as median with 95% confidence interval (CI) of an experiment performed in triplicate of each volunteer ($^{*}P < 0.05$ compared to growth control).

E. coli and *S. aureus* strains had DNA damage and protein denaturation compromising cellular growth [28].

Opportunistic Gram-positive staphylococci are appointed as cause of approximately 75% of osteomyelitis cases, while the most severe infections are caused by *Staphylococcus aureus* [29]. The repair of such infected bone defects is a concern in implantology and orthopedics areas. To avoid such complication and offer more predictable treatment outcomes, the association between antibacterial and osteoinductive properties is encouraged. Local delivery of alternative antimicrobials has advantages over to systemic antibiotics: broader bactericidal spectrum and nearly no resistance [30, 31]. Prevention methods as coating on implants and antimicrobial materials application are key to prevent osteomyelitis [29].

In addition, Pires et al. [18] observed that the present BGAg samples, instead of neat BG, exhibited therapeutic potential to treat infections caused by *Leishmania* parasites. The growth and proliferation inhibition of promastigote and metacyclic infective forms of the parasites occurred in the presence of 0,003% BGAg. In parallel to that study, the BGAg effective concentration allowed a PBMC viability of 65.5% after 24 hours of incubation. However, for other cell types, e.g., osteoblasts and fibroblasts, this relationship between therapeutic concentrations and cell viability lacks definition.

3.2. Oxidative Stress. Both samples of BG and BGAg alone were unable to induce intra- and extracellular ROS production above baseline parameters (Figure 3). Therefore, the higher dilution of neat BG decreased ROS detection when coincubated with opsonized zymosan. This compound activates an oxidative burst by binding itself to complement receptors, leading transduction signal to protein kinase C activation and consequent activation of NADPH-oxidase, the key enzyme of oxidative burst [32]. The oxidative stress reduction could be explained by the following: BG dissolved products like silica, calcium, phosphate, and sodium ions contribute to the balance of the oxidative status, or they may interfere with zymosan-receptor complex, or they might have the ability to act as free radicals and superoxides scavengers. The *in vivo* redox activity of bioglass compounds was previously reported [30]; thus the exact mechanism of action is still not clear. Such modulatory effect is of great relevance in osteogenesis by induction of osteoblasts metabolism and differentiation.

On the other hand, ROS production is a common finding on *in vitro* and *in vivo* models due to Ag presence in different biological systems. Overproduction of free radicals is appointed as a mechanism of cytotoxicity by oxidative stress, resulting in genotoxicity and cells breakdown [25]. BGAg samples unhanged ROS levels in culture medium; this finding may justify why the concentrations applied were not cytotoxic for PMN's cultures.

3.3. Cytokine Modulation. Quantification of TNF-α, IL-1β, IL-6, and IL-10 at 24h PBMC's culture supernatant performed by sandwich ELISA showed no significant differences between the treatments with three subtoxic BG and BGAg suspensions and baseline control (Figure 4). At some sample concentrations, TNF-α, IL-1β, and IL-10 release were lower than detection limits of the method. Interestingly, however, all BG and BGAg samples induced IL-4 production to similar levels than PHA stimulus (Figure 4). This result cannot be attributed to the action of biomaterials since the production of IL-4 by unstimulated cells was not significantly different. The presence of bioactive glasses did not change TNF-α, IL-1β, IL-6, and IL-10 secretion profile compared to basal levels or PHA stimulated cells. These results suggest that bioactive glasses particles even when doped with silver ions do not change the levels of releasing proinflammatory and anti-inflammatory cytokines by human PBMC.

Immunomodulatory effects of bioactive glasses were investigated by previous studies. Particles belonging to system 60S did not change significantly IL-4 secretion profile

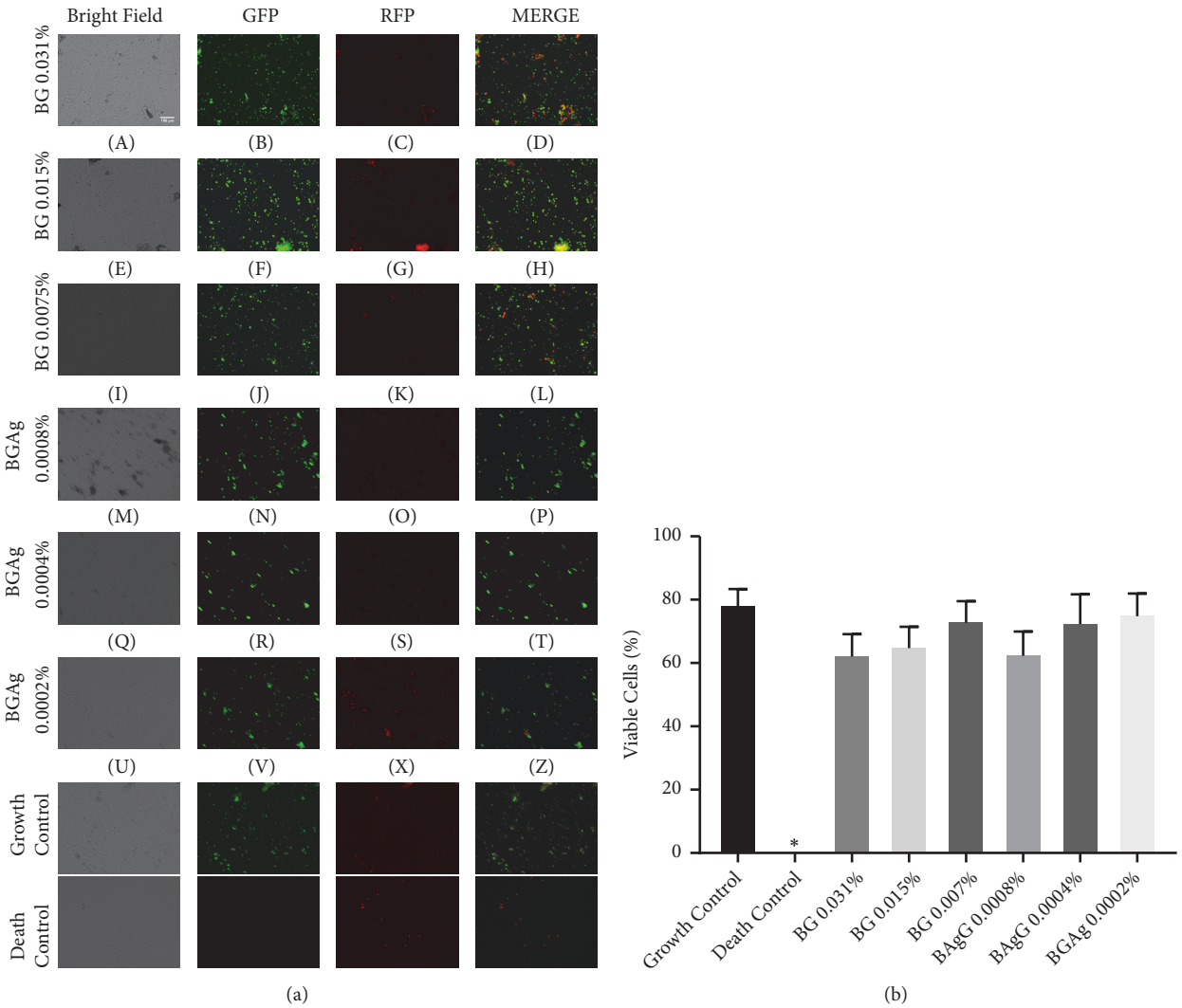

Figure 2: *PMN viability in presence of BG (A-L) and BGAg (M-Z)*. Demonstrative images of Live/Dead™ assay captured by 40x objective (a). The bright field shows cell morphology, GFP shows live cells green stained by calcein, and RFP shows dead cells stained by ethidium homodimer. For growth and death controls, cells were incubated, respectively, with, medium alone or 80% methanol. (b) Percentage of viable PMNs were counted on three aleatory fields. PMNs incubated with different concentrations of BG and BGAg have a similar number of viable cells compared to growth control. Results were expressed as median with 95% CI ($^{*}P < 0.05$ compared to growth control).

by PBMCs [33]. In agreement with our current results, other studies found that 45S5 glass did not interfere with IL-6, IL-10, and TNF-α secretion by nonstimulated macrophages and monocytes cultures [7]. This same study observed a decrease in TNF-α production when the cells were incubated with LPS. On the other hand, another study showed that 45S5 powders upregulated TNF-α secretion by peritoneal macrophages [34]. Beyond cell population variances, differences on cytokine modulation may be explained by different factors that induce immune response by biomaterials, such as BG composition, particle size, surface chemistry, plasma protein binding, and exposure model [35].

The literature has a great extended relates about therapeutic perspectives for bioactive glasses, including implant coatings, alloplastic grafts for sinus lift (micro particles formulation) or replacement after tumor removal (scaffolds), and dental composites [3]. Beyond the hard tissues engineering, bioactive glasses can also be applied in the soft tissue manipulation. Several studies report on the application of BGs for wound healing by mechanisms of stimulation of angiogenesis, establishment of bg-collagenous bonding, and accelerated rate of blood coagulation [36]. The described biological properties are relevant in the context of management of chronic wounds including, for example, diabetic foot ulcers, venous leg ulcers, and pressure ulcers [37].

In some therapies against cancer, arthritis, and allergies, an immunomodulatory capacity of the therapeutic agent is highly desirable. However, an unbalanced immunosuppression or immunostimulation might be associated with many of the undesirable side effects observed in most cases. Thus, the study of interactions between biomaterials and the immune system is key for safe medicinal use of recently developed

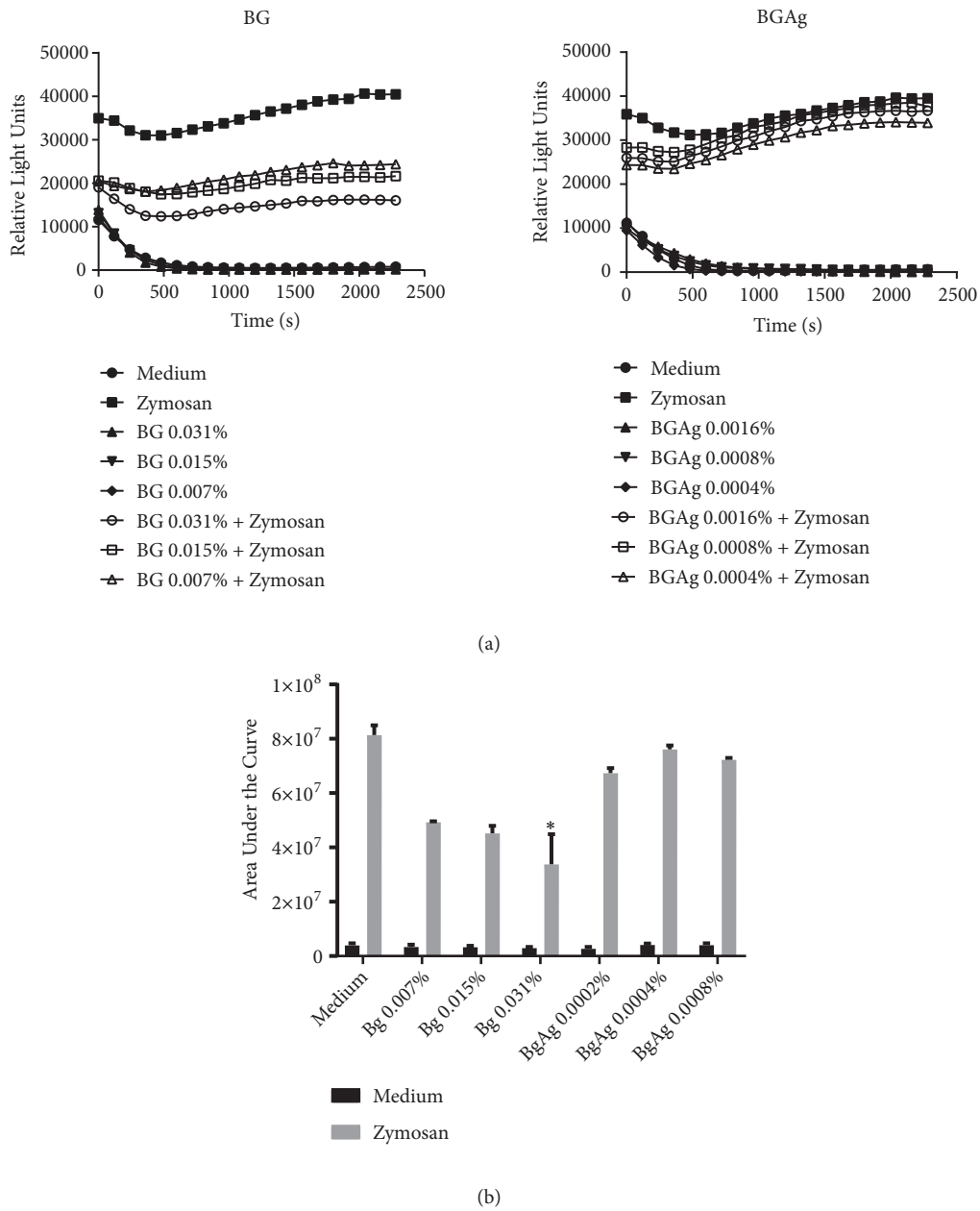

Figure 3: *ROS production in PMNs*. (a) Chemiluminescent curves showing similar relative light units (RLU) detection between BG and BGAg samples when compared to with negative control (medium only). BG samples decreased ROS production when coincubated with zymosan (positive control). Each point represents the median of triplicate readings of ex vivo PMN cultures (n=3). (b) Area under the curve (AUC) values plotted for each stimulus. The sample BG 0.031% reduced significantly ROS production in comparison with only zymosan as stimulus. Values were expressed as median with CI ($^{*}P < 0.05$ compared to positive control).

biomaterials. A recent work questioned the actual capacity to examine the real function of biomaterials within both innate and adaptive immune responses, mainly concerning the B and T cell responses [38]. Although models for determining acute and long-term immune toxicities have been developed, studies on the treatment and prediction of immunomodulatory activity are scarce [35, 38]. One study showed that some biomaterials modified the adaptive immunity (cell phenotype and cytokine release) and promoted tissue repair [39]. Our results follow these studies which contribute to expanding the knowledge about materials science and biomedical engineering applications in humans [40].

4. Conclusions

The presence of silver increased the glass cytotoxicity against human PBMCs. The 58S BG and BGAg subtoxic concentrations did not interfere with patterns associated with release of main regulatory, pro- and anti-inflammatory cytokines by cultured PMBCs. Both BG and BGAg were unable to induce

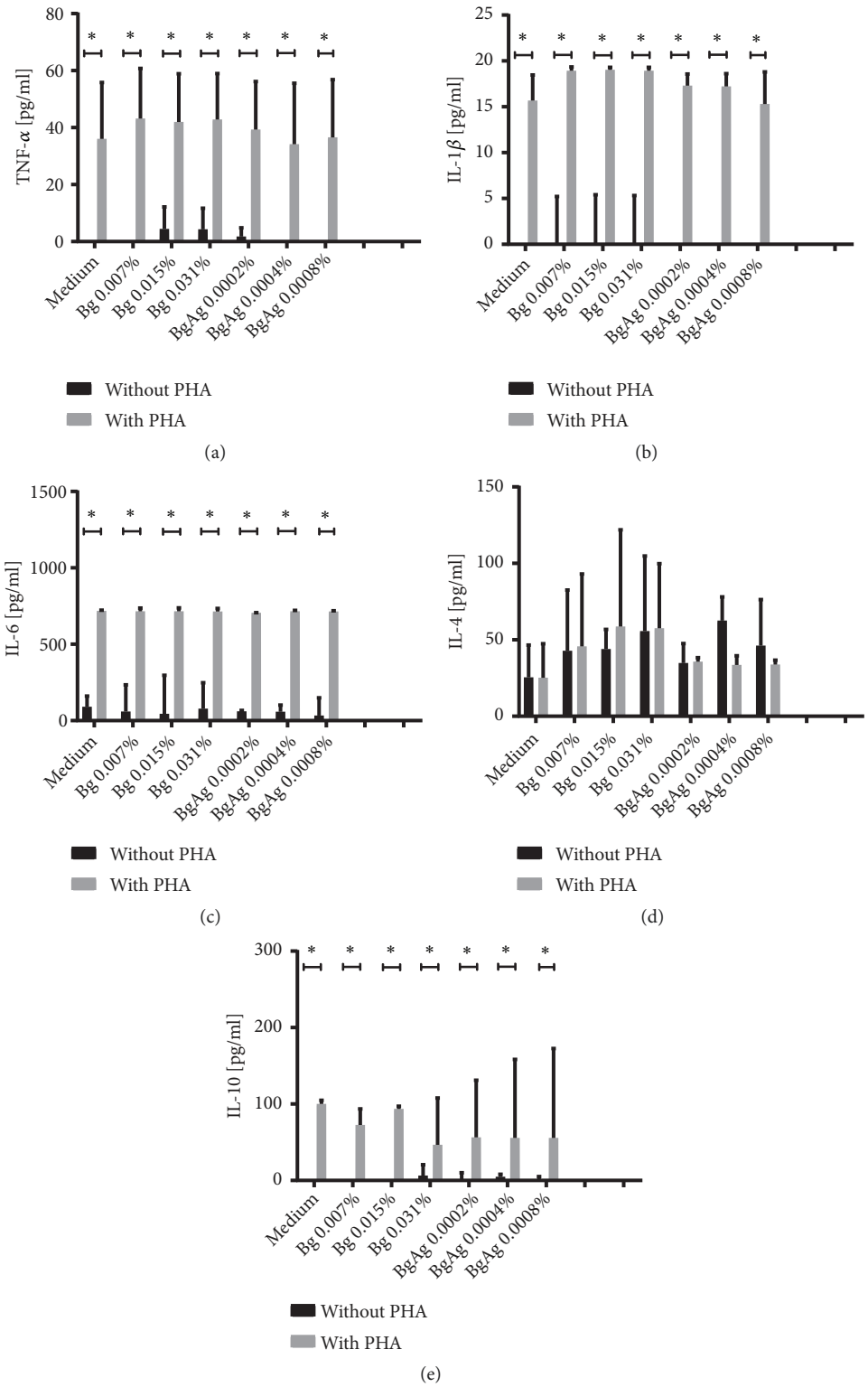

Figure 4: *Cytokine release by PBMC cultures incubated with BG or BGAg*. Titration of TNF-α (a), IL-1β (b), IL-6 (c), IL-4 (d), and IL-10 (e) released at 24-hour culture supernatant of PBMC's cultured with or without 5 μg/ml PHA stimulation. There were no significant differences on cytokine's production between BG and BGAg stimulus and medium alone treatment. Bioactive glasses were unable to reduce cytokine levels after PHA coincubation. *Correspond to the statistical difference ($p<0,05$). Data were presented as the median ± 95% CI of triplicates of each volunteer (n=3).

ROS production, while neat BG decreased ROS production when coincubated with serum-opsonized zymosan, suggesting its potential scavenger activity. Further studies of silver dissolution in culture medium, *in vivo* Ag^+ biodistribution and the development of mechanisms for ion release control according to desirable dose are necessary and important next steps to increase our current knowledge about therapeutic applications of BG and BGAg.

Data Availability

Previously reported BG and BGAg synthesis and characterization data were used to support this study and are available at https://doi.org/10.1111/ijag.12285. This prior study is cited at relevant places within the text as [18].

Ethical Approval

This study was approved by the Research Ethics Committee of the Universidade Federal da Paraíba under Protocol no. 61192816.6.0000.5188.

Consent

All study participants signed an informed consent in accordance to the Resolution 466/2012 from the Brazilian National Council of Health.

Disclosure

The main findings of the study have been presented in poster format at the Academy of Dental Materials Annual Meeting 2018 and the abstract is available at https://doi.org/10.1016/j.dental.2018.08.050.

Conflicts of Interest

The authors declare that the research was conducted in the absence of any commercial or financial relationships that could be construed as potential conflicts of interest.

Acknowledgments

This study was financially supported by the Universidade Federal da Paraíba, Coordenação de Aperfeiçoamento de Pessoal de Nível Superior (CAPES, Brazil, fellowship to JL), and Conselho Nacional de Desenvolvimento Científico eTecnológico (CNPq, Brazil)/INCT-TeraNano (Grant no. 465669/2014-0). In addition, we are grateful to Rebeca Tibau, MSc, for technical support during the study.

References

[1] V. J. Shirtliff and L. L. Hench, "Bioactive materials for tissue engineering, regeneration and repair," *Journal of Materials Science*, vol. 38, no. 23, pp. 4697–4707, 2003.

[2] L. L. Hench, R. J. Splinter, W. C. Allen, and T. K. Greenlee, "Bonding mechanisms at the interface of ceramic prosthetic materials," *Journal of Biomedical Materials Research Part B: Applied Biomaterials*, vol. 5, no. 6, pp. 117–141, 1971.

[3] J. R. Jones, L. M. Ehrenfried, and L. L. Hench, "Optimising bioactive glass scaffolds for bone tissue engineering," *Biomaterials*, vol. 27, no. 7, pp. 964–973, 2006.

[4] G. Chouzouri and M. Xanthos, "In vitro bioactivity and degradation of polycaprolactone composites containing silicate fillers," *Acta Biomaterialia*, vol. 3, no. 5, pp. 745–756, 2007.

[5] A. Al-Noaman, S. C. F. Rawlinson, and R. G. Hill, "Bioactive glass-stoichimetric wollastonite glass alloys to reduce TEC of bioactive glass coatings for dental implants," *Materials Letters*, vol. 94, pp. 69–71, 2013.

[6] A. Al-Noaman, N. Karpukhina, S. C. F. Rawlinson, and R. G. Hill, "Effect of FA addition on bioactivity of bioactive glass coating for titanium dental implant: Part II— Composite coating," *Journal of Non-Crystalline Solids*, vol. 364, pp. 99–106, 2013.

[7] R. M. Day, A. R. Boccaccini, S. Shurey et al., "Assessment of polyglycolic acid mesh and bioactive glass for soft-tissue engineering scaffolds," *Biomaterials*, vol. 25, no. 27, pp. 5857–5866, 2004.

[8] C. Lin, C. Mao, J. Zhang, Y. Li, and X. Chen, "Healing effect of bioactive glass ointment on full-thickness skin wounds," *Biomedical Materials*, vol. 7, no. 4, Article ID 045017, 2012.

[9] L. L. Hench and J. R. Jones, "Bioactive glasses: frontiers and challenges," *Frontiers in Bioengineering and Biotechnology*, vol. 3, 2015.

[10] A. Balamurugan, G. Balossier, D. Laurent-Maquin et al., "An *in vitro* biological and anti-bacterial study on a sol–gel derived silver-incorporated bioglass system," *Dental Materials*, vol. 24, no. 10, pp. 1343–1351, 2008.

[11] H. Zhu, C. Hu, F. Zhang et al., "Preparation and antibacterial property of silver-containing mesoporous 58S bioactive glass," *Materials Science and Engineering C: Materials for Biological Applications*, vol. 42, pp. 22–30, 2014.

[12] A. A. El-Rashidy, G. Waly, A. Gad et al., "Antibacterial activity and biocompatibility of zein scaffolds containing silver-doped bioactive glass," *Biomedical Materials*, vol. 13, no. 6, Article ID 065006, 2018.

[13] F. Baghbani, F. Moztarzadeh, M. Mozafari, M. Raz, and H. Rezvani, "Production and characterization of a Ag- and Zn-doped glass-ceramic material and in vitro evaluation of its biological effects," *Journal of Materials Engineering and Performance*, vol. 25, no. 8, pp. 3398–3408, 2016.

[14] A. M. El-Kady, A. F. Ali, R. A. Rizk, and M. M. Ahmed, "Synthesis, characterization and microbiological response of silver doped bioactive glass nanoparticles," *Ceramics International*, vol. 38, no. 1, pp. 177–188, 2012.

[15] M. M. Abudabbus, I. Jevremović, A. Janković et al., "Biological activity of electrochemically synthesized silver doped polyvinyl alcohol/graphene composite hydrogel discs for biomedical applications," *Composites Part B: Engineering*, vol. 104, pp. 26–34, 2016.

[16] R. M. Day and A. R. Boccaccini, "Effect of particulate bioactive glasses on human macrophages and monocytes in vitro," *Journal of Biomedical Materials Research Part A*, vol. 73, no. 1, pp. 73–79, 2005.

[17] I. M. M. Paino and V. Zucolotto, "Poly(vinyl alcohol)-coated silver nanoparticles: Activation of neutrophils and nanotoxicology effects in human hepatocarcinoma and mononuclear cells," *Environmental Toxicology and Pharmacology*, vol. 39, no. 2, pp. 614–621, 2015.

[18] E. G. Pires, R. F. Bonan, Í. M. Rocha et al., "Silver-doped 58S bioactive glass as an anti-Leishmania agent," *International Journal of Applied Glass Science*, 2017.

[19] G. Katara, N. Hemvani, S. Chitnis, V. Chitnis, and D. Chitnis, "Surface disinfection by exposure to germicidal UV light," *Indian Journal of Medical Microbiology*, vol. 26, no. 3, pp. 241-242, 2008.

[20] S. Janetzki, C. M. Britten, M. Kalos et al., "'MIATA'-minimal information about T cell assays," *Immunity*, vol. 31, no. 4, pp. 527-528, 2009.

[21] C. F. Arkin, J. D. Bessman, R. R. Calam, D. J. Ernst, G. T. Parish, and D. I. Szamosi, "Procedures for the collection of diagnostic blood specimens by venipuncture; approved standard," *Clinical and Laboratory Standards Institute*, vol. 23, no. 32, p. 52, 2003.

[22] L. R. Castellano, D. C. Filho, L. Argiro et al., "Th1/Th2 immune responses are associated with active cutaneous leishmaniasis and clinical cure is associated with strong interferon-γ production," *Human Immunology*, vol. 70, no. 6, pp. 383–390, 2009.

[23] P. Spaepen, S. De Boodt, J.-M. Aerts, and J. V. Sloten, "Digital image processing of live/dead staining," *Mammalian Cell Viability: Methods and Protocols*, vol. 740, pp. 209–230, 2011.

[24] D. Rendina, C. Ryff, and C. Coe, "Concordance of serum cytokines and stimulated mononuclear cell responses in older adults," *Brain, Behavior, and Immunity*, vol. 49, p. e39, 2015.

[25] J. A. Lemire, J. J. Harrison, and R. J. Turner, "Antimicrobial activity of metals: mechanisms, molecular targets and applications," *Nature Reviews Microbiology*, vol. 11, no. 6, pp. 371–384, 2013.

[26] Y.-H Hsueh, K.-S Lin, W.-J Ke et al., "The antimicrobial properties of silver nanoparticles in bacillus subtilis are mediated by released Ag+ ions," *PLoS ONE*, vol. 10, no. 12, p. e0144306, 2015.

[27] M. Bellantone, H. D. Williams, and L. L. Hench, "Broad-spectrum bactericidal activity of Ag2O-doped bioactive glass," *Antimicrobial Agents and Chemotherapy*, vol. 46, no. 6, pp. 1940–1945, 2002.

[28] Q. L. Feng, J. Wu, G. Q. Chen, F. Z. Cui, T. N. Kim, and J. O. Kim, "A mechanistic study of the antibacterial effect of silver ions on *Escherichia coli* and *Staphylococcus aureus*," *Journal of Biomedical Materials Research Part B: Applied Biomaterials*, vol. 52, no. 4, pp. 662–668, 2000.

[29] G. Walter, M. Kemmerer, C. Kappler, and R. Hoffmann, "Treatment algorithms for chronic osteomyelitis," *Deutsches Ärzteblatt International*, vol. 109, no. 14, pp. 257–264, 2012.

[30] J. A. Inzana, E. M. Schwarz, S. L. Kates, and H. A. Awad, "Biomaterials approaches to treating implant-associated osteomyelitis," *Biomaterials*, vol. 81, pp. 58–71, 2016.

[31] H. Lu, Y. Liu, J. Guo, H. Wu, J. Wang, and G. Wu, "Biomaterials with antibacterial and osteoinductive properties to repair infected bone defects," *International Journal of Molecular Sciences*, vol. 17, no. 3, p. 334, 2016.

[32] S. Sergeant and L. C. McPhail, "Opsonized zymosan stimulates the redistribution of protein kinase C isoforms in human neutrophils," *The Journal of Immunology*, vol. 159, no. 6, pp. 2877–2885, 1997.

[33] C. Silva, A. Bozzi, M. Pereira, A. Goes, and M. F. Leite, "Effects of bioactive glass 60S and biphasic calcium phosphate on human peripheral blood mononuclear cells," in *Key Engineering Materials*, vol. 254-256, pp. 841–844, Trans Tech Publisher, 2004.

[34] M. Bosetti, L. Hench, and M. Cannas, "Interaction of bioactive glasses with peritoneal macrophages and monocytes in vitro," *Journal of Biomedical Materials Research Part B: Applied Biomaterials*, vol. 60, no. 1, pp. 79–85, 2002.

[35] Q. Jiao, L. Li, Q. Mu, and Q. Zhang, "Immunomodulation of nanoparticles in nanomedicine applications," *BioMed Research International*, vol. 2014, Article ID 426028, 19 pages, 2014.

[36] V. Miguez-Pacheco, L. L. Hench, and A. R. Boccaccini, "Bioactive glasses beyond bone and teeth: Emerging applications in contact with soft tissues," *Acta Biomaterialia*, vol. 13, pp. 1–15, 2015.

[37] R. G. Frykberg and J. Banks, "Challenges in the treatment of chronic wounds," *Advances in Wound Care*, vol. 4, no. 9, pp. 560–582, 2015.

[38] A. Vishwakarma, N. S. Bhise, M. B. Evangelista et al., "Engineering immunomodulatory biomaterials to tune the inflammatory response," *Trends in Biotechnology*, vol. 34, no. 6, pp. 470–482, 2016.

[39] K. Sadtler, K. Estrellas, B. W. Allen et al., "Developing a pro-regenerative biomaterial scaffold microenvironment requires T helper 2 cells," *Science*, vol. 352, no. 6283, pp. 366–370, 2016.

[40] S. F. Badylak, "A scafold immune microenvironment," *Science*, vol. 352, no. 6283, p. 298, 2016.

Hindawi
BioMed Research International
Volume 2019, Article ID 3610785, 11 pages
https://doi.org/10.1155/2019/3610785

Research Article

Evaluation and Prediction of Mass Transport Properties for Porous Implant with Different Unit Cells: A Numerical Study

Jian Li,[1,2,3] **Diansheng Chen**,[1,3] **and Yubo Fan**[2,3,4]

[1] *Robotic Institute, Beihang University, Beijing 100191, China*
[2] *Beijing Key Laboratory of Rehabilitation Technical Aids for Old-Age Disability and Key Laboratory of Rehabilitation Aids Technology and System of The Ministry of Civil Affairs, National Research Center for Rehabilitation Technical Aids, Beijing 100176, China*
[3] *Beijing Advanced Innovation Center for Biomedical Engineering, Beihang University, Beijing 100191, China*
[4] *Key Laboratory for Biomechanics and Mechanobiology of Ministry of Education, School of Biological Science and Medical Engineering, Beihang University, Beijing 100191, China*

Correspondence should be addressed to Diansheng Chen; chends@163.com and Yubo Fan; yubofan@buaa.edu.cn

Received 25 February 2019; Accepted 11 April 2019; Published 23 April 2019

Guest Editor: Francesca Salamanna

Efficient exchange of nutrients and wastes required for cell proliferation and differentiation plays a pivotal role in improving the service life of porous implants. In this study, mass transport properties for porous implant with different unit cells were evaluated and predicted when the porosities are kept the same. To this end, three typical unit cells (diamond (DO), rhombic dodecahedron (RD), and octet truss (OT)) were selected, in which DO displayed diagonal-symmetrical shape, while RD and OT share midline-symmetrical structure. Then, single unit cells were designed quantitatively, and its shape parameters were measured and calculated. Moreover, corresponding porous scaffolds with same outline size were created, respectively. Furthermore, using computational fluid dynamics (CFD) methodology, flow performances with Dulbecco's Modified Eagle's Medium (DMEM) in vitro were simulated for three different porous implants, and flow trajectory, velocity, and wall shear stress which could reflect the properties of mass transfer and tissue regeneration were compared and predicted numerically. Results demonstrated that different unit cell could directly lead to different mass transport properties for porous implant, in spite of same porosity, scaffold size, and service environment. Additionally, by the results, DO displayed greater tortuosity, more appropriate areas, and smoother shear stress distribution than RD and OT, which would provide better surroundings for implant fixation and tissue regeneration. However, RD and OT showed better mass transport properties because of bigger maximum velocity (5.177 mm/s, 4.381 mm/s) than DO (3.941 mm/s). This study would provide great helps for unit cell selection and biological performance optimization for 3D printed bone implants.

1. Introduction

It is well known that an ideal bone implant should match the mechanical properties of the host bone, but, importantly, efficient exchange of nutrients and wastes required for cell proliferation and differentiation also plays a pivotal role in improving the service life of bone implants [1]. To this end, many conventional fabrication techniques, such as gas foaming, solvent casting, particle leaching, fiber meshes, and freeze drying [2], were used to create porous structure to lower the strength and promote cell proliferation and differentiation. Herein, porosity, as an important parameter for porous structure [3], attracted a lot of attentions in the recent years. For porous implant, porosity not only plays a critical role in the mechanical properties [4–6] but also affects biological performances, such as cell attachment, proliferation, and differentiation [7], and transport of nutrients and metabolic waste [8]. In contrast to the solid metal implant, conventional fabrication techniques could provide porous implant with different porosity and low strength. It is, however, that the pore distribution usually has random features for porous implant manufactured by conventional fabrication techniques, and its connectivity may not keep the same and control accurately. Additive manufacturing (AM), also, namely, 3D printing or rapid prototyping, is a process of join materials layer by layer, which provides

required ability to deliver a high level of control over the complex architecture of the construct [9]. With the advent of additive manufacturing (AM), many applications benefit from it. Particularly, 3D printed porous implant is one of the medical applications, which has been widely acknowledged as an important and hopeful future development for bone tissue engineering because of personalized customization and controllability [10]. In this regard, many studies had been involved and performed recently [11], and also some patient-specific implants were designed and printed [12, 13], although the abovementioned studies confirmed 3D porous implants have lighter weight, lower stiffness, and a controlled structure [10], which could be optimized and tailored to avoid stress shielding and promote mass transfer, cell adhesion, and differentiation effectively [14]. However, different pore shapes and porosity usually have completely different mass transport properties. As mentioned before, this would lead to different regeneration efficiency and service efficiency for the tissue and implant. To some extent, some improper porous structure creation may be detrimental to cell proliferation and tissue regeneration, thereby affecting implant fixation and long-term service. Meanwhile, ideally, porous implant design is a key step to 'fit' the implant with appropriate mechanical properties and biological performance in a typical design [15]. However, currently in literature, most of the different kinds of pores are selected just by engineers' experience, lacking quantitative assessment and prediction. In particular far less attention has been paid to mass transport properties. In addition, although literatures had studied different kinds of pores [16]; to date, a significant amount of work has not focused on different symmetric types with same porosity together for the porous structure's mass transport performances in the application of bone implant.

Accordingly, for the evaluation of biological performances of bone implant, methodology in vivo and in vitro could be divided into four kinds: (1) cell culture in vitro; (2) animal experiment in vivo; (3) clinical trial in vivo; (4) numerical analysis in vitro. In general, cell culture, animal experiment, and clinical trial often need long period and lots of money as well as many times' repetition. In the meantime, the results of above methods could be affected by many factors. Relatively, numerical analysis with computational fluid dynamics (CFD) provides potential assistance for bone implant because of quick speed, low cost, and good anti-interference performance. In the aspect of blood vessels, CFD is a reliable and fast method for the flow fluid evaluation, and the validity was confirmed by many researchers [17, 18]. Furthermore, recently, lots of previous studies had evaluated the biological properties of porous implant with CFD method [19–22] and found many useful and amazing results.

Therefore, based on the above state and our previous study [23], this study focused on the regular unit cell and chose one diagonal-symmetrical regular unit cell and two midline-symmetrical regular unit cells, which are commonly used in actual design. From the biological viewpoints, singe unit cells were design quantitatively, and corresponding scaffolds were created with same porosity and scaffold size. Using CFD method, flow trajectory, flow velocity, and flow shear stress of different porous scaffolds in Dulbecco's modified Eagle's medium (DMEM) were predicted for mass transport properties numerically.

2. Methods

2.1. Pore Preparation and Scaffold Design. As shown in Figure 1(a), three unit cells (Diamond (DO) [24], rhombic dodecahedron (RD) [25], and Octet truss (OT) [26]) were selected in this study, which are commonly used in porous implant design, and RD and OT share same midline-symmetrical structure both on the coronal plane and the sagittal plane, while DO displays diagonal-symmetrical shape. Furthermore, porosity as an important parameter for porous implant and its biological properties was kept same (70%) when the three shapes of unit cells (5×5×5mm, Figure 1(a)) were designed in the commercial 3D-design software of SolidWorks (Dassault Systems, Velizy-Villacoublay, France). Accordingly, taking into account quantitative assessment, factors affecting the biological performance were paid more attentions, and unit cell's volume, max-pore size, surface area, and surface-to volume ratio were recorded, computed and compared in Figure 1(b). Specifically, volume and surface area were analyzed automatically in the SolidWorks software, and max-pore size could be measured manually. Further on, porosity and surface-to volume ratio were calculated as [23, 27]

$$p = \frac{V_0 - V}{V_0} \times 100\% \tag{1}$$

$$s = \frac{V}{S^*} \tag{2}$$

where V_0 and V are the volumes of the solid initial structure and porous structure, respectively, and S^* is the surface area of porous structure.

With regard to porosity, because DO, RD, and OT were recorded as same volume and unit cells size (5×5×5mm), the same porosity was tested by (1). It is, however, that max-pore size, surface area, and surface-to volume ratio are quite different from each other in spite of sharing same volume and porosity, which could be indicated different biological performance and mechanical properties in the future.

In the case of same porosity (70%) and equal unit cells size (5×5×5mm), single unit cells were repeated along X, Y, and Z axis periodically. Then, three kinds of porous scaffolds with the size of 10 mm in diameter and 25 mm in height were constructed by Boolean operations (Figure 1(c)), respectively.

2.2. Mass Transport Properties Prediction. Learn from literatures [19–22] that in order to predict the mass transport properties of different porous implants with midline-symmetrical and diagonal-symmetrical unit cells, CFD methodologies were used in this study. Moreover, in the SolidWorks software, corresponding CFD plugin was used to simulate the porous scaffolds in vitro, and flow trajectory, velocity, and wall shear stress which could reflect the properties of mass transport and tissue regeneration were studied. As illustrated in Figure 2, porous models (Figure 2(a), Φ10×25mm) were limited in an enclosed tube (Figure 2(a)), respectively, and

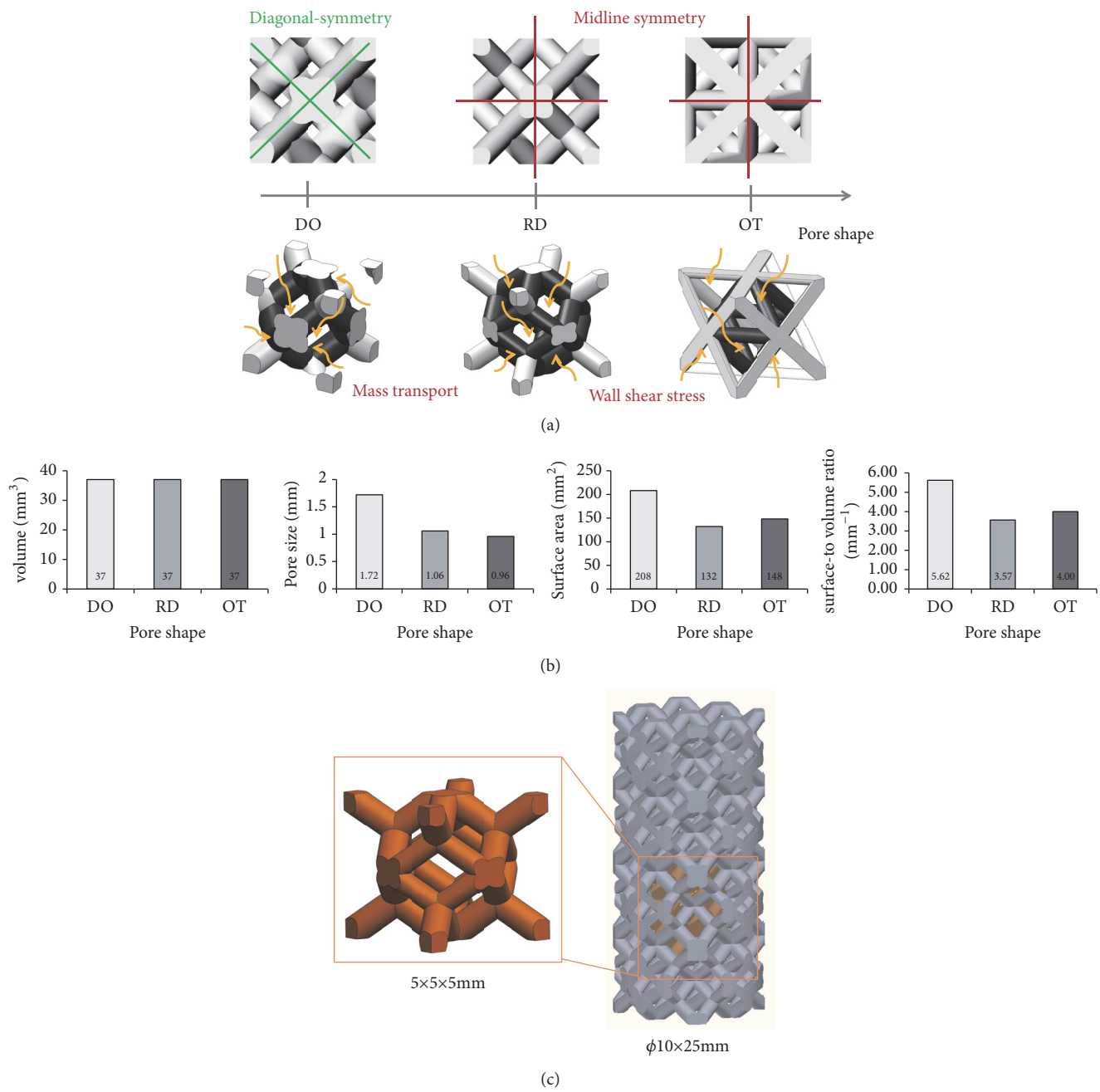

Figure 1: Different unit cells and related porous scaffold: (a) DO, RD, and OT shape; (b) physical parameters of three shapes; (c) schematic diagram of porous structure building. Importantly, the midline-symmetry and diagonal-symmetry described herein are relative to the cube outline.

one side of the tube was assumed as the inlet, whilst the opposite side was assumed as the outlet. In this study, DMEM commonly used in cell culture was represented as fluid material (incompressible and continuous Newtonian fluid) to simulate a steady state in vitro, whose viscosity and density are 1.45Pa·s and 1000 kg/m^3 [28]. Namely, the enclosed tube was filled with DMEM, and then porous scaffolds were immersed in one by one. Meanwhile, for the three shapes, the same boundary conditions were defined as: an inlet velocity (v_i = 1 mm/s) at the inlet-flow side and an output environmental pressure (one Atm pressure) at the opposite-flow side [23]. It is worth noting that the aim of the chosen boundary conditions was to imitate cell culture of porous implant in vitro. Besides, diagonal section, middle section (Figure 2(c)), and middle line views (Figure 2(d)) of the porous scaffolds were stressed and used to display inner flow velocity and shear stress [23]. Furthermore, the governing equation underlying the calculation was the Navier-Stokes

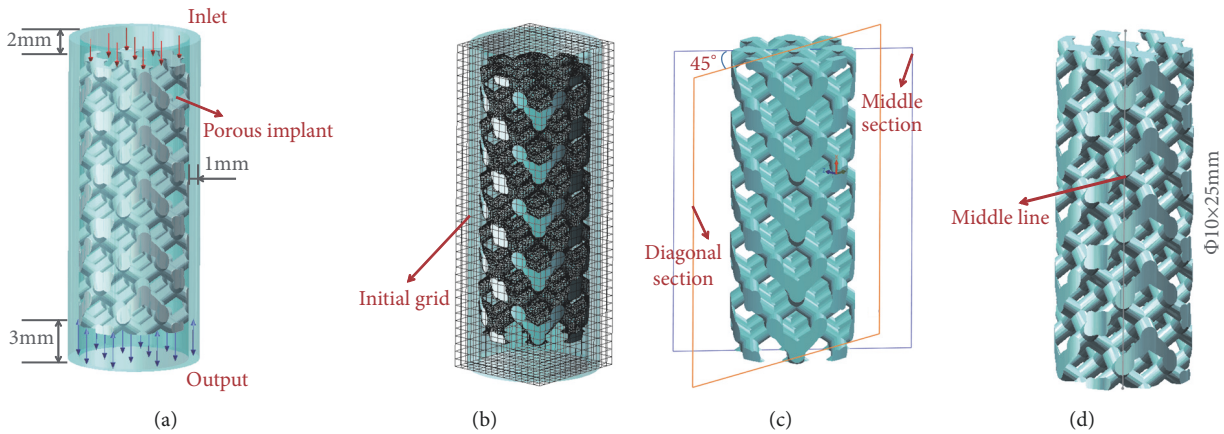

Figure 2: Schematic diagram of CFD model: (a) computational domain; (b) Initial grids and meshing; (c) diagonal section and middle section views; (d) middle line view of the porous scaffold.

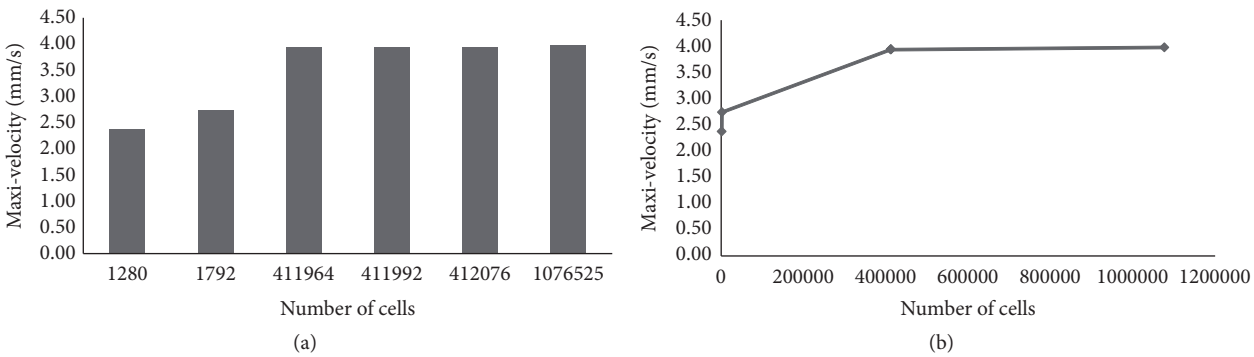

Figure 3: Convergence analysis of CFD model: (a) maximum velocity of the same model with different mesh sizes; (b) change trend of the values of maximum velocity for same model.

formulation in this study, which could be expressed as (3). Conventionally, Navier-Stokes usually describes the motion of viscous fluid substances and reflects the basic mechanical law of viscous fluid flow, which has great significance in fluid mechanics.

$$\frac{\partial v}{\partial t} + (v \bullet \nabla) v = -\frac{1}{\rho}\nabla p + \frac{\mu}{\rho}\nabla^2 v \tag{3}$$

where v is the flow velocity, which varies with the time; ρ and μ denote the density and dynamical viscosity of DMEM, respectively, which usually have constant value; p is the pressure. Accordingly, tetrahedron was used for the models' meshing (Figure 2(b)) in the flow simulation, and adaptive optimization is performed in the software. Moreover, in order to provide accurate computation and reliable results, convergence studies with different initial grids (Figure 2(b)) and mesh sizes (Figure 3(a)) were also conducted to evaluate mesh size as well as calculating time. Meanwhile, change trend of the values of maximum velocity for same model was performed (Figure 3(b)). As Table 1 shown, more than 380000 tetrahedral elements and 260 iterations were included in the three classes of simulations, respectively, in order to bring credible solutions.

3. Results

3.1. Flow Trajectory and Velocity. As illustrated in Figure 4, flow trajectory and velocity distributions of the three porous scaffolds (DO, RD, and OT) with the same porosity are elaborated in the global view, in which maximum velocity values observed in were 3.941 mm/s, 5.177 mm/s, and 4.381 mm/s, respectively. Besides, in order to compare the results intuitively, the same numbers of trajectory lines were depicted and amplified by the uniform multiple. In the meantime, one cloud chart was shared for the three shapes [23]. Obviously, curvatures of the trajectories were quite different from each other, and the descending order of flow velocity is RD, OT, and DO. In addition, for an easy understanding of the inner flow velocities, flow velocity distributions on the diagonal section and middle section could be found in Figure 5, and corresponding data analysis of maximum velocity values in global view, diagonal section, and middle section were was directly in Figure 6. Furthermore, in Figure 7, flow velocities along the middle line were illustrated and compared for the three shapes. As expected, above details also showed quite difference for DO, RD, and OT shapes, such as the biggest peak values along the middle line and their change trends.

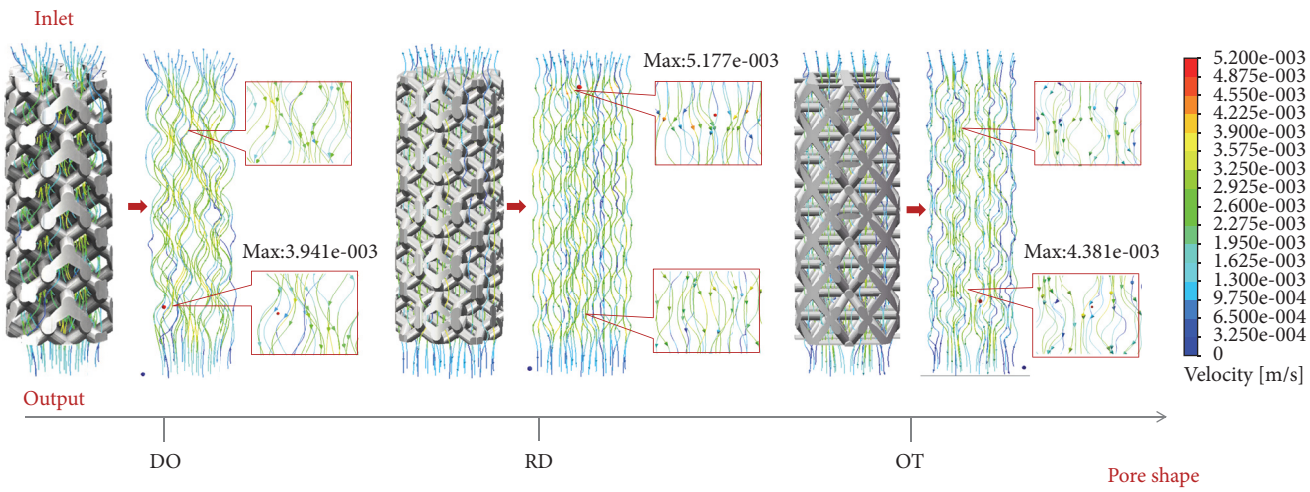

Figure 4: Flow trajectory and velocity distributions of the three porous scaffolds.

Table 1: Details of CFD simulations.

Unit cell	Scaffolds	Cells	Fluid cells	Solid cells	Partial cells	Iteration	Time∗ (Min)	Cell volume (mm^3)
DO		411978	251099	56395	104484	264	37	0.46
RD	φ10×25	388431	202221	64009	122201	411	68	0.50
OT		405924	211140	68686	126098	391	46	0.50

∗*Computer configuration*
CPU: Intel(R) Xeon(R) CPU E5-2620 v3 @ 2.40GHz; memory (RAM):32.0GB; OS:64 bits.

3.2. Wall Shear Stress. Figure 8 showed the shear stress distributions on the wall surface of the three porous structures. Taking into account previous findings [28–30] the cloud chart were limited to from 0.05 to 25 mPa. The black color marked (>25 mPa or <0.05 mPa) in the figures mean that wall shear stress were not suitable for cell viability and proliferation, and the red color marked usually suggested bigger value than others. Undoubtedly, DO had the least black colors in the three shapes, while RD had the most black colors. However, RD (peak value: 0.558 Pa) and OT (peak value: 0.526 Pa) were seemed to have bigger wall shear stress than DO (peak value: 0.133 Pa). Further on, subtle shear stress distributions and change trends of the wall shear stresses along the middle line were displayed in Figure 9, and significantly difference were depicted vividly.

4. Discussions

It is well known that tortuosity (τ) is a property of curve and commonly used to describe diffusion in porous media. The mathematical formula of tortuosity is

$$\tau = \frac{L}{L_0} \tag{4}$$

where L and L_0 are the actual length and straight length of fluid channel, respectively. When L_0 keeps same, τ would increase with the increasing of L. As illustrated in Figure 4, it was evident that flow trajectory (L) of DO was more tortuous than OT and RD visually. In this sense, DO should display the biggest tortuosity (τ) in the three shapes. According to Xiao [31] and Fan's [32] views, the greater tortuosity is conducive to improving the degree of tissue adhesion and implant fixation when the pore size is enough large, and the channels for fresh tissue and nutrient transport are smoother. Considering that the aperture of DO was the largest (Figure 1(b)) in the three shapes, it could be predicted that DO may have more implant fixation advantages than OT and RD due to the biggest tortuosity.

In addition, flow velocity is another indicator to evaluate the properties of mass transfer [33–35]. Considering descending order of the maximum flow velocities was RD (5.177 mm/s), OT (4.381 mm/s), and DO (3.941 mm/s) in the global view (Figure 4). It was worth noting that RD and OT have better mass transfer performance than DO shapes. Fortunately, inner flow velocities on the diagonal section and middle section (Figure 5) showed completely same global maximum values and same sequence (RD>OT>OT) as Figure 4 portrayed. As a result, abovementioned conclusion should be proved and trusted directly. Along this line of consideration, for DO shape, it could be found that peak velocity on the diagonal section (3.867 mm/s) was closer to the global maximum values (3.941 mm/s) than middle section (3.425 mm/s); namely, diagonal unit cell was likely to bring bigger velocity near to the diagonal section (Figure 6). However, for RD and OT shapes, it was well documented that the discrepancies of global maximum values and peak values on diagonal and middle section were bigger than DO shape (Figure 6). Perhaps, there was no clear rule for RD and OT, but it was worth noting that the maximum values should not appear on the diagonal section and middle section. Further

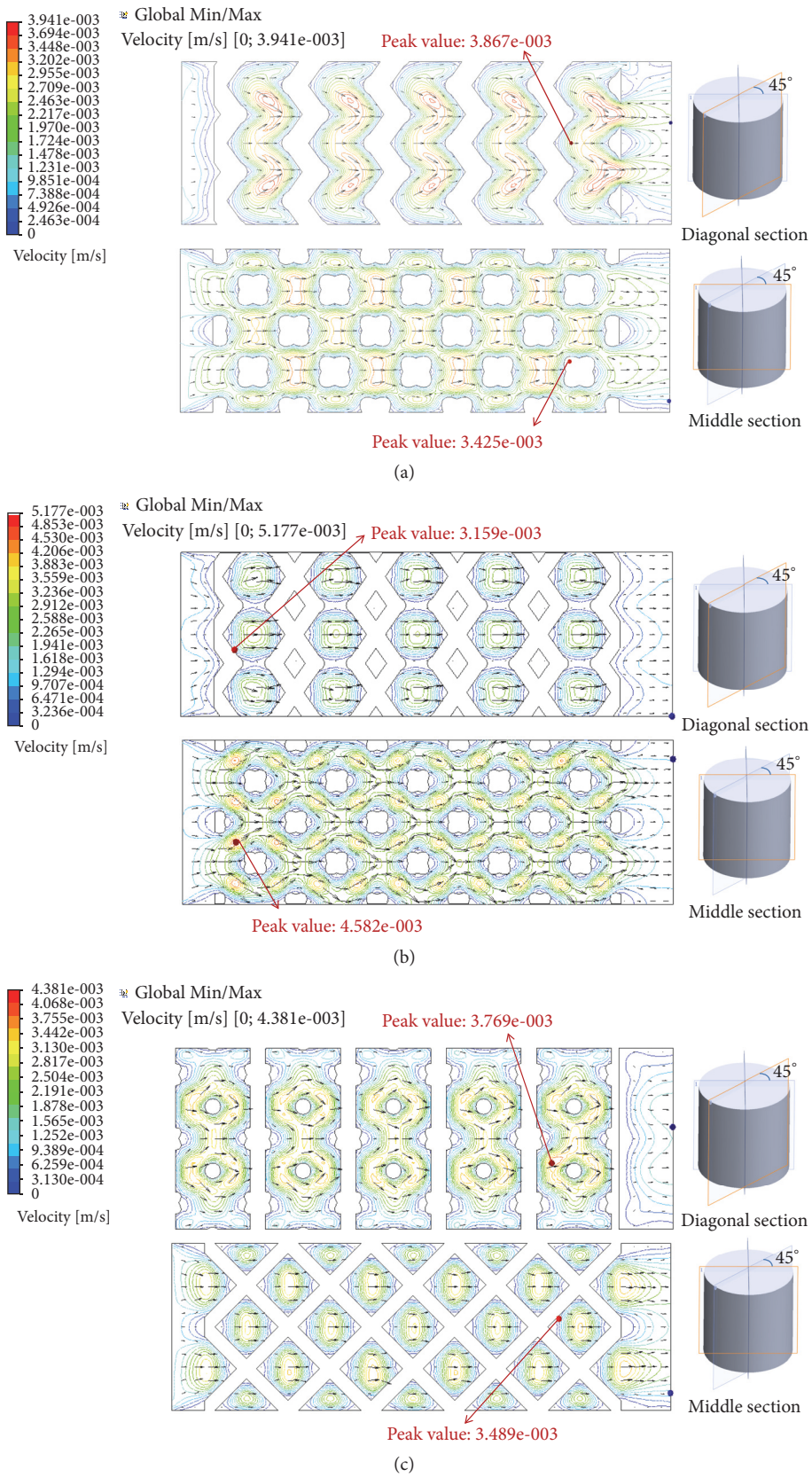

Figure 5: Flow velocity distributions on the diagonal section and middle section: (a) DO; (b) RD; (c) OT.

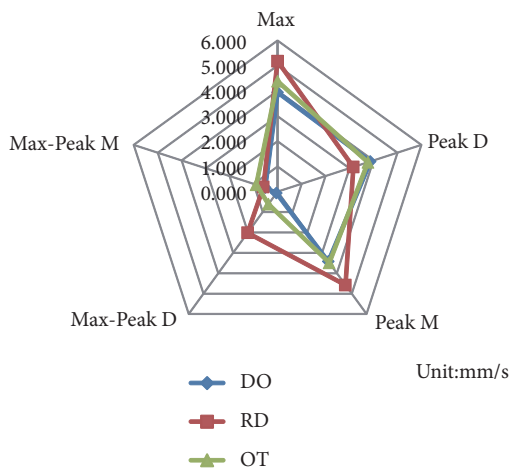

Figure 6: Data analysis of maximum flow velocity in the global view, diagonal section, and middle section.

on, as illustrated in Figure 7, different locations of the biggest peak values for flow velocity along the middle line were found. For the DO shape, the biggest peak value was found on the third crest, which was located in the intermediate of the inlet and outlet (Figure 2). However, for RD and OT shapes, their biggest peak values were on the first crest, which were near to the inlet (Figure 2). In the meantime, it is of interest that different change trends of the flow velocities were also found along the middle line in spite of similar waveforms (Figure 7). From the first crest to the fifth crest, RD and OT displayed decreasing peak values gradually, but for DO, the peak value increased firstly and then decreased (Figure 7). It should be noted that pore shape and symmetrical type may be the only causes for these results. Eventually, from the point of flow trajectory and velocity, it could be inferred that DO shape exhibits more advantages on implant fixation than OT and RD, but OT and RD presented better mass transfer performance than DO shape.

Additionally, in this study, by the results of wall shear stress (Figure 8), the least black colors were found on DO shape, and RD and OT displayed more black colors. According to the views of Cartmell [29] and Raimondi [30], it could be concluded that DO has more appropriate adhesion areas than OT and RD, which would provide a better surroundings for cell adhesion and tissue regeneration [36, 37]. Meanwhile, as illustrated in Figure 1(b), DO also had bigger surface area and surface-to volume ratio than DO and OT. Then, above conclusion would be more persuasive and confirmed. Moreover, maximum values of wall shear stress on RD and OT shapes were observed bigger than DO due to more red colors appearing (Figure 8). It could be guessed that DO porous implant may have homogeneous and gentle growth environment for cell proliferation relatively, but for RD and OT, uneven shear stress stimulation would lead to differentiation and asynchrony in different regions of the wall surface. In this regard, the type and growth characteristics of the cell should play a critical role in unit cell selection and tissue regeneration [37].

Further on, change trends of wall shear stresses along the middle line (Figure 9) also had confirmed above difference and relationships in Figure 8. It seemed that DO displayed similar and gentle value along the middle line, and some change trend should be found (Figure 9). However, OT and RD showed unstable values and messy trends. Taking into consideration previous studies [19], unit cell also influenced cell proliferation and activity by affecting the efficiency of shear stimuli to cells under perfused culture, and stress with some frequency had been shown to be favorable for bone regeneration in vitro [38]. Herein, from the point of wall shear stress, it could be concluded that DO shape has some advantages than RD and OT shapes because of more appropriate adhesion areas and regular mechanical stimulation.

As already stated above, although the same porosities (70%), scaffold size ($\phi 10\times 25$), and simulation environment (DMEM) were shared for DO, RD, and OT, different flow trajectory, velocity, and wall shear stress were found because of unit cell morphology and symmetrical type. Towards this end, the differences between diagonal-symmetrical unit cell and midline-symmetrical unit cell were tentatively confirmed. These findings could provide proofs for the difference between diagonal-symmetrical and midline-symmetrical unit cells and related porous implants. In the meantime, the importance of pore morphology and symmetrical type was also demonstrated [7, 8]. Comprehensively considering the results of flow trajectory, velocity, and wall shear stress, it could be deduced that diagonal-symmetrical shape may have some advantages on implant fixation (bigger tortuosity), cell adhesion (more appropriate adhesion areas), and tissue regeneration (regular mechanical stimulation) compared to midline-symmetrical shape, but midline-symmetrical shape is likely to have super mass transfer performance (bigger flow velocity) compared to diagonal-symmetrical shape. Overall, the results and validity in this study are credible. On the one hand, above findings and inference are not contradict each other, and all the results could be explained and complemented. Meanwhile, as studied before, some findings of this study are consistent with previous literatures [39–41], such as the importance of pore morphology, pore size, surface area, and the advantages of DO shape. On the other hand, in contrast to the conventional cell culture [6] and animal experiment [42], CFD is also an reliable and fast and of low cost method for the flow fluid evaluation for porous implant [37] and regarded as one of the most potential candidates for future patient-specific implants' inspection [43], whose validity was also confirmed by Gómez [20], Olivares [21], Ardiyansyah Syahrom [22], H. Montazerian [19], Chen [28], and so on. Finally, in fluidic optimization, a level-set algorithm for the steady-state Navier–Stokes flow was established, where the solid–fluid interface was determined for maximizing permeability and minimizing energy dissipation in the periodic porous materials [44, 45]. Therefore, the findings in this study are reliable, which could be used to predict biological performance of porous structure with different unit cells.

Eventually, there are also some limitations and future works in this study. Firstly, only three shapes of unit cells

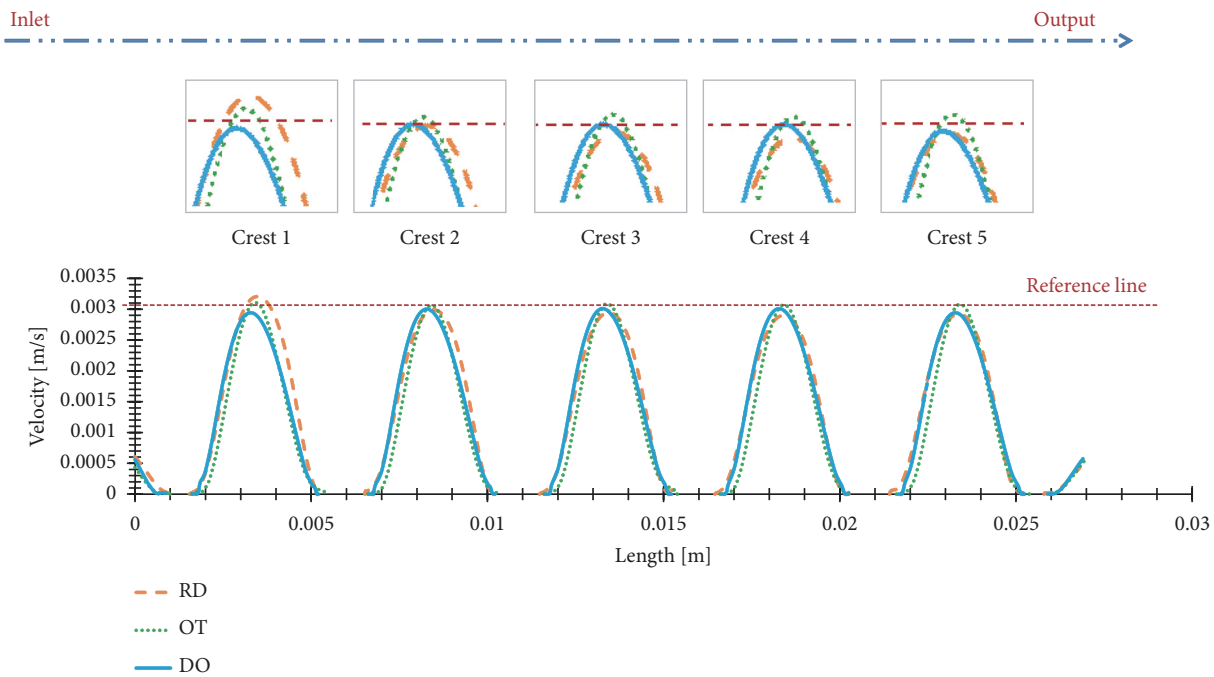

Figure 7: Flow velocity distributions of the three porous scaffolds along the middle line.

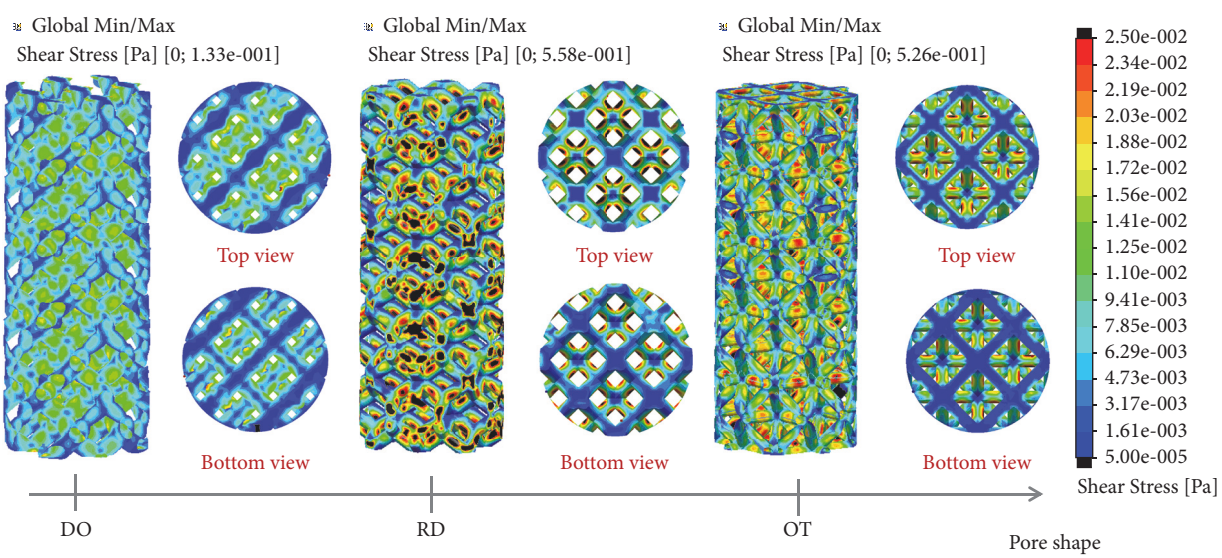

Figure 8: Flow shear stress distributions of the three porous scaffolds.

with 70% porosity were studied and simulated, which is not enough to meet various needs in practice. In order to create a useful unit cell library, mass transport properties of more unit cells and porosities should be studied in the future. Secondly, cell and animal experiments with the three unit cells were not involved in this study. Future work in vitro and in vivo should be conducted systematically.

5. Conclusions

In this study, flow performance of porous structure with diagonal-symmetrical and midline-symmetrical unit cells was evaluated and predicted when the porosities are same. By the results, it can be inferred that porous structures with midline-symmetrical unit cell may have superior mass transport properties than diagonal-symmetrical structure because of bigger flow velocity. However, it seemed that diagonal-symmetrical shape has bigger tortuosity, more appropriate adhesion areas, and more homogeneous and regular shear stimuli than midline-symmetrical shape, which could provide a better environment for implant fixation, cell adhesion, and tissue growth. Additionally, the importance and difference of pore morphology and symmetrical type were also demonstrated. In summary, each unit cell has its

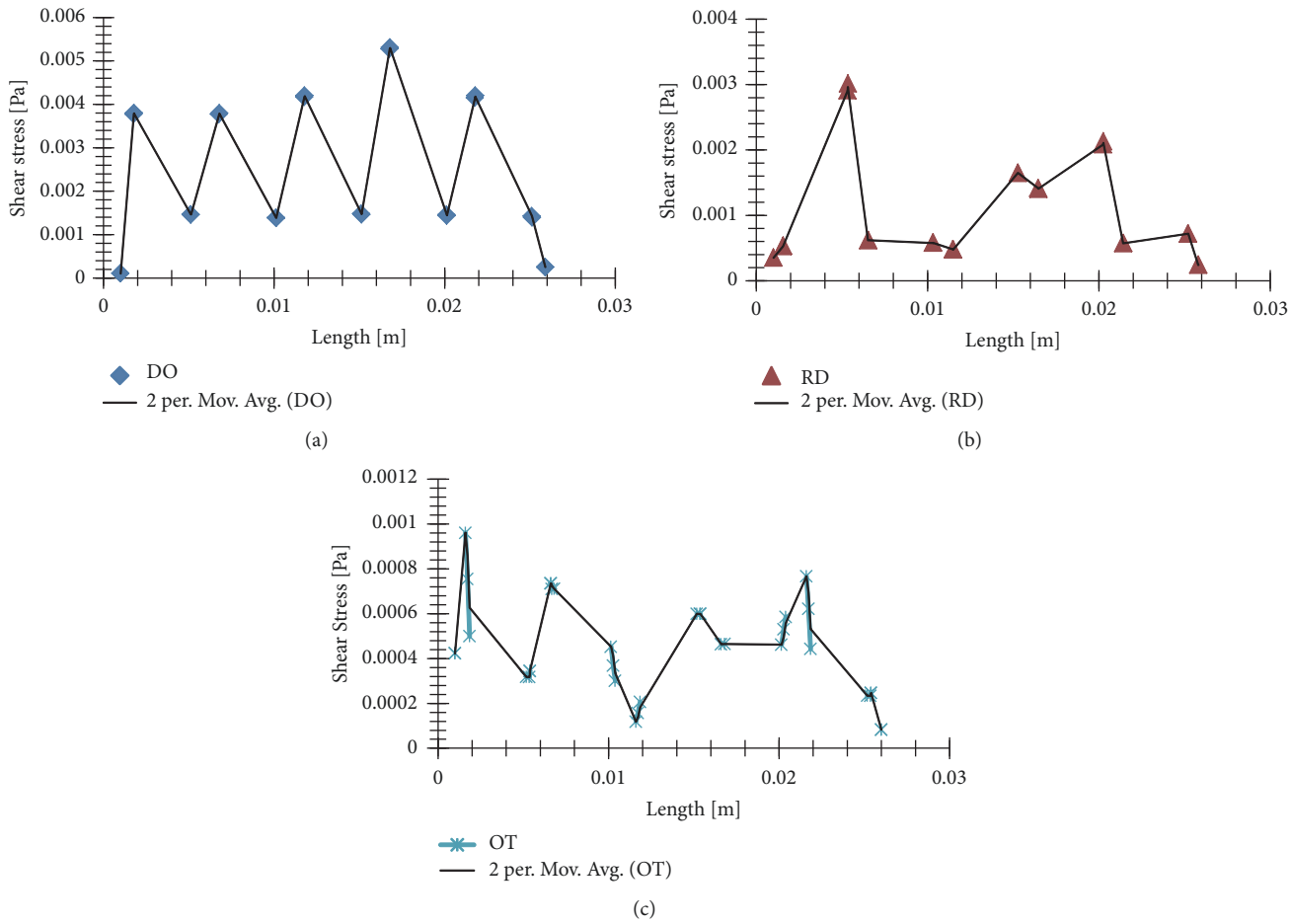

Figure 9: Flow shear stress distributions and change trends along the middle line: (a) DO; (b) RD; (c) OT.

own share of merits and demerit;, this study can be utilized to tailor and evaluate the design quantitatively, each with its mass transport properties and tissue regeneration properties.

Data Availability

The figure and table data used to support the findings of this study are included within the article.

Conflicts of Interest

None of the authors has any conflicts of interest.

Acknowledgments

Special thanks are due to China National Key Research and Development Plan Project (Nos. 2016YFB1101101 and 2016YFB1101102), Beijing Outstanding Young Backbone Personnel Training Project (No. 2017000026825G280), Sichuan Science and Technology Program (No. 18ZDYF1362), Fundamental Research Funds for Central Public Welfare Research Institutes (118009001000160001), and National Natural Science Foundation of China (Nos. 11421202 and 11572029).

References

[1] D. Hutmacher, "Scaffolds in tissue engineering bone and cartilage," *Biomaterials*, vol. 21, no. 24, pp. 2529–2543, 2000.

[2] S. S. Preethi, M. A. Haritha, C. S. Viji et al., "Bone tissue engineering: scaffold preparation using chitosan and other biomaterials with different design and fabrication techniques," *International Journal of Biological Macromolecules*, vol. 119, pp. 1228–1239, 2018.

[3] V. Karageorgiou and D. Kaplan, "Porosity of 3D biomaterial scaffolds and osteogenesis," *Biomaterials*, vol. 26, no. 27, pp. 5474–5491, 2005.

[4] F. Senatov, N. Anisimova, M. Kiselevskiy et al., "Polyhydroxybutyrate/hydroxyapatite highly porous scaffold for small bone defects replacement in the nonload-bearing parts," *Journal of Bionic Engineering*, vol. 14, no. 4, pp. 648–658, 2017.

[5] F. N. Habib, M. Nikzad, S. H. Masood, and A. B. M. Saifullah, "Design and development of scaffolds for tissue engineering using three-dimensional printing for bio-based applications," *3D Printing and Additive Manufacturing*, vol. 3, no. 2, pp. 119–127, 2016.

[6] Q. Liu, W. Li, L. Cao et al., "Response of MG63 osteoblast cells to surface modification of Ti-6Al-4V implant alloy by laser interference lithography," *Journal of Bionic Engineering*, vol. 14, no. 3, pp. 448–458, 2017.

[7] Q.-M. Jin, H. Takita, T. Kohgo et al., "Effects of geometry of hydroxyapatite as a cell substratum in BMP-induced ectopic bone formation," *Journal of Biomedical Materials Research*, vol. 52, no. 4, pp. 841–851, 2000.

[8] A. Kumar, K. Biswas, and B. Basu, "Hydroxyapatite-titanium bulk composites for bone tissue engineering applications," *Journal of Biomedical Materials Research Part A*, vol. 103, no. 2, pp. 791–806, 2015.

[9] K. Wong and P. Scheinemann, "Additive manufactured metallic implants for orthopaedic applications," *Science China Materials*, vol. 61, no. 4, pp. 440–454, 2018.

[10] L. E. Murr, S. M. Gaytan, E. Martinez, F. Medina, and R. B. Wicker, "Next generation orthopaedic implants by additive manufacturing using electron beam melting," *International Journal of Biomaterials*, vol. 2012, Article ID 245727, 14 pages, 2012.

[11] A. Hooyar, E. H. Shima, K. Damon et al., "Recent developments and opportunities in additive manufacturing of titanium-based matrix composites: a review," *International Journal of Machine Tools and Manufacture*, vol. 2018, no. 133, pp. 85–102, 2018 (Arabic).

[12] J.-K. Kim, S.-B. Lee, and S.-Y. Yang, "Cranioplasty using autologous bone versus porous polyethylene versus custom-made titanium mesh: a retrospective review of 108 patients," *Journal of Korean Neurosurgical Society*, vol. 61, no. 6, pp. 737–746, 2018.

[13] K. Yang, C. Zhou, H. Fan et al., "Bio-functional design, application and trends in metallic biomaterials," *International Journal of Molecular Sciences*, vol. 19, no. 1, pp. 1–21, 2017.

[14] D. Tang, R. S. Tare, L.-Y. Yang, D. F. Williams, K.-L. Ou, and R. O. C. Oreffo, "Biofabrication of bone tissue: approaches, challenges and translation for bone regeneration," *Biomaterials*, vol. 83, pp. 363–382, 2016.

[15] A. A. Zadpoor, "Mechanics of additively manufactured biomaterials," *Journal of the Mechanical Behavior of Biomedical Materials*, vol. 70, pp. 1–6, 2017.

[16] X. Wang, S. Xu, S. Zhou et al., "Topological design and additive manufacturing of porous metals for bone scaffolds and orthopaedic implants: a review," *Biomaterials*, vol. 83, no. 6, pp. 127–141, 2016.

[17] C. Zhang, S. Xie, S. Li et al., "Flow patterns and wall shear stress distribution in human internal carotid arteries: the geometric effect on the risk for stenosis," *Journal of Biomechanics*, vol. 45, no. 1, pp. 83–89, 2012.

[18] X. Liu, Y. Fan, A. Sun, and X. Deng, "Numerical simulation of nucleotide transport in the human thoracic aorta," *Journal of Biomechanics*, vol. 46, no. 4, pp. 819–827, 2013.

[19] H. Montazerian, M. Zhianmanesh, E. Davoodi et al., "Longitudinal and radial permeability analysis of additively manufactured porous scaffolds: effect of pore shape and porosity," *Materials and Corrosion*, vol. 122, no. 2017, pp. 146–156, 2017.

[20] S. Gómez, M. D. Vlad, J. López, and E. Fernández, "Design and properties of 3D scaffolds for bone tissue engineering," *Acta Biomaterialia*, vol. 42, pp. 341–350, 2016.

[21] A. L. Olivares, È. Marsal, J. A. Planell, and D. Lacroix, "Finite element study of scaffold architecture design and culture conditions for tissue engineering," *Biomaterials*, vol. 30, no. 30, pp. 6142–6149, 2009.

[22] A. Syahrom, M. R. Abdul Kadir, J. Abdullah, and A. Öchsner, "Permeability studies of artificial and natural cancellous bone structures," *Medical Engineering & Physics*, vol. 35, no. 6, pp. 792–799, 2013.

[23] J. Li, D. Chen, H. Luan, Y. Zhang, and Y. Fan, "Numerical evaluation and prediction of porous implant design and flow performance," *BioMed Research International*, vol. 2018, Article ID 1215021, 13 pages, 2018.

[24] S. M. Ahmadi, R. Hedayati, Y. Li et al., "Fatigue performance of additively manufactured meta-biomaterials: The effects of topology and material type," *Acta Biomaterialia*, vol. 65, pp. 292–304, 2018.

[25] S. J. Li, Q. S. Xu, Z. Wang et al., "Influence of cell shape on mechanical properties of Ti-6Al-4V meshes fabricated by electron beam melting method," *Acta Biomaterialia*, vol. 10, no. 10, pp. 4537–4547, 2014.

[26] D. Snelling, Q. Li, N. Meisel, C. B. Williams, R. C. Batra, and A. P. Druschitz, "Lightweight metal cellular structures fabricated via 3D printing of sand cast molds," *Advanced Engineering Materials*, vol. 17, no. 7, pp. 923–932, 2015.

[27] J. Li, D. S. Chen, H. Q. Luan et al., "Mechanical performance of porous implant with different unit cells," *Journal of Mechanics in Medicine & Biology*, vol. 17, no. 17, pp. 1–18, 2017.

[28] Y. Chen, S. Zhou, J. Cadman, and Q. Li, "Design of cellular porous biomaterials for wall shear stress criterion," *Biotechnology and Bioengineering*, vol. 107, no. 4, pp. 737–746, 2010.

[29] S. H. Cartmell, B. D. Porter, A. J. García, and R. E. Guldberg, "Effects of medium perfusion rate on cell-seeded three-dimensional bone constructs in vitro," *Tissue Engineering Part A*, vol. 9, no. 6, pp. 1197–1203, 2003.

[30] M. T. Raimondi, F. Boschetti, L. Falcone et al., "Mechanobiology of engineered cartilage cultured under a quantified fluid-dynamic environment," *Biomechanics & Modeling in Mechanobiology*, vol. 1, no. 1, pp. 69–82, 2002.

[31] D. Xiao, Y. Yang, X. Su, D. Wang, and J. Sun, "An integrated approach of topology optimized design and selective laser melting process for titanium implants materials," *Bio-Medical Materials and Engineering*, vol. 23, no. 5, pp. 433–445, 2013.

[32] J. Fan, X. Jia, Y. Huang, B. M. Fu, and Y. Fan, "Greater scaffold permeability promotes growth of osteoblastic cells in a perfused bioreactor," *Journal of Tissue Engineering and Regenerative Medicine*, vol. 9, no. 12, pp. E210–E218, 2016.

[33] R. Singh, P. D. Lee, T. C. Lindley, R. J. Dashwood, E. Ferrie, and T. Imwinkelried, "Characterization of the structure and permeability of titanium foams for spinal fusion devices," *Acta Biomaterialia*, vol. 5, no. 1, pp. 477–487, 2009.

[34] B. Porter, R. Zauel, H. Stockman, R. Guldberg, and D. Fyhrie, "3-D computational modeling of media flow through scaffolds in a perfusion bioreactor," *Journal of Biomechanics*, vol. 38, no. 3, pp. 543–549, 2005.

[35] Z. Zhang, L. Yuan, P. D. Lee, E. Jones, and J. R. Jones, "Modeling of time dependent localized flow shear stress and its impact on cellular growth within additive manufactured titanium implants," *Journal of Biomedical Materials Research Part B: Applied Biomaterials*, vol. 102, no. 8, pp. 1689–1699, 2014.

[36] R. G. Bacabac, T. H. Smit, S. C. Cowin et al., "Dynamic shear stress in parallel-plate flow chambers," *Journal of Biomechanics*, vol. 38, no. 1, pp. 159–167, 2005.

[37] R. Dholakia, C. Sadasivan, D. J. Fiorella, H. H. Woo, and B. B. Lieber, "Hemodynamics of flow diverters," *Journal of Biomechanical Engineering*, vol. 139, no. 2, Article ID 021001, 2017.

[38] D. Jing, S. Tong, M. Zhai et al., "Effect of low-level mechanical vibration on osteogenesis and osseointegration of porous titanium implants in the repair of long bone defects," *Scientific Reports*, vol. 5, article 17134, pp. 1–13, 2015.

[39] M. Cavo and S. Scaglione, "Scaffold microstructure effects on functional and mechanical performance: Integration of theoretical and experimental approaches for bone tissue engineering applications," *Materials Science and Engineering C: Materials for Biological Applications*, vol. 68, pp. 872–879, 2016.

[40] Z. Wang, C. Wang, C. Li et al., "Analysis of factors influencing bone ingrowth into three-dimensional printed porous metal scaffolds: a review," *Journal of Alloys and Compounds*, vol. 717, pp. 271–285, 2017.

[41] X. Pei, B. Zhang, Y. Fan et al., "Bionic mechanical design of titanium bone tissue implants and 3D printing manufacture," *Materials Letters*, vol. 208, pp. 133–137, 2017.

[42] B. A. J. A. Van Oirschot, R. M. Eman, P. Habibovic et al., "Osteophilic properties of bone implant surface modifications in a cassette model on a decorticated goat spinal transverse process," *Acta Biomaterialia*, vol. 37, pp. 195–205, 2016.

[43] T. Lemaire, J. Kaiser, S. Naili et al., "Three-scale multiphysics modeling of transport phenomena within cortical bone," *Mathematical Problems in Engineering*, vol. 2015, Article ID 398970, 10 pages, 2015.

[44] M. I. S. Azzam and F. A. L. Dullien, "Calculation of the permeability of porous media from the navier-stokes equation," *Industrial & Engineering Chemistry Fundamentals*, vol. 15, no. 4, pp. 281–285, 1976.

[45] S. Zhou and Q. Li, "A variational level set method for the topology optimization of steady-state Navier-Stokes flow," *Journal of Computational Physics*, vol. 227, no. 24, pp. 10178–10195, 2008.